

Robotic Assembly of Integrally-Attached Timber Plate Structures: From Computational Design to Automated Construction

Présentée le 3 mars 2023

Faculté de l'environnement naturel, architectural et construit
Laboratoire de construction en bois
Programme doctoral en architecture et sciences de la ville

pour l'obtention du grade de Docteur ès Sciences

par

Nicolas Henry Pierre Louis ROGEAU

Acceptée sur proposition du jury

Dr E. Cogato Lanza, présidente du jury
Prof. Y. Weinand, Prof. P. Latteur, directeurs de thèse
Prof. S. Brell-Cokcan, rapporteuse
Prof. J. Gattas, rapporteur
Prof. S. Parascho, rapporteuse

To my grandmother who instilled in me her passion for art, science, and teaching...

Acknowledgements

Thesis advisors

First of all, I would like to thank my thesis director, Prof. Dr. Yves Weinand, for giving me the opportunity to conduct this exciting research at the Laboratory for Timber Constructions (IBOIS) and for putting his trust in me throughout these four years. I am also grateful to have had the opportunity to be deeply involved in teaching, notably through the supervision of the design studio. Furthermore, I would like to give special thanks to my thesis co-director, Prof. Dr. Pierre Latteur, for his continuous support, his precious help in proofreading all my publications, and his encouragement and guidance in my early academic career.

Jury members

I am also very grateful to the jury members of the doctoral oral exam committee who accepted to review my dissertation and provided constructive feedback on my research: Prof. Dr. Sigrid Brell-Cockan, Prof. Dr. Joe Gattas, Prof. Dr. Stefana Parascho, and Prof. Dr. Elena Cogato Lanza. Similarly, I am grateful to the jury members of my candidacy examination for their valuable inputs at the beginning of my research work: Dr. Aleksandra Anna Apolinarska and Prof. Dr. Bernard Cache.

Internal and external collaborations

I would also like to thank all the brilliant people I met at Ecole Polytechnique Fédérale de Lausanne (EPFL) and at the National Center of Competence in Research (NCCR) Digital Fabrication. I learned a lot through our passionate exchanges and fruitful collaborations. I also met some fantastic people at the Laboratory for Timber Constructions (IBOIS) who supported me in my research and with whom I had the chance to collaborate on several publications. I am particularly grateful to Prof. Dr. Aryan Rezaei Rad for his highly valuable support as a colleague and friend.

Industrial partners

I also had the chance of collaborating with very professional people from IMAX Pro and Mobic. I would especially like to thank Cedric Moutschen and his team for their support in the robotic integration and for taking the time to answer all my questions about their automated workflow. I am also very grateful for their hospitality and trust during my stays at their production site

in Harzé which allowed me to better understand the functioning and the needs of a timber construction company.

Technical and administrative staff

I would also like to express my special appreciation to the technicians of the Groupe Ingénierie des Structures (GIS) at EPFL who spent a lot of time helping me with my robotic experiments. A particular thanks to François Perrin for his precious technical advice, his kind words of encouragement, and his ski tips. In addition, I would like to acknowledge the important work of the administrative staff at IBOIS and at the doctoral program Architecture and Sciences of the City (EDAR). Their help and support were also really appreciated.

Family and friends

My deepest gratitude goes to my family and my friends who encouraged me to do this thesis and supported me throughout these 4 years. I am really lucky to be surrounded by so many fantastic people. I especially thank my parents, Olivier and Isabelle, and my siblings, Damien and Anaïs, who have always been there for me despite the distance. Thank you so much for your affection and for believing in me! Lastly, I would like to thank a really wonderful person who always finds the right words when I need it the most, my best friend and partner, Sandra. Thank you for your unfailing support and for making me laugh even in the most difficult times!

Lausanne, February 2, 2023

Nicolas Rogeau

Abstract

The digitization of timber construction, the emergence of engineered wood products, and the urgent need to drastically reduce buildings' environmental impact have given a rebirth to wood as a construction material. On the one hand, increasing the use of timber in building technology has the potential to transform cities into carbon sinks. On the other hand, the growing availability of Computer Numerical Control (CNC) machines and industrial robotic arms makes woodworking less labor-intensive, less time-consuming, and thus more cost-effective. Besides, recent advances in Computer-Aided Design and Manufacturing (CAD/CAM) have paved the way for a wide range of architectural and structural design possibilities by overcoming this organic material's inherent limitations.

It is within this context that a significant focus has been put on Integrally-Attached Timber Plate Structures (IATPS) at the Laboratory for Timber Constructions (IBOIS, EPFL) since the last decade. This innovative yet sustainable construction system combines traditional craft with state-of-the-art technology. Timber panels are cut with a CNC and connected with timber joints inspired by ancient woodworking techniques to create spatial structures that can reach up to 50 m without glue or screws. A significant asset lies in the possibility of building both standard and bespoke buildings from simple flat-packed panels whose pre-cut shape informs the assembly. While previous research has focused on the computational design and digital fabrication of IATPS, this thesis has, for the first time, investigated the automation of the assembly process. The objective was to determine the feasibility of assembling these structures with a robotic arm and to identify the influence of assembly constraints on the design.

The methodology adopted a multidisciplinary approach integrating architectural, civil engineering, robotics, and computer science considerations. First, a computational framework was developed to enable a streamlined workflow from architectural design to robotic construction. This included the parametrization of timber joints, the implementation of algorithms to address modular assembly sequences, and a collaboration with an industrial partner to simulate robot trajectories within the design interface. Second, full-scale experiments were carried out with a 6-axis industrial robotic arm to assess and tackle the challenges associated with the robotic insertion of timber panels. A feedback loop relying on computer vision was developed to improve the robot's accuracy. In addition, design guidelines were established to determine an optimal shape for timber joints to reduce friction forces during insertion.

Abstract

A key achievement of the thesis is to have made IATPS more accessible to the Architecture, Engineering, and Construction (AEC) community through the release of Manis, an open-source Grasshopper plugin. This integrated design tool automates the 3D modeling of timber joints, the generation of CNC cutting files and robot instructions, as well as the creation of Finite Element meshes for subsequent structural analysis. Furthermore, the thesis gives new perspectives on mass timber construction by providing a framework for the industrial implementation of wood-wood connections in automated prefabrication lines. It proposes an innovative assembly process that requires no mechanical fasteners or chemical bonding and is fully automated from design to construction.

Keywords: timber plates; timber panels; timber joints; IATPS; robotic assembly; robotic insertion; insertion vector; construction automation; prefabrication; design for manufacture and assembly (DFMA).

Résumé

La digitalisation du secteur de la construction en bois, l'émergence du bois d'ingénierie ainsi que la nécessité de réduire drastiquement l'impact environnemental des bâtiments ont suscité un regain d'intérêt pour le bois en tant que matériau de construction. D'une part, l'augmentation de l'utilisation du bois dans la construction a le potentiel de transformer les villes en puits de carbone. D'autre part, l'accessibilité croissante des machines-outils à commande numérique (CNC) et des bras robotisés rend le travail du bois moins difficile, moins long et moins coûteux. En outre, les récentes avancées dans le domaine de la conception et de la fabrication assistées par ordinateur (CAO/FAO) ouvrent de nouvelles possibilités conceptuelles en permettant de surmonter les limites inhérentes à ce matériau organique.

Dans ce contexte, les Integrally-Attached Timber Plate Structures (IATPS) ont été développées au cours de la dernière décennie au Laboratoire de Construction en Bois (IBOIS, EPFL). Ce système de construction innovant et durable associe artisanat traditionnel et technologie de pointe. Des panneaux de bois connectés par des joints s'inspirant des anciennes techniques de menuiserie, sont découpés à l'aide d'une CNC et assemblés en structures spatiales pouvant atteindre des portées de 50 m sans colle ni vis. Un atout majeur réside dans la possibilité de créer des structures tant conventionnelles que complexes à partir de simples panneaux pouvant être transportés à plat et dont la forme prédécoupée informe l'assemblage. Alors que les recherches antérieures se sont concentrées sur l'automatisation du processus de conception et de fabrication des IATPS, cette thèse investigate pour la première fois l'automatisation de leur assemblage. L'objectif principal était de déterminer la faisabilité d'assembler ces structures avec un bras robotisé et d'identifier l'influence des contraintes de l'assemblage robotisé sur la géométrie des connections.

Une approche multidisciplinaire intégrant des considérations liées à l'architecture, au génie civil, à la robotique, et à l'informatique a été adoptée. Premièrement, un environnement computationnel a été développé afin de rationaliser l'ensemble des étapes de production. Cela inclut la paramétrisation de joints en bois, l'implémentation d'un algorithme pour résoudre les séquences d'assemblage modulaire, et la simulation des trajectoires robotiques. Deuxièmement, des expériences d'insertion robotisée ont été menées. Une boucle de rétroaction reposant sur la vision par ordinateur a été développée pour améliorer la précision du robot. Par ailleurs, un guide de conception pour les joints a été établi afin de proposer une forme

Résumé

optimale réduisant la friction lors de l'insertion.

Cette thèse constitue une avancée majeure vers une plus large adoption des IATPS. L'une des réalisations est la publication de Manis, un plugin pour Grasshopper disponible en accès libre. Cet outil automatise la modélisation 3D des joints en bois, la génération des fichiers de découpe CNC et des instructions pour l'assemblage robotisé, ainsi que la création de maillages aux éléments finis pour l'analyse structurelle. En outre, ce travail ouvre de nouvelles perspectives pour les acteurs du secteur de la construction en bois concernant l'utilisation des connecteurs bois-bois sur les lignes de préfabrication. La thèse propose ainsi un processus d'assemblage innovant et entièrement automatisé de la conception jusqu'à la construction.

Mots clefs : plaques de bois ; panneaux de bois ; joints en bois ; IATPS ; assemblage robotisé ; insertion robotisée ; vecteur d'insertion ; construction automatisée ; préfabrication ; conception pour la fabrication et l'assemblage.

Contents

Acknowledgements	i
Abstract (English)	iii
Résumé (Français)	v
List of figures	xiii
List of tables	xix
I Introduction and state of the art	1
1 Introduction	3
1.1 A renewed interest in wood	3
1.1.1 A brief history of timber construction	3
1.1.2 Engineered wood products	4
1.1.3 Lowering embodied carbon in buildings	4
1.2 Digitization of the timber construction sector	5
1.2.1 Computer-Aided Design	5
1.2.2 Automated production	6
1.2.3 From standard to free-form architecture	7
2 State of the art	9
2.1 Integrally-Attached Timber Plate Structures	9
2.2 Robotic assembly of timber structures	11
2.3 Research questions and objectives	12
II Computational design framework	15
3 Generation of joint geometry, fabrication toolpath, and robot trajectories	17
3.1 Abstract	17
3.2 Introduction	18
3.2.1 From traditional timber joints to Integrally-Attached Timber Plate Structures (IATPS)	18
	vii

Contents

3.2.2	Existing computational workflows for IATPS	19
3.2.3	Existing computational design tools for timber joints	21
3.3	Solver implementation and user interface	22
3.3.1	Implementation of a new data structure	22
3.3.2	User interface for iterative design workflows	23
3.4	Solver inputs	23
3.4.1	Hypothesis about the initial 3D model	23
3.4.2	Assembly sequence and modular construction approach	24
3.4.3	Insertion constraints for timber joints	25
3.5	Solver algorithms	26
3.5.1	Computing adjacency information from plate contacts	27
3.5.2	Computing assembly steps from the assembly sequence	27
3.5.3	Computing compatible insertion vectors for each plate and module	29
3.6	Solver outputs	30
3.6.1	Generating joint geometry	30
3.6.2	Generating fabrication toolpath for CNC machining	33
3.6.3	Generating robot trajectories for an automated assembly process	35
3.7	Solver application and performance	36
3.7.1	Case study 1: curved beam	36
3.7.2	Case study 2: boxed vault	36
3.7.3	Case study 3: timber frame	37
3.7.4	Computational performance	38
3.8	Conclusion and outlook	39
3.9	Acknowledgements	40
3.10	Addendum: Details on the integrated robotic simulation	41
3.10.1	Robotic simulation in Grasshopper	41
3.10.2	Robotic simulation in Unity	42
3.10.3	Synchronization Unity-Grasshopper	43
4	Integration of structural engineering considerations	45
4.1	Abstract	45
4.2	Introduction	46
4.2.1	Interdisciplinarity as a driver of sustainability	46
4.2.2	Interactive computational workflows	47
4.3	Method	48
4.3.1	Developing a collaborative design interface	48
4.3.2	Integrating numerical simulation	49
4.4	Results	50
4.4.1	First case study: orthogonal timber slab	50
4.4.2	Second case study: doubly-curved timber vault	51
4.5	Conclusion	53
4.6	Acknowledgements	54

4.7	Addendum: A computational design framework for the structure of Annen . . .	54
4.7.1	A streamlined and automated data exchange from CAD to CAE	55
4.7.2	Generating the macro model	56
4.7.3	Indexing system	57
4.7.4	Performance of the algorithm, conclusion, and outlook	59
III	Automated construction workflow	61
5	Insertion of timber joints with a visual feedback loop	63
5.1	Abstract	63
5.2	Introduction	64
5.3	State of the art of robotic insertion	65
5.3.1	Shape adaptation	65
5.3.2	Force monitoring	65
5.3.3	Visual feedback	66
5.3.4	Strategy comparison and research objective	67
5.4	Methodology	67
5.4.1	Integrated design framework	67
5.4.2	Insertion vectors	68
5.4.3	Position detection using fiducial markers	68
5.4.4	Fail-safe process	70
5.4.5	Robotic workflow	70
5.4.6	Intermediate robot language	71
5.5	Tests and results	72
5.5.1	Experimental set up	72
5.5.2	Insertion without visual feedback loop	74
5.5.3	Precision of the visual feedback loop	75
5.5.4	Insertion with visual feedback loop	76
5.6	Conclusion	77
5.7	Acknowledgements	78
5.8	Addendum: Further improvements to the visual feedback loop	78
5.8.1	Integrating Time of Flight sensors	78
5.8.2	Improving marker detection	81
5.8.3	Detecting the square to compute glyph orientation	81
5.8.4	Detecting the circle to compute glyph translation	82
5.8.5	Detecting crosses to compute glyph ID	83
5.8.6	Conclusion	84
6	Design considerations for robotically assembled through-tenon joints	85
6.1	Abstract	85
6.2	Introduction	86
6.3	State of the Art	87

Contents

6.4	Material and methods	88
6.4.1	Experimental set up	88
6.4.2	Experimental parameters	89
6.4.3	Fabrication of the samples	90
6.4.4	Experimental protocol	91
6.5	Results and discussion	92
6.5.1	Offset parameter	92
6.5.2	Chamfer and offset parameter	93
6.5.3	Angle parameter	95
6.5.4	Combined parameters	97
6.5.5	Extrapolation to a box girder	98
6.6	Conclusion	98
6.7	Acknowledgments	101
IV	Conclusion and outlook	103
7	Research output	105
7.1	Summary of research achievements	105
7.1.1	Computational design framework	105
7.1.2	Automated Construction workflow	106
7.2	Impact of the research	106
7.2.1	Impact on the design team	106
7.2.2	Impact on timber construction companies	108
7.2.3	Impact on society	108
7.2.4	Impact on architectural education	109
8	Research outlook	111
8.1	Limitations and future research needs	111
8.1.1	Computational design framework	111
8.1.2	Automated Construction workflow	112
8.2	Perspectives for robotic timber construction	113
8.2.1	Toward automated on-site construction	113
8.2.2	Toward human-robot collaboration	114
A	Appendix	115
A.1	UML diagram of the joinery solver	116
A.2	Mathematical parametrization of timber joints	117
A.3	Examples of structures designed with Manis	125
A.3.1	Projects of Master students from the architecture studio at EPFL)	125
A.3.2	Workshop at the 2022 CAADRIA conference in Sydney	127
A.3.3	Architectural investigations	128
A.4	Pseudo-code of the indexing algorithm for the macro model of the structure of Annen	130

A.5	Global overview of the robotic insertion test campaign	134
A.6	Insertion graphs for different joint parameters	135
A.6.1	Offset only	135
A.6.2	Offset and angle	137
Bibliography		153
Glossary		155
Curriculum Vitae		157

List of Figures

1	Introduction	3
2	State of the art	9
3	Generation of joint geometry, fabrication toolpath, and robot trajectories	17
3.1	Graphical abstract.	18
3.2	Three large-scale projects showcasing IATPS (from left to right): The folded structure of the Vidy theater (IBOIS, 2018) [RGW17], the segmented shell of the Buga Wood Pavilion (ICD/ITKE, 2019) [Wag+20a], the double-layered vault of the Annen head office (IBOIS, 2021) [Rob+16].	20
3.3	Different methods for 3D modeling IATPS: using a mesh data structure (a), using aggregation rules for a set of two tiles (b), using standard CAD software without a specific data structure (c).	21
3.4	Plate faces refer to the two largest surfaces of the poly-surface while other surfaces are designated as sides.	24
3.5	Possible contact types for an assembly of two plates and their associated timber joints.	24
3.6	A modular assembly sequence of timber plates expressed as a list of lists of integers.	25
3.7	Generating joints without considering the assembly sequence can lead to blocking situations (a). The goal of the solver is to first compute a compatible direction of assembly before generating the joint geometry (b).	26
3.8	Each timber joint has an insertion domain that represents all possible insertion vectors for assembling the pieces (a). Without any joint, the insertion domain is represented by a half-sphere (b). Insertion constraints ensure joints can be generated once the insertion vector has been deduced (c).	26
3.9	The solver provides a default insertion constraint for each contact type.	27
3.10	Decision tree of the algorithm used to identify the different contact types.	28

List of Figures

3.11 Plate contacts can be represented with an adjacency graph where each link represents a contact between two plates. Contact types, contact zones, contact planes, and insertion constraints are stored in parallel lists inside the model instance.	28
3.12 Developing all subsequences from the input sequence allows ordering the assembly steps.	29
3.13 Plate 4 has three contact zones (C1, C2, C3) and two insertion vectors (V1 and V2) since it is involved in two subsequences. The aim of the algorithm is to associate one insertion vector to each contact zone by crossing adjacency and assembly information.	29
3.14 A compatible insertion vector is found by intersecting the insertion constraints from the contact zones between the plate(s) to assemble and the plate(s) already in place.	31
3.15 Five types of joints have been parametrized and can be generated with the solver.	31
3.16 Parametric construction of the half-lap joint as implemented in the solver. The use of solid Boolean operations to get the chamfer planes precluded a purely mathematical description of the joint geometry. For the other joints, the equations can be found in Appendix A.2.	32
3.17 Joint geometry is stored as three lists of solids and kept separated from the plate geometry until the design is fixed. Solid Boolean operations allow the integration of the joints inside the plates to display the result.	33
3.18 Integrating corner notches into fabrication toolpath.	34
3.19 The different steps of the robotic trajectory are similar for each plate. However, distances can be adjusted, and intermediary points can be added to work around obstacles and avoid collisions.	35
3.20 Application of the solver to a segmented curved beam of 18 panels.	37
3.21 Application of the solver to a vault composed of 20 hexagonal modules of 7 plates.	37
3.22 Application of the solver to a timber frame composed of two arches of 13 pieces each and 21 purlins.	38
3.23 Flowchart representing the algorithm developed to simulate the motion of the robot and the plates. Inputs are displayed in grey, and outputs are in color. . . .	42
3.24 Robotic simulation within the design interface. If a valid trajectory can be computed, the robot turns green (a). Otherwise, it turns red (b), and the blocking situation is displayed. On the right, the robot cannot insert the second plate as it is beyond reach.	42
3.25 Robotic interface developed by ImaxPro in Unity.	43
3.26 Communication protocol to synchronize two robot models in Unity and Grasshopper and enable direct feedback about robotic constraints inside the design interface.	44

4 Integration of structural engineering considerations

45

4.1	Two examples of IATPS: the theatre of Vidy in Lausanne (left, © Ilka Kramer) and the multipurpose hall of Annen in Manternach (right, © Valentin Bianchi).	47
4.2	Standard software focuses on one part of the design process leading to siloed workflows. Collaborative design workflows focus instead on one building typology.	48
4.3	The algorithm enables collaboration by integrating structural performance as well as fabrication and assembly constraints into the design process.	49
4.4	Integrating engineering feedback from Abaqus and OpenSees into the collaborative design plugin "Manis" via COMPAS open-source platform.	49
4.5	Automated conversion of architectural 3D models to Finite Element models. . .	50
4.6	The developed plugin enables the integration of fabrication, assembly, and structural constraints into the design process of an orthogonal slab made of 4 timber panels.	51
4.7	The tool design space ranges from standard to bespoke timber plate structures, as demonstrated with this doubly-curved timber vault made of 9 boxes of 4 plates each.	52
4.8	CNC cutting and robotic assembly of one module of the doubly-curved vault prototype.	53
4.9	The 23 doubly-curved vaults of the Annen headquarters are composed of hundreds of timber panels with thousands of joints.	55
4.10	Assembly sequence of the arches of the Annen structure.	56
4.11	The different steps of the geometric algorithm developed to convert the detailed 3D model of the structure of the Annen project to a macro model suitable for structural analysis in OpenSees.	57
4.12	Algorithm for the indexing of the elements of the macro model and the generation of the .tcl file for the subsequent OpenSees analysis.	58
5	Insertion of timber joints with a visual feedback loop	63
5.1	Three types of self-centering connections: conic joint (left), drone-compatible joint for interlocked timber beams (middle), and chamfered through-tenon joint (right).	66
5.2	Integrated design framework linking design to robotics constraints.	67
5.3	Insertion vectors are inducing the shape of the connections as well as the robot trajectory.	69
5.4	Image processing of an ArUco Marker using OpenCV library to get the position and orientation of a timber panel.	69
5.5	Robotic workflow: camera shooting with the robot moving according to model (green), image processing (orange), picking phase with the robot moving according to the stack of panels (blue), insertion phase with the robot moving according to marker (purple).	71
5.6	Robotic trajectory based on the vector of insertion.	72

List of Figures

5.7	Samples of a text file interpreted by our custom application in Unity to send instructions to the robot controller: Activation of the visual feedback loop (a) and joint move above a marker (b).	73
5.8	Robot end effector equipped with a vacuum gripper and camera for visual feedback.	73
5.9	Assembly of 13 non-orthogonal timber panels without using the visual feedback loop. Discrepancies of about 1 cm between the virtual and physical models were reported when trying to assemble the panels. Manual adjustments were, therefore, required to perform the assembly with the robot.	74
5.10	Finding the relative camera position by comparing manually referenced coordinates with computed values from the visual feedback.	75
5.11	Maximum distance between the target position and the results obtained with the visual feedback loop.	76
5.12	Variation of accuracy according to the orientation of the camera.	76
5.13	Chamfered tenon based on the measured precision of the visual feedback loop.	77
5.14	Insertion of a Laminated Veneer Lumber (LVL) panel with the visual feedback loop.	77
5.15	Improved visual sensor with four ToF lasers and a camera connected to a single-board computer and fixed on a steel plate.	79
5.16	First, the four lasers are used to accurately adjust the distance to the target plate (Z translation) and to ensure the camera lens is parallel to the plane of the panel (XY rotation). Then a picture of the marker can be taken, and the image can be processed to find the center of the panel (XY translation) and its 2D orientation (Z rotation).	80
5.17	Computing the rotation angle by detecting the square in the engraved glyph.	82
5.18	Varying the low and high threshold values of the intensity gradient of the Canny filter maximize the chances of getting the correct lines in the glyph image.	82
5.19	Only the longest detected lines are kept, allowing to discard the natural lines of the wood and only detect the edges of the marker.	82
5.20	The center of the glyph is obtained by detecting the engraved circle.	83
5.21	By detecting the presence of crosses in the glyph, the panel ID can be retrieved. The ID is stored as a binary number between 0 and 511 (in this example, the panel ID is 110010101 = 405).	84
6	Design considerations for robotically assembled through-tenon joints	85
6.1	Robotic assembly of a timber frame structure (credit: IMAX Pro S.A., Belgium).	87
6.2	Custom setup developed to evaluate the insertion performance of the joints.	89
6.3	Geometric parameters for the male and female parts of the joints.	90
6.4	Variation of fabrication tolerance for the different faces of the male and female parts.	91
6.5	Procedure for testing each sample with the 6-axis robotic arm.	93
6.6	Influence of the offset parameter on the insertion of 2 tenons with a chamfer of 5 by 5 mm (angle parameter: 0 degree).	95

6.7	Influence of the angle parameter on the insertion of 2 tenons (offset parameter: 0 mm, chamfer: 5 by 5 mm).	96
6.8	Progressive diminution of clearance for a bevel angle of 5 degrees without offset and with a chamfer of 5 by 5 mm. The clearance (C) is defined as the distance between the edges of the tenon and the internal faces of the mortise hole. The distance is measured perpendicularly to the vector of insertion.	96
6.9	Robotic assembly of a box girder. The four plates are connected by eight through-tenon joints each.	99
6.10	Successful insertion of the three elements of the box girder.	99
7	Research output	105
7.1	Using the developed tool, custom IATPS can be built with a fully automated process combining the advantages of modular prefabrication and bespoke architecture. (Credits for left and right pictures: Blumer Lehmann AG).	107
8	Research outlook	111
A	Appendices	115
A.1	Using Manis for a renovation project in a Swiss castle (student: Nicolas Otti, Spring 2020).	125
A.2	Using Manis for a bespoke timber shell (student: Nicolas Otti, Spring 2020). . .	126
A.3	Using Manis for prefabricated housing boxes (student: Tomohiko Nakamura, Spring 2020).	126
A.4	Using Manis for a bike shelter (participant: Jacinta Alves, April 2022).	127
A.5	Using Manis for a reciprocal structure (participant: Rin Masuda, April 2022). . .	127
A.6	Using Manis to design a boxed vault.	128
A.7	Using Manis to design zome structures (spiral-shaped domes).	129
A.8	Influence of the offset parameter (mm) on the insertion of 2 tenons (angle parameter: 0 degree, chamfer: none).	135
A.9	Influence of the offset parameter (mm) on the insertion of 3 tenons (angle parameter: 0 degree, chamfer: none).	135
A.10	Influence of the offset parameter (mm) on the insertion of 4 tenons (angle parameter: 0 degree, chamfer: none).	136
A.11	Influence of the offset parameter (mm) on the insertion of 5 tenons (angle parameter: 0 degree, chamfer: none).	136
A.12	Influence of the offset parameter (mm) on the insertion of 2 tenons (angle parameter: 5 degree, chamfer: 5 by 5 mm).	137
A.13	Influence of the offset parameter (mm) on the insertion of 3 tenons (angle parameter: 5 degree, chamfer: 5 by 5 mm).	137
A.14	Influence of the offset parameter (mm) on the insertion of 4 tenons (angle parameter: 5 degree, chamfer: 5 by 5 mm).	138

List of Figures

A.15 Influence of the offset parameter (mm) on the insertion of 5 tenons (angle
parameter: 5 degree, chamfer: 5 by 5 mm). 138

List of Tables

1	Introduction	3
2	State of the art	9
3	Generation of joint geometry, fabrication toolpath, and robot trajectories	17
3.1	Computational time of each operation for each case study. Joints abbreviations: DJ = Dowel joint, TT = through-tenon joint, SD = Sunrise Dovetails, FJ = Finger Joint, HL = Half-lap joint.	39
4	Integration of structural engineering considerations	45
4.1	Performance comparison between Finite Element (FE) and Macro models. . . .	59
5	Insertion of timber joints with a visual feedback loop	63
5.1	Comparison of fault tolerant assembly techniques.	67
6	Design considerations for robotically assembled through-tenon joints	85
6.1	Geometric parameters of the tested samples.	90
6.2	Fabrication time in 3 and 5-axis according to the number of tenons.	91
6.3	Insertion completion as a function of the offset parameter and number of tenons. Orange cells represent samples with partial insertion while green cells represent fully inserted samples.	94
6.4	Maximum load (F) as a function of the offset parameter and number of tenons.	94
6.5	Insertion completion and maximum load (F) as a function of the offset parameter with a chamfer of 5 by 5 mm.	94
6.6	Insertion completion and maximum load (F) as a function of the angle parameter	97
6.7	Insertion completion as a function of the offset parameter and the number of tenons with an additional angle of 5 degrees.	97
6.8	Maximum load (F) with an additional angle of 5 degrees.	97
7	Research output	105

List of Tables

8	Research outlook	111
A	Appendices	115
A.1	List of tested samples (each sample was tested three times).	134

Introduction and state of the art

Part I

1 Introduction

1.1 A renewed interest in wood

1.1.1 A brief history of timber construction

Wood is one of the oldest building materials known to humans. Archaeological surveys have reported traces of timber dwellings dating back to the neolithic [Nob06] [PB15]. Its high strength-to-weight ratio and the ease with which it can be worked made it ideal for building nomadic shelters in prehistoric times. Until the industrial revolution, the fabrication and assembly of timber buildings remained a highly manual process relying on hand tools. However, Roman bridges, Viking ships, and Japanese temples testify to the richness, complexity, and diversity of woodworking techniques developed before the industrial era.

In medieval Europe, the extensive use of wood combined with agricultural expansion led to severe deforestation [Rad12]. The decreasing availability of large trees fostered the adoption of timber framing [HaB05]. As the timber pieces were smaller than before, ingenious joinery techniques were invented by high-skilled carpenters to connect the different structural elements. Notably, the art of the French scribing tradition ("trait de charpente") allowed the realization of complex timber roofs in castles and cathedrals [Def81]. Ultimately, the shortage of wood and the fear of fire in cities led builders to turn to other materials such as stone or bricks [Rad12].

In North America, the use of wood in construction followed a similar course with an offset of about two centuries [See21]. In the 16th century, early settlers inhabited log cabins made out of long round wood [Mor87]. Then, colonization, population growth, and European exports led to a massive expansion of wood demand. This resulted in a reduction in the size of the timber pieces and the spread of stick-built construction [Tak81]. However, unlike in Europe, the emergence of metal fasteners has favored nailing connections instead of complex and expensive timber joints. Later, the arrival of reinforced concrete at the beginning of the 20th century relegated the use of wood to single-story houses.

1.1.2 Engineered wood products

Reinforced concrete combines the ductility of steel with the compressive strength of concrete, resulting in a material with very high structural resistance. This enabled the construction of skyscrapers and bridges with previously unimaginable heights and spans. The isotropic properties of steel and concrete have also facilitated building standardization and mass production, which pushed concrete to be the most consumed resource on earth after water. Conversely, wood is a natural material with anisotropic properties depending on the direction of the fibers. Moreover, depending on the tree's growing conditions, knots, and internal stresses can weaken it locally.

The purpose of Engineered Wood Products (EWP) is to improve both the reliability and performance of solid wood. The manufacturing process involves binding wooden boards, veneers, or particles with adhesives, nails, or dowels to create large structural beams, posts, and panels with standardized dimensions and properties. Plywood boards and Glue Laminated Timber (GLT) are examples of EWP that have been commercialized since the beginning of the 20th century. However, it is essentially the invention of Cross-Laminated Timber (CLT) by Gerhard Schickhofer at the end of the 1990s that initiated the broader adoption of EWP by the construction sector [SB13].

During the last decade, mass timber construction has gained popularity among architects and real estate developers. Although construction costs are higher than for concrete, the possibilities of prefabrication and the ease of transport make it possible to construct multi-story buildings in a very short time [Gui09]. In addition, the growing awareness of environmental challenges is pushing the sector to reevaluate existing construction methods. Mass timber construction could be vital to cutting carbon emissions from buildings.

1.1.3 Lowering embodied carbon in buildings

The construction sector is a significant contributor to environmental pollution and global warming. The operational energy used for heating, cooling, and lighting buildings, accounts for 28% of global greenhouse gas emissions [Uni20]. In addition, the embodied energy associated with the construction of buildings accounts for another 11% [Uni20]. In 2020, construction and demolition waste were also responsible for 37,1% of all waste generated in the European Union [Eur21], with the proportion of waste from mineral materials reaching two-thirds of this [Eur11].

Recent technological advances in energy efficiency should make it possible to significantly reduce operational energy in the coming years, provided that the entire building stock is renovated quickly enough [Dil+19]. Nevertheless, to reach the objectives of the Paris Agreement and the Sustainable Development Goals, those innovations must be coupled with substantial progress in reducing embodied energy and building waste [WMR21]. This is a significant challenge considering the current growth of the world population and the expected need for

new housing and facilities [Uni18].

Through carbon storage, bio-based materials like wood can contribute to decarbonizing the construction industry, and mitigating climate change [Ing11] [Ami+20]. Coming from renewable sources and being more easily recycled, they have a lower global environmental impact than their mineral counterparts [De +16]. Their manufacturing and transport are also less carbon-intensive. In addition, timber buildings are usually lighter than concrete or steel constructions and, therefore, require smaller foundations. Furthermore, studies have shown that bio-based materials positively affect human health [KK14].

However, sustainable forest management upstream of the construction process is necessary to avoid deforestation and biodiversity losses. While forest area has increased by 9% since 1990 in Europe, the world has lost an estimated 420 million hectares of forest in the same time [For20]. Despite standards and certificates being increasingly used, significant efforts are still required to ensure the sustainable management of the world's forests.

Nonetheless, the global environmental benefits of bio-based materials have spurred ambitious policies to encourage building with wood. For example, Finland is committed to doubling the use of timber in buildings to reach carbon neutrality by 2035 [Pel21]. Japan also passed a law in 2010 requiring the use of wood for public buildings that have three stories or less [Jap22]. Cities like Amsterdam [Gem] or Paris [FIB] are also planning to build new neighborhoods almost entirely with wood. Several other countries have taken similar resolutions to increase the share of reused and bio-based materials in the construction sector in the coming decades. An increasing number of high-rise buildings are also being built of wood, with the current record being held by the Mjøstårnet tower and its 18 stories.

The growing demand for wood challenges the industry along the whole value chain [HP20]. This goes from the extraction of raw logs through the processing and manufacturing of engineered timber products to their implementation in buildings. Besides, lumber prices in 2021 and 2022 have reached four to five times the usual rate due to the cumulative effects of the high demand and low supply following the COVID-19 pandemic [ZS21]. However, the rapid digitization of the sector could increase productivity and make wood more competitive [ACS16].

1.2 Digitization of the timber construction sector

1.2.1 Computer-Aided Design

In the second half of the 20th century, the invention of Computer-Aided Design (CAD) drastically improved the communication of project data between designers and builders by reducing drawing flaws and enabling more back and forth in the design process [Car13]. The development of 3D modeling software with accessible interfaces in the 1990s led to the massive adoption of CAD in design offices. Initially, the main interest in using the computer to draw

plans was to be more precise and faster than by hand. However, another major asset of CAD became the possibility to associate data with drawings [Pic10]. Information such as material performance, surface finishing, element cost, and assembly sequence can be added on top of the geometry of the building components. This principle is at the core of Building Information Modeling (BIM) processes.

Progressively, buildings are not only drawn but also coded. Custom algorithms are being developed to optimize architectural shapes and to integrate constraints from other disciplines (environmental, social, economic, structural, logistic, etc.). Consequently, parametric design, which mixes geometric drawing and computer science, is increasingly taught in architecture schools [Boi20]. Although the recent appropriation of these new tools has so far mainly produced organic shapes and intricate geometries, parametric design should not be reduced to a stylistic trend. Its potential lies more in the adaptive and iterative process than in the appearance of the built result.

The timber construction sector has particularly benefited from the emergence of CAD tools. Connection details that used to be complex and time-consuming to draw can now be generated automatically from pre-established databases. Furthermore, dedicated pieces of software, such as Cadwork [Cad] or SEMA [SEM], are offering "all-in-one" digital solutions from planning to assembly. One single virtual model gathers all project data avoiding file transfers and enabling the automated prefabrication of building components.

1.2.2 Automated production

In addition to CAD, the digitization of the timber construction sector has been characterized by the introduction of Computer Numerical Control (CNC) machines. CNC wood-cutting processes were first used in the furniture industry to accelerate production rates and reduce manufacturing costs [Rat22]. The difference with the construction sector is that buildings are much less standardized than furniture. They are made of many different parts that can be unique to the project. Therefore, automating the production of building components also requires automating the generation of cutting files. Computer-Aided Design and Manufacturing (CAD/CAM) workflows allow the generation of machining instructions directly from 3D models. The constraints of manufacturing processes are integrated into the design through the possibility of simulating the machining toolpath inside an interactive interface.

The spread of CNC machining has gradually transformed small traditional sawmills, where a lot of manual work was necessary, into larger automated production lines. With the rise of automation, the quality and accuracy of production have considerably increased [Mac+19]. However, while industries and workers now benefit from an overall safer and more productive environment, digitization has also led to more standardization and the demise of many small businesses. Therefore, the issue of accessibility to digital tools remains crucial to guarantee a democratic use of the technology and ensure that it has a positive impact on the whole of society.

Furthermore, the specific needs of architectural projects prevent the implementation of a logic similar to the one used in the production of cars and smartphones. Before filing for bankruptcy in 2021, Katterra was one of the biggest off-site timber construction companies with more than 1300 employees working in several gigafactories spread across the United States [Cur20]. Its business model consisted in providing turnkey services, including all steps from design to construction. Katterra's failure showed the difficulty of disrupting current practices in the construction industry. While encompassing the entire construction process within a single industry provides clear efficiency gains, the broad diversity of components and operations makes any attempt at harmonization difficult.

In the last years, leading timber construction companies [ERN22] [Gru22] [Mob22] have started to implement 6-axis Industrial Robotic Arms (IRA) in their production lines. The main advantage of IRAs is their versatility, as they are multipurpose and reprogrammable. A wider variety of tasks can therefore be performed than with other machines. Besides, they have large working envelopes and more degrees of freedom (usually 6 axes) than conventional CNC (usually 3 to 5 axes). Consequently, IRAs make it possible to overcome some of the manufacturing limitations imposed by CNCs and allow even more architectural freedom.

With the increasing presence of robots on prefabrication lines (and on construction sites), new questions arise. In particular: how the implementation of these new technologies can benefit workers? And how can robots and humans collaborate in the same environment? This also raises new political debates in our society: Should we tax the use of robots to fight income inequality? And should we only automate painful jobs where there are labor shortages? Although this thesis is primarily concerned with technical considerations, tools are not innocent and their potential societal impact must be addressed upstream of their development.

1.2.3 From standard to free-form architecture

Over the last two decades, architects have explored digital fabrication's new possibilities. CAD/-CAM workflows enabled the design and fabrication of complex geometry while maintaining a rational production in terms of cost and time through modular prefabrication. Furthermore, since wood is a material that can be easily milled or bent to give it the desired shape, it has generated a lot of interest from architects wishing to build free-form structures. Although various manufacturing and assembly techniques have been developed, two categories can be distinguished.

The first category comprises structures with linear load-bearing elements. It includes timber framing, post and beam systems, and gridshells. The new Swatch headquarters designed by Shigeru Ban [Shi19] and the Cambridge Mosque by Marks Barfield [Mar22] are among the most iconic examples of free-form timber structures with double-curved linear elements. Both buildings feature a network of custom Glued Laminated (Glulam) timber beams. First, the wooden lamellas are bent and glued on custom jigs. Then, they are robotically milled to obtain

the double curvature [Leh22].

This thesis focuses on the second category, which includes all structures made out of planar elements. The recent emergence of EWP has made it possible to build structural envelopes where the panels are load-bearing. This simplifies the construction process as fewer elements are necessary. Mass timber buildings composed of prefabricated CLT walls and slabs represent the most widespread system in this category. The curved tubular structure of "The Smile", an installation by architect Alison Brooks for the 2016 London Design [Ali16], demonstrates that the use of timber panels is not limited to standard orthogonal structures. Free-form building envelopes can also be built out of panels by tessellating a target surface with planar polygons. While this technique is still experimental, several large-scale demonstrators showcasing this technique have been realized by different research institutes in the last decade. Consequently, the next chapter establishes the state of the art of those Timber Plate Structures (TPS) and further introduces the research question and objectives.

2 State of the art

2.1 Integrally-Attached Timber Plate Structures

The increasing accessibility of digital fabrication tools has spurred the realization of many architectural research pavilions with timber panels featuring different design processes and construction systems. Simultaneously, various connection strategies have been developed to attach the panels while ensuring adequate load transfer. Early prototypes developed at the Laboratory for Timber Constructions (IBOIS) at Ecole Polytechnique Fédérale de Lausanne (EPFL) showcased folded structures inspired by origami patterns [Bur10]. The panels were first connected by miter joints combined with nails as in the Chapel of Saint-Loup (Pompaples, 2008) [Han08]. However, subsequent investigations have led to the integration of the connections directly into the geometry of the timber panels resulting in the development of Integrally-Attached Timber Plate Structures (IATPS). Inspired by traditional Japanese joinery, the assembly of the pieces relies only on interlocking principles, removing the need for additional mechanical fasteners.

The renewed interest in timber joints was only possible because of the new opportunities offered by CNC machining. As their design and fabrication can be fully automated, integrating timber joints is no longer as time-consuming and expensive as when they had to be produced by hand. At IBOIS, Christopher Robeller's thesis highlighted both the potential and constraints of the digital fabrication of timber joints [Rob15]. In 2013, a thin folded shell was assembled in Mendrisio [RNW14]. Curved CLT panels featuring dovetail joints were cut using a convex formwork and a robotic arm equipped with a saw blade. In 2017, the construction of a folded and double-layered IATPS covering up to 20 m for the theater of Vidy in Lausanne demonstrated the feasibility of using timber joints for large-scale spatial structures [RGW17].

Other IBOIS works focused on the mechanical behavior of timber joints and the structural analysis of IATPS. The semi-rigidity of through-tenon joints was studied by Stéphane Roche [Roc17] while a calculation method for orthogonal timber slabs with wood-wood connections was established by Julien Gamero [Gam20]. In addition, a Finite Element method and a macro modeling approach for IATPS were respectively developed by Anh Chi Nguyen [Ngu20] and

Aryan Rezaei Rad [Rez20]. The research performed in those two theses was ultimately applied to analyze the doubly-curved vaults of the Annen headquarters with spans ranging from 22.5 to 53.7 m [NVW19] [Rez+21]. The building is currently under construction in Manternach, Luxembourg.

IBOIS research was also continued by Christopher Robeller with the Digital Timber Construction group at the Technical University of Kaiserslautern. The HexBox Canopy project was assembled in collaboration with the University of Sydney in 2019 [Tag20]. The vault was composed of hexagonal timber boxes made from plywood panels and connected by wedge joints. The Recycleshell was inaugurated the same year [RV20]. This demonstrator consisted of 230 panels sourced from CLT wall cutouts and connected by X-Fix butterfly joints.

Since 2010, the Institute for Computational Design and Construction (ICD) at the University of Stuttgart has also explored the potential of digital tools to design and build free-form timber structures inspired by nature [Sch+19]. Four iterations of IATPS based on the plate skeleton of sea urchins and featuring panels connected by finger joints were successively developed: the 2011 research pavilion [KM13], the Landesgartenschau Exhibition Hall in 2014 [Kri+15], the Segmented Timber Shell of the Rosenstein Museum in 2017 [Sch+19], and the BUGA Wood Pavilion in 2019 [Wag+20a]. A collaborative workflow was developed and improved with each pavilion to integrate robotic manufacturing and structural engineering requirements in the design process. A decade of research made it possible to progressively reduce the quantity of wood per square meter and create an effective and lightweight construction system. The BUGA Wood Pavilion, the last iteration, spans 30 m for a weight of 36 kg/m² [Wag+20a].

IATPS research is deeply applied and project-oriented. For all structures cited above, custom algorithms were developed to generate the 3D geometry of the panels and their connections, automate their fabrication, and integrate structural engineering considerations. However, two research gaps can be pointed out.

First, custom computational workflows are being developed for each new project. Code reusability is, therefore, very low. While some tools have been created to solve some specific tasks, such as automating the generation of fabrication files or the 3D modeling of some particular joints, the range of applications is currently very limited. There have not yet been any attempts to generalize the IATPS design process by integrating all the constructive constraints into one tool.

Second, while research has been actively performed on the digital fabrication of panels and joints, the assembly remains primarily manual. Moreover, there is a lack of research on the robotic insertion of timber joints, especially on tolerance issues. The following section introduces the state of the art in robotic timber construction and underlines the need for more research on the automation of the assembly of IATPS.

2.2 Robotic assembly of timber structures

A unique experiment on the robotic assembly of IATPS was carried out in 2017 by Christopher Robeller et al. at the Swiss National Centre of Competence in Research (NCCR) Digital Fabrication [Rob+17]. It highlighted the difficulty of inserting tight-fitting connections with a robotic arm as friction forces can rapidly exceed the robot's strength. Furthermore, a major challenge involved assembling multiple joints simultaneously on different panels. Collaborative robots have also been used at ICD to assemble the timber boxes of the BUGA Wood Pavilion. However, the robotic process consisted in gluing the pieces instead of using timber joints [Wag+20a].

Other research at the NCCR Digital Fabrication focused on the robotic assembly of timber beams to realize complex structures. For example, 168 trusses were assembled with a robotic gantry for the Sequential Roof project [Apo+16], making it the largest robotically built timber structure. The developed workflow included the automation of the nailing of the pieces. Bespoke timber frame modules were also assembled with collaborative robots for the DFAB House project [Tho+20]. While human assistance was required to screw the beams together, the robots allowed the precise positioning of the pieces. Similarly, the elements composing the reciprocal timber grid of the Future Tree project were cut and positioned by a robotic arm [Apo+21a].

Subsequent investigations aimed at replacing the screws with timber joints. Victor Leung's thesis focused on the design of detachable robotic clamps to assemble timber beams connected by half-lap joints [Leu+21]. Several demonstrators were also assembled throughout the development of this technique. Furthermore, a complementary research project was developed at Gramazio Kohler Research in collaboration with Autodesk to explore the use of Deep Reinforcement Learning for inserting half-lap joints [Apo+21b].

The research group CREATE at the University of Southern Denmark also explored the robotic assembly of beams connected by timber joints. An assembly policy based on prior human demonstrations was developed to teach the robot to insert a half-lap joint [Kra+22]. Spherical connectors cut with a round CNC milling bit were also designed to enable the robotic assembly of reconfigurable timber structures [HKN21]. In addition, a modular building system consisting of robotically prefabricated timber blocks was developed by the Automated Architecture Lab (AUAR) at the Bartlett School of Architecture [Cla+21]. The panels forming the blocks are connected by through-tenon joints.

Other remarkable wooden structures have been built with the help of robots, although mechanical fasteners were used instead of timber joints in those projects. For example, the Fusta Robotica pavilion and the Digital Urban Orchard are two spatial structures composed of several hundred wooden sticks and robotically assembled at the Institute for Advanced Architecture of Catalonia [BFD19]. Furthermore, haptic feedback and human-robot collaboration strategies were developed by the Chair for Individualized Production at RWTH Aachen University to assemble a twisted arch made from timber sticks [DSB19].

The robotic assembly of timber beams shares similar challenges to the robotic assembly of IATPS, such as joint tolerance and robot path planning. Nevertheless, some differences are induced by the geometry of the plates. Panels are less slender than beams and less likely to bend. However, they are usually heavier and more difficult to manipulate with a robot. Large vacuum grippers are required to lift the panels, potentially reducing the pick-and-place operation's accuracy. The manufacturing process is also more restrictive for panels as they need to be cut with one of the two main faces lying against the CNC table. Conversely, beams can be more easily placed on a stand to cut from below and rotated a quarter turn if needed.

While several research groups are working on the robotic assembly of timber structures, the challenge of inserting timber joints with a robotic arm has been only slightly addressed so far. In addition, most of the experiments involved the insertion of half-lap joints for timber beams. Consequently, further research is required on the assembly of panels, and the insertion of other types of joints is still to be investigated.

2.3 Research questions and objectives

Considering the research gaps identified in the state of the art, two questions related respectively to the computational design and automated construction of IATPS arise:

- Would it be possible to create an intuitive interface to facilitate the design of IATPS by generalizing existing project-oriented algorithms and integrating the various engineering constraints?
- What are the challenges of robotically assembling IATPS, and what solutions can be implemented to overcome them?

Consequently, the objective of this thesis is twofold. First, develop an integrated design tool that will apply to all kinds of IATPS. The goal is to provide a computational framework that integrates robotic assembly constraints in addition to manufacturing and engineering considerations. The tool will be implemented as an open-source Grasshopper plugin to make IATPS more accessible to non-experts. Second, to tackle the challenges linked to the robotic assembly of panels connected by timber joints and determine the conditions for inserting tight-fitting connectors. The research will ultimately produce guidelines for timber construction companies in order to enable the use of robotically-assembled wood-wood connections as an alternative to glued and screwed connections.

The research presented in this manuscript is therefore divided into two parts. The first part addresses the development of the computational design framework, while the second covers the implementation of a fully automated construction workflow for IATPS. Each part is again divided into two chapters based on published and peer-reviewed publications. Additional investigations conducted after an article's publication are also presented in the *Addendum* section of the corresponding chapter.

For the first part, Chapter 3 introduces the different algorithms constituting the computational design framework. This includes the parametrization of 5 types of timber joints, as well as the integration of fabrication and assembly constraints in the design interface. Then, Chapter 4 completes the framework description by detailing the integration of structural engineering considerations. The performance of the solver is also demonstrated through several study cases.

For the second part, Chapter 5 presents experiments conducted with fiducial markers and computer vision algorithms to increase the accuracy of robotic insertion tasks. Next, Chapter 6 provides design guidelines based on experimental tests to reduce friction forces during the insertion of through-tenon joints while ensuring tight-fitting connections.

In the last part of the manuscript, the output and outlooks of the research are reported. The main scientific contributions and the potential applications of the thesis are highlighted in Chapter 7. Lastly, the limitations of the work, the future research needs, and the longer-term perspectives are discussed in Chapter 8.

Computational design framework **Part II**

3 Generation of joint geometry, fabrication toolpath, and robot trajectories

The texts and figures presented in this section were reproduced from the postprint version of the following peer-reviewed paper available in open access:

Rogean, N., Latteur, P., & Weinand, Y. (2021). An integrated design tool for timber plate structures to generate joints geometry, fabrication toolpath, and robot trajectories. *Automation in Construction*, 130, 103875. doi:10.1016/j.autcon.2021.103875.

The doctoral candidate was responsible for the entire development of the scientific work as well as for the writing of the article. The second and third authors of the paper contributed equally as scientific advisors and proofreaders.

3.1 Abstract

This paper presents an integrated design tool for structures composed of engineered timber panels connected by traditional wood joints. Recent advances in computational architecture have permitted the automation of fabrication and assembly of such structures using Computer Numerical Control (CNC) machines and industrial robotic arms. However, while several large-scale demonstrators have been realized, most developed algorithms are closed-source or project-oriented. Furthermore, the lack of a general framework makes it difficult for architects, engineers, and designers to effectively manipulate this innovative construction system. Therefore, this research aims at developing a holistic design tool targeting a wide range of architectural applications. Main achievements include: (1) a new data structure to deal with modular assemblies, (2) an analytical parametrization of the geometry of five timber joints, (3) a method to generate CNC toolpaths while integrating fabrication constraints, and (4) a method to automatically compute robot trajectories for a given stack of timber plates.

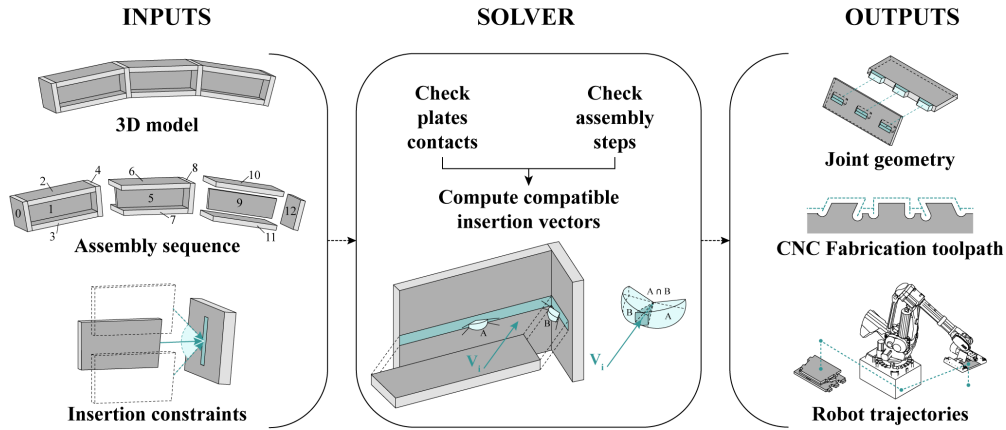


Figure 3.1: Graphical abstract.

3.2 Introduction

3.2.1 From traditional timber joints to Integrally-Attached Timber Plate Structures (IATPS)

Early wood architecture traces have revealed timber joints dating back more than 7000 years ago [Teg+12]. Until the industrial revolution, it remained the most common technique to assemble wooden pieces. Two primary structural purposes of timber joints can be distinguished: increasing the length of the elements to achieve longer spans (e.g., roof framing, bridge trusses) or increasing the width of the elements to cover a larger surface (e.g., stacked walls, roof cladding). For each situation, various joining techniques adapted to the local context were developed and transmitted by carpenters over time [Gra92].

With the spread of metallic connectors (e.g., screws, bolts), which can be easily mass-produced, and the rising cost of skilled labor in developed countries, timber joints have gradually been abandoned by construction companies in favor of less expensive practices that could be more easily automated [Ben81]. New gluing processes have also made it possible to overcome the natural size of trees. Indeed, engineered wood products such as glued laminated timber (Glulam) and cross-laminated timber (CLT) can cover large spans and broad surfaces with a single element whose dimensions are limited only by logistical constraints. With the industrialization of the construction sector, timber joint craft was narrowed down mainly to vernacular architecture and cabinet making.

However, the recent emergence of robotics in the construction sector has made it possible to revive ancient techniques such as traditional timber joinery. Computer Numerical Control machines (CNC) and Industrial Robotic Arms (IRA) allow for the automation of complex fabrication and assembly processes that would otherwise be too time-consuming for cost-effective applications. This opportunity led to the development of so-called Integrally Attached Timber Plate Structures (IATPS) [Rob15]. IATPS combine modern engineered wood panels

with traditional timber joints that are digitally fabricated. Beyond their aesthetic appeal, these joints also fulfill a functional role, allowing each construction element to be precisely positioned. They also reduce the need for additional connectors, such as screws or nails, as the assembly is performed solely by geometrical interlocking. Furthermore, experimental studies and numerical analysis of IATPS have demonstrated the positive influence of wood-wood connections on the structural performance of the system [GLW18].

The main interest of IATPS lies in the fact that they allow a high degree of prefabrication. However, designing such structures is not straightforward, as multiple constraints influence the shape of the connections between the panels. Several workflows have been showcased through the construction of demonstrators and real-scale flagship projects (Section 1.2), and different computational tools have been developed to assist in the 3D modeling of timber joints (Section 1.3). However, there is a lack of a general framework linking all constraints of the system together to allow non-experts to design IATPS and enable broader applications of the system. A general framework for the structural design of IATPS has been proposed by Rad and al. [Rez+21] [RBW20]. This contribution aims at completing this framework by integrating fabrication and assembly constraints in the 3D modeling of the connections.

3.2.2 Existing computational workflows for IATPS

IATPS have been showcased in several research pavilions and flagship buildings during the last decade (Figure 3.2). Several large-scale demonstrators featuring finger joints have been built by researchers from the University of Stuttgart [Kri+15] [Sch+19]. For the recent Buga Wood pavilion [Wag+20a], so-called "co-design" algorithms were developed to integrate structural requirements and robotic fabrication aspects into the design process. A high level of automation was reached as each unique module of the structure was carefully assembled by two collaborative robots.

Recent projects from the Digital Timber Construction chair of Kaiserslautern University have used wedge-joints [Tag20] and butterfly joints [RV18] [RV20] between hexagonal pieces to build doubly-curved timber vaults. For each project, global geometry and local connection details were controlled by custom scripts. The machining toolpath has also been automatically generated and simulated before exporting fabrication files to a 5-axis CNC.

Previous research conducted at the Laboratory for Timber Constructions at Ecole Polytechnique Fédérale de Lausanne has led to the construction of two full-scale projects: the theater of Vidy [RGW17] in Lausanne and Annen head office in Manternach [Rob+16]. The first project is a double-layered folded structure inspired by Japanese origami patterns, and the second consists of 23 doubly-curved vaults made of timber boxes. Through-tenon joints were used in both structures as connections between timber panels. As for the pavilions mentioned above, parametric scripts were developed to integrate fabrication constraints in the design process.

For all projects presented above, the global shape was first discretized using a mesh where each



Figure 3.2: Three large-scale projects showcasing IATPS (from left to right): The folded structure of the Vidy theater (IBOIS, 2018) [RGW17], the segmented shell of the Buga Wood Pavilion (ICD/ITKE, 2019) [Wag+20a], the double-layered vault of the Annen head office (IBOIS, 2021) [Rob+16].

mesh face represents a timber panel. A mesh data structure keeps track of the links between the elements. This adjacency information is essential for modeling joints between two timber plates, as the shape of the connection is influenced by the relative position of the plates. As timber panels are planar elements, all mesh faces must be planar. Planarization algorithms are used to approximate curved surfaces with planar panels [Wan+08] [Mes18]. In addition, as timber panels are standardized products, it is often required to work with panels of constant thickness. Ensuring both planarity and constant thickness heavily constrains the design space to certain types of meshes. Hexagonal patterns with trivalent vertices (Figure 3.3a) allow meeting both requirements [Pot+08].

However, mesh discretization is not the only possibility for modeling IATPS. One alternative is to rely on procedural generation algorithms such as the one developed by Rossi and al. [RT17]. Complex assemblies can be created from aggregation rules operating on a predefined set of tiles (Figure 3.3b). Aggregation is the inverse operation of discretization. Instead of dividing a complex geometry into panels, panels are assembled iteratively to form a complex structure based on topological constraints. As for meshes, aggregation methods produce an organized data structure that contains the adjacency information necessary to model the joints.

Another possibility is to manually draw the elements in 3D without relying on specific data structures (Figure 3.3c). While aggregation and discretization are potent tools to tackle complex geometries, most architectural projects are drawn using standard CAD software without using any computational methods. In that case, the only information contained in the model is the plate geometry and its position in an arbitrarily defined frame. Therefore, automating the 3d modeling of the connections for such structures requires first determining the relative position of the plates to each other.

The integrated design approach employed in all the projects cited above was based on a predefined data structure that facilitated the modeling of connections between elements and the integration of fabrication and assembly constraints. The drawback is that each architectural project is different, so a unique algorithm must be thought out for each new construction system. This research aims to develop a holistic design tool to generalize joinery modeling between timber plates independently of the global geometry of a project.

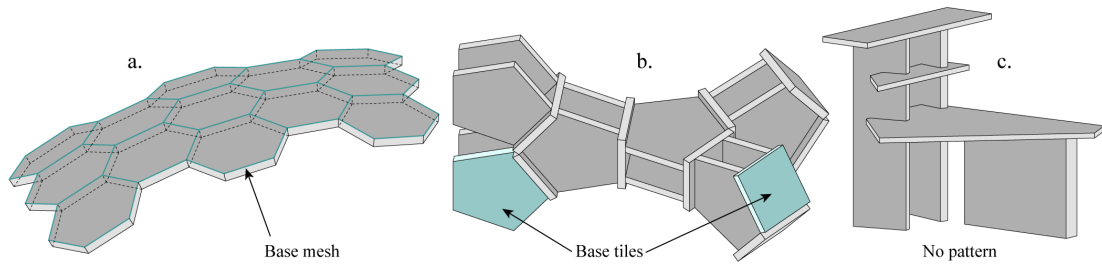


Figure 3.3: Different methods for 3D modeling IATPS: using a mesh data structure (a), using aggregation rules for a set of two tiles (b), using standard CAD software without a specific data structure (c).

3.2.3 Existing computational design tools for timber joints

The resurgence of timber joints in contemporary architecture has been facilitated by the development of 3D modeling tools to automatically generate geometry and fabrication files for these types of connections. Several Computer-Aided Design and Manufacturing (CAD/CAM) software such as CadWork [Cad], Sema [SEM], and Lignocam [Lig] integrate dedicated joinery modules for timber frame structures and can export machining toolpath from 3D models. Similarly, open access web applications such as MakerCase [Hol], CutCad [Hel+18], Kyub [Bau+19], and Joinery [ZDB17] allow readily creating joints between planar pieces which can then be cut and assembled in 3D. Another approach based on voxels was taken by Larsson and al. [Lar+20] to develop Tsugite, an interactive interface to explore, design, and manufacture complex joints between timber beams. By restricting the design space to a 9x9x9 voxel grid, a multi-criteria analysis of the joint performance can be shown to the user after each iteration, and the design can be accordingly improved.

Custom plugins for Grasshopper, the visual scripting interface of Rhinoceros by McNeel and Associates [Maa], have also been developed. Timber Plate Structure plugin (TPS) [RW15] allows users to create origami patterns with dovetails, finger joints, or miter joints. Reindeer [Mor+17] open-source set of tools focuses on timber frame connections with structural analysis feedback. GluLamb [Svi20] addresses the specific case of curved glued laminated timber (GLT) pieces. Finally, Emarf [VUI] offers various tools to generate timber joints between extruded solids and export fabrication files. The main advantage of those parametric solvers is the direct feedback that makes it possible to adapt the joint geometry according to fabrication constraints. Typically, the machining toolpath can be visualized without leaving the design interface, and its impact on the global project can be considered ahead of execution.

Assembly constraints can also inform the shape of a joint. Most solvers leave it up to the user to assess the feasibility of the assembly as they are tailored for standard applications. When complexity rises, two strategies can be employed: (1) solving assembly constraints for a given set of joints and refining the design until the assembly works, or (2) constraining the design space to generate only compatible joints. Tsugite solver belongs to the first category as it

evaluates friction areas to assess the ease of insertion of each proposed joint. On the contrary, the TPS plugin computes a compatible vector of insertion for each piece in the structure before generating the joints to avoid any blocking situation.

The interlocking properties of timber joints can also be exploited in the design of a structure. For example, DESIA framework [WSP18] uses directed graphs to compute assembly sequences and vectors of insertion for a set of discrete elements where the last piece acts as a blocking key. Graph theory was also applied to compute assembly sequences of waffle structures composed of intersecting planar pieces connected by half-lap joints [SP13].

This research aims to provide a computational design tool for timber plate structures that may have a large number of connections. Therefore, fabrication and assembly constraints must be treated automatically and cannot be left under the user's responsibility. The main challenge was to provide a high level of automation while keeping a design space as ample as possible to accommodate different typologies: from structures with a regular pattern (e.g., shell, vaults, slabs) to more irregular assemblies. Furthermore, by concentrating the research scope on timber plates, a systematic methodology could be employed to cover all topological cases.

The developed tool is introduced in the following sections. First, the implementation of the solver and its interface are presented in Section 3.3. Required inputs and working hypotheses are then detailed in Section 3.4. Next, the algorithmic framework allowing the computation of compatible insertion vectors is explained in Section 3.5. Then, the generation of the solver outputs (joint geometry, fabrication toolpath, and robotic trajectories) is covered in Section 3.6. Finally, the performance of the solver is demonstrated in Section 3.7 through three case studies.

3.3 Solver implementation and user interface

The main concept of this new integrated design tool is to convert a 3D model into an organized data structure, allowing for generating joint geometry, fabrication toolpath, and robotic trajectories. Before detailing the different parts of the algorithm, its general implementation and interface are presented here.

3.3.1 Implementation of a new data structure

The solver has been coded in Python 2.7 [Pyt] (for compatibility with the Rhinoceros framework) and relies on the RhinoCommon [Mac] library for geometric operations. The code is structured as four python classes (see Appendix A.1 for further details):

- Plate model: methods and attributes applying to the full structure.
- Plate module: methods and attributes applying to a group of plates.
- Plate: methods and attributes applying to one single plate.

- Toolbox: helper functions.

Taking advantage of the concept of object-oriented programming (OOP) [Mol], a 3D model is converted into an instance of the plate model class. For each plate in the 3D model, an instance of the plate class is also created. Similarly, plate modules are instantiated for each group of plates specified by the user. This will be more detailed in Section 3.2 about the modular construction approach.

By converting 3D geometries into class instances, additional information can be attached to the elements of the structure. For example, a plate instance carries more data than just the plate geometry. The plate thickness, the plane in which the plate stands, and other specific attributes are all computed during the object's instantiation and stored as variables that can be later accessed. Besides, those elements can be grouped into different hierarchic levels (Module, Model) to store topological data about how the elements are connected.

Adding this layer of information during the conversion of the 3D model into a class instance also allows faster feedback when performing operations on the model. Typically, a modification of the joint geometry can be executed without the need to compute all topological information again, as it is already stored in the data structure.

3.3.2 User interface for iterative design workflows

To facilitate the manipulation of the integrated design tool by architects and structural designers, a custom plugin has been developed in the visual scripting environment of Grasshopper. This node-based interface makes the tool usable without any programming knowledge. Class methods and attributes can be accessed through different Grasshopper components. A parametric design workflow can be easily set up to generate different types of joints in an iterative process. This is further demonstrated in Section 3.7 through three case studies.

3.4 Solver inputs

The solver requires three types of inputs: a 3D model containing all the elements of the structure, an assembly sequence defining the order in which to assemble the different parts, and insertion constraints depending on the type of joints to generate. Each solver input is described here.

3.4.1 Hypothesis about the initial 3D model

To run the solver, a 3D model of the global geometry of a timber plate structure first needs to be provided. At this stage, joints are not modeled yet. The 3D model is a collection of timber plates that can be manually drawn or algorithmically generated in Rhinoceros CAD software. A plate is defined as a planar structural element with a small thickness compared to the planar

dimensions [TW+59]. It is geometrically represented as a collection of connected surfaces forming a closed polyhedron (see Figure 3.4). Besides, a plate must follow the following requirements: (1) all surfaces composing the plate should be planar, (2) all vertices should be trivalent (having exactly three neighbors), and (3) each vertex of the top face should be directly connected to exactly one vertex of the bottom face and conversely. Plates with internal holes are included in this definition, while those with curved edges or warped faces are excluded. However, curved edges can be approximated by linear segments.

The type of joint generated between two plates is conditioned by their relative position. Five topological cases are supported by the solver (Figure 3.5). The contact zone is defined as the surface (or the volume for intersecting plates) shared by two adjacent plates. Edgewise connections are a specific type of side-to-face connection with the contact zone located on the edge of the plate. For each relative position, a type of joint has been studied and parametrized (see Appendix A.2). To ensure the 3D model can be properly interpreted by the solver, each pair of adjacent plates must respect one of the five contact types.

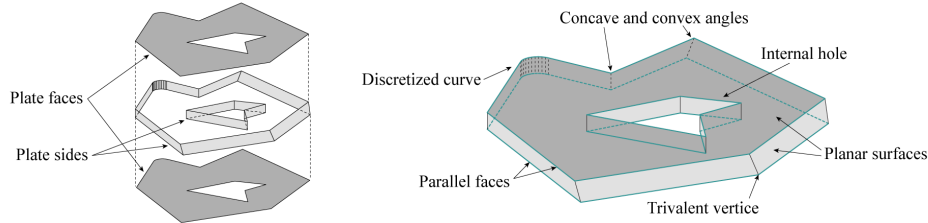


Figure 3.4: Plate faces refer to the two largest surfaces of the poly-surface while other surfaces are designated as sides.

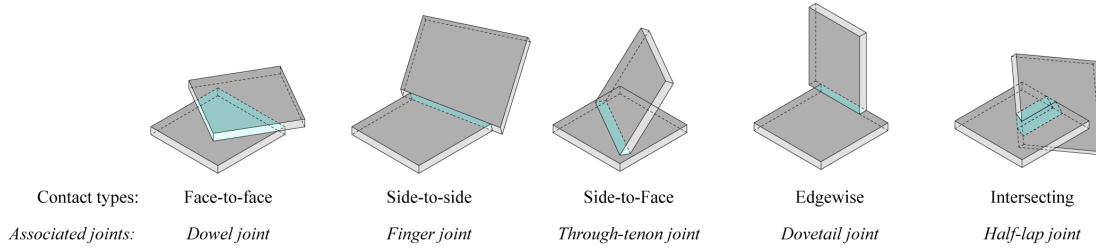


Figure 3.5: Possible contact types for an assembly of two plates and their associated timber joints.

3.4.2 Assembly sequence and modular construction approach

In addition to the 3D model, the user is asked to provide an assembly sequence defining the order of assembly of the elements. Some solvers, such as DESIA [WSP18], can automatically compute an assembly sequence for a given set of elements. However, for real construction projects, assembly steps are often constrained by factors other than the geometry of the pieces. Besides, large-scale structures are often subdivided into smaller modules that can be

preassembled off-site. The range of possibilities for a modular assembly sequence is extensive, as plates can be grouped in many different ways. To avoid constraining the solver to linear assemblies and enable the use of modules, the assembly sequence is here considered a design variable under the user's responsibility. The sequence input is written as a list of integers using Python syntax (Figure 3.6). Each integer refers to a plate in the list of elements of the 3D model. To change the order of the assembly, the user can either change the order of the collection of plates or swap integers in the assembly sequence.

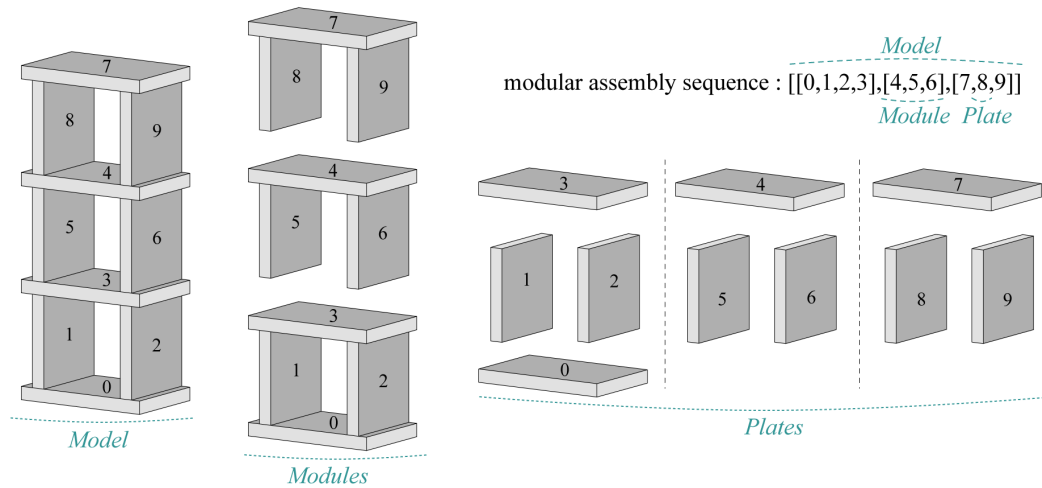


Figure 3.6: A modular assembly sequence of timber plates expressed as a list of lists of integers.

3.4.3 Insertion constraints for timber joints

The goal of the solver is to generate timber joints compatible with the assembly sequence. To do so, the direction of the assembly has to be predetermined before generating joint geometry. Otherwise, non-compatible joints could lead to blocking situations where pieces cannot be assembled (Figure 3.7). To summarize, the shape of a connection is induced by the type of joint, the assembly sequence, and the adjacent plates. The algorithms leading to determining the assembly direction are detailed in Section 3.5.

Timber joints can be inserted in one or more directions depending on their geometry. The direction of the assembly is represented by an insertion vector, while the insertion domain shows all possible insertion vectors for a given joint (Figure 3.8a). Before adding a joint between two plates, the assembly can potentially be performed from all directions. Therefore, the largest insertion domain is a hemisphere oriented to the normal of the contact zone (Figure 3.8b). However, most types of joints cannot be adapted to work for any insertion vector. Therefore, to ensure the generation of the joint geometry remains possible, it is necessary to constrain the insertion domain to a portion of that sphere before computing the insertion vectors (Figure 3.8c). This is a way of informing the solver about the type of joint that will later be created.

Mathematically, an insertion constraint is defined as the locus of all the points on the unit sphere from which an insertion vector can be created by linking the sphere center. The locus can be tridimensional (a piece of the unit sphere), bidimensional (an arc on a unit circle), or unidimensional (a point on the surface of the sphere). The solver supports five contact types (see Figure 3.5). By default, it provides a different insertion constraint for each of them (Figure 3.9). Custom constraints can also be specified by the user via the Grasshopper plugin interface.

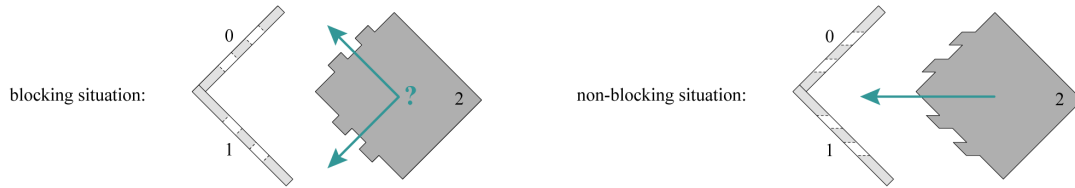


Figure 3.7: Generating joints without considering the assembly sequence can lead to blocking situations (a). The goal of the solver is to first compute a compatible direction of assembly before generating the joint geometry (b).

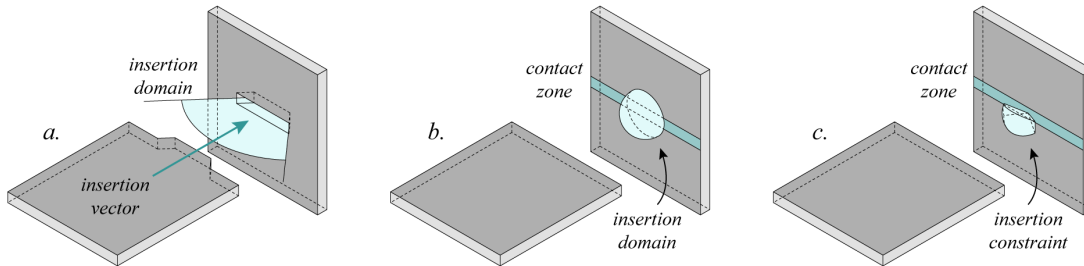


Figure 3.8: Each timber joint has an insertion domain that represents all possible insertion vectors for assembling the pieces (a). Without any joint, the insertion domain is represented by a half-sphere (b). Insertion constraints ensure joints can be generated once the insertion vector has been deduced (c).

3.5 Solver algorithms

This section describes all the necessary steps to transform the 3D model into an instance of the "Model" class (see Section 3.3) using the inputs provided by the user. The topology of the structure is first computed by looking at the contacts between the plates. Then, the assembly sequence is parsed to extract the different assembly steps. Finally, insertion vectors are computed for each plate and module in the structure.

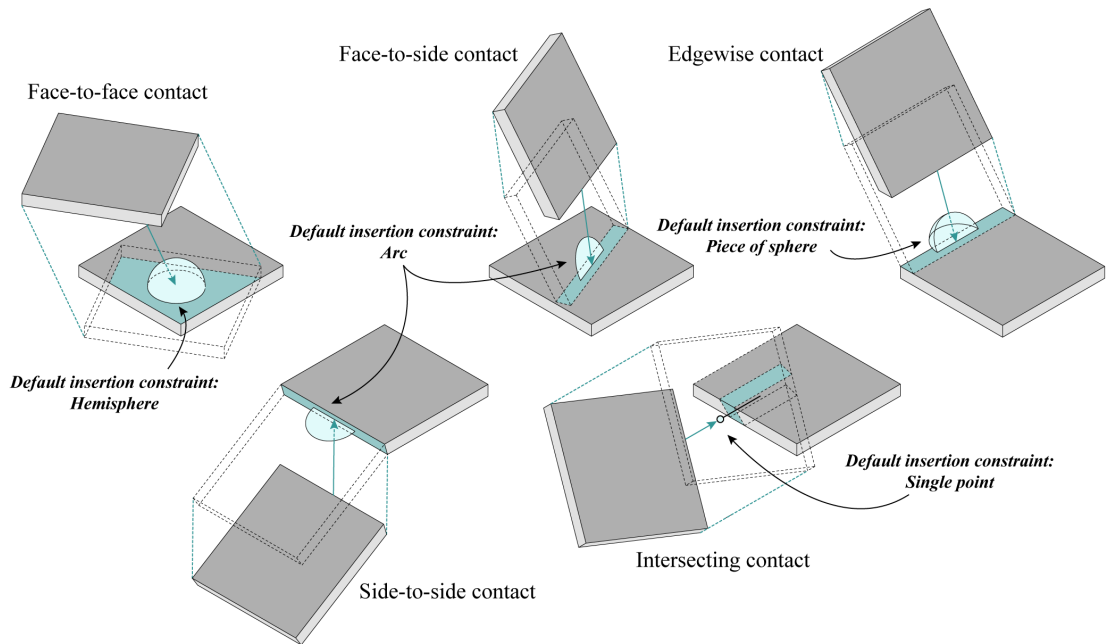


Figure 3.9: The solver provides a default insertion constraint for each contact type.

3.5.1 Computing adjacency information from plate contacts

The 3D model input only provides geometries without any attached data. Conversely, a mesh data structure stores information about the adjacency of its elements. Therefore, the first step of the algorithmic framework is to find all contact zones where a joint could be created. This is achieved by intersecting the plates with each other. If the intersection returns neither a surface nor a volume, the pair is discarded. Otherwise, the contact type is determined by comparing the orientation of the normal to each neighboring plate with the normal of the contact zone (Figure 3.10). Finally, a plane is also generated at the center of the contact zone. It will be the frame of reference for the joint that will later be created between both plates.

Adjacency information can be represented using a graph where each node of the graph is a plate, and each link represents a contact between two plates (Figure 3.11, left). In the model instance, this information is stored using a list of pairs of integers based on plate numbers (Figure 3.11, right). Parallel lists are used to store the contact type, the contact zone, and the contact plane for each pair of plates. In addition, an insertion constraint is selected in function of the contact type and oriented according to the contact plane.

3.5.2 Computing assembly steps from the assembly sequence

The second step of the algorithmic framework is to parse the assembly sequence input. Each pair of square brackets implies the instantiation of a module. A module is a preassembled group of plates moving as one object. Modules and plates can be combined to form larger modules. In the example of Figure 3.12, the module "[1,2,3]" is associated with the plates "0"

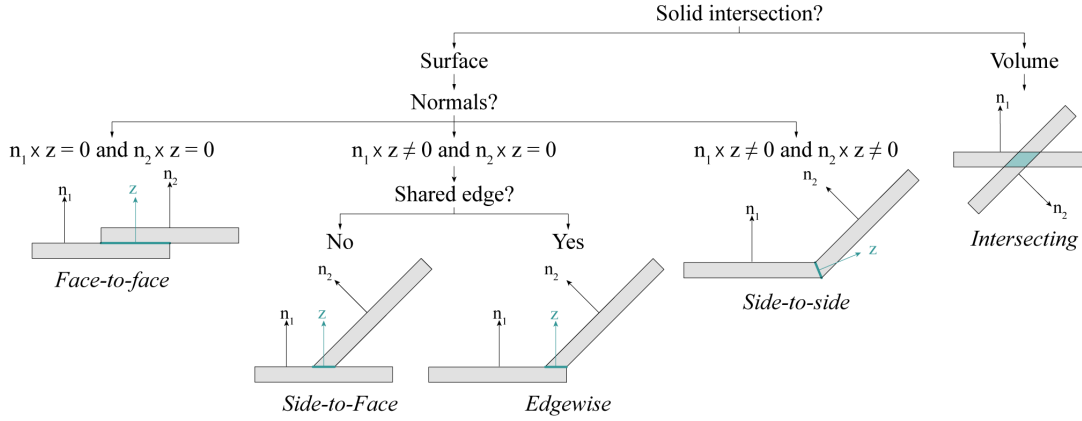


Figure 3.10: Decision tree of the algorithm used to identify the different contact types.

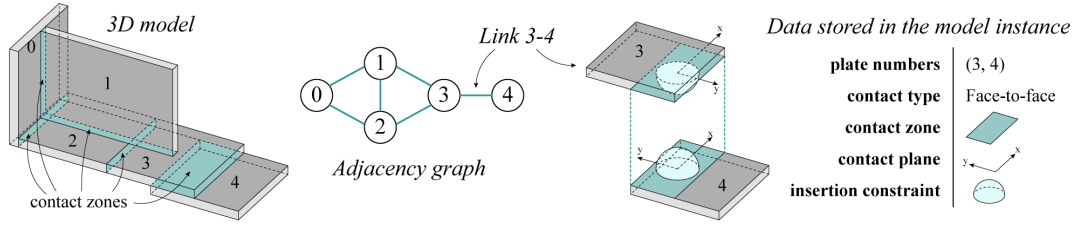


Figure 3.11: Plate contacts can be represented with an adjacency graph where each link represents a contact between two plates. Contact types, contact zones, contact planes, and insertion constraints are stored in parallel lists inside the model instance.

and "4" to form the module "[0,[1,2,3],4]". This module is then assembled with the module "[[5,[6,7]], [8,9]]" to complete the model. As for a simple plate, an insertion vector must be associated with each module to specify the assembly direction. However, at this stage, insertion vectors are not yet determined.

The assembly sequence is successively divided into different subsequences that define the order of assembly of the elements constituting each module. A tree graph can be used to represent the development of the assembly sequence associated with the model into the subsequences associated with all modules (Figure 3.12, top left). Since a plate can be part of several modules, smaller modules must be assembled first. Therefore, the order of the assembly steps is obtained by navigating the tree from bottom to top (Figure 3.12, top right). Consequently, in the example of Figure 3.12, the first module to assemble is "[6,7]". Modules on the same level of the tree graph are assembled from left to right, respecting the ascending order of the plate integers. Hence, the next module to assemble is "[1,2,3]", followed by "[5,[6,7]]" and "[8,9]". Several steps can be required to assemble a module. For example, for the module "[1,2,3]", plate "2" is first inserted into plate "1". Then, plate "3" is inserted into plate "2". A total of nine steps are necessary to complete the assembly of the input geometry of Figure 3.12.

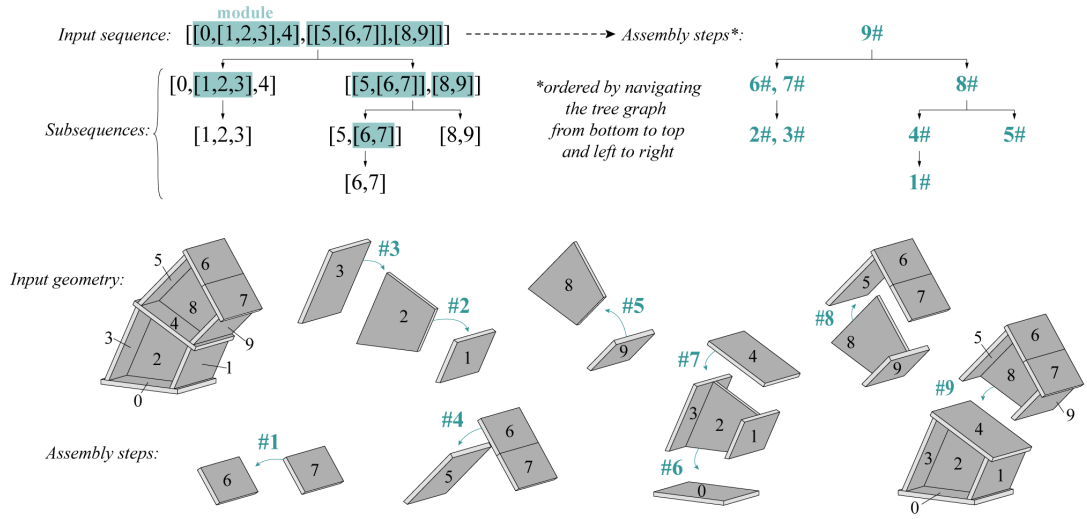


Figure 3.12: Developing all subsequences from the input sequence allows ordering the assembly steps.

3.5.3 Computing compatible insertion vectors for each plate and module

At this stage, contact types and assembly steps have been retrieved from user inputs. The purpose of this third part of the algorithmic framework is to compute insertion vectors for all the model elements (plates and modules) at each assembly step. With modular assemblies, a single element can be part of several subsequences. Therefore, while each contact zone needs to be associated with only one insertion vector to generate a joint, the contact zones of one plate can have different insertion vectors (like C1 and C2 in Figure 3.13). However, if two contact zones are involved in the same assembly step (like C2 and C3 in Figure 3.13), the same insertion vector must be applied.

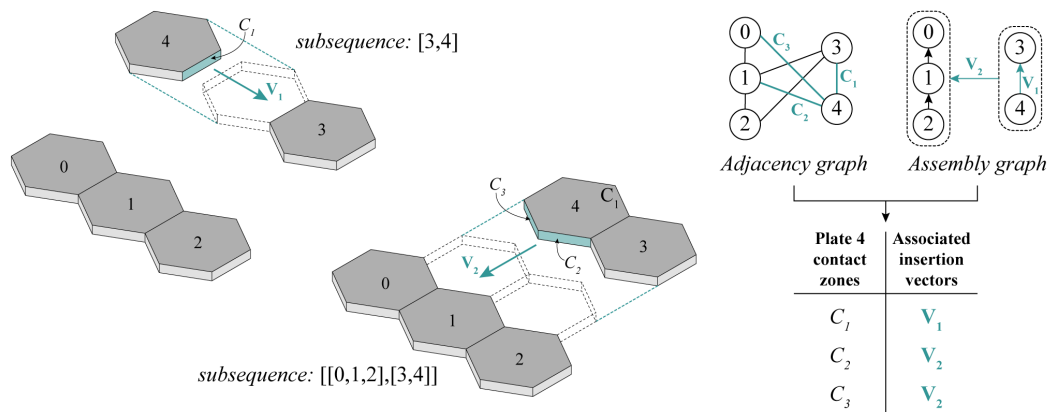


Figure 3.13: Plate 4 has three contact zones (C1, C2, C3) and two insertion vectors (V1 and V2) since it is involved in two subsequences. The aim of the algorithm is to associate one insertion vector to each contact zone by crossing adjacency and assembly information.

By representing the assembly sequence as a graph, adjacency and assembly information can be compared. To find the insertion vector associated with an assembly step, all contacts between the plate(s) to assemble and the plate(s) appearing before it in the subsequence are considered. In the example of Fig. 12, the first subsequence only implies plates 3 and 4. Therefore, only one contact will be involved in the determination of the insertion vector. On the contrary, for the second subsequence, the module "[3,4]" has four contacts reported on the adjacency graph with plates 0, 1, and 2. As those plate numbers appear before "[3,4]" in the subsequence, a common insertion vector will be generated for the four contacts.

Insertion constraints are used to compute an insertion vector for all contact zones involved in an assembly step. Four different cases can be considered depending on whether the element to be assembled is a plate or a module and the number of adjacent plates. (Figure 3.14). When assembling a plate that has only one contact with one adjacent plate (Figure 3.14, top left), the insertion vector is directly found by taking the average point on the domain of the insertion constraint. When assembling a plate that has more than one contact (Figure 3.14, bottom left), the vector is found by intersecting the domains of all the insertion constraints associated with those contacts. A similar method is described in Chapter 4 of Christopher Robeller's thesis [Rob15]. This method is here extended to modular assemblies. When a module is inserted in the structure (Figure 3.14, top and bottom right), all the insertion constraints associated with the contacts between the plates of the module and the plate(s) already in place are regrouped and intersected to compute a compatible insertion vector. The intersection process has also been optimized compared to the initial method, as it does not rely on solid intersections but only on faster point-point, point-curve, and point-surface intersections. Finally, if the intersection of the constraints returns no result for one assembly step, the solver asks the user to modify one of the solver inputs.

3.6 Solver outputs

Once an insertion vector has been computed for each assembly step and associated with each contact zone, joints can finally be generated. In this section, the parametrization of five different joints (one for each contact type) is presented. The generation of CNC toolpath and robotic trajectories to automate the fabrication and assembly of the pieces is also detailed.

3.6.1 Generating joint geometry

For each contact type, one timber joint has been studied and parametrized (Figure 3.15). Those joints have been selected for their common use in timber construction or their geometric and aesthetic interest. However, other joints could easily be parametrized by following a similar logic to the one presented here. The shape of each joint can be controlled by a set of user-defined parameters. For example, for the dowel joint, the number of dowels, their radius, and their inclination can be adjusted. Similarly, for the through-tenon joint, parameters allow modifying the number of tenons as well as their dimensions and spacing.

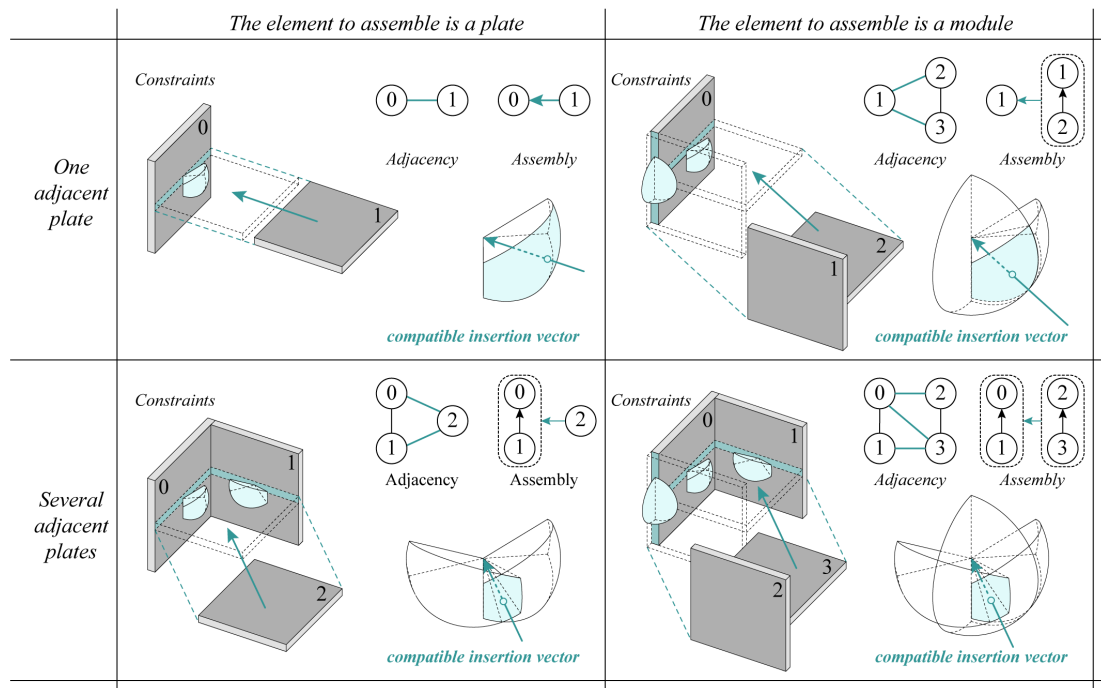


Figure 3.14: A compatible insertion vector is found by intersecting the insertion constraints from the contact zones between the plate(s) to assemble and the plate(s) already in place.

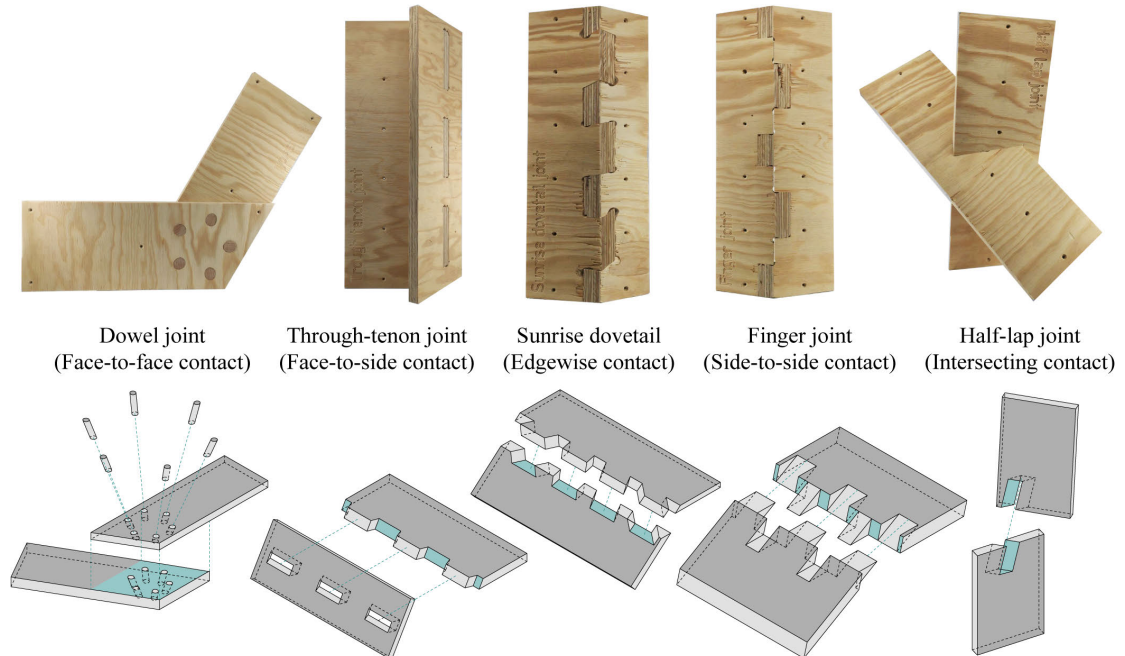


Figure 3.15: Five types of joints have been parametrized and can be generated with the solver.

The objective was to provide a purely analytical description of the shape of each joint to remain independent of any computational library or programming language. The parametric equations of all the points necessary to create four of those five joints are given in Appendix A.2. The half-lap joint is here the only exception. Its geometric construction requires solid Boolean operations that prevent a purely mathematical approach. Therefore, it is necessary to rely on an existing library of geometric algorithms for this particular type of joint. The parameterization of the half-lap joint is nevertheless detailed in Figure 3.16.

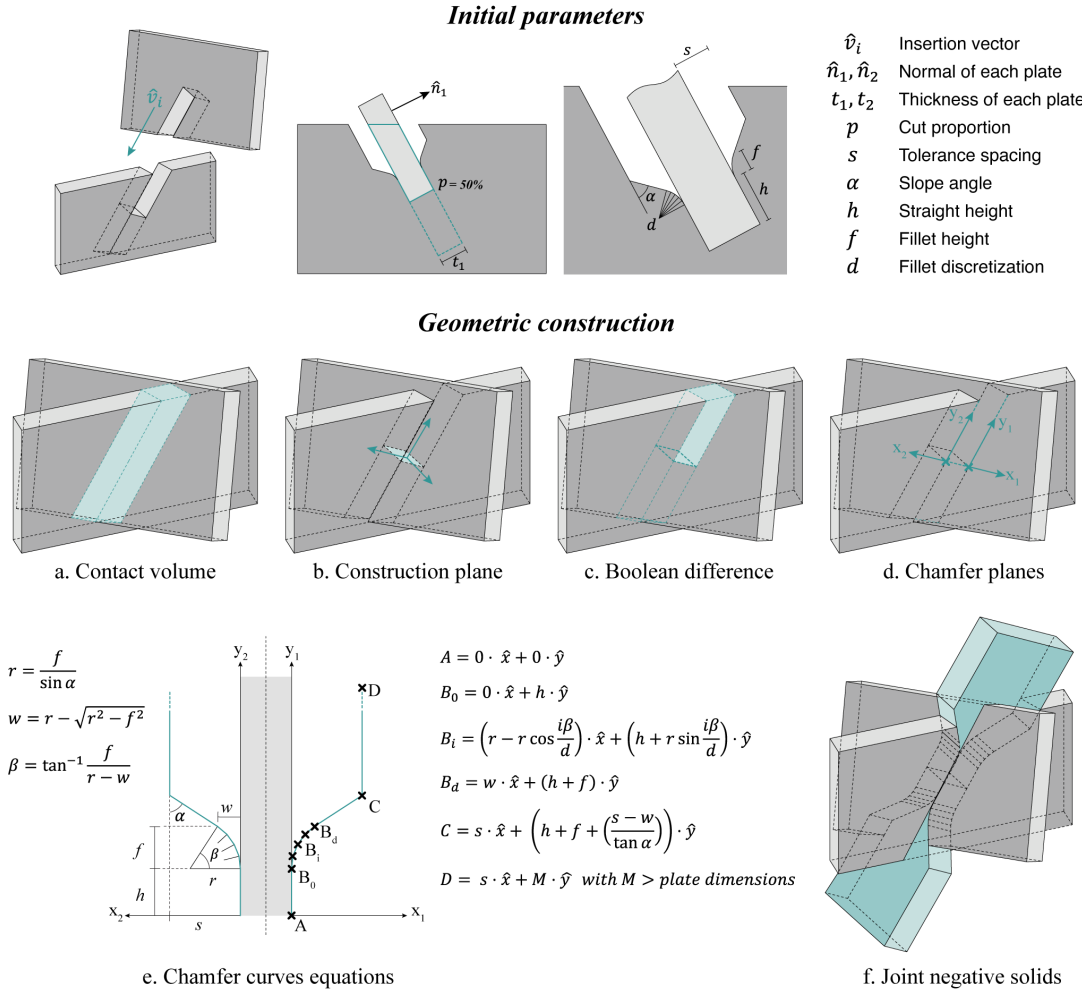


Figure 3.16: Parametric construction of the half-lap joint as implemented in the solver. The use of solid Boolean operations to get the chamfer planes precluded a purely mathematical description of the joint geometry. For the other joints, the equations can be found in Appendix A.2.

For all timber joints, the solver splits the output into three lists: one list of 3D solids to add to the plate geometry, another to subtract from the plate, and the last one for independent solids such as external keys or dowels (Figure 3.17). The final geometry of each plate is obtained by

performing Boolean operations with the solids of the first two lists (e.g., tenons are merged with the plate's initial geometry while mortises are subtracted). However, those operations require a high computational time. Therefore, the solver keeps all joints as distinct geometries separated from the plate to keep fast feedback and enable an iterative process. When the user is satisfied with the design, joints are ultimately merged within the plate for visualization purposes.

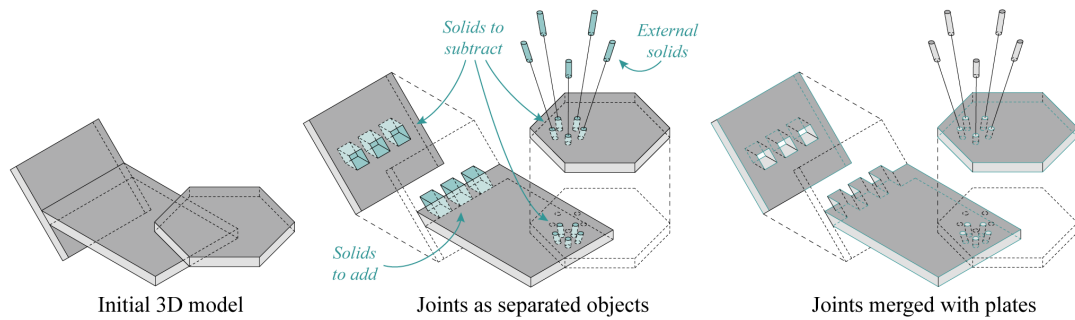


Figure 3.17: Joint geometry is stored as three lists of solids and kept separated from the plate geometry until the design is fixed. Solid Boolean operations allow the integration of the joints inside the plates to display the result.

3.6.2 Generating fabrication toolpath for CNC machining

Developing an accurate 3D modeling tool for timber joints in IATPS enables a direct workflow from design to fabrication. The parameterization of each joint presented in this paper encompasses creating a 3D solid for visualization purposes and polylines and surfaces informing the milling process. This geometric data can be interpreted by CAD-CAM software to generate a machining toolpath which can then be exported to a CNC using a standard machine language as G-Code [Int]. Although a CNC router allows cutting complex joints into standardized timber panels, it also brings some constraints to the design, mainly due to axis reachability and cutting tool characteristics.

The "inside corner" problem is a well-known example of CNC fabrication constraints (see Figure 3.18a). Due to the circular cross-section of CNC milling bits, it is impossible to cut sharp corners with a CNC. For timber joints, this is typically problematic to fabricate a mortise matching a rectangular tenon. To make both parts compatible, removing a bit more material is necessary. This can be done by extending the cutting toolpath to create notches in the corners. As those fabrication details can impact the structural performance and the aesthetic of the connections, there is an interest in integrating them into an iterative design workflow [Rob15]. Consequently, the developed tool automates the generation of those notches and updates the machining toolpath accordingly. It also provides the possibility to choose between two alternatives: dogbone fillets (Figure 3.18b) or T-bone fillets (Figure 3.18c) [Pad].

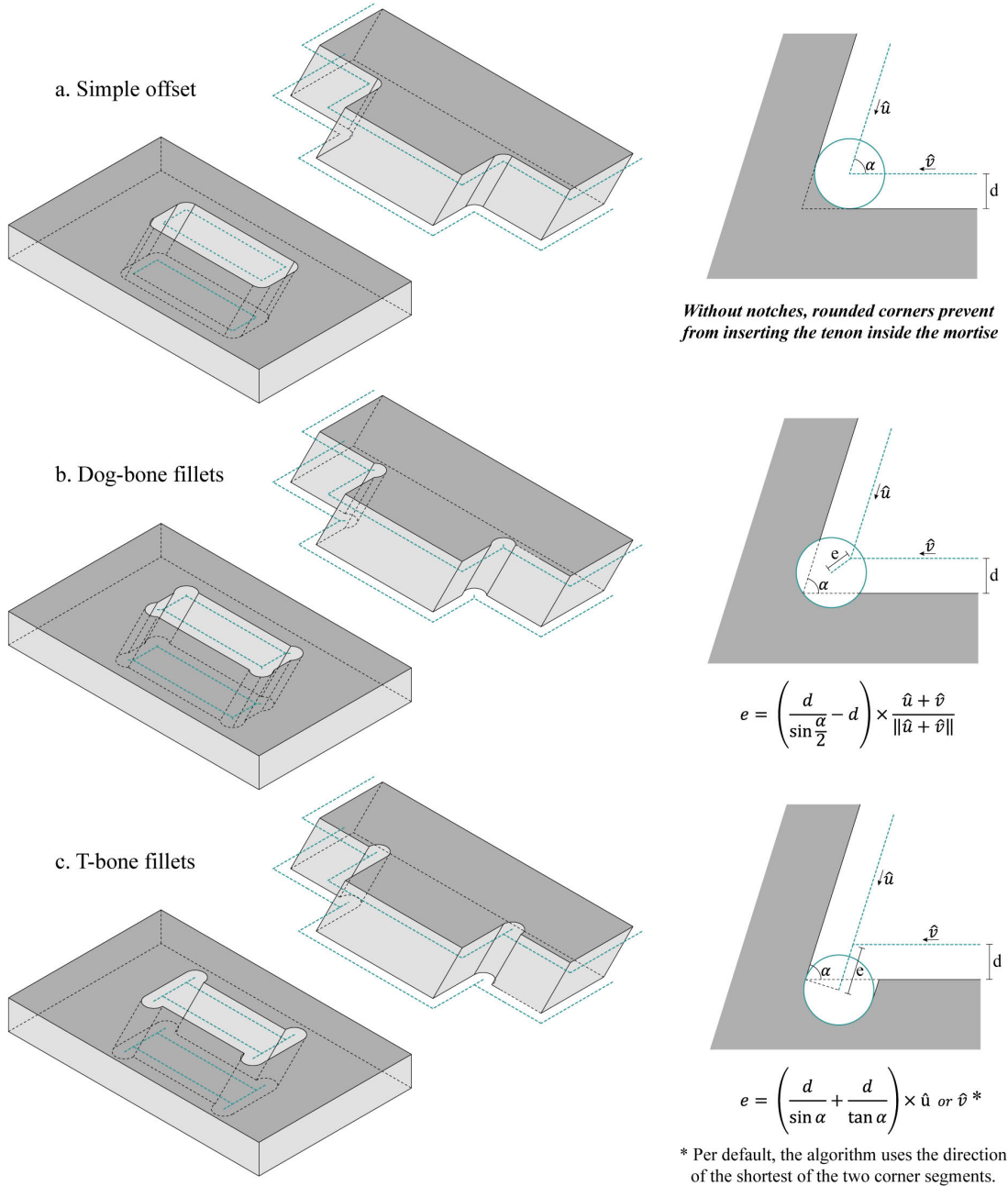


Figure 3.18: Integrating corner notches into fabrication toolpath.

Other functionalities have also been developed to ease the manipulation of the 3D model. For example, all plates can be scaled and reoriented independently with their attributes. They can also be automatically laid flat in an array or a grid to visualize fabrication toolpath better or stacked on top of each other to prepare robotic trajectories. Per default, the bottom face of each plate faces downward. However, the top and bottom faces can be inverted by the user to specify the best cutting approach for non-orthogonal machining (using more than three axes).

The solver returns two types of outputs for fabrication purposes: contours and surfaces. Contours are pairs of closed polylines that can be interpolated to create multiple milling passes. The orientation of the cutting tool is given by joining each pair of corresponding vertices from the top polyline to the bottom polyline. Surfaces are typically used to chamfer tenons (as illustrated in Appendix A.2). The orientation of the cutting tool is here given by the normal of the surface, and a snake-like surfacing toolpath can then be generated according to the tool radius.

3.6.3 Generating robot trajectories for an automated assembly process

One objective of this research is to propose a general framework for the automated assembly of timber plate structures. By splitting the assembly sequence into modules, groups of plates can be preassembled off-site with an industrial robotic arm. A robotic insertion strategy for timber joints based on the visual detection of fiducial markers has already been detailed in a previous paper [Rog+20]. Therefore, only geometrical considerations about the robot trajectories will be discussed here. Tridimensional path planning usually requires a long computational time as checking for object collisions is a complex task, and the solution space is vast [Gan+18]. To enable fast feedback for designers, a more straightforward approach was taken. A potential trajectory based on nine predefined moves is extrapolated from the vector of insertion associated with each plate (Figure 3.19). The open-source plugin Robots [Sol] is then used to check if there are no obstructions and if the robot can reach all positions. Note that other robotic simulation plugins could also be used according to the model of the robot. If necessary, the user can tweak the trajectory with some additional parameters. The direction of each movement is fixed, but lengths can be modified. While this semi-automated method eventually requires some manual adjustment, it simplifies the assembly process using a predictive but parametric trajectory.

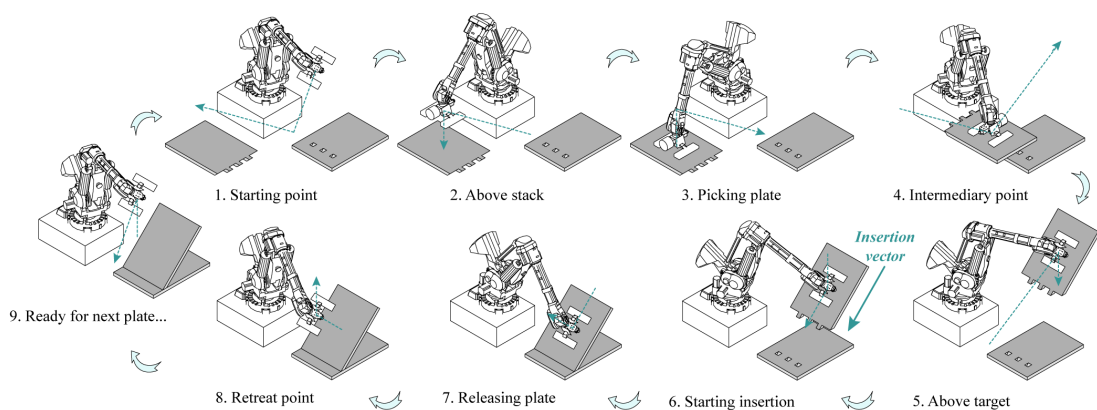


Figure 3.19: The different steps of the robotic trajectory are similar for each plate. However, distances can be adjusted, and intermediary points can be added to work around obstacles and avoid collisions.

3.7 Solver application and performance

The developed solver has been tested on different 3D models to assess its performance. This section presents three structures for which joint geometry, fabrication toolpath, and robotic trajectories have been automatically generated. Further investigations are still required to tackle the physical assembly of those structures with a robotic arm as considerable challenges remain to insert all types of joints with varying plate configurations [Rog+20]. The purpose of those case studies is to demonstrate the range of applications of the integrated design tool by applying the solver to different geometries.

3.7.1 Case study 1: curved beam

For the first case study (Figure 3.20), a 4-m-long curved beam made of 18 timber panels was considered. Through-tenons joints were applied on face-to-side contacts to connect the beam web with both flanges. The top flange is more segmented. It is composed of 7 panels to obtain a curved shape. The bottom flange is formed of three longer panels. Therefore, different parameters were used for the top and bottom layers. A single 10 cm wide tenon was generated for each contact zone in the top flange, while two tenons of 5 cm were used for the contact zones in the lower flange. Finger joints were used for side-to-side connections in both flanges. However, all contacts between web elements were discarded to avoid assembly issues. Due to the angle between the top flange plates, a slight chamfer needs to be surfaced on top of the fingers, as shown on the bottom right of Figure 3.20. The fabrication toolpath also includes dogbone notches for outer and inner milling curves. To simulate the robotic assembly of the structure, an ABB 6400 robot equipped with a gripping end-effector was reproduced in the parametric environment. The trajectory of each plate was validated after adjusting the position of the plate stack and the other parameters mentioned in the previous section.

3.7.2 Case study 2: boxed vault

The second case study is a boxed vault composed of 20 hexagonal modules of 7 plates (Figure 3.21). A doubly-curved NURBS surface was first segmented by projecting a hexagonal tiling pattern. Boxes were then extruded by intersecting bisector planes from each mesh edge [Ves+20]. Boxes are slightly shifted about each other, as no optimization algorithm was used to planarize the initial geometry. For this example, a modular assembly sequence was set as input: each group of seven plates forms a module to which a vector of insertion and a subsequence are assigned. Regarding the joints, sunrise dovetails were applied on all edgewise connections to connect the plates of the box, while dowel joints were used to connect the boxes. Figure 3.21 highlights how the solver not only creates the joint geometry but also gives a complete overview of the different steps of the construction process. This goes from the preview of t-bone notches for the manufacturing process to the simulation of the insertion of the other elements (here performed manually) for the assembly of the structure.

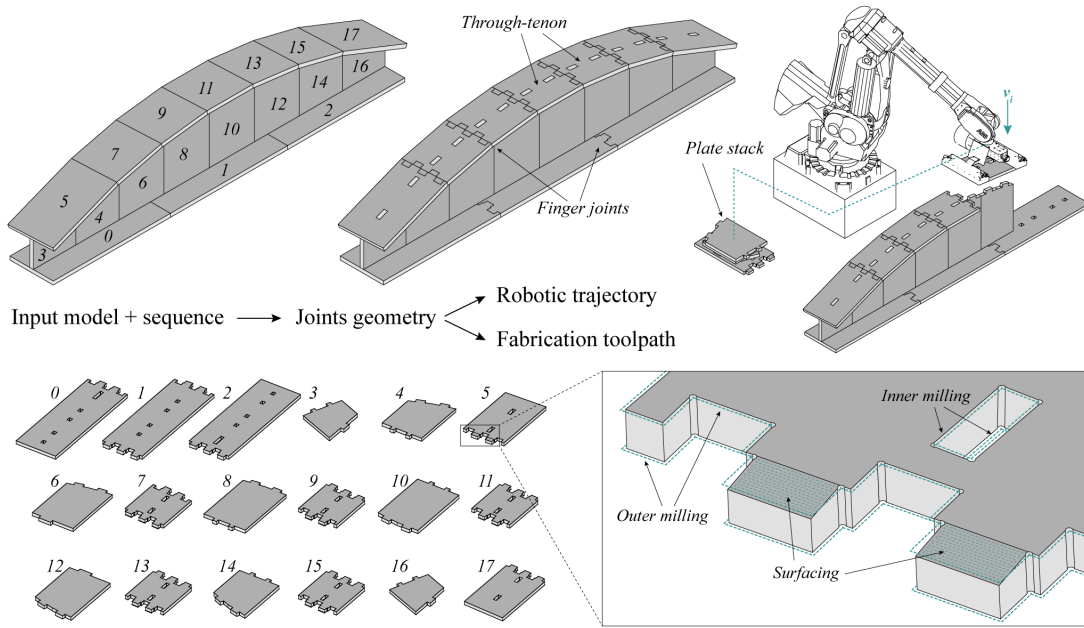


Figure 3.20: Application of the solver to a segmented curved beam of 18 panels.

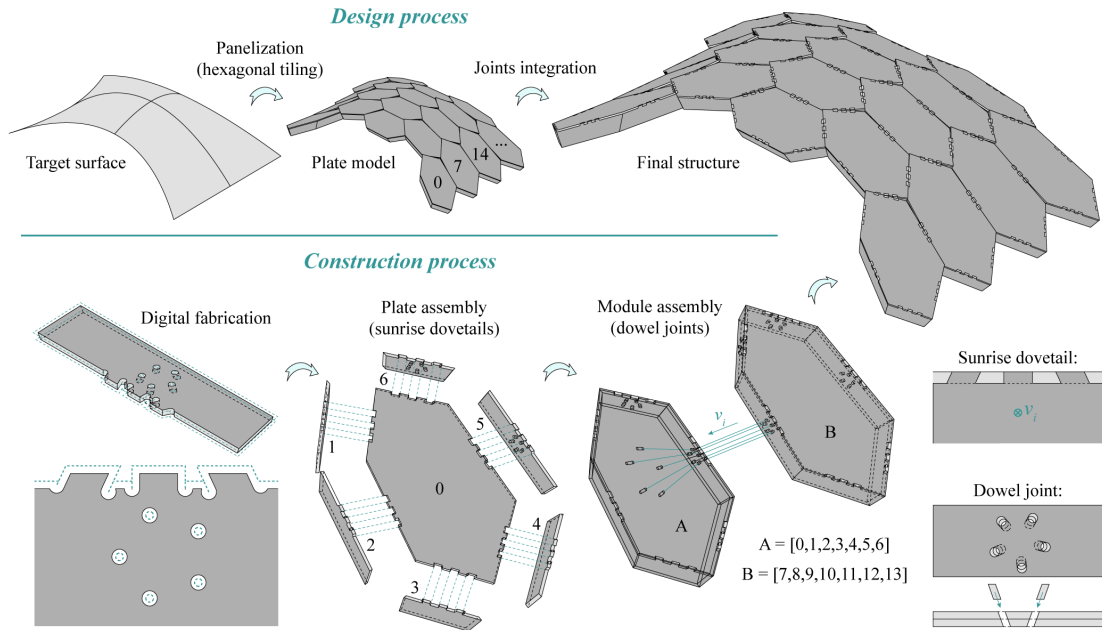


Figure 3.21: Application of the solver to a vault composed of 20 hexagonal modules of 7 plates.

3.7.3 Case study 3: timber frame

For the third case study, a modular assembly sequence was also used. The structure comprises two arches of 13 plates each and 21 purlins (Figure 3.22). In this scenario, both arches are preassembled with a robot while the purlins are added manually. Therefore, the plates of

the arches are grouped in two distinct modules in the input sequence. Dowel joints were generated at each face-to-face contact to create a rigid connection between the arches pieces. Half-lap joints were used for the purlins with a guiding slope to ease the assembly and dog-bone notches in the corners. Robotic trajectories have been generated for one of the arch modules after scaling it down according to the size of our robot model. The entire assembly sequence for this module was successfully simulated using the solver's output.

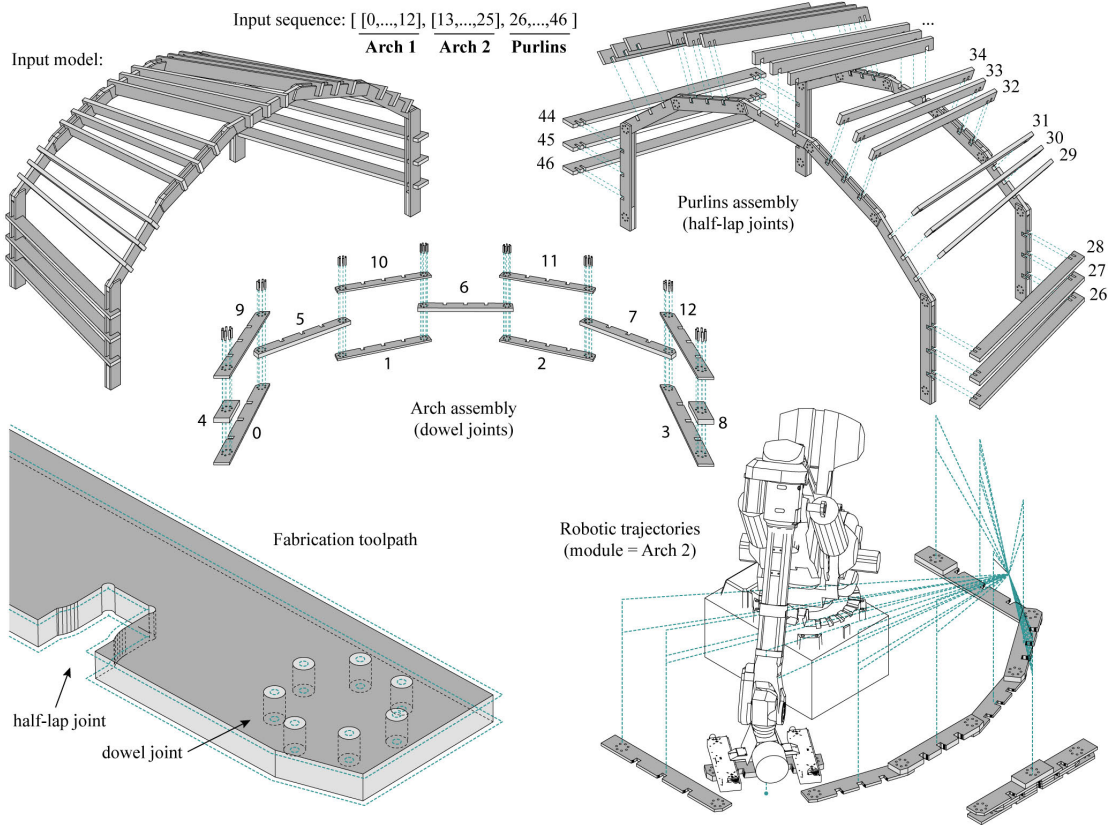


Figure 3.22: Application of the solver to a timber frame composed of two arches of 13 pieces each and 21 purlins.

3.7.4 Computational performance

The solver performance is presented in Table 3.1 for the three case studies. The computational time associated with each step of the algorithm is detailed. Boolean operations remain the most computationally intensive task, with more than 2 min required to merge the joints and the notches of the complete boxed vault. The model instantiation also requires a consequent time to compute since finding all contact zones relies on Boolean operations. Besides, this part of the algorithm runs in the order of n^2 as each pair of plates needs to be tested. Therefore, computing the adjacency of an assembly of a thousand plates might take considerable time. However, only generating joint geometry remains quite fast. For the second case study, 1365 solids were generated in less than 5 s. This maintains the possibility to explore different design

options quickly before performing the Boolean operations. The time needed to create a joint depends on its geometric complexity. For example, the simple cylinder of a dowel joint is typically much faster to generate than a half-lap joint with rounded guiding slopes. It should also be noted that working inside the Grasshopper environment requires creating a new copy of the model instance before executing any task, which adds between 1 and 2 s of delay to every step. Finally, working on the entire model at once is rarely necessary. Only performing Boolean operations on one plate or module dramatically enhances the solver's responsivity.

<i>Case study</i>	<i>Model instantiation</i>	<i>Joints generation</i>	<i>Toolpath generation</i>	<i>Boolean operations</i>	<i>Robotic simulation</i>
#1 Curved beam 18 plates	39 contacts 2.9 s	136 solids (8 FJ, 22 TT) 2.9 s	322 notches 0.8 s	without notches / with notches 2.7 s / 22.6 s	234 planes 1.0 s
#2 Boxed vault 140 plates	409 contacts 39.1 s	1365 solids (43 DJ, 120 SD) 4.6 s	1440 notches 10.3 s	without notches / with notches 25.5 s / 126 s	/ /
#3 Timber frame 46 plates	196 contacts 6.6 s	804 solids (64 DJ, 66 HL) 6.3 s	264 notches 8.4 s	without notches / with notches 18.1 s / 30.8 s	169 planes (1 arch) 3.2 s

System specifications: CPU: Intel(R) Xeon(R) E3-1505M v6 @ 3.00GHz, RAM: 16 Go, GPU: NVIDIA Quadro M2200

Table 3.1: Computational time of each operation for each case study. Joints abbreviations: DJ = Dowel joint, TT = through-tenon joint, SD = Sunrise Dovetails, FJ = Finger Joint, HL = Half-lap joint.

The solver was also tested in different workshops with architecture students who had only very limited knowledge of parametric design (see Appendix A.3). This was an excellent opportunity for testing the user experience of the developed Grasshopper plugin for non-experts. Surprisingly, students were rapidly capable of designing relatively complex assemblies of a dozen plates. The tool also proved particularly effective in explaining and visualizing assembly constraints. The documentation of the potential sources of error in the workflow was also significantly improved after students' feedback.

3.8 Conclusion and outlook

An integrated design tool for timber plate structures connected by wooden joints has been developed and tested through three case studies. It offers an effective way to integrate digital fabrication and robotic assembly constraints into the design of standard and bespoke structures. Compatible timber joints are automatically created by interpreting an assembly sequence set by the user. This sequence can also be divided into modules allowing a multi-step assembly. By generalizing the joinery system, more freedom is given to the designer, and the impact of construction constraints on the project can be better understood. Besides, this opens the possibility to easily extend the library of joints by following the same framework.

The application of the algorithm to three case studies resulted in a relatively high calculation time, especially for large assemblies. This is caused mainly by three factors. First, the solver must look for all contacts between the elements since no information about adjacency is provided. Second, Boolean operations are computationally-intensive tasks. Third, the Grasshopper environment requires creating a new copy of all properties stored in the model

at each step to avoid conflicts when running parallel tasks. However, using this node-based visual scripting platform, it is possible to complete the complex modeling of all timber joints independently of the model instantiation. This drastically reduces the delay between two iterations, maintaining a high level of interactivity. Besides, it is unnecessary to merge the joints with their parent plate to visualize them. Boolean operations can therefore be postponed after the end of the design process.

The solver could also be optimized to reduce calculation times. For example, a list of all adjacent plates could optionally be provided by the user in addition to the assembly sequence, avoiding the need to compute plate intersections. In addition, if the global shape of the model is designed using a mesh data structure, adjacency information could easily be transferred from the mesh to the plate model. Finally, implementing external libraries optimized for Boolean operations could also speed up the process.

The joinery solver could also be extended to beam elements or more complex polyhedra. Similar logic to plates could be considered, although plates have the advantage of having only two possible orientations, which reduces the amount of user input required. The current framework targets translational assemblies with pieces moving according to one insertion vector. More complex insertion trajectories involving rotations could also be considered.

In conclusion, this research constitutes a first attempt at generalizing the design process of IATPS. While the computational performance of the solver could still be improved, its application to three case studies demonstrated the interest in connecting architectural design, digital fabrication, and robotic assembly under one roof. Furthermore, parallel investigations have been carried out on the mechanical characterization of such structures [Rez+21], and a logical development would be to integrate structural feedback into this general design framework.

This contribution opens new perspectives for IATPS. The development of this new tool facilitates the manipulation of this innovative structural system by architects and structural designers who are not necessarily familiar with coding. Consequently, this fosters the shift in the status of IATPS from iconic research pavilions to a more widespread and highly automated building system that allows for both standardized and bespoke structures.

3.9 Acknowledgements

This research was supported by the NCCR Digital Fabrication, funded by the Swiss National Science Foundation (NCCR Digital Fabrication Agreement #51NF40-141853). The authors would like to thank Alexandre Flamant for his contribution to the equations describing joint geometry and Dr. Julien Gamero and Dr. Aryan Rezaei Rad for their support in reviewing the paper.

3.10 Addendum: Details on the integrated robotic simulation

The algorithm for generating the joints has been extensively discussed in the above paper. However, the simulation of the robotic trajectories has only been briefly addressed so far. Consequently, further explanations are given in this section. Part of this research benefited from the collaboration with an industrial partner specialized in developing robotic solutions for timber construction companies (Imax Pro SA, Belgium). This company developed a custom application in Unity [Uni] to solve the inverse kinematics of a 6-axis robotic arm and detect potential collisions. The robot can also be controlled directly from the application, and custom commands can be programmed. The doctoral candidate's contribution consisted in establishing a communication protocol between the design and robotic interface to simulate and execute the robotic trajectories. While the protocol for sending the instructions to the real robot is presented in Chapter 5, the integration of the robotic simulation into the design interface is detailed here.

The collaboration with an industrial partner allowed studying the challenges of implementing the integrated design tool into an existing industrial workflow. The primary difficulty consisted in enabling the interoperability between the design platform (Rhino, Grasshopper) and the robotics simulation platform (Unity). The objective was to give the possibility to simulate a robotic trajectory inside Grasshopper while integrating the constraints of a real robotic setup. First, two robotic simulations were developed independently in Grasshopper and Unity. Next, a streamlined data exchange protocol was established to synchronize both simulations and benefit from the advantages of both platforms.

3.10.1 Robotic simulation in Grasshopper

Several plugins are available in the Grasshopper ecosystem to simulate robot trajectories (Kuka Prc [Ass], Taco ABB [WSF], Hal Robotics [Sch]). The plugin *Robots* [Sol], developed at the Bartlett School of Architecture, was selected to be implemented within the computational framework for designing IATPS. It has the advantage of being fully open-source, well-documented, and compatible with a wide range of robot models (ABB, KUKA, UR, and Staubli). Existing robot 3D models, as well as XML files containing robot joint dimensions and properties, can be downloaded from *Robots* public GitHub repository [Sol]. However, the model of the robot hosted at IBOIS (ABB 6400) did not feature on this list yet and was, therefore, created using the data provided by the industrial partner.

A custom workflow relying on the Grasshopper components of *Robots* plugin was developed (Figure 3.23). It solves the inverse kinematics equations to compute a robot trajectory that satisfies the robot constraints and passes through a list of planes given as input (Figure 3.24a). As explained in Section 3.6, this list of planes is one of the outputs of the integrated design tool for IATPS. It is automatically computed according to the vectors of insertion of the timber plates. The parametric interface allows adjusting the trajectory based on the feedback of the robot solver. If no valid robot position can be found to reach one or several planes of the

trajectory, the robot will instantaneously appear in red in the design interface (Figure 3.24b). A slider allows animating the robot to identify problematic positions. In addition, a custom component was scripted to display the timber plates that are being assembled.

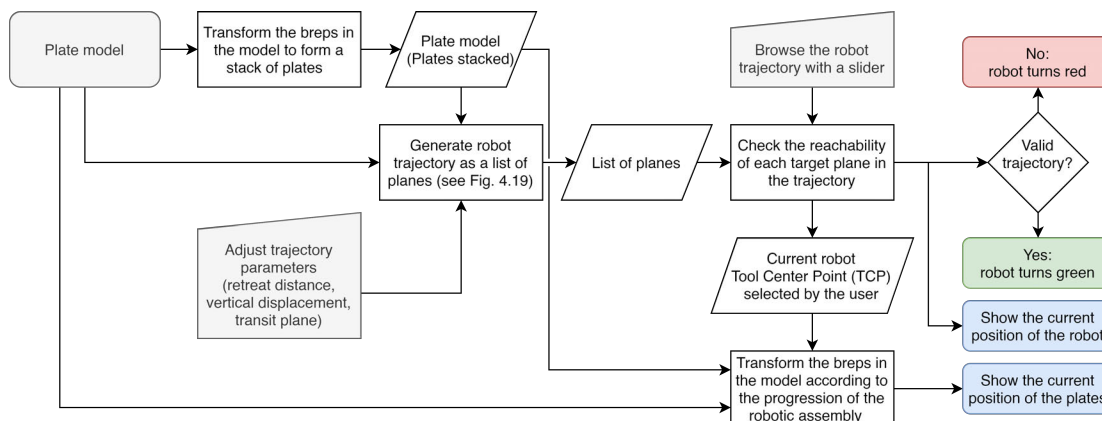


Figure 3.23: Flowchart representing the algorithm developed to simulate the motion of the robot and the plates. Inputs are displayed in grey, and outputs are in color.

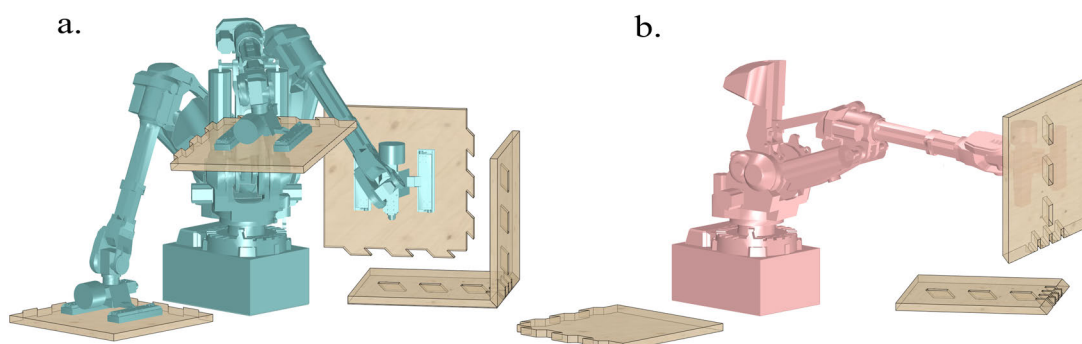


Figure 3.24: Robotic simulation within the design interface. If a valid trajectory can be computed, the robot turns green (a). Otherwise, it turns red (b), and the blocking situation is displayed. On the right, the robot cannot insert the second plate as it is beyond reach.

3.10.2 Robotic simulation in Unity

Whereas the robot model in the Grasshopper interface approximates the real robot, the one implemented by our industrial partner in Unity is a more accurate replica (Figure 3.25). It includes all physical limitations in the robotic cell (e.g., surrounding walls, joint restrictions due to equipped tools, etc.) and goes as far as showing the state of the electronic circuits that activate the vacuum gripper. Besides, while Rhino is a 3D modeling software, Unity is a game engine that can simulate physical interactions such as collisions between objects. This makes it particularly interesting for robotic applications. The interface consists mainly of a 3D scene where the robot is displayed, a hierarchy tab listing all elements in the scene, and an inspector tab detailing object properties (e.g., position, scripted behavior, etc.).

3.10 Addendum: Details on the integrated robotic simulation

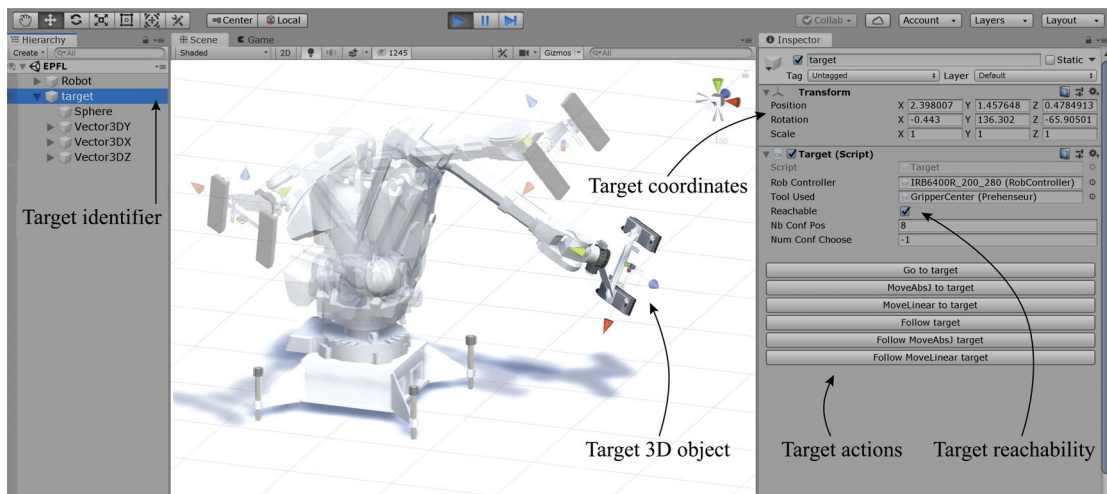


Figure 3.25: Robotic interface developed by ImaxPro in Unity.

In an industrial context, robotic trajectories are usually programmed manually. Standard workflows require workers to move the robot in manual mode and save the different positions. Subsequently, the robot repeats the trajectory autonomously. With the custom Unity application, the same can be achieved on the computer. A list of targets can be programmed by the operator by manually entering spatial coordinates and rotation angles. First, the application will deduce if each target is reachable. Second, the whole robotic trajectory will be computed to check if there is a valid sequence of moves between the different targets. Finally, the user can use custom action buttons to ask the virtual robot to reach or follow a specific target, which facilitates the detection of potential collisions or problematic motions.

3.10.3 Synchronization Unity-Grasshopper

On the one hand, the Unity simulation has the advantage of being directly connected to the robot controller and faithfully reproducing the real robot. On the other hand, the Grasshopper simulation has the advantage of being fully parametric and enabling synergy with the different modules of the developed computational framework for IATPS. To benefit from the advantages of both platforms, a streamlined data exchange protocol was developed (Figure 3.26). It works both ways, from Unity to Grasshopper and conversely. The principle is that one robot takes the role of *guide* and the other that of *follower*. The position of the *guide* is encoded in a text file which is instantaneously read and reproduced by the *follower*.

A major challenge was the different conventions of coordinate systems used by the two software. While Rhino follows the standard right-hand convention, Unity has the particularity of having a left-handed coordinate system with the Z axis pointing in the opposite direction. To facilitate data exchanges, it was decided to swap the Y and Z axes in Unity (see Figure 3.26). Therefore, the spatial coordinates representing the position of the planes have to be changed from XYZ to XZY.

Chapter 3. Generation of joint geometry, fabrication toolpath, and robot trajectories

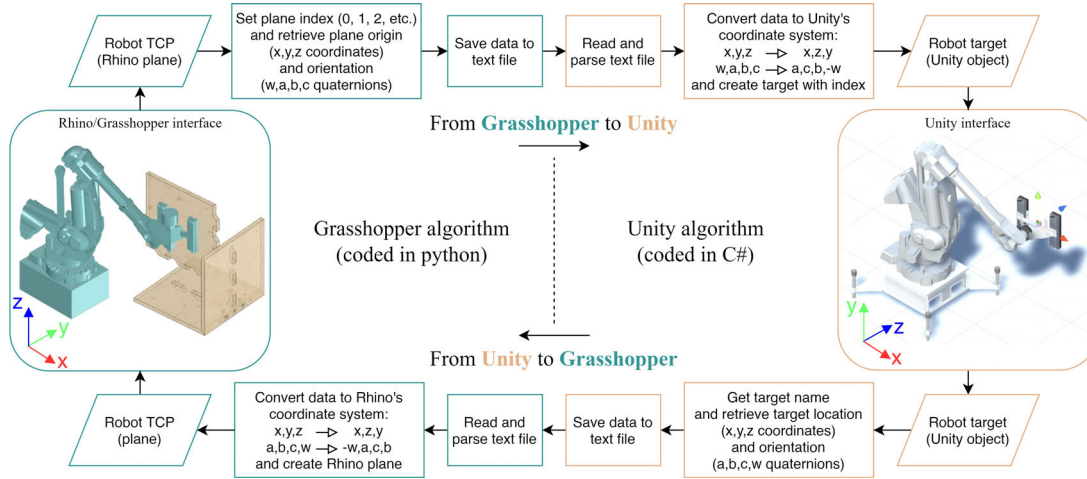


Figure 3.26: Communication protocol to synchronize two robot models in Unity and Grasshopper and enable direct feedback about robotic constraints inside the design interface.

The orientation of the planes is also impacted by the change of axis. In Rhino, planes are usually described using two vectors (origin, X axis, Y axis), while in Unity, their orientation is stored as quaternion [SE] (in the form a, b, c, w with w being the real part) but displayed in the editor as Euler angles (using the *pitch, roll, yaw* convention). The quaternion representation is the most common in robotics as it is not impacted by the gimbal lock problem [HO18]. Therefore, it was used to store the orientation of the planes in the text file. However, quaternion notation also differs between both software as it starts with the real part in Rhino (giving: w, a, b, c). Finally, considering both the change of axis and of notation, a quaternion in the form w, a, b, c in Rhino gives $a, b, c, -w$ in Unity. In the other direction, a quaternion in the form a, b, c, w in Unity gives $-w, a, c, b$ in Rhino.

In conclusion, streamlined data exchange was established between the design and robotic interfaces. The response time is in the order of a tenth of a second. This enables direct feedback regarding the possibility of assembling the plates of an IATPS with a robotic arm. This also demonstrated the feasibility of integrating an existing industrial workflow with different software. Further developments could include valuable features such as displaying the plates generated in Rhino inside Unity and automating the evaluation of the robotic simulation to determine a collision-free path without any manual intervention. However, as it stands, the implemented code already allows interactive modification of the design of an IATPS based on the reachability constraints of a given robotic arm.

4 Integration of structural engineering considerations

The texts and figures presented in this section were reproduced from the postprint version of the following peer-reviewed paper available in open access:

Rogean, N., Rezaei Rad, A., Vestartas, P., Latteur, P., & Weinand, Y. (2022). A collaborative workflow to automate the design, analysis, and construction of Integrally-Attached Timber Plate Structures. In: *POST-CARBON, Proceedings of the 27th International Conference of the Association for Computer-Aided Architectural Design Research in Asia (CAADRIA) Sydney 2022*, Volume 2, pp.151-160, CAADRIA, Honk-Kong. doi:10.52842/conf.caadria.2022.2.151.

The doctoral candidate was responsible for the writing of the article as well as for the coordination of the scientific project. In particular, this consisted in enabling interoperability with algorithms previously developed by the second and third authors and creating an intuitive design interface. The second author also contributed to the writing of Section 4.3. The third author was involved in the development of a design-to-fabrication workflow to facilitate the simulation and export of CNC toolpaths. The fourth and fifth authors of the paper contributed equally as scientific advisors and proofreaders.

4.1 Abstract

This paper introduces a computational framework that fosters collaboration between architects, engineers, and contractors by bridging the gap between architectural design, structural analysis, and digital construction. The present research is oriented toward the formulation of an automatic design-to-construction pipeline for Integrally-Attached Timber Plate Structures (IATPS). This construction system is based on assembling timber panels through the sole interlocking of wood-wood connections inspired by traditional Japanese joinery. Prior research focused on developing distinct computational workflows and dealt with the automation of 3D modeling, numerical simulation, fabrication, and assembly separately. In the current study, a single and interactive design tool is presented. Its versatility is demonstrated through

two case studies, as well as the assembly of a physical prototype with a robotic arm. Results indicate that efficiency in terms of data flow and stakeholder synergy is considerably increased. The proposed approach contributes to the Sustainable Development Goal (SDG) 11 by facilitating the collaborative design of sustainable timber structures. Besides, the research also contributes to SDG 9 as it paves the way for sustainable industrialization of the timber construction sector through streamlined digital fabrication and robotic assembly processes. This reduces manufacturing time and associated costs while leveraging richer design possibilities.

4.2 Introduction

4.2.1 Interdisciplinarity as a driver of sustainability

In 2020, the construction sector was responsible for 37% of energy-related CO₂ emissions. A decrease in economic activities due to the COVID-19 pandemic has led to temporary improvements. However, the decarbonization of buildings is currently not on track to reach the goals of the Paris Agreement [Uni20]. While there is a clear reduction trend in life-cycle greenhouse gas emissions due to improved operational energy performance, researchers have reported an increase in embodied emissions arising from the manufacturing and processing of building materials [Zim+21]. Given the high demand for new housing, the entire life cycle of buildings should be taken into consideration during the design phase to mitigate the environmental impact of construction.

Digitization can enhance the productivity of the construction sector and help deliver the required building stock. However, automating existing workflows without a paradigm shift would only increase the environmental impact of building activities. To reach United Nations Sustainable Development Goal 11 – Making cities and human settlements inclusive, safe, resilient, and sustainable – it is necessary to both rethink standard design workflows and develop more sustainable construction processes. On the one hand, given the increasing complexity of architectural projects, interdisciplinary collaboration needs to be strengthened [Kni+21]. Physical considerations such as material properties, structural performance, and prefabrication constraints need to be included upstream in the design process. On the other hand, low-carbon materials and efficient manufacturing techniques need to be more broadly adopted.

This research focuses on Integrally-Attached Timber Plate Structures (IATPS) – an innovative building system relying on the interlocking of engineered timber panels. Drawing inspiration from traditional Japanese carpentry, the elements are connected solely by wooden joints (i.e., mortises and tenons), reducing the need for additional metallic fasteners (Figure 4.1). The advantages of IATPS are double. Firstly, this construction technique offers the possibility of creating complex shapes out of flat standard wooden panels. It, therefore, provides a low-carbon alternative for creating architecturally appealing structures, relying mainly on a natural and renewable resource. Secondly, recent advances in digital timber construction allow a high

degree of automation for IATPS. Panels can be cut with a Computer Numerical Control (CNC) machine and assembled into larger modules with an industrial robotic arm [RLW21]. The main objective of this research is to ease the design of IATPS by facilitating the data flow from architectural design to structural analysis and automated construction. To enable reciprocal feedback between the different fields of expertise involved in the project (i.e., architecture, engineering, and robotics), a collaborative computational design tool has been developed and is presented in this paper.

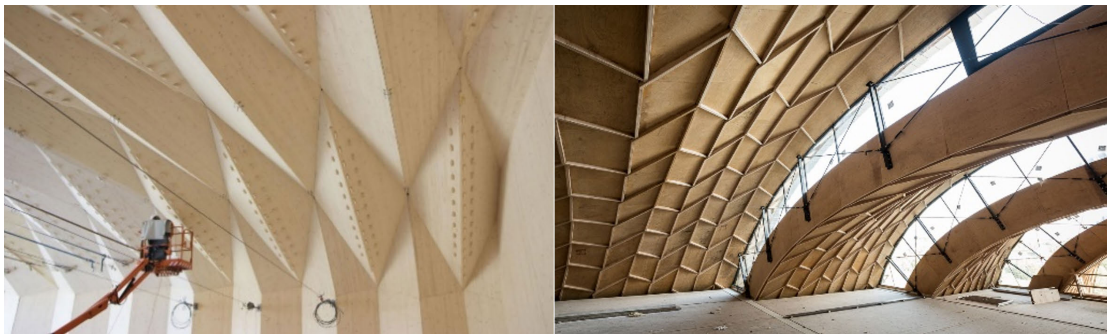


Figure 4.1: Two examples of IATPS: the theatre of Vidy in Lausanne (left, © Ilka Kramer) and the multipurpose hall of Annen in Manternach (right, © Valentin Bianchi).

4.2.2 Interactive computational workflows

Despite the progressive adoption of Computer-Aided Design (CAD) software that increased drafting productivity in architectural and engineering offices, standard design-to-construction workflows have barely changed and remained very linear [Car17]. However, as design teams keep getting bigger and their members more specialized, collaboration is both more essential and more complex than ever [Dal21]. One major challenge lies in the diversity of digital tools used by architects, engineers, and contractors, as proprietary file formats lack interoperability to enable a real collaborative design workflow [OT10]. Indeed, most professional software focuses on one part of the design process (drafting, analyzing, manufacturing...) and ensures that its functionalities are generic enough to accommodate all building typologies (Figure 4.2, left).

As developing custom software, applications, and plugins become more accessible, collaborative design workflows tailored for specific building typologies (Figure 4.2, right) have been elaborated and tested by different researchers. So-called “Interactive co-design methods” have been used to realize the BUGA wood [Wag+20a] and fiber [Bod+19] pavilions. Computational developments consisted notably in integrating physical constraints linked to the robotic pre-fabrication of the elements into the 3D design model. This was achieved by allowing designers to simulate fabrication toolpath and assembly sequences inside the design interface.

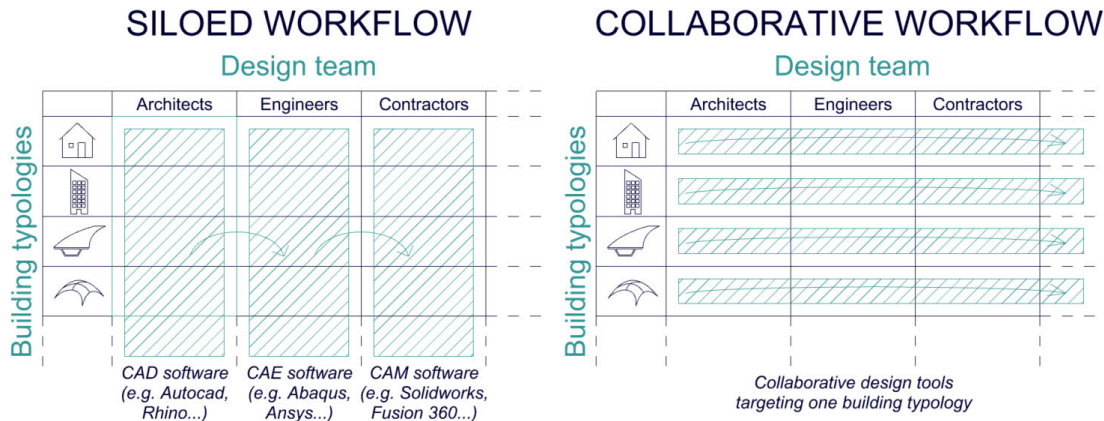


Figure 4.2: Standard software focuses on one part of the design process leading to siloed workflows. Collaborative design workflows focus instead on one building typology.

4.3 Method

4.3.1 Developing a collaborative design interface

The methodology builds on previous work on Integrally-Attached Timber Plate Structures (IATPS) conducted at the laboratory for timber constructions (IBOIS, EPFL). An integrated design tool to generate joint geometry, fabrication toolpath, and robot trajectories [RLW21], as well as a framework for the structural analysis of IATPS [Rez+21], were separately introduced. The novelty of this contribution lies in the integration of the structural engineering feedback directly into the design interface. This is achieved through the systematic conversion of architectural 3D models to Finite Element (FE) meshes and will be further detailed in the following sections.

The collaborative design workflow was implemented in Grasshopper – the parametric interface of Rhinoceros 3D software and released as an open-source plugin named Manis. The algorithm automatically outputs visual information on the structural performance and the construction feasibility of a timber plate structure based on an initial 3D model (Figure 4.3). Interdisciplinary collaboration is thereby made possible by following an iterative design process. The collection of 3D panels that composes the structure is converted to a *plate model object*. This custom python class instance automatically generates an additional layer of data based on the order of the elements (assembly sequence) and how they are connected (adjacency graph). A set of components that operate on the plate model is then available to: (1) simulate the computed assembly sequence, (2) generate parametric timber joints between the pieces, (3) generate a FE model and run a FE analysis, (4) generate, simulate, and execute CNC fabrication toolpath, (5) generate, simulate, and execute robotic trajectories.

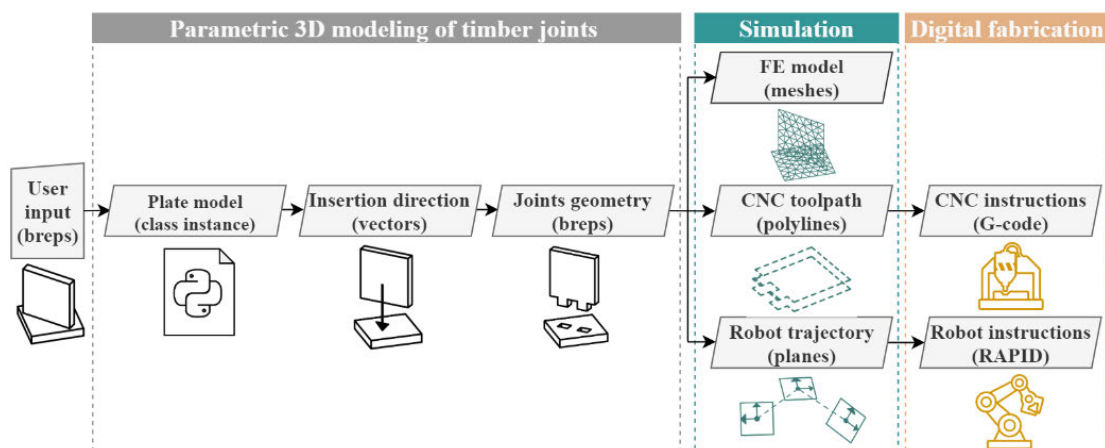


Figure 4.3: The algorithm enables collaboration by integrating structural performance as well as fabrication and assembly constraints into the design process.

4.3.2 Integrating numerical simulation

The integration of the numerical simulation is achieved through COMPAS – an open-source python-based platform developed at the NCCR Digital Fabrication to enhance code reusability and facilitate the development of collaborative design workflows [Van+17]. The COMPAS_FEA extension aims to provide a smooth interface between CAD and FEA. First, this Python package creates a *structure* object associated with the 3D model. It includes geometric information, element, section, and material properties. Then, it enables the user to specify loads and boundary conditions for structural analysis. The construction of the *structure* object is performed using various modules that exist in the core COMPAS library (i.e., data structure, mesh) and the FEA extension. Accordingly, the majority of the repetitive scripting tasks are eliminated while streamlined data post-processing and visualization support are provided. Once the *structure* object is constructed, COMPAS_FEA writes the native input file for the FE software. In this case, the model is generated in either ABAQUS or OpenSees. It is then sent to the original solver for analysis. Lastly, the data from the analysis results are extracted and returned to the collaborative design interface (Figure 4.4).

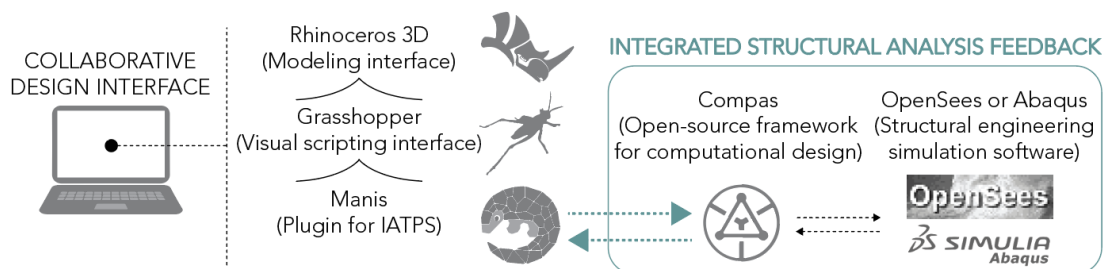


Figure 4.4: Integrating engineering feedback from Abaqus and OpenSees into the collaborative design plugin "Manis" via COMPAS open-source platform.

In detail, each plate is simulated using a conventional shell element with a homogeneous section property. The thickness, the integration rule (i.e., Simpson's rule), and the number of integration points are also specified in this step. General-purpose thin shell elements are used to account for finite membrane strains, as well as large rotations. In particular, a finite-strain shell element with four nodes (S4R), which uses lower-order integration to compute the element stiffness, is employed. This type of shell element has six degrees of freedom and enables thickness changes, leading to a realistic evaluation of the performance of the *structure*. Also, a free meshing technique is used to convert each plate mid-surface to a triangular mesh while line segments are created to represent the connections between the plates (Figure 4.5). Those connection links are integrated into the simulation by defining spring elements between the shell elements. The algorithm ensures that the nodes of each connection link correspond to the vertices of the plate meshes. Finally, mesh data and connection links are added to the *structure* object to perform the analysis.

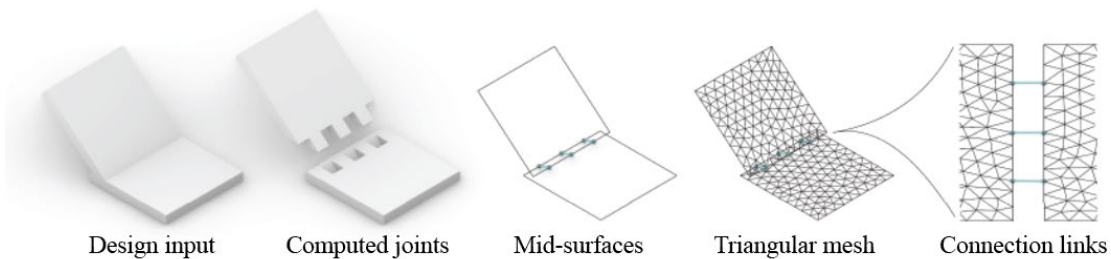


Figure 4.5: Automated conversion of architectural 3D models to Finite Element models.

4.4 Results

4.4.1 First case study: orthogonal timber slab

Our collaborative design workflow was first tested on a piece of timber slab consisting of 4 panels connected by through tenon joints (Figure 4.6). This construction system was initially developed with the idea of shipping flat packs of timber panels to be assembled on-site [GBW20b]. Using our parametric tool, timber joints are automatically generated between the panels. The influence of the number of tenons, their dimensions, and spacing on the structural performance is systematically visualized through the integrated numerical simulation module. Load and support points for the analysis are parametrically defined through a complementary script. The deformation of the structure is displayed in the design interface. In addition, von Mises stresses are computed to evaluate yield and failure states near the connections. The simulation of the CNC toolpath, as well as the robotic trajectory, is performed in the same environment. This allows modifying the design at any time while ensuring compliance with fabrication and assembly constraints.

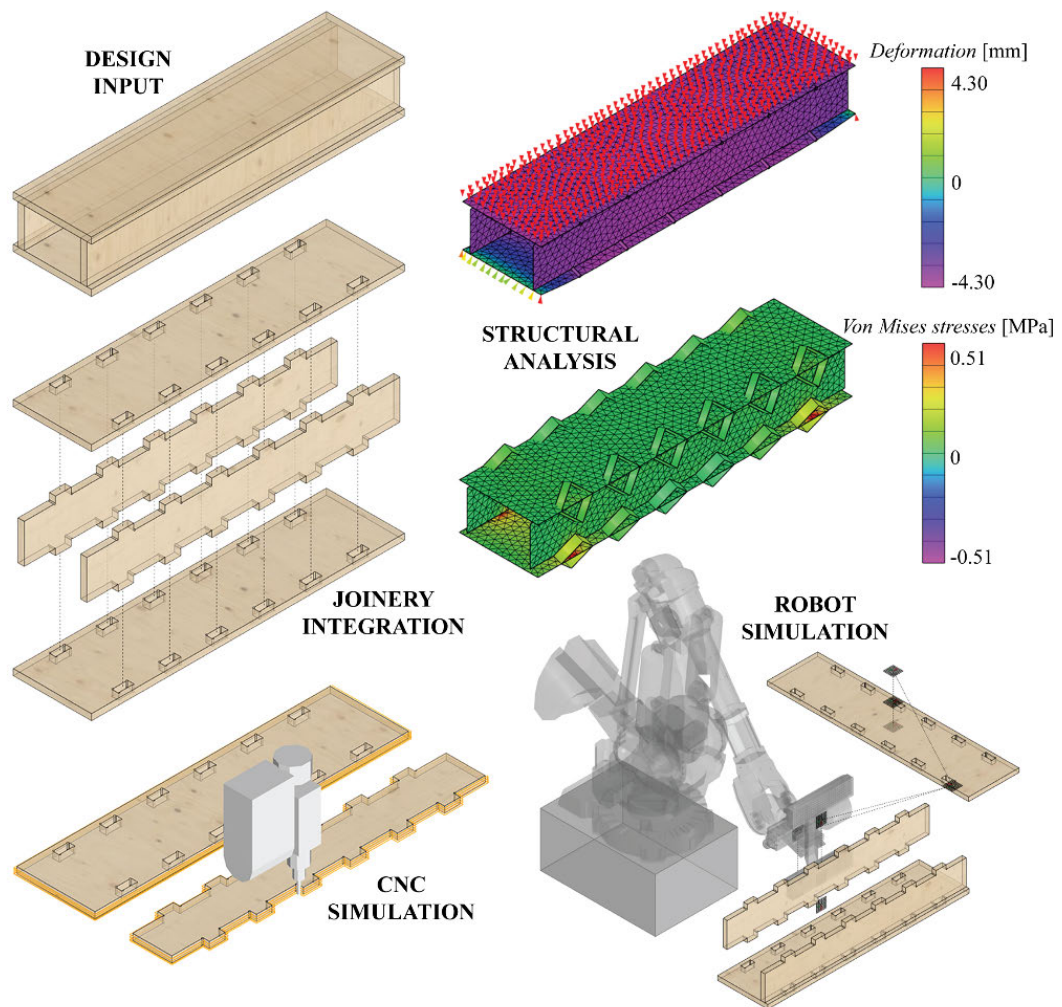


Figure 4.6: The developed plugin enables the integration of fabrication, assembly, and structural constraints into the design process of an orthogonal slab made of 4 timber panels.

4.4.2 Second case study: doubly-curved timber vault

A piece of the doubly-curved timber structure of Annen's head office in Manternach [Rez+21] has been chosen as the second case study. The prototype is a modular structure composed of 9 boxes with 4 panels each (Figure 4.7). Sunrise dovetails and through tenon joints connect the pieces to each other. The choice of the joint is automatically determined according to the relative position of the plates [RLW21]. As for the previous case study, the algorithm allows us to test different joinery configurations while visualizing their influence on structural performance. A uniform load is applied to the top layer of the vault, and subsequent deformations and stresses are automatically retrieved. The Finite Element Analysis of all 36 plates is performed with a computational time of approximately 1 minute, which maintains the possibility of evaluating several design iterations. The entire design workflow has also been recorded and is available on Vimeo [Rog21] [RR21].

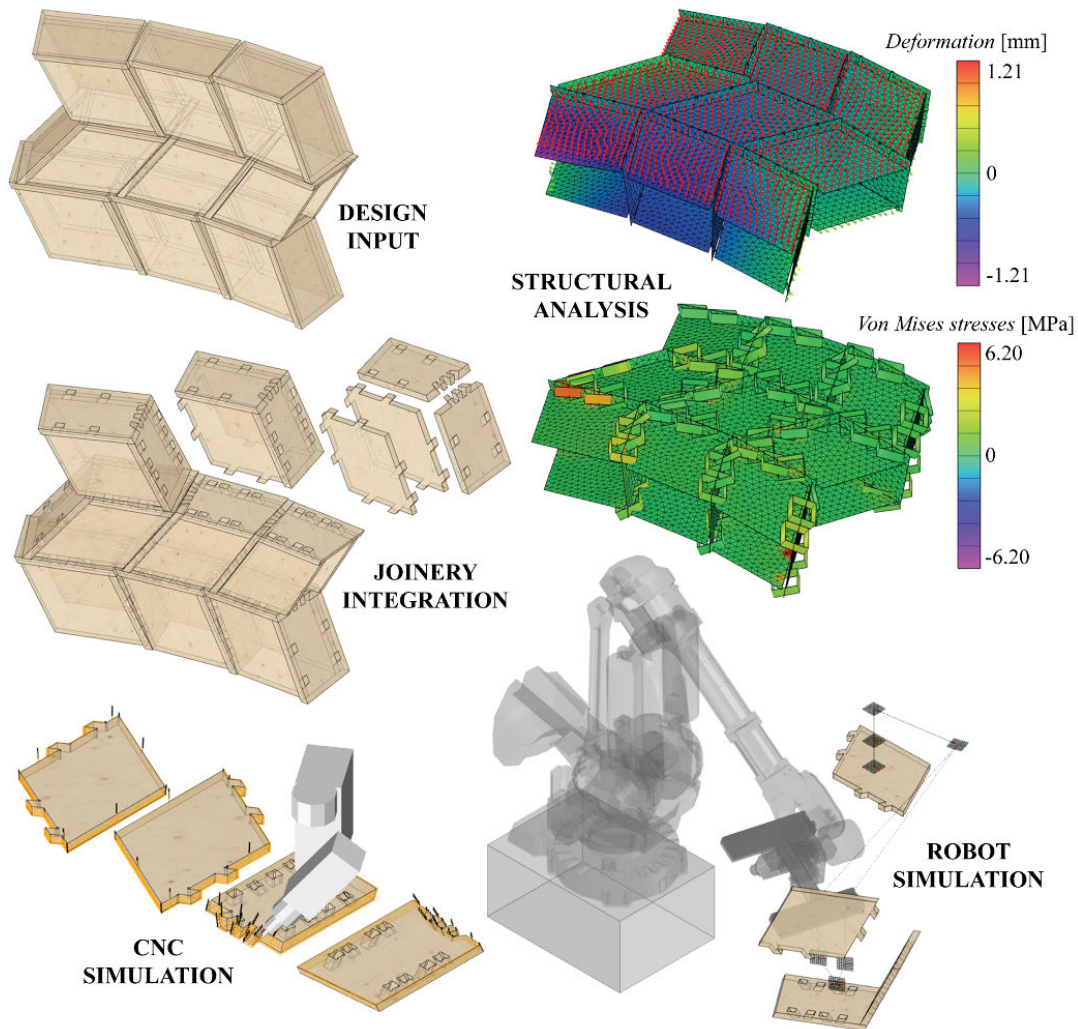


Figure 4.7: The tool design space ranges from standard to bespoke timber plate structures, as demonstrated with this doubly-curved timber vault made of 9 boxes of 4 plates each.

To assess all steps of the design-to-fabrication pipeline, one box of the doubly-curved vault prototype was fabricated (Figure 4.8). The four panels of the box were cut with a 5-axis CNC after simulating the toolpath in the design interface. Next, robot trajectories, computed by the algorithm, made it possible to perform the assembly by seamlessly transferring the data to a 6-axis robotic arm (ABB 6400). The position of the first plate of the box was manually referenced. Then, the three remaining plates were lifted from a square base with a vacuum gripper attached to the robot end effector. The joints were manually sanded beforehand to ease the insertion with the robot. This proved particularly necessary when inserting the last two plates of the module as 4 tenons had to be assembled simultaneously in two adjacent plates (Figure 4.8.7). This made it possible to compensate for the slight differences between the virtual model and the prototype.

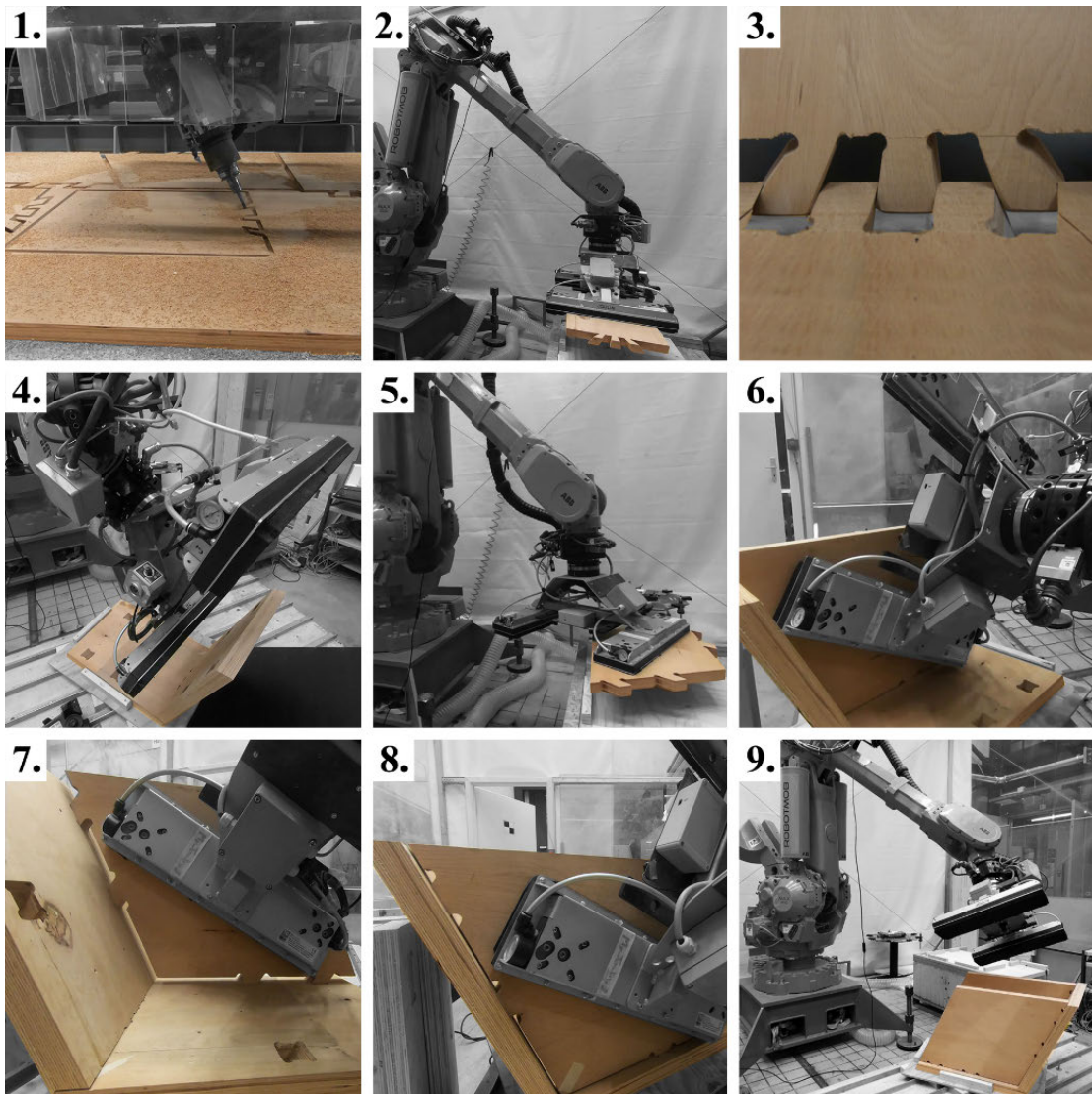


Figure 4.8: CNC cutting and robotic assembly of one module of the doubly-curved vault prototype.

4.5 Conclusion

An open-source collaborative design workflow for Integrally-Attached Timber Plate Structures (IATPS) has been developed and tested through two case studies. Using COMPAS and COMPAS_FEA frameworks makes it possible to remain independent of the structural analysis back-end. A significant achievement consisted in unifying architectural design, structural analysis, digital fabrication, and robotic assembly in one single interface. Consequently, barriers among construction stakeholders are removed, and the integration of physical constraints in the project can happen at a very early stage of the design process. Furthermore, both standard and bespoke geometries have been handled by the algorithm, demonstrating that a wide range of architectural applications can be explored.

While the present research facilitated the design of IATPS by enabling a collaborative design workflow, future research should focus on the construction phase and its automation. Indeed, to foster the use of timber in standard and bespoke architecture, streamlined prefabrication processes need to be developed and implemented. More specifically, upcoming investigations on IATPS should tackle challenges linked to the insertion of the joints with a robotic arm. Parameters such as the tolerance and the shape of the connections have a significant impact on the success of the robotic assembly as well as on the rigidity of the connections. Further experimental studies are therefore required to understand the influence of those design parameters better. From a broader perspective, future robotic setups should aim for more flexibility by allowing the assembly of different types of joints in various configurations.

As far as structural engineering and associated simulation are concerned, the computational cost could be reduced by employing reduced-order Finite Element models for timber plates, i.e., macroscopic elements. The interdisciplinary aspect of this collaborative design workflow could also be expanded further by integrating other design considerations, such as economic factors and environmental impact measures. Quantitative data about material savings and avoided CO₂ emissions would typically be a great addition to better inform the design team. Assembling the knowledge of different fields of expertise in a single platform will contribute to better design decisions and lead to a more sustainable building environment. In this regard, the particular focus should be to develop design tools that allow a holistic approach to specific building systems instead of generic tools dedicated to one professional discipline.

4.6 Acknowledgements

This research was supported by the NCCR Digital Fabrication, funded by the Swiss National Science Foundation (NCCR Digital Fabrication Agreement #51NF40-141853). In addition, the authors would like to acknowledge Imax Pro S.A. and Maka GmbH for their assistance with the robotic arm and CNC, respectively. The authors are also grateful to the COMPAS development team and to especially Dr. Tom Van Mele for his support with COMPAS FEA.

4.7 Addendum: A computational design framework for the structure of Annen

The integration of a structural analysis module within the framework introduced in Chapter 3 made it possible to automatically convert a 3D model into a mesh suitable for Finite Element Analysis (FEA). The objective was to provide an integrated design tool compatible with all types of IATPS. However, widening the scope of application required making some trade-offs in terms of computational performance. For architectural projects with complex geometry and many elements, such as the structure of the multipurpose hall of Annen in Manternach (Figure 4.9), a tailored workflow remains necessary to optimize computational times. Consequently, this section presents an algorithm that was specifically developed to automate data exchanges

between the architectural and engineering models of the Annen structure. While the text and figures are original, this research is also featured in the following peer-reviewed paper available in open access:

Rezaei Rad, A., Burton, H., Rogeau, N., Vestartas, P., & Weinand, Y. (2021). A framework to automate the design of digitally-fabricated timber plate structures. *Computers & Structures*, Volume 244, February 2021, 106456. doi: 10.1016/j.compstruc.2020.106456.



Figure 4.9: The 23 doubly-curved vaults of the Annen headquarters are composed of hundreds of timber panels with thousands of joints.

4.7.1 A streamlined and automated data exchange from CAD to CAE

This particular project was designed by Valentiny hpv architects and Yves Weinand. A computational design workflow was first proposed by Robeller et al. [Rob+16] to discretize the target surface into planar panels, compute the orientation of the joints, and generate fabrication files. Each arch is composed of rows of boxes made of 4 beech Laminated Veneer Lumber (LVL) panels connected by timber joints (Figure 4.10). Furthermore, there is only one possible assembly sequence, as each box fits into the previous one, with the last box locking the system.

Then, the structural analysis of the arches was approached separately through two distinct methods at the Laboratory for Timber Constructions (IBOIS, EPFL). On one side, a tridimensional FE model including the semi-rigid behavior of the connections and relying on the Abaqus solver [Das] was investigated in the thesis of Dr. Anh Chi Nguyen [Ngu20]. On the other side, a simplified macro model based on the OpenSees framework [Maz+] was developed in the thesis of Dr. Aryan Rezaei Rad [Rez20]. The macro modeling technique has the advantage of drastically reducing computational time. Only 2 s were needed to run the analysis of one full arch of 200 boxes [Rez+21] whereas the FE analysis took more than 20 s for only 15 boxes with a mesh size of 2.5 mm [Ngu20].

For both methods, a significant challenge consisted in automating the conversion of the architectural 3D model to a model suitable for structural analysis. Since there are no two identical panels in the project and 23 arches composed of several hundred panels need to be modeled, an automated workflow is required. Regarding the FE method, such workflow had already been developed in Grasshopper to generate suitable meshes for each timber

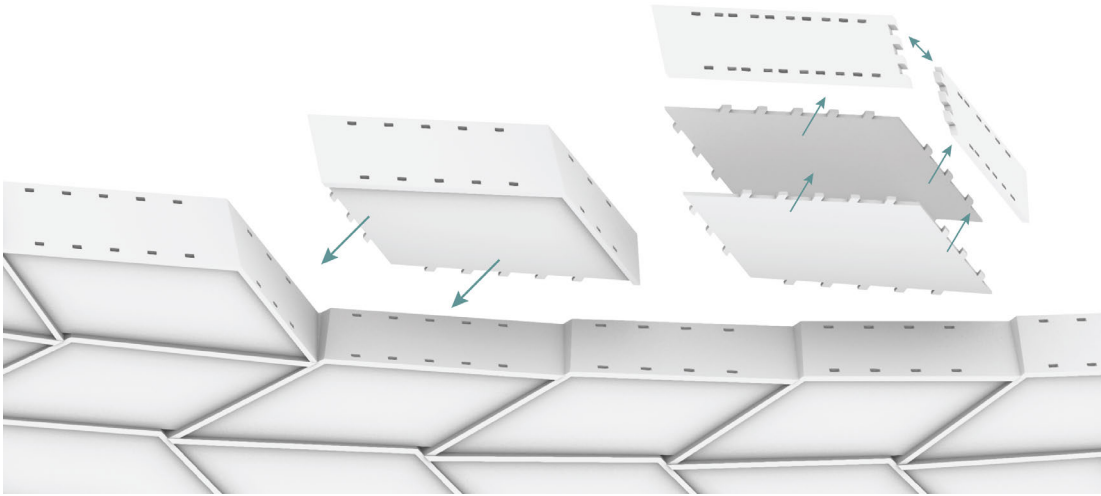


Figure 4.10: Assembly sequence of the arches of the Annen structure.

panel [NVW19]. However, the vast number of elements and the density of the meshes led to a computational time of 64.2 min for an arch of 200 boxes. Therefore, the objective was to develop a similar workflow for the macro modeling method with the ambition to generate the required elements in a considerably shorter time and provide more interactive design feedback. The algorithm was coded in Python and implemented in Grasshopper. It takes the 3D model of an arch of the Annen structure as input and outputs a text file (.tcl) containing all data of the generated macro model to be analyzed in OpenSees.

4.7.2 Generating the macro model

A macro model is constituted of springs and beams. It is a discrete representation based on unidimensional elements, unlike FE models, which are continuous. The methodology consisted in representing each timber plate with a grid of orthogonal beams and each joint with a spring. The orthogonal beams emulate the orthotropic properties of the LVL panels, while the springs simulate the semi-rigid behavior of the connections.

The construction of the macro model from the architectural 3D model is detailed in Figure 4.11. First, the mid-surface of each plate is computed (4.11.b). Then the joints are simplified into segments linking the edges of the adjacent planar surfaces. The base contour of each plate is also extracted as a polyline (4.11.c). The corner nodes are identified, and two additional nodes (adjacent hinges) are created on both sides of each corner (4.11.d). Next, the grid of orthogonal beam elements is generated (4.11.e and 4.11.f). Since all the plates in the structure have relatively similar proportions, the number of inner beams in the direction perpendicular and parallel to the fibers is constant and set to 6 and 4, respectively. Their end nodes are also computed and added to the model. Likewise, the spring elements representing the joints and their end nodes are generated (4.11.g). Lastly, all computed nodes are collected and ordered around the plate polyline to create the boundary elements (4.11.h).

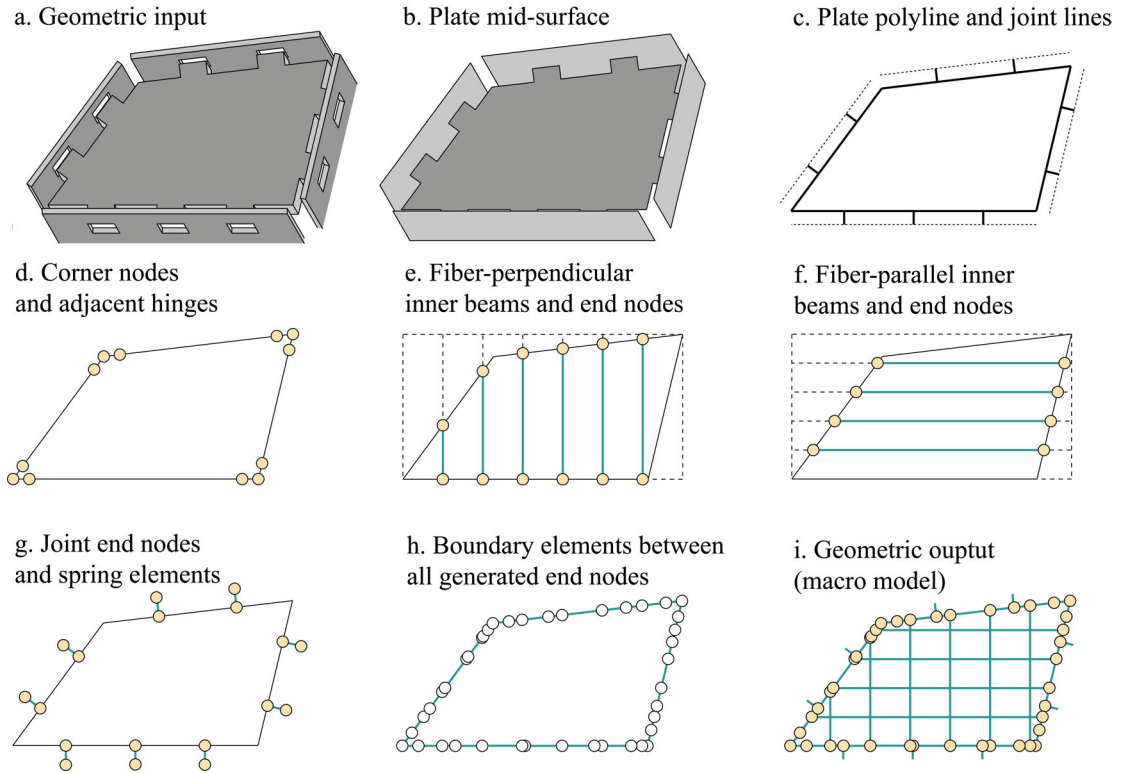


Figure 4.11: The different steps of the geometric algorithm developed to convert the detailed 3D model of the structure of the Annen project to a macro model suitable for structural analysis in OpenSees.

4.7.3 Indexing system

In order to analyze the structure with OpenSees, the nodes, springs, and beam elements need to be exported as textual information in *.tcl* format. Consequently, a custom indexing system was developed in order to set a unique tag number for each element. To ease their identification, this number was directly derived from their position in the macro model. The indexing logic is summarized in Figure 4.12, and the associated pseudo-code is given in Appendix A.4. Each tag begins with four digits identifying the panel's position in the structure. For example, the index of the fourth plate of the twelfth box of the third row of an arch is 3124 (row 3, box 12, plate 4). The following digit corresponds to the element type: 0 for the corner nodes, 1 and 2 for the inner beams, 3 for the joints, 4 for the boundary elements, and 5 for the corner hinges. The next digits are used to number the elements. The end points of the beam and joint elements reuse the same tags with an additional 1 to label the start point or a 2 for the end point.

Once a unique identifier has been assigned to each element, the data is exported following OpenSees syntax. The nodes are defined by their spatial coordinates using the *node* command. The command *elasticBeamColumn* is used for the beams. Different material properties (elastic modulus, shear modulus, torsional moment of inertia, second moment of area, etc.) are

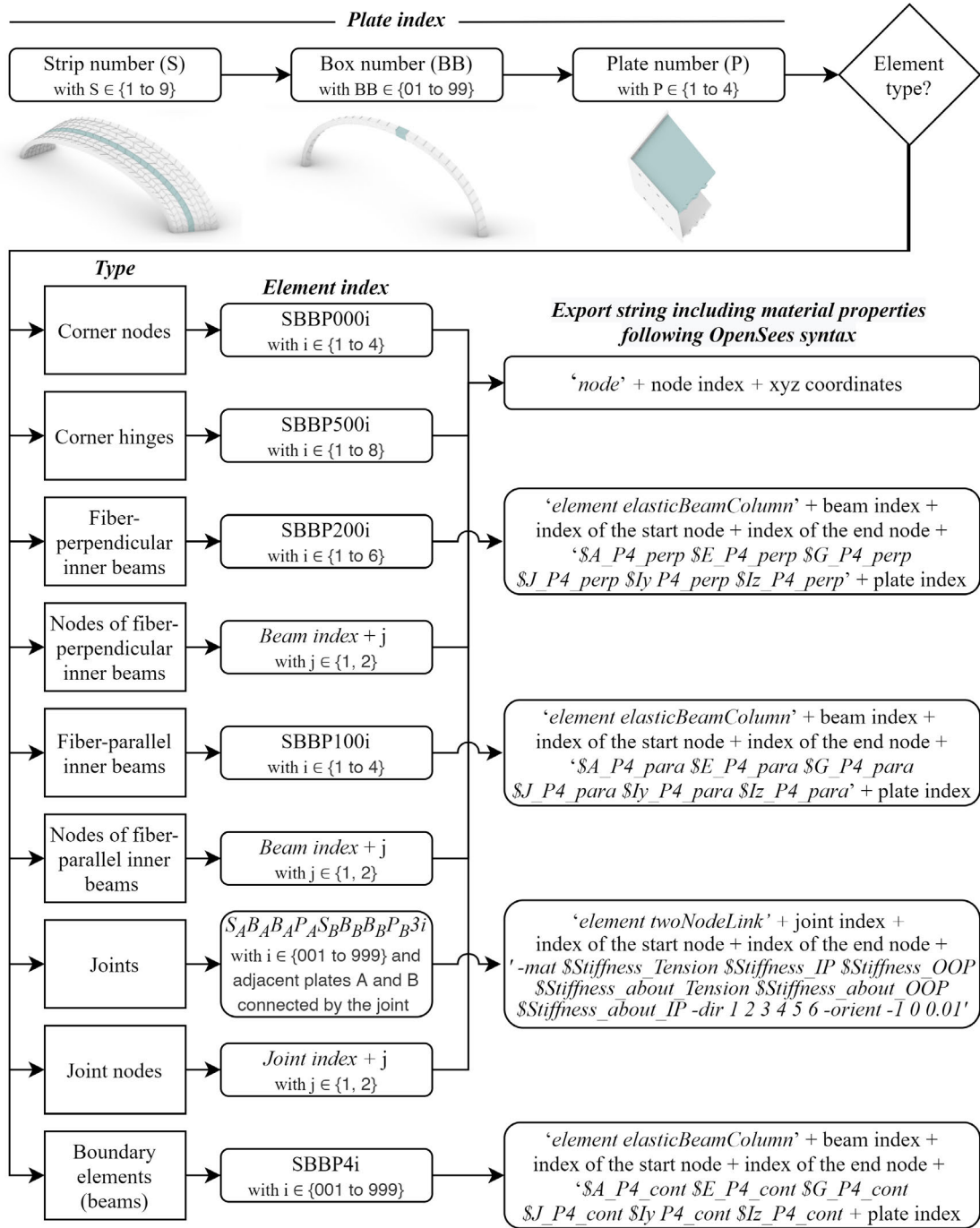


Figure 4.12: Algorithm for the indexing of the elements of the macro model and the generation of the .tcl file for the subsequent OpenSees analysis.

assigned to the fiber-parallel, fiber-perpendicular, and boundary beams according to the information provided by the LVL manufacturer [VTT16]. Lastly, the springs are created with the command *twoNodeLink*, which requires specifying the stiffness for the 6 degrees of freedom (3 translations and 3 rotations according to the local system of axes). Those coefficients were evaluated through a series of experimental activities previously carried out by Dr. Rad [Rez20].

4.7.4 Performance of the algorithm, conclusion, and outlook

The algorithm was tested on an arch of 200 boxes. The generation of the macro model and the associated text file took 1 min and 3 s (with an Intel Core i7-4800MQ CPU @2.7 GHz and 16 GB of RAM). This is about 60 times faster than the mesh generation for the FE analysis of the same arch. Besides, the analysis runtime for the macro model took only 11 min and 27 s, which is about 170 times faster than the corresponding FE analysis [Ngu20]. This demonstrates a clear advantage for the macro modeling approach coupled with the indexing strategy. In addition to saving computational time, the automatic conversion from CAD to CAE also considerably reduces the risk of errors compared to manual modeling approaches.

Table 4.1: Performance comparison between Finite Element (FE) and Macro models.

Method (for 200 boxes)	Model generation (s)	Simulation (s)
FE Model	3840	111842
Macro Model	63	687

The structural analysis module described in Section 4.3 relies on FE solvers. It has the advantage of working for all types of IATPS, independently of the configuration of the plates or the type of joints. While generating a FE mesh is more time-consuming, the technique is more versatile as the creation of the mesh is independent of the topology of the structure. In contrast, the algorithm developed for the Annen structure requires a specific indexing logic and the establishment of simplification hypotheses beforehand.

A modified version of the algorithm developed for Annen was applied to an orthogonal boxed beam designed by Gamarro et al. [GBW20b] and similar to the one shown in Figure 4.6. While a new algorithm had to be developed specifically for the beam in order to automate the generation of the geometric elements of the macro model, a methodology similar to the case of the Annen structure was followed. Besides, most of the indexing logic was reused. The only difference was that since there was only one box to consider, the first three digits of the element tags were dropped. Ultimately, the analysis of this second macro model led to convincing results both in terms of computational time and relevance of the results. Further details can be found in the referenced publication and will not be discussed here. While more research is necessary to study how the macro modeling approach could be generalized to any IATPS, this research highlighted the interest in implementing this alternative to FE modeling inside the developed integrated design tool.

Automated construction workflow

Part III

5 Insertion of timber joints with a visual feedback loop

The texts and figures presented in this section were reproduced from the postprint version of the following open-source peer-reviewed paper:

Rogean, N., Tiberghien, V., Latteur, P., & Weinand, Y. (2020). Robotic Insertion of Timber Joints using Visual Detection of Fiducial Markers. In: Hisashi Osumi, Hiroshi Furuya, Kazuyoshi Tateyama (Eds.) *Proceedings of the 37th International Symposium on Automation and Robotics in Construction (ISARC 2020)*, Kitakyushu, Japan, International Association for Automation and Robotics in Construction (IAARC), pp.491-498. doi:10.22260/ISARC2020/0068.

The doctoral candidate was responsible for the writing of the article as well as for the coordination of the scientific project. In particular, this consisted in creating a streamlined workflow to exchange data between the design interface and the robot controller. In addition, a visual feedback loop based on the detection of fiducial markers was developed in collaboration with the second author and integrated by the doctoral candidate into the workflow. The third and fourth authors of the paper contributed equally as scientific advisors and proofreaders.

5.1 Abstract

The timber building industry is facing a major transformation, with digitization and automation being more broadly adopted. Prefabricated timber frame structures can be mass-produced on large robotic assembly lines, increasing the productivity and competitiveness of wood over standard inorganic materials such as steel or concrete. While standardization is likely to limit creativity, new digital tools, on the contrary, give the possibility to design and build complex and unique geometries. Recent research in bespoke digital prefabrication notably led to the development of Integrally Attached Timber Plate Structures (IATPS). This system consists in assembling wooden panels connected only with timber joints inspired by traditional Japanese carpentry. The elements are digitally prefabricated and inserted into one another to form bespoke architectural structures. To propose a fully automated process for

IATPS from design to construction, this paper investigates a method for assembling the panels with a 6-axis robotic arm. Preliminary studies have shown that significant discrepancies can occur between virtual models and physical prototypes due to joint tolerances, hygrometric variations, and self-weight deformations. To address this challenge and to adapt the robot's position to the actual location of the elements, a visual feedback loop was developed using fiducial markers. Several tests were performed with structural wood panels to assess the method's accuracy for different configurations and adapt the geometry of the joints in consequence. Finally, the insertion of a panel with two through-tenon joints was achieved by taking pictures of the target with a camera mounted on the robot's end effector.

5.2 Introduction

The construction sector is recognized as one of the main contributors to the current ecological crisis. The production of new construction materials is responsible for a significant share of CO₂ emissions and plays a major role in landfill waste generation. Therefore, to reach the Sustainable Development Goals set by the United Nations for 2030 [Nat], it is necessary to reconsider the whole construction process and take material life cycles into account upstream in the design phase.

Engineered wood products have been identified as an alternative to commonly used concrete and steel components, which could lead to more sustainable construction systems by lowering the embodied carbon energy of the structure [Chu+20]. In addition, connections between timber panels can be integrated into the element geometry taking inspiration from traditional timber joinery techniques and benefiting from recent advances in digital fabrication to generate the toolpath [Rob15]. This construction system, also referred to as Integrally-Attached Timber Plate Structures (IATPS), reduces steel fasteners and improves structural performance. Furthermore, since additional connectors are not required, the amount of time allocated to the construction phase can also be reduced.

Previous research has both demonstrated the architectural and structural interest of IATPS, leading to the realization of large-scale projects such as the theater of Vidy [RGW17], the BUGA wood pavilion [Wag+20a], and the Annen's head office [NVW19]. Different workflows have been set up for each of those projects to integrate fabrication constraints in the design and automate the cutting of the different pieces using a CNC machine or a 6-axis robotic arm. For the BUGA wood pavilion, collaborative robots have also been used to glue the construction components. However, for each of the three projects, the assembly of the different modules remained a manual process.

First investigations about the robotic assembly of IATPS have highlighted two main challenges for automating the insertion of timber joints [Rob+17]. First, friction forces grow with the number of connections and can hinder the insertion. Second, the robotic insertion has to be performed with enough precision to avoid the introduction of gaps, which would decrease the rigidity of the connections. This paper focuses on developing a method combining different

strategies to automate the insertion of the panels.

5.3 State of the art of robotic insertion

Pick and place operations are usual tasks that can be handled by industrial robotic arms. Suppose the initial and final positions of the objects relative to the robot are known. In that case, the trajectory can be easily computed, and the precision of the insertion will only depend on the accuracy of the robot from point to point. However, for large and heavy construction elements, significant discrepancies between virtual and real models can occur. For example, timber panels are typically subject to slight dimensional changes over time and are very sensitive to hygrometric variations. Even for standardized elements, fabrication tolerances are usually around 1 mm. Besides, wood-wood connections are not ideally rigid, and gaps in the joints can add up through the structure causing large deviations and preventing the robot from assembling the pieces. Three strategies, which can be combined to ensure a precise insertion, have been identified in the literature and presented here.

5.3.1 Shape adaptation

The first method consists in adapting the design of the connections to enhance the tolerance and progressively guide the pieces to the final position (Figure 5.1). Usually, the modification consists in chamfering one or both pieces or adding a separate guide. Conic joints with a tolerance of about 4 cm have been used in the FutureHome Project [Bal+02] to compensate for the swing of the automated crane, which was used to assemble the large modules. The cone's slope was related to the friction forces between the different parts.

In the extreme case of structures assembled by drones where precision is an even more significant challenge, specific joints have also been developed for masonry and timber elements [Goe+18]. Chamfering through-tenon joints is a commonly used technique in traditional woodworking. Such joints have notably been optimized for inserting the panels of the double-layered timber plate structure of the Vidy Theater [RGW17]. However, a potential downside of self-centering connections is the diminution of the rigidity of the joint as the induced slopes lead to smaller bending resistance.

5.3.2 Force monitoring

As manual insertion relies mainly on haptic feedback, another strategy is to use torque sensors to adapt the robot's position according to the measured forces. A classic example consists of trying to insert a peg in a hole using integrated force sensors to align the robot's position [Str88]. The need to manage material tolerances by developing robot sensitivity has also been illustrated in the DIANA project [Ode+19], where a robotic arm was interactively taught how to insert wooden rods to shape a ruled surface.

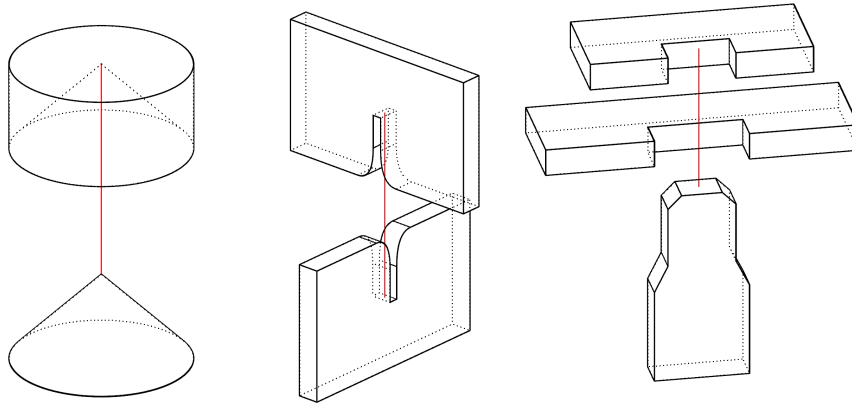


Figure 5.1: Three types of self-centering connections: conic joint (left), drone-compatible joint for interlocked timber beams (middle), and chamfered through-tenon joint (right).

Impedance control has also been used to insert gear-shaft mechanisms with a precision of around $5\text{ }\mu\text{m}$ for applications in medical fields or aeronautics [Guo+19]. In addition, more complex feedback loops using behavior-based or machine-learning approaches have also been used to develop optimal strategies for inserting pieces into one another [EG14].

However, the interpretation of the measured force is always dependent on the shape and weight of the piece to insert, and the techniques mentioned above are established for standard symmetrical elements. Developing an adaptive strategy for the case of timber joinery is challenging as elements come in different sizes, and the number and type of connections can also vary.

5.3.3 Visual feedback

Different position-tracking systems based on visual feedback loops have already been developed for on-site applications and could also be applied off-site. For example, a total station can be used to track selected points and deduce the robot's position by triangulation. Another possibility is to rely on cameras and image recognition. A comparative study has highlighted the performance of fiducial markers for reducing deviation with a clear advantage regarding the execution speed [IKB19]. Fiducial markers have also been used to guide the In-situ Fabricator developed at ETH Zurich [Gif+17].

Other visual detection applications include precisely laying mortar on a brick wall [EG14] and assembling large modular frames [Qin+16] using a combination of cameras and lasers to guide the insertion. Photogrammetry and laser scanning technologies have also been combined with robotic arms to gather data on-site for indoor and outdoor localization [VBV19] [KCC] [Gaw+19]. However, image reconstruction, point cloud acquisition, and mesh post-processing are all computationally intensive, and data interpretation requires complex machine-learning algorithms in order to work with different geometries.

5.3.4 Strategy comparison and research objective

Each strategy has its advantages and drawbacks which are listed in Table 5.1. Adapting the shape of the connection is probably the easiest solution to implement and will be discussed in the next chapter. However, the tolerance that can be gained with that solution is limited by the size of the objects to insert. Considering that tolerances can accumulate through a structure and cause significant discrepancies between physical and virtual models, it is necessary to be able to tackle large deviations up to several centimeters. As force monitoring is more suited for small adjustments and requires to train specific models for each type of connection, it was decided to focus first on the implementation of a visual feedback loop which can accommodate larger deviations and be compatible with all kind of joints.

Table 5.1: Comparison of fault tolerant assembly techniques.

	Shape adaptation	Force monitoring	Visual feedback
Pros	Integrated to the design Low-tech approach	Precise local feedback Sense physical reality	Work for larger deviations Work for all kind of joints
Cons	Loss of structural rigidity Not always possible	Limited deviations Difficult to generalize	Need to see the object Need markers

5.4 Methodology

5.4.1 Integrated design framework

Our approach links project design and technical constraints by means of computational geometry. Instead of locally solving the insertion problem, the goal is to inform the designer of fabrication and assembly constraints by developing a cross-platform workflow. Custom scripts are used to convey the geometric information between software (Figure 5.2).

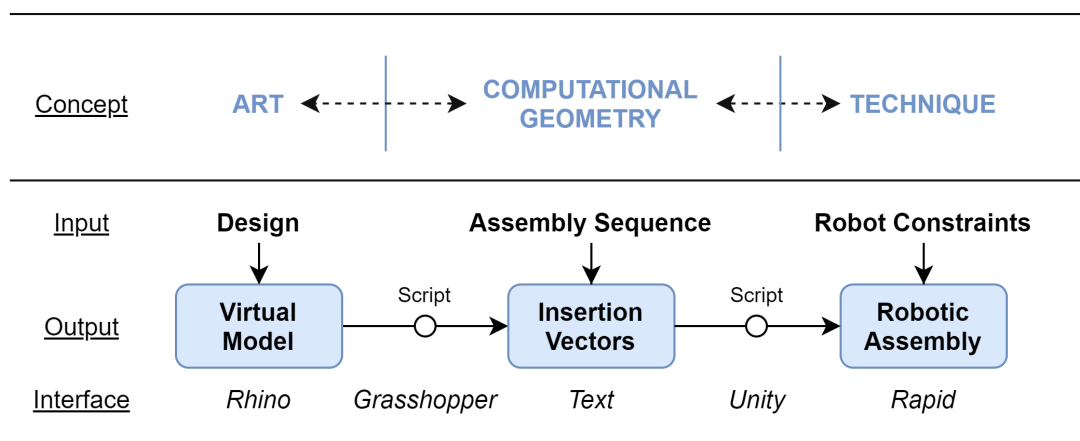


Figure 5.2: Integrated design framework linking design to robotics constraints.

The assembly is driven by three major inputs: design, assembly sequence, and robot constraints. In a traditional workflow, each input is integrated one at a time in the construction process. Digitization allows for more agility since parameters can be modified and information can flow back and forth.

It was decided to rely on existing specialized software for each part of the workflow instead of building a single custom program from scratch. Rhinoceros 7 [Mab] was chosen as the design interface, and the plugin Grasshopper as a tool to extract and manipulate data from the model. To simulate and execute the robot trajectory, the research benefited from a collaboration with a specialized industrial partner (ImaxPro S.A). A custom application was developed, for the purpose of the research project, on the game engine Unity [Uni] to convert geometric data from a text file to robot instructions.

Splitting the workflow between different software avoids making compromises between design possibilities and robotic performance. Meanwhile, custom scripts ensured a smooth transition between the different interfaces allowing almost instantaneous feedback and testing of multiple design iterations.

5.4.2 Insertion vectors

Insertion vectors are an essential parameter for IATPS as the geometry of the joints is tightly connected to the assembly sequence (Figure 5.3). It is impossible to design the connectors' shape without knowing the insertion's trajectory beforehand. Therefore, the integration of fabrication and assembly constraints follows an iterative process and is inherent to the design of IATPS.

A parametric script was thus coded inside the Grasshopper interface to deduce insertion vectors from a geometric input and a specific assembly sequence. Contact zones are identified by computing intersections between the panels. The type of joints that is generated depends on which faces are connected (e.g., through-tenon joints are created for a connection between the side of a panel and the face of its neighbor). Once the 3D model is created, the contour of the panel can be extracted, and the panels can be cut using a CNC. Then insertion vectors are used a second time to generate the robot trajectory.

5.4.3 Position detection using fiducial markers

Given the variety of possible configurations for IATPS, using fiducial markers was found to be the most efficient method to keep track of the position of the different timber panels. Furthermore, the open-source library OpenCV [Gar+14] provides a robust solution for estimating the position of fiducial markers (ArUco) from various sizes. Therefore, a custom python executable was developed to assess the detection performance before being integrated into the global workflow.

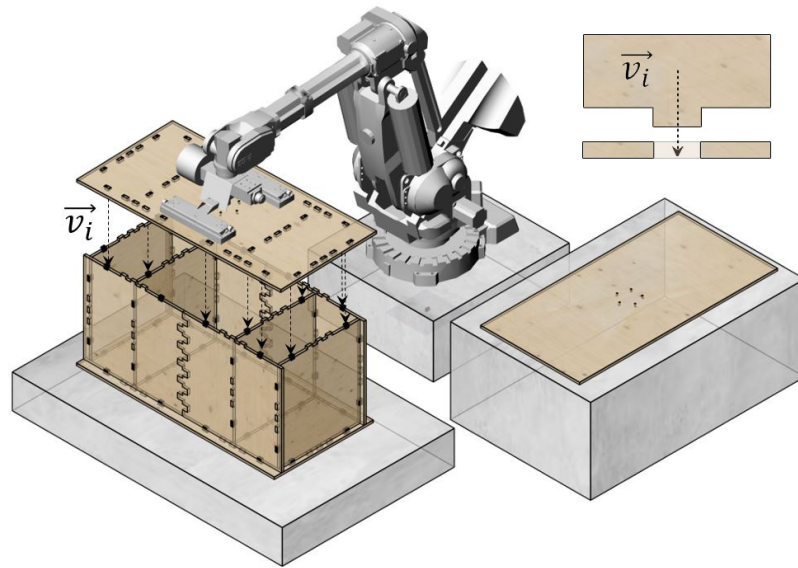


Figure 5.3: Insertion vectors are inducing the shape of the connections as well as the robot trajectory.

The algorithm consists in taking one picture from a targeted marker on a panel, computing its orientation and position coordinates (Figure 5.4), and saving those results in a text file. This information is later accessed by the robot controller to update the trajectory. The image is processed by applying perspective transformation and thresholding to get potential markers from the pixels. Analyzing the color of the 36 cells composing the ArUco provides the unique identification number of the marker. The position and the orientation are obtained by finding the tridimensional transformation from the camera's coordinate system to the marker's coordinate system. Rotations are obtained in Euler angles but converted to quaternions to ease the conversion to Unity software, which uses another axes convention.

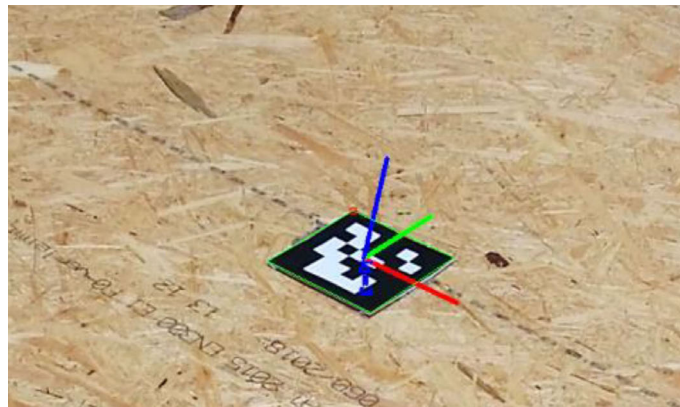


Figure 5.4: Image processing of an ArUco Marker using OpenCV library to get the position and orientation of a timber panel.

A key feature of the developed application is that the position of the different targets constituting the robot trajectory is expressed in different coordinate systems. The position of some targets is associated with the coordinate system of the starting location. In contrast, the position of some other targets is expressed according to the position and orientation of an ArUco marker. Hence, updating the position of this marker will automatically update the absolute coordinates of all associated targets, while others will remain unchanged.

A unique marker has to be assigned to each panel and glued at its center. Although the point of reference can be set arbitrarily, making it coincide with the point from which the tool would lift the panel seems the most logical. The potential bending of the panel is minimized by picking it from its center of gravity.

Before proceeding to the robotic assembly, the position of the stack of panels is precisely referenced. Hence applying the visual feedback loop to adjust the starting location of the panels is not necessary, and only the end point of each trajectory is updated using fiducial markers. Prior to each pick and place operation, pictures of a marker placed on the panels on which the insertion will occur are taken with a camera mounted on the robotic arm (technical specifications are given in Section 5.5).

5.4.4 Fail-safe process

One drawback of working with relative positions (instead of absolute) and a feedback loop is that detection errors can potentially lead to unexpected trajectories different from the simulation. Indeed, under certain circumstances, such as in the case of insufficient luminosity or when the marker is too far or in the periphery of the camera's angle of view, the detection's precision significantly decreases.

To prevent updating the position of the marker with inaccurate coordinates, it was decided to take three pictures of each marker at different angles and set two tolerance parameters. If the dispersion of the results or the deviation from the model is too high, new pictures are taken, and the updated values are again compared.

5.4.5 Robotic workflow

Putting together the initial information given by the insertion vectors with the visual feedback loop, a complete workflow was established to insert the timber panels with a robotic arm (Figure 5.5). No path-planning algorithm was used for the robot trajectory. Instead, a strategic approach was preferred.

After the first panel of the sequence is placed, the robot positions itself above the marker using the information of the model as a reference. Next, the visual feedback loop is executed, and pictures are taken from different angles at a distance of about 50 cm. Then the position of the marker in the virtual model is updated through image processing.

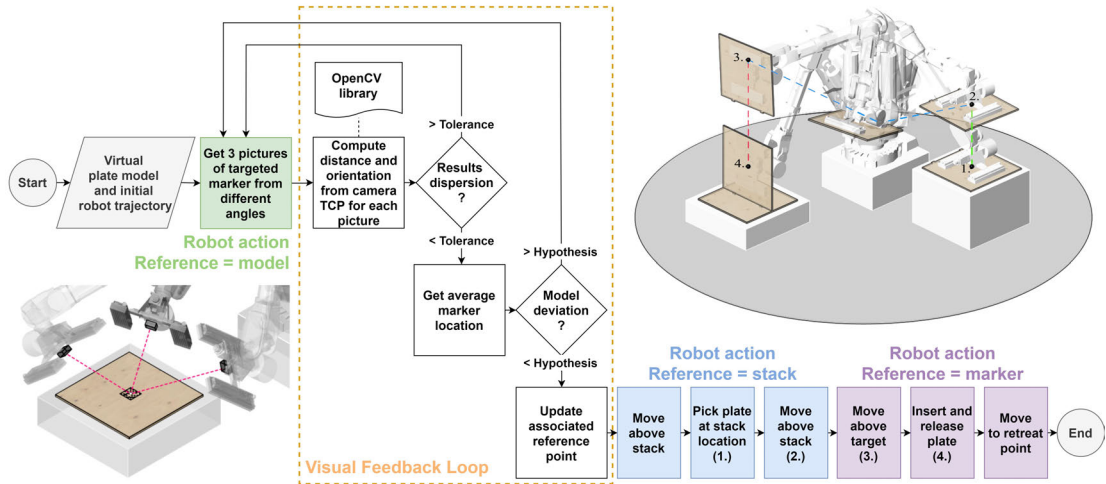


Figure 5.5: Robotic workflow: camera shooting with the robot moving according to model (green), image processing (orange), picking phase with the robot moving according to the stack of panels (blue), insertion phase with the robot moving according to marker (purple).

The second step consists in picking the next panel at the stack location. Then, as the position of the stack, as well as the dimensions of the panels, are known, the robot uses that information to move right above the stack and lift the panel from its center of gravity.

For the third step, the updated position of the fiducial marker is used as the new system of reference, and a target is generated above the place of assembly. As a *linear move* is not always possible between those two positions, a *joint move* is preferred for this part of the trajectory. To constrain the interpolation, additional targets can eventually be created in between.

For the last step, the panel insertion is finally performed (Figure 5.6). The robot reaches a target a few centimeters away from the final position, in the opposite direction of the vector of insertion associated with the panel. Then it follows that vector until the panel is inserted. The panel is released by the vacuum gripper, and the robot retracts along the panel's normal before returning to the safety plane. A structure is gradually assembled by repeating the process with the next panels.

5.4.6 Intermediate robot language

Once established, the workflow was converted to robot instructions. Target positions and special actions, such as taking a picture or activating the vacuum gripper, were interpreted from a text file, which was manually typed or automatically generated by a script (e.g., in the case of complex assemblies or when a high number of elements needs to be inserted). An intermediate programming language with a high level of abstraction was therefore developed to integrate custom commands.

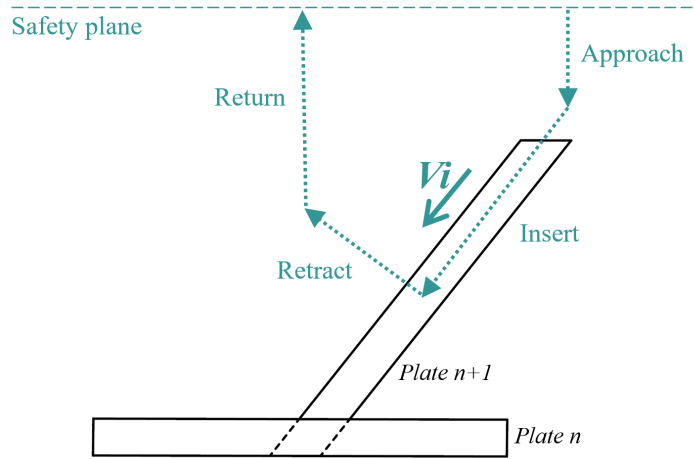


Figure 5.6: Robotic trajectory based on the vector of insertion.

Two examples of instructions are given in Figure 5.7. The number of parameters on each line depends on the first keyword: Camera will start the visual feedback loop and requires four additional parameters. In comparison, *JointMove* requires up to 12 parameters, including the coordinates of the targeted position to execute an unconstrained motion between the actual position of the robot and the specified point.

Other typical commands include *LinearMove*, which takes the same parameters as *JointMove*, *Vacuum On/Off*, which is used to activate the suction of the gripper and *Wait* followed by a number to pause the execution of the code during a certain amount of time.

Finally, each line of the code is parsed by our application in Unity for simulation and converted to the specific programming language of the robot for execution. On a side note, the additional layer of abstraction added by this intermediate language proved to significantly enrich the user experience by providing an explicit workflow.

5.5 Tests and results

5.5.1 Experimental set up

Experiments were led with a 6-axis robotic arm (ABB IRB 6400R) with a reach of 2.5 m. The end effector was equipped with two vacuum grippers, which can lift panels up to 80 kg. In addition, a standard webcam (Logitech C270) with a resolution of 1 megapixel was mounted on top of the robot end effector and connected by a USB cable to take pictures of the ArUco markers (Figure 5.8). First, calibration was carried out by taking a series of 20 pictures of an ArUco board from different angles to get the camera's intrinsic parameters, such as the focal distance and camera center. Then, fiducial markers were printed as 10 cm square and precisely fixed to the center of the panels following guiding lines previously engraved with a CNC.

a. Camera Marker12 3 0.005 2.0

Start visual feedback loop	Number of pictures to compare	Marker to update	Tolerance factors (distance/angle)

b. JointMove Gripper Marker12 500 10 0.00 0.00 500.00

Type of Move (Linear/Joint)	Tool in use	Frame of reference	Interpolation factor	Maximum speed	Position Coordinates (x, y, z)

Quaternion 0.0000000 0.0000000 0.0000000 1.0000000

Rotation format (Quaternion/Euler)	Rotation values (qw,qx,qy,qz or rx,ry,rz)

Figure 5.7: Samples of a text file interpreted by our custom application in Unity to send instructions to the robot controller: Activation of the visual feedback loop (a) and joint move above a marker (b).

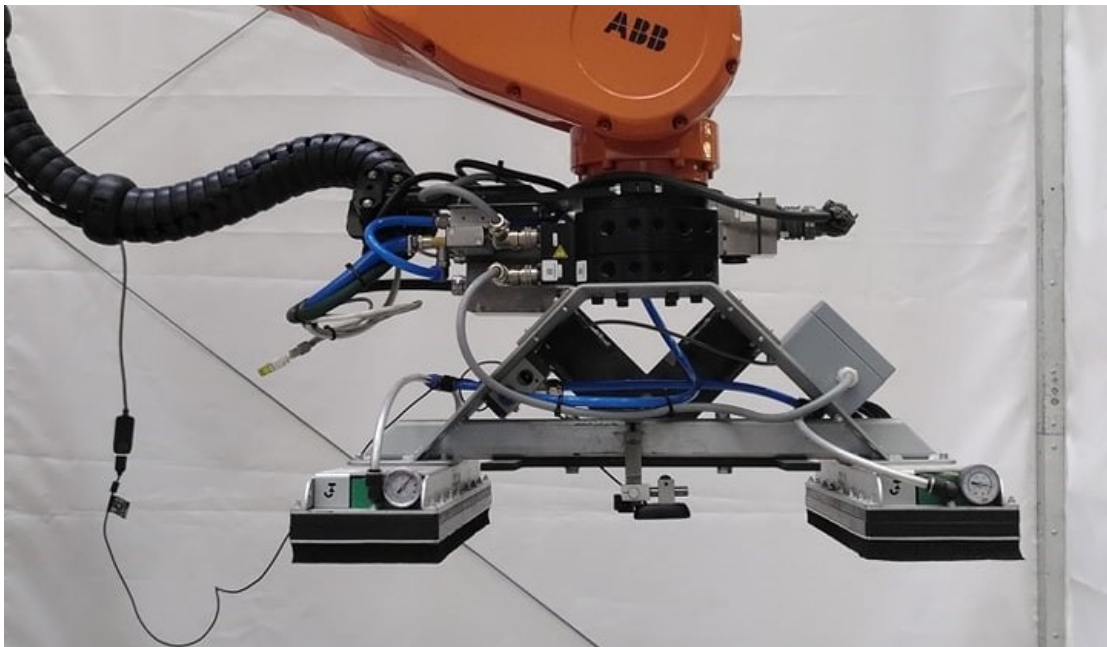


Figure 5.8: Robot end effector equipped with a vacuum gripper and camera for visual feedback.

5.5.2 Insertion without visual feedback loop

A first test was led without the visual feedback loop to evaluate the difficulty of inserting panels with a robotic arm. The objective was to automate the assembly of 3 non-orthogonal timber boxes composed of 13 panels of 45 mm thick cross-laminated timber (CLT) (Figure 5.9). The gap between the tenon and the mortise was set to 0.5 mm to reduce friction forces and reached up to 0.7 mm in some cases due to slight material deformations in addition to the tolerance of fabrication.

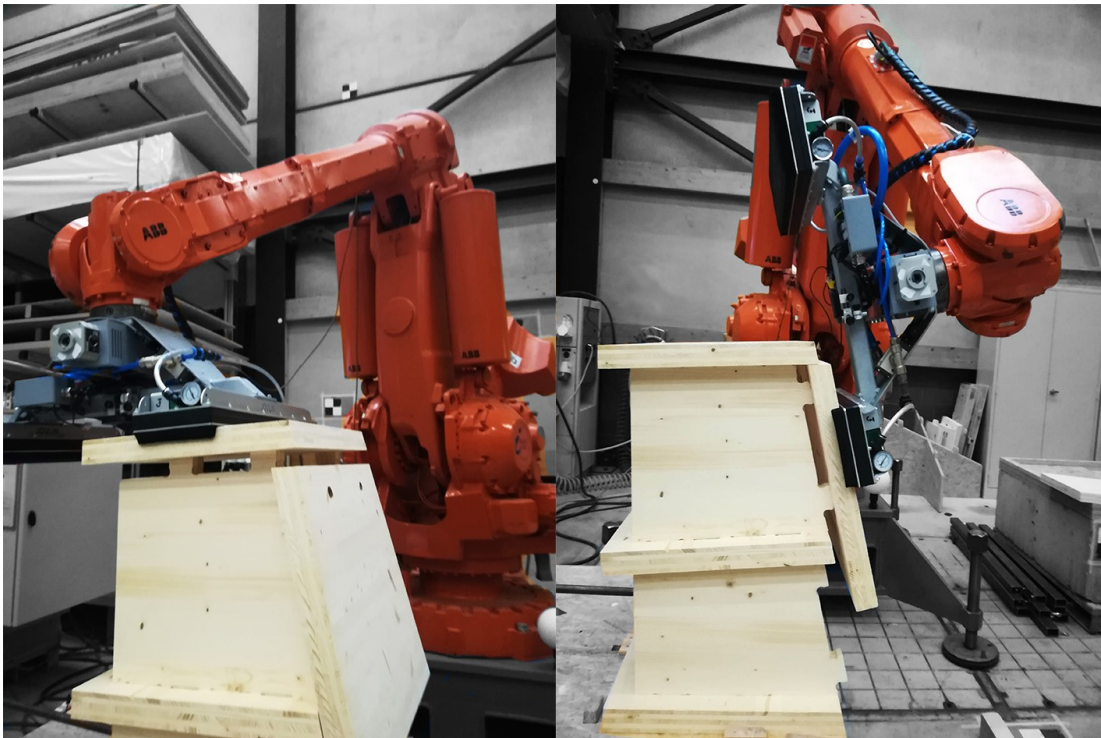


Figure 5.9: Assembly of 13 non-orthogonal timber panels without using the visual feedback loop. Discrepancies of about 1 cm between the virtual and physical models were reported when trying to assemble the panels. Manual adjustments were, therefore, required to perform the assembly with the robot.

The accumulation of small discrepancies due to the clearance in the joints and the dimensional variation of the panels caused large deviations between the virtual model and the physical prototype. For example, when inserting the last panel, a difference of about 1 cm was measured at the top of the structure. This could be explained by the fact that only the first panel was anchored, while the rigidity of the connections for the other panels was not enough to prevent them from rotating slightly. This led to the impossibility of assembling the pieces without manual intervention. In conclusion, as inaccuracy increases with the number and the size of the elements in the structure, a visual feedback loop was found to be necessary.

5.5.3 Precision of the visual feedback loop

Before testing the panels' insertion, the visual feedback accuracy was evaluated. The camera's position in relation to the end effector of the robotic arm was found by referencing the position of 4 markers in manual mode (Figure 5.10) and matching the values obtained by taking a picture. It is assumed that both the sharp tool's calibration and the markers' referencing were achieved with a precision of about 0.5 mm. Once the camera position was properly set up, new pictures were taken with multiple camera orientations and distances. Then, the acquired data were compared with the coordinates of the manually referenced markers. Three pictures were taken at each location to assess the consistency of the results.

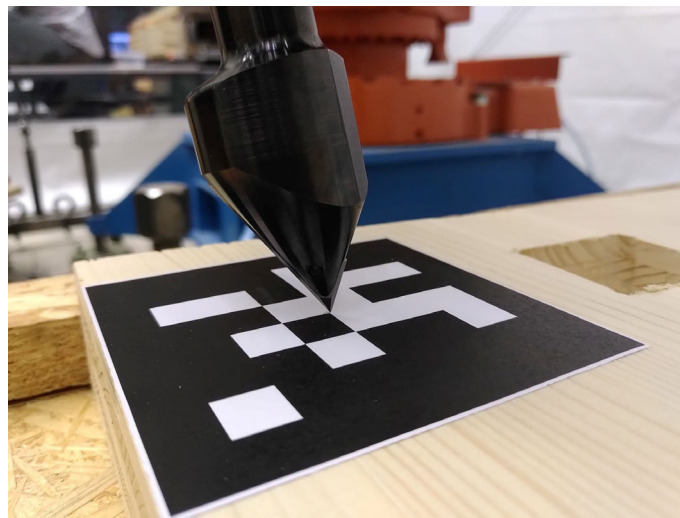


Figure 5.10: Finding the relative camera position by comparing manually referenced coordinates with computed values from the visual feedback.

Extreme values for distances of 30, 50, and 80 cm between the camera and the fiducial marker are reported in (Figure 5.11). Both precision and accuracy were affected by the distance from which the picture was taken. However, below 30 cm, the dispersion of the results stayed below 1 mm, which remains in the range of precision of the manual measurements. Further than 50 cm, the visual detection accuracy decreased considerably, reaching several millimeters at 80 cm. In addition, a loss of precision was also observed as the dispersion of the results, which were obtained from the same camera position, raised to 2 mm at 80 cm.

Additional tests were performed with different orientations of the robot end effector (Figure 5.12) and also produced slight deviations from the referenced point. Targets on the edge of the camera's field of view were particularly misinterpreted by the algorithm and reported position errors up to 2 cm. On the one hand, the calibration of the camera was found to be a key parameter to reaching more accurate results. However, it was also limited by the precision of the manual measurements. On the other hand, the precision of the detection was also limited by the algorithm itself and the exactitude of the spatial transformation.

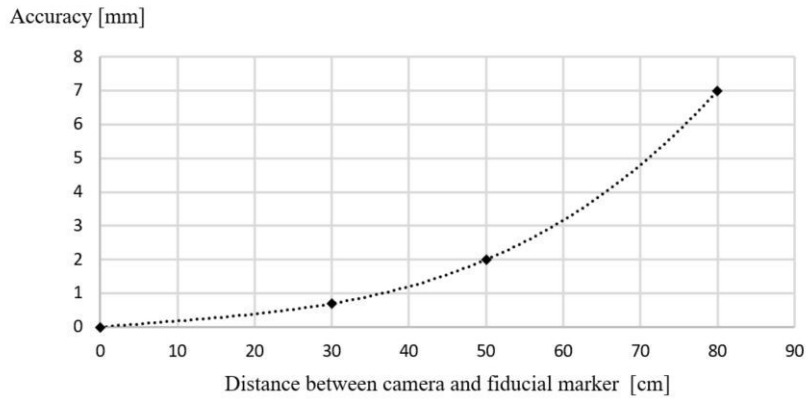


Figure 5.11: Maximum distance between the target position and the results obtained with the visual feedback loop.

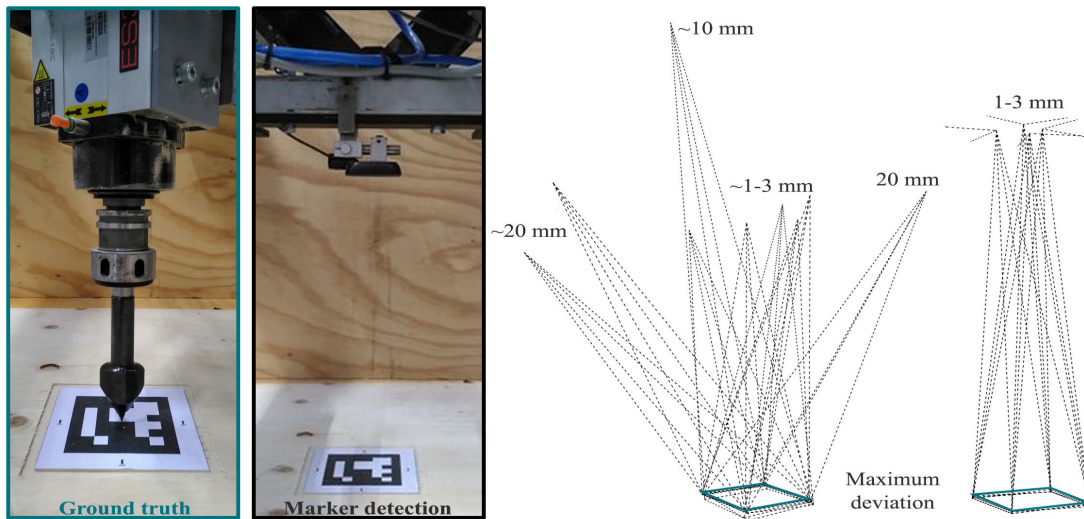


Figure 5.12: Variation of accuracy according to the orientation of the camera.

5.5.4 Insertion with visual feedback loop

Based on the previous results, a tolerance threshold was established. It was shown that all pictures taken at a distance below 50 cm, with the camera parallel to the marker, were interpreted with a maximum error of 3 mm. The design of the timber joints was therefore adapted in consequence to match that tolerance threshold as shown in Figure 5.13.

A test of insertion was conducted using two panels of 1 m^2 each connected by 2 trough-tenon joints. Following the principles of auto-centering connections, a chamfer of 4 mm was applied to tenons and mortises. As the fabrication process excluded cutting the panel from below, the chamfer was doubled on top of the tenon instead of being equally distributed (see Figure 5.13). Using the visual feedback loop, the two panels could finally be inserted into one another (Figure 5.14).

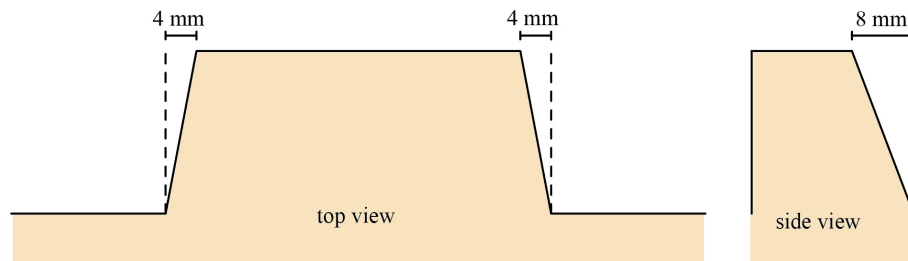


Figure 5.13: Chamfered tenon based on the measured precision of the visual feedback loop.

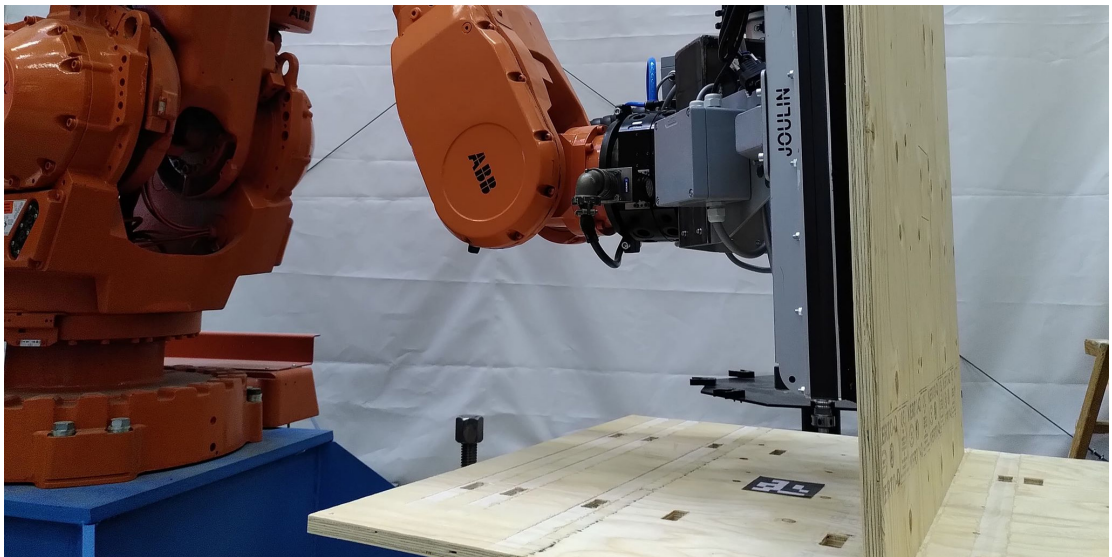


Figure 5.14: Insertion of a Laminated Veneer Lumber(LVL) panel with the visual feedback loop.

5.6 Conclusion

A complete workflow was established to assemble prefabricated timber panels connected by wood-wood connections with a robotic arm. The study included the development of a strategy of insertion using different software and linking design and assembly constraints by means of computational geometry. In addition, an explicit programming language was introduced to ease the interactions between the designer and the machine.

A particular focus was set on performing a precise insertion despite the large deviations that might occur between physical prototypes and virtual models. In addition, the visual detection of fiducial markers, which can easily be placed on top of timber plates, was found to be a cheap and effective solution for updating the position of the panels through a feedback loop. The evaluation of the method performance showed satisfying results at distances up to 50 cm. For larger distances, the precision of the detection of the markers showed some limitations but could probably be enhanced by refining camera calibration. Eventually, increasing the camera resolution or the size of the ArUco markers could improve the quality of image processing and lead to better outcomes.

Finally, applying the visual feedback loop to the assembly of two timber plates demonstrated the potential of the concept and the feasibility of the proposed workflow to automate the assembly of Integrally Attached Timber Plate Structures. The method presented in this paper could have applications on-site. However, further research is still required to extend the workflow to the architectural scale, such as solving friction-related issues when inserting multiple joints simultaneously.

5.7 Acknowledgements

This research was supported by the NCCR Digital Fabrication, funded by the Swiss National Science Foundation (NCCR Digital Fabrication Agreement #51NF40-141853). In addition, the authors would also like to acknowledge Imax Pro S.A. for the technical support regarding the integration of the robotic system.

5.8 Addendum: Further improvements to the visual feedback loop

Following the publication of the above article, further research was conducted on the visual feedback loop. These investigations have not been published and are, therefore, presented here as an addendum to the previous paper. This work was performed in collaboration with Mr. Florian Genilloud, who conducted a semester project from September to December 2020 at the Laboratory for Timber Constructions under the supervision of the author of the thesis.

5.8.1 Integrating Time of Flight sensors

The first objective was to improve the accuracy of the visual detection of the fiducial markers to better align the robot end effector with its target plate. Previous results obtained with a standard webcam highlighted the necessity for the camera to be as parallel as possible to the markers. Some discrepancies were reported in the results when processing pictures with different orientations of the robot end effector. Therefore, the integration of additional sensors was explored to measure and compensate for the potential difference in orientation between the robot and its target.

Time of Flight (ToF) laser range sensors are ideally suited for this kind of application as they can measure the distance to a surface at a high frame rate while remaining relatively affordable [Koh+13]. To compute the orientation of a plane, a minimum of three points is required. However, four ToF lasers (TFmini Plus, Benewake) were added around the camera to have some redundancy in the measured values. In addition, the standard webcam used in previous experiments was replaced by a high-definition camera (CS-Mount Lens, Arducam).

Furthermore, to avoid the use of many cables, the lasers and the camera were connected to a single-board computer (Raspberry Pi 4), which enabled data to be sent via WiFi to the

5.8 Addendum: Further improvements to the visual feedback loop

computer of the robot controller. The connection between the Raspberry and the sensors was made using a standard breadboard. The Raspberry, the breadboard, and the cables were all regrouped in a closed box to protect the electronic circuits from dust and potential impacts. Consequently, the only cable coming out of the system was the power cable which could be easily replaced by a power bank for more flexibility in future developments.

To ease the calibration of their respective position and orientation, the lasers and the camera were all fixed on a steel plate pre-cut by a water jet machine and attached to the robot end effector (Figure 5.15). The electronic box was also screwed to the back of this plate. Besides, the lasers were positioned as far apart as possible to increase the precision of the measurements. Finally, their calibration was achieved by setting to zero the distances measured by each sensor when a panel was being lifted by the vacuum gripper.

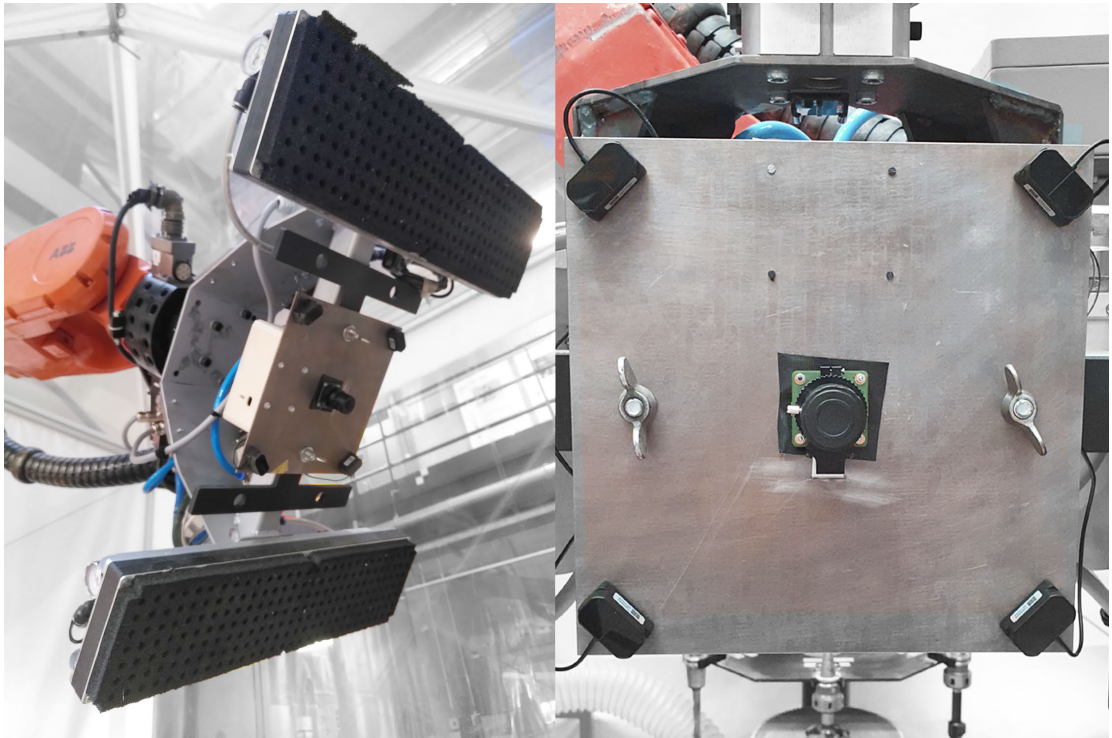


Figure 5.15: Improved visual sensor with four ToF lasers and a camera connected to a single-board computer and fixed on a steel plate.

The lasers are controlled by the Raspberry Pi to operate alternately. This prevents their light from interfering with that of their neighbors. Besides, the communication interface of the Raspberry Pi is a Universal Asynchronous Receiver Transmitter (UART), which works in a serial mode and can read only one value at a time. 50 measurements per second are taken by each laser with a time interval of 0.005 s between each measurement. This makes it possible to remove potential outliers to increase the consistency of the results.

After calibration, preliminary tests were carried out to evaluate the accuracy of the laser

measurements for distances ranging from 20 to 50 cm between the robot end effector and a test plate (see Figure 5.16). An accuracy of 1 mm on average, with a standard deviation of less than 0.4 mm, was obtained for the four lasers. The maximum angular deviation from the target plane is given by the following trigonometric relation (equation 5.1) where t is the laser tolerance, and s is the shortest distance between two lasers:

$$\alpha = \tan^{-1} \frac{t}{s} \quad (5.1)$$

In this setup, the lasers were positioned 21.5 cm apart. With a margin of error of 1.5 mm for the measurements, the maximum angular deviation between the computed plane and the plane of the target plate in the real world is only about 0.4 degrees. Therefore, with the help of the lasers, the robot can adjust its position to be almost entirely parallel to the panel before taking a picture of the marker. This ensures that the detection of the position and orientation of the ArUco markers will be within 2 mm for a picture taken at a distance of 50 cm, as shown in Figure 5.10.

A new command was created in our custom Unity application (see Section 5.4) to retrieve the average distance measured by each laser (d_1, d_2, d_3, d_4 in Figure 5.16) from the Raspberry Pi.

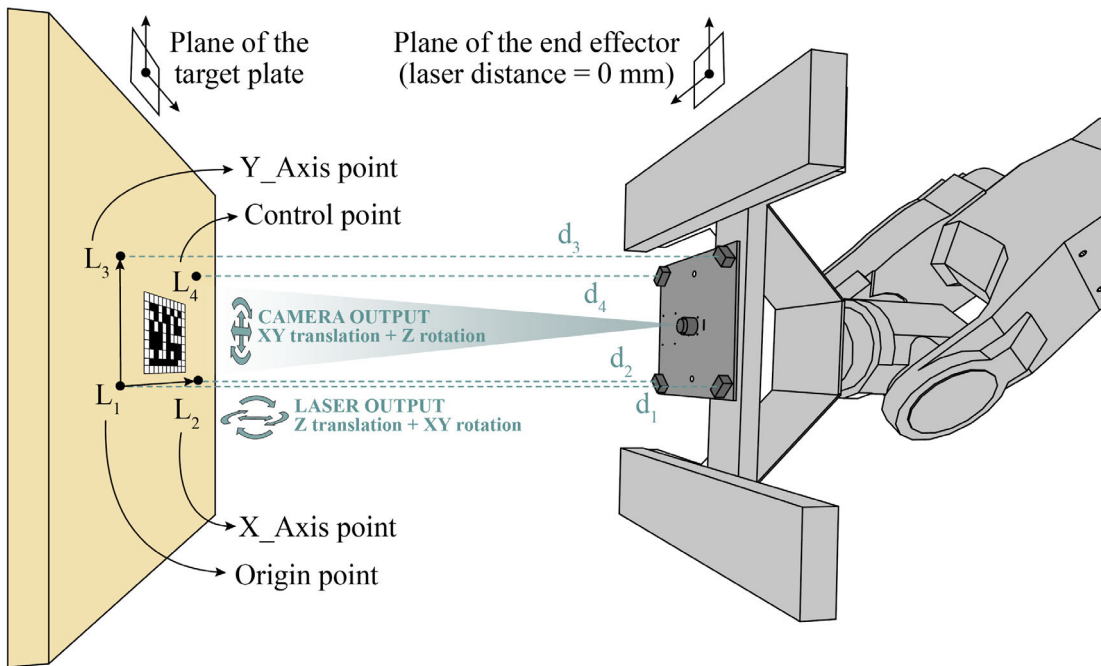


Figure 5.16: First, the four lasers are used to accurately adjust the distance to the target plate (Z translation) and to ensure the camera lens is parallel to the plane of the panel (XY rotation). Then a picture of the marker can be taken, and the image can be processed to find the center of the panel (XY translation) and its 2D orientation (Z rotation).

The target plane is then computed using the points L_1 , L_2 , and L_3 . If the position of point L_4 is more than 2 mm away from the generated plane, new values are requested. Otherwise, the robot will adjust its position to be parallel to the target plane.

5.8.2 Improving marker detection

CNC-engraved glyphs were also explored as an alternative to fiducial markers. The advantage is that engraving is faster and more precise than gluing markers after cutting the panels. However, detecting the orientation and position of a glyph is more complex than detecting conventional black-and-white markers. Therefore, a new image processing algorithm relying on the OpenCV library [Gar+14] was developed with the aim of detecting the edges of the engravings and retrieving the necessary information.

To ensure constant lighting condition, a standard flashlight was also attached next to the camera on the the robot end effector. After testing different glyph patterns for detection, it was determined that the most effective design should be composed of three elements, each encoding a distinct piece of information:

- An engraved square of 110x110 mm is used to compute the 2D orientation of the glyph (rotation of the robot end effector in the plane of the panel).
- An engraved circle with a radius of 65 mm is used to find the center of the glyph (translation of the robot end effector in the plane of the panel).
- Nine engraved crosses of 25x25 mm are used to determine the panel ID encoded as a binary number (from 0 to $2^9 - 1 = 511$).

The three following sections detail how each piece of information is retrieved from the glyph.

5.8.3 Detecting the square to compute glyph orientation

The algorithm's steps to compute the rotation angle are shown in Figure 5.17. First, the image is converted to black and white and slightly blurred using a Gaussian mask. Then, the contours are obtained using the Canny edge detector algorithm [Can86]. To maximize the chances of getting a valid result, the Canny filter is applied several times with different threshold parameters (Figure 5.18). Then, the lines are identified with the Line Hough Transform (LHT) function implemented in OpenCV. While lines are naturally present in the wood texture, those can be discarded based on their length to select only the marker lines (Figure 5.19). Next, the angle between the bottom edge of the source picture and each detected line is measured. Outliers are discarded, and the remaining values are averaged to obtain the rotation angle.

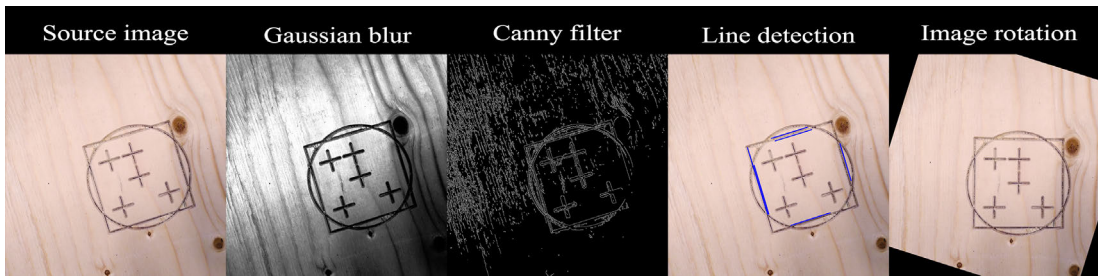


Figure 5.17: Computing the rotation angle by detecting the square in the engraved glyph.

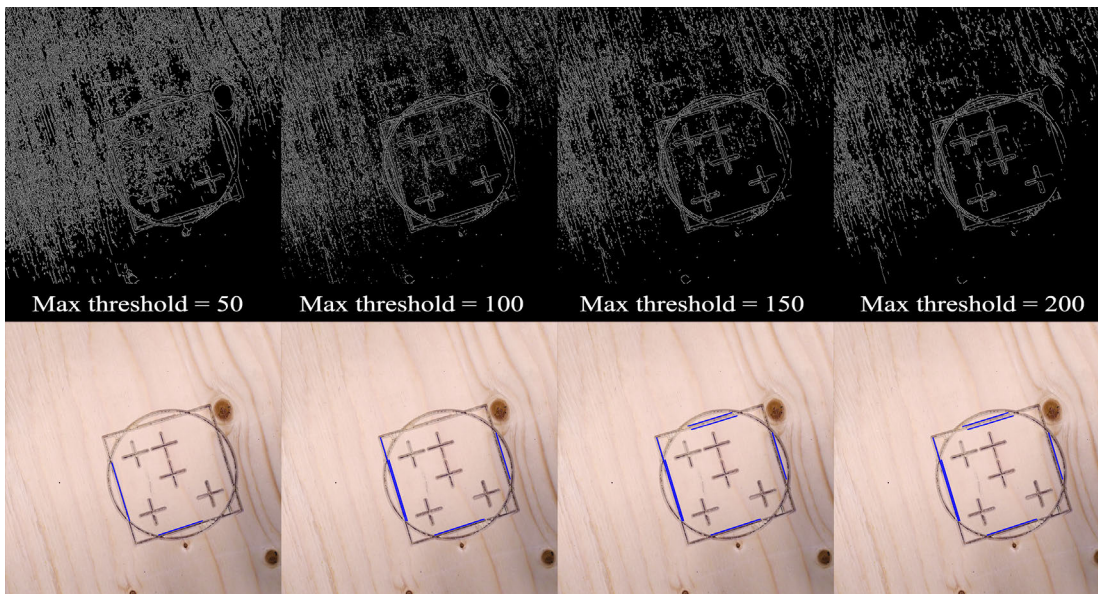


Figure 5.18: Varying the low and high threshold values of the intensity gradient of the Canny filter maximize the chances of getting the correct lines in the glyph image.

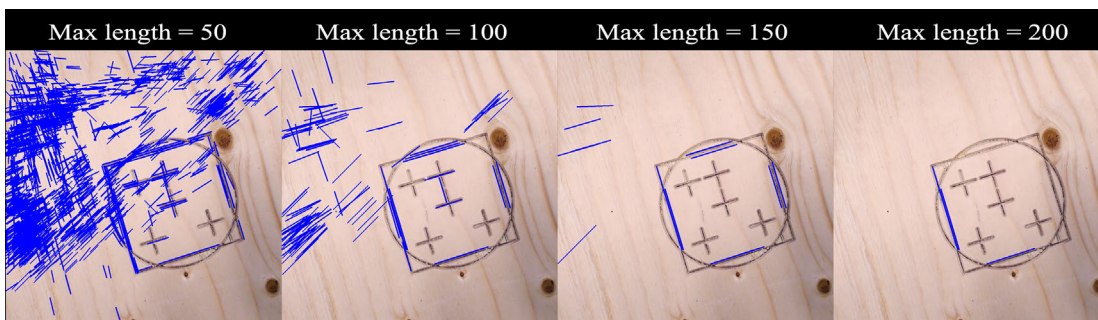


Figure 5.19: Only the longest detected lines are kept, allowing to discard the natural lines of the wood and only detect the edges of the marker.

5.8.4 Detecting the circle to compute glyph translation

As can be observed in Figures 5.18 and 5.19, it is not always possible to detect the four edges of the engraved square. As at least three edges of the square would be necessary to find the center

of the glyph, a more reliable method based on circle detection was preferred. The first idea was to drill a hole in the center of the glyph with a 2 cm diameter CNC milling bit. However, the presence of knots of 1 to 4 cm in diameter in the wood could have misled the detection algorithm. Therefore, it was decided to engrave a larger circle of 11 cm around the glyph.

Circle detection works similarly to line detection (Figure 5.20). However, this time the Canny filter is not required. The engravings are again emphasized by applying a Gaussian mask. Then, the circle is identified using a Circle Hough Transform (CHT) function implemented in OpenCV. The function gives the possibility to specify a minimal and maximal radius for the detection of the circle. Pictures are taken with a constant distance of 50 cm. This is ensured by the first part of the visual feedback loop, which relies on laser measurements to update the robot's position (See Section 5.8.1). Therefore, the size of the circle in the source image is also constant, which facilitates the detection. Next, the image translation (T_i) is obtained by measuring the distance between the circle's center and the image's center. Finally, the robot translation (T_r) can be computed by applying a correction factor equal to the ratio between the diameters of the circle engraved on the panel (d_p) and its image (d_i):

$$T_r = T_i * \frac{d_p}{d_i} \quad (5.2)$$

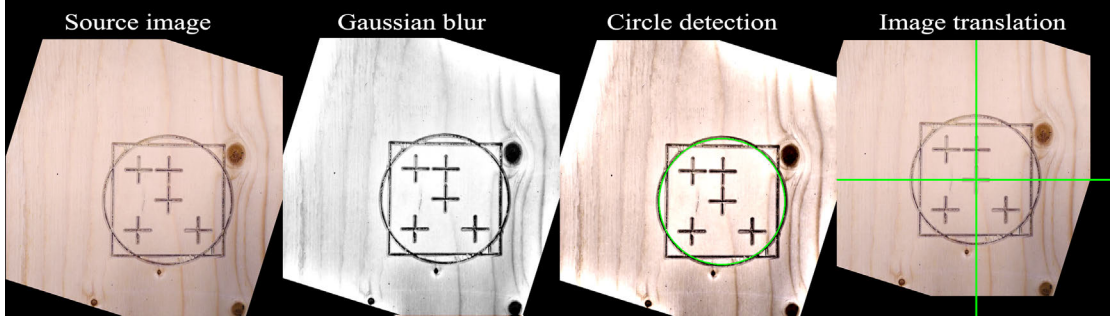


Figure 5.20: The center of the glyph is obtained by detecting the engraved circle.

5.8.5 Detecting crosses to compute glyph ID

The last information encoded in the glyph is the panel ID. Crosses were found to be the most effective to store this information. This symbol is only composed of orthogonal lines parallel to the square sides. Therefore, the lines of the crosses contribute to the detection of the glyph orientation described in section 5.8.3. Moreover, engraving this glyph with a CNC machine is fast, as only two lines are necessary for each cross.

The detection algorithm relies again on a Canny filter and the Line Hough Transform function of Open CV to detect the number of crosses present in the glyph (Figure 5.21). A different set

of threshold parameters is used to detect smaller lines than for the detection of the square. As the glyph orientation is already known, all lines that are not orthogonal within a tolerance of 5 degrees are discarded. The image is then segmented into nine squares based on the glyph dimensions. If lines are present inside a square, the algorithm adds a 1. Otherwise, it adds a 0. The panel ID is obtained by converting the nine digits binary number into the decimal system.

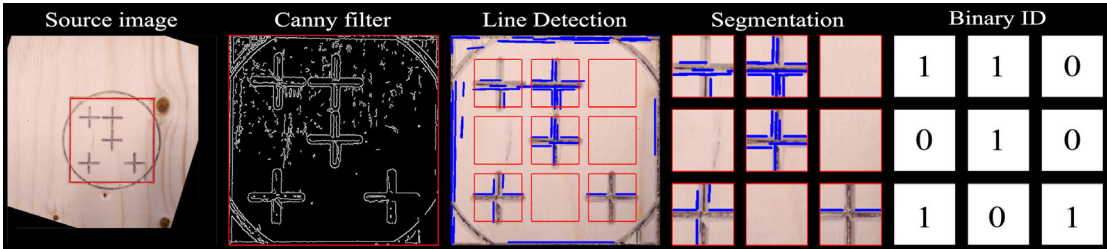


Figure 5.21: By detecting the presence of crosses in the glyph, the panel ID can be retrieved. The ID is stored as a binary number between 0 and 511 (in this example, the panel ID is $110010101 = 405$).

5.8.6 Conclusion

This additional piece of research completes the previous findings of the original paper. An updated version of the visual feedback loop is proposed to improve the performance of the marker detection. It highlights the interest of combining lasers and camera to precisely compute the six degrees of freedom of the spatial transformation. It also brings an alternative to glued markers, increasing the robustness of the methodology. The whole system described in this chapter allows the correction of the robot's position with an accuracy of about 2 mm when inserting the panels. The remaining tolerance is inherent to the model of the robotic arm, the different calibration processes and the dimensional variations of the wood panels. Consequently, the research presented in the next chapter focuses on adapting the shape of the joints to tackle this remaining tolerance and provide guidelines for robot-compatible connections.

6 Design considerations for robotically assembled through-tenon joints

The texts and figures presented in this section were reproduced from the postprint version of the following peer-reviewed paper available in open access:

Rogean, N., Gamarro, J., Latteur, P., & Weinand, Y. (2022). Design considerations for robotically assembled through-tenon timber joints. *Construction Robotics*, doi:10.1007/s41693-022-00080-5.

The doctoral candidate was responsible for the entire development of the scientific work as well as for the writing of the article. The second author was involved in supporting the development of the experimental activities and processing the data. The third and fourth authors of the paper contributed equally as scientific advisors and proofreaders.

6.1 Abstract

This research investigates the robotic assembly of timber structures connected by wood-wood connections. As the digitization of the timber construction sector progresses, digital tools, such as industrial robotic arms and Computer Numerical Control machines, are becoming increasingly accessible. The new-found ease with which wood can be processed stimulates a renewed interest in traditional joinery, where pieces are interlocked instead of being connected by additional metallic parts. Previous research established a computational workflow for the robotic assembly of timber plate structures connected by wood-wood connections. This paper focuses on determining the physical conditions that allow inserting through-tenon joints with a robot. The main challenge lies in minimizing the clearance between the tenon and the mortise in order to keep the connections as tight as possible. An experimental protocol has, therefore, been developed to quantitatively assess the performance of the insertion according to different geometric parameters. Robotic insertion tests have been carried out on over 50 samples of 39 mm Laminated Veneer Lumber. Results showed the advantage of tapering the joint with a 5 degrees angle, in addition to introducing an offset of 0.05 mm, to

minimize friction forces during the insertion. This configuration was confirmed by successfully assembling a 2,50 m long box girder with the same parameters.

6.2 Introduction

The digitization of the timber construction sector is one of the key factors in reducing buildings' embodied carbon and ultimately lower carbon emissions in the built environment [Rey+21]. In the last two decades, technological advances have enabled the spread of Computer Numerical Control (CNC) machines and engineered wood products such as Cross and Glued Laminated Timber (CLT and Glulam). Those innovations favor a return to wood construction after a century focusing mainly on two mineral materials: concrete and steel. Aside from environmental considerations, another main advantage of contemporary timber constructions lies in the ease of prefabrication relying on standardized elements. Indeed, this reduced construction time leads to cost-competitive solutions [HHT17].

However, many challenges remain for the sector to have the capacity to increase its market share largely covered by mineral materials, particularly with the expected growth in housing demand [Uni20]. Therefore, timber construction companies have started investigating the use of Industrial Robotic Arms (IRA) to automate part of their workflow and increase productivity. The main application is the robotic assembly of timber frame structures, as it is the most widespread timber construction system [Dan16]. Panels and studs are first placed on an inclined plane with a vacuum gripper equipped on the robot end effector. Then, the elements are fixed using a pneumatic nail gun (see Figure 6.1).

This research aims at proposing an alternative to standard timber frame structures by replacing the screws with through-tenon joints and the beams with largely available wood-engineered panels that can be more easily processed by a CNC machine [Ope]. This solution offers three advantages. First, it reduces the number of steps in the prefabrication process as the joints provide both a guide for the assembly and a means to connect the elements. Second, it decreases the embodied carbon of the construction system by avoiding metallic connectors [FM21]. Third, it increases the structural performance by geometrically interlocking the pieces through form closure [GBW20a; GBW20b].

However, inserting timber joints with a robotic arm is more complex than nailing, as tolerances are much smaller. Indeed, with too much clearance between the tenon and the mortise, the joint is loose, and it reduces the rigidity of the connection. On the other hand, too little clearance hinders the insertion of the joint, either partially or completely, as friction forces exceed the robot threshold. Therefore, this experimental study focuses on determining the adequate design for the geometry of the joints that would make the robotic insertion of through-tenon joints possible.

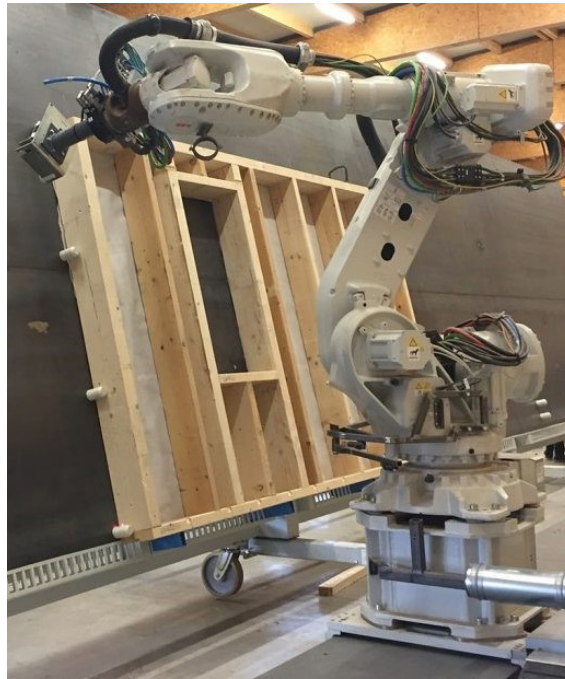


Figure 6.1: Robotic assembly of a timber frame structure (credit: IMAX Pro S.A., Belgium).

6.3 State of the Art

The problem of inserting one part into another with a robotic arm dates back to the early days of robotics. A classic example extensively covered in the literature is peg-in-hole insertion. Existing strategies generally rely on an initial robot trajectory that spirals around the hole [SZP18]. In addition, a force and torque sensor allows for adjusting the trajectory in real-time by comparing the data to a predetermined force pattern [Tan+16]. Most recent works also integrate reinforcement learning algorithms to improve the reliability of the insertion [GFB94]. However, the objects concerned are generally small, cylindrical, and smooth (made from metal or plastic). Conversely, timber pieces are large, with more complex geometries, and a relatively rough surface. It is, therefore, harder to predict and interpret the force patterns to correctly adjust the robot's trajectory.

Reinforcement learning and force sensors were also used by Apolinarska et al. to automate the insertion of half-lap joints [Apo+21b]. A virtual robot was first trained in simulation so that the real robot could learn how to compensate for translational and rotational offsets. Although the results were promising, tight-fitting joints with a clearance inferior to 1 mm could not be inserted due to the limitations of the setup. An alternative method for training a robot was also proposed by Kramberger et al. [Kra+22]. Relying on the principles of Learning from Demonstration (LfD), the robot was taught how to insert half-lap joints by first analyzing the motion and force pattern of hand-guided examples. Both training methods make the insertion more reliable by compensating for potential misalignment. However, it is still necessary to add a considerable amount of clearance to ensure the robotic insertion.

To eliminate gaps and overcome induced friction forces, Robeller et al. exploited the elastic properties of wood through snap-fit joints [Rob+17]. As those joints can bend slightly, it makes it possible to insert oversized tenons without requiring too much force. However, the experiments highlighted the difficulties of inserting several joints simultaneously. Despite the presence of a vibration device on the robot end effector, the sum of the resulting friction forces was too high, and the joints required manual hammering to be inserted. In addition, the bending properties of snap-fit joints are conditioned by their small cross-section, which considerably reduces the shear resistance of the connection.

Another strategy consists in increasing the force of the robot end effector. Remote-controlled robotic clamps were developed by Leung et al. for the insertion of half-lap joints [Leu+21]. The clamps can detach from the robot and synchronously apply a 3 kN force. The main advantage is that the strength or number of clamps can be increased to meet the required insertion force. However, the industrial implementation of this solution is constrained by the development of those specific pieces of hardware and by its limited application to timber beams connected by half-lap joints.

Most existing research on the topic has explored solutions based on software or hardware development. This paper proposes a more low-tech approach focusing on the joints themselves. A testing protocol to assess the performance of the robotic insertion is presented in Section 6.4. The results of the experiments on small and large samples are reported in section 6.5. Finally, the influence of the geometric parameters on the progression of friction forces is discussed in section 6.6.

6.4 Material and methods

6.4.1 Experimental set up

The experiments were all conducted with a 6-axis robotic arm (ABB 6400R/2.5-200) [ABB01] equipped with two vacuum grippers capable of lifting timber panels up to 200 kg for a maximum reach of 3 m. In addition, a custom testing setup was developed to measure the performance of the robotic insertion (see Figure 6.2). A concrete block covered with a dense timber board was used as a flat and stable base on which to execute the robotic assembly. A square corner enables the precise positioning of the male piece before it is picked by the robot while the female piece is clamped inside a reserved hollow socket. The position of both pieces relative to the robot frame is, therefore, known with a tolerance inferior to one millimeter.

To measure the reaction forces during the insertion, a 6-axis force/torque sensor (Schunk, FT Omega160) was attached to the robot end effector. Besides, two Linear Variable Differential Transformers (LVDT) were fixed on the male piece to measure the vertical displacement and report eventual rotations in the plane of the inserted piece. Finally, the presence of a cavity under the female piece should also be noted. This prevents any contact between the tenons and the support and avoids interfering reaction forces.

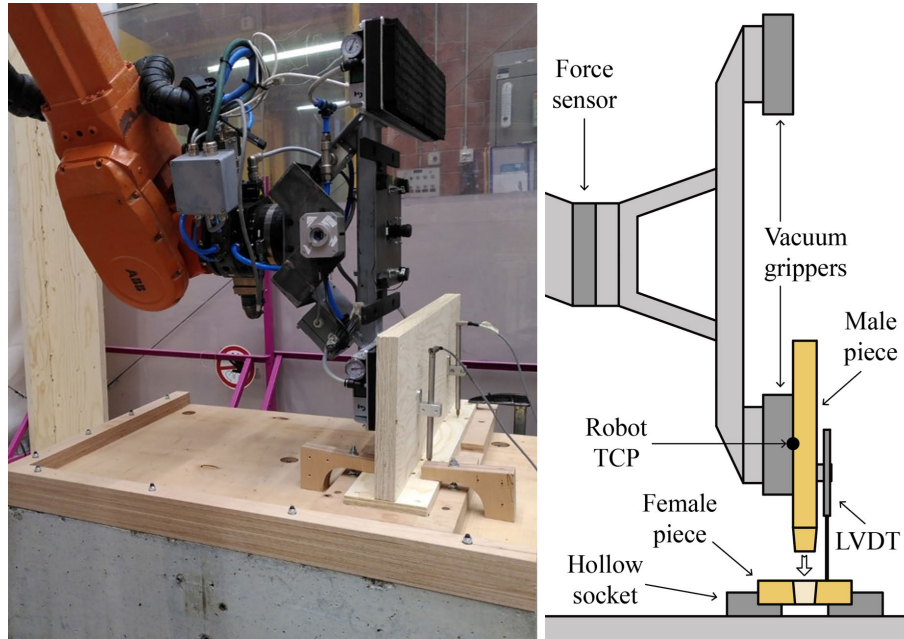


Figure 6.2: Custom setup developed to evaluate the insertion performance of the joints.

6.4.2 Experimental parameters

Fixed and variable experimental parameters are reported in Table 6.1 and represented in Figure 6.3. It was decided to work with 39 mm thick spruce Laminated Veneer Lumber (LVL) panels as this is a commonly used product in the timber construction sector. Its high strength-to-weight ratio makes it an ideal material for load-bearing applications, and one of the study's objectives was to get as close as possible to real industry conditions. However, to avoid wasting wood, the dimensions of the samples were kept to a minimum by matching the size of the robot end effector and performing the tests with only one vacuum gripper. Hardwood panels were not investigated in this research as they are less used in construction for now.

The robot speed was set to 1 mm/sec during the insertion. While this is relatively slow in comparison with industrial standards, this allowed a better assessment of the influence of the shape of the connections on the robotic insertion. Besides, by working at a reduced speed, we place ourselves in the most unfavorable case as we no longer benefit from the robot's acceleration when inserting the joint.

Regarding the parameters associated with the geometry of the mortises and the tenons, a length of 100 mm and a minimum distance of 50 mm from the edge of the board have been set for all joints. This follows the design guidelines provided by Gamarro et al. for orthogonal timber slabs connected by mortise and tenon joints [Gam20]. Therefore, the remaining variable parameters of the experimental campaign were the offset, the angle, the number of joints, and the size of the chamfer.

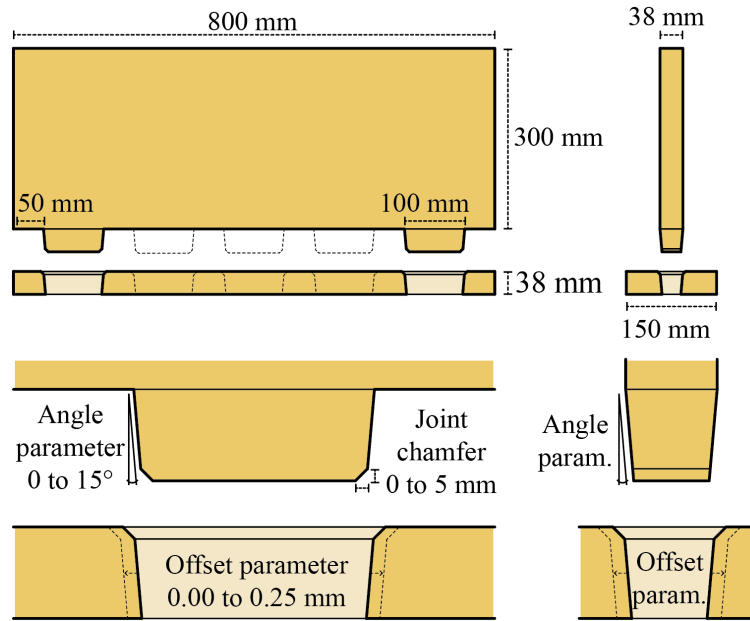


Figure 6.3: Geometric parameters for the male and female parts of the joints.

Table 6.1: Geometric parameters of the tested samples.

Fixed Parameters	
Panel material	Kerto® LVL Q-panel
Panel thickness	39 mm (13 plies)
Sample dimensions (male)	800 x 300 x 38 mm
Sample dimensions (female)	800 x 150 x 38 mm
Robotic insertion speed	1 mm/sec
Joint length	100 mm
Joint distance from the edge	50 mm
Variable Parameters	
Joint offset	0.00 to 0.25 mm
Joint angle	0 to 15 degrees
Joint number	2 to 5
Joint chamfer	0 to 5 mm

6.4.3 Fabrication of the samples

The geometry of the joints was parametrically generated using the grasshopper plugin Manis [Rog+22]. The plugin also allowed the generation of the fabrication files and the robotic trajectories for the subsequent insertion tests. All samples were then cut with a 5-axis CNC machine. However, only those with an angle parameter greater than 0 degrees actually required 5-axis machining, whereas 3-axis machining was sufficient for the other samples. In addition, the introduction of this bevel required milling the four faces of the tenons. This implies flipping the piece on the CNC table and repositioning them with a corner square

to mill the side of the tenon that was previously facing the table. Table 6.2 shows that the fabrication time for joints requiring 5-axis milling is increased by 30 to 40% compared to 3-axis. Calculations include both drilling and cutting steps. The time for flipping the pieces is also taken into account and was measured at 1 min per sample on average.

Table 6.2: Fabrication time in 3 and 5-axis according to the number of tenons.

Time (s)		Nbr Tenons			
		2	3	4	5
Nbr Axis	3	652	732	859	1050
	5	859	1057	1299	1490

Fabrication tolerance is one of the main challenges for the robotic insertion of timber joints. While our CNC is accurate to within 0.05 mm, irregularities in the interface between the martyr table and the panel can reduce the accuracy of the cut in the vertical axis to approximately 0.25 mm. The thickness of the panels can also vary by about 1 mm depending on production and storage conditions. Therefore, to compensate for material tolerances, the female pieces, as well as the tenons of the male pieces, were surfaced to 38 mm. To avoid potential dimensional variations induced by external factors, the pieces were assembled directly after being cut. Figure 6.4 summarizes the dimensional tolerances obtained after CNC machining.

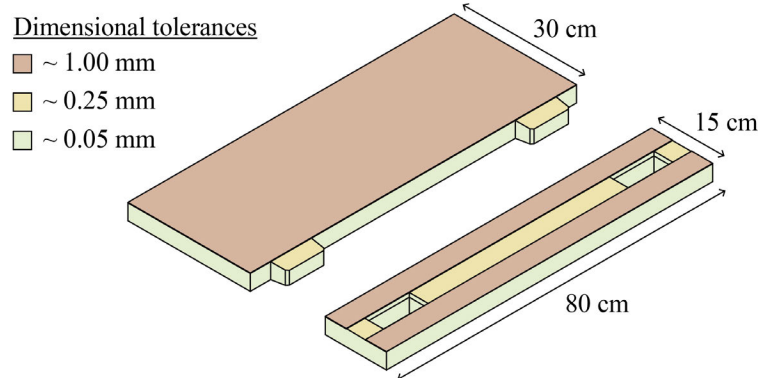


Figure 6.4: Variation of fabrication tolerance for the different faces of the male and female parts.

6.4.4 Experimental protocol

After fabrication, each sample was brought to the insertion table (Figure 6.5.1) and tested with the robotic arm. The male and female pieces were first positioned in their dedicated slots (Figure 6.5.2). Then, the male piece was lifted by the vacuum gripper (Figure 6.5.3) and rotated 38 mm above the female piece (Figure 6.5.4). Next, the two LVDTs were attached and centered on the most extreme tenons (Figure 6.5.5).

To compare the progression of the insertion for different samples, the precise height of the starting point of each test was measured. It was obtained by controlling the distance between the male and female pieces with each LVDT and averaging both values. In addition, using two distance sensors allowed for measuring the rotation of the male piece in its plane, which could reach up to 2 degrees. However, this variation remained negligible as the male piece would always align itself with the female piece during the insertion of the joints.

Before initiating the data recording, all sensors were reset, and the synchronization of the measurements between the force sensor and the LVDTs was ensured. Finally, the robotic insertion was started. In order to prevent the robot from stopping the insertion too early due to frictional forces, the final point of the robot path was shifted 5 mm lower for all tests. Once the insertion was completed (Figure 6.5.6), the male part was removed and reinserted two more times to investigate possible variations in the results. However, only the first insertion was considered for the final result. Taking into account the overall tolerances of the machining and panels, the insertion was considered complete if the tenon was at least 95% inserted into the mortise. This corresponds to a traveled distance of 36 mm out of the 38 mm of the total plate thickness. Complete insertions were also confirmed by visual inspection and manual measurement at the end of each test.

6.5 Results and discussion

38 different samples have been tested by following the experimental protocol described above. An overview of the entire testing campaign is given in Appendix A.5. The detailed results are further discussed in the next sections.

6.5.1 Offset parameter

The first experiments focused on studying the influence of the offset parameter (see Figure 6.3). The percentage of insertion and the maximum friction forces are reported respectively in Table 6.3 and 6.4. Detailed graphs are reported in Appendix A.6.1. In this configuration, the threshold force for the robot varies between 1700 N and 2100 N. Under 0.10 mm of offset, the robot detected a collision almost instantaneously. For 0.10 mm and 0.15 mm, the robot managed to insert the tenons about halfway through the mortise before the forces were too high. From 0.2 mm, recorded forces did not exceed 1500 N, and the insertion was fully achieved. However, with this amount of clearance, the joints were already considerably loose. It was observed that the pieces could rotate freely in a range of about 3 degrees leading to potentially large discrepancies during the assembly.

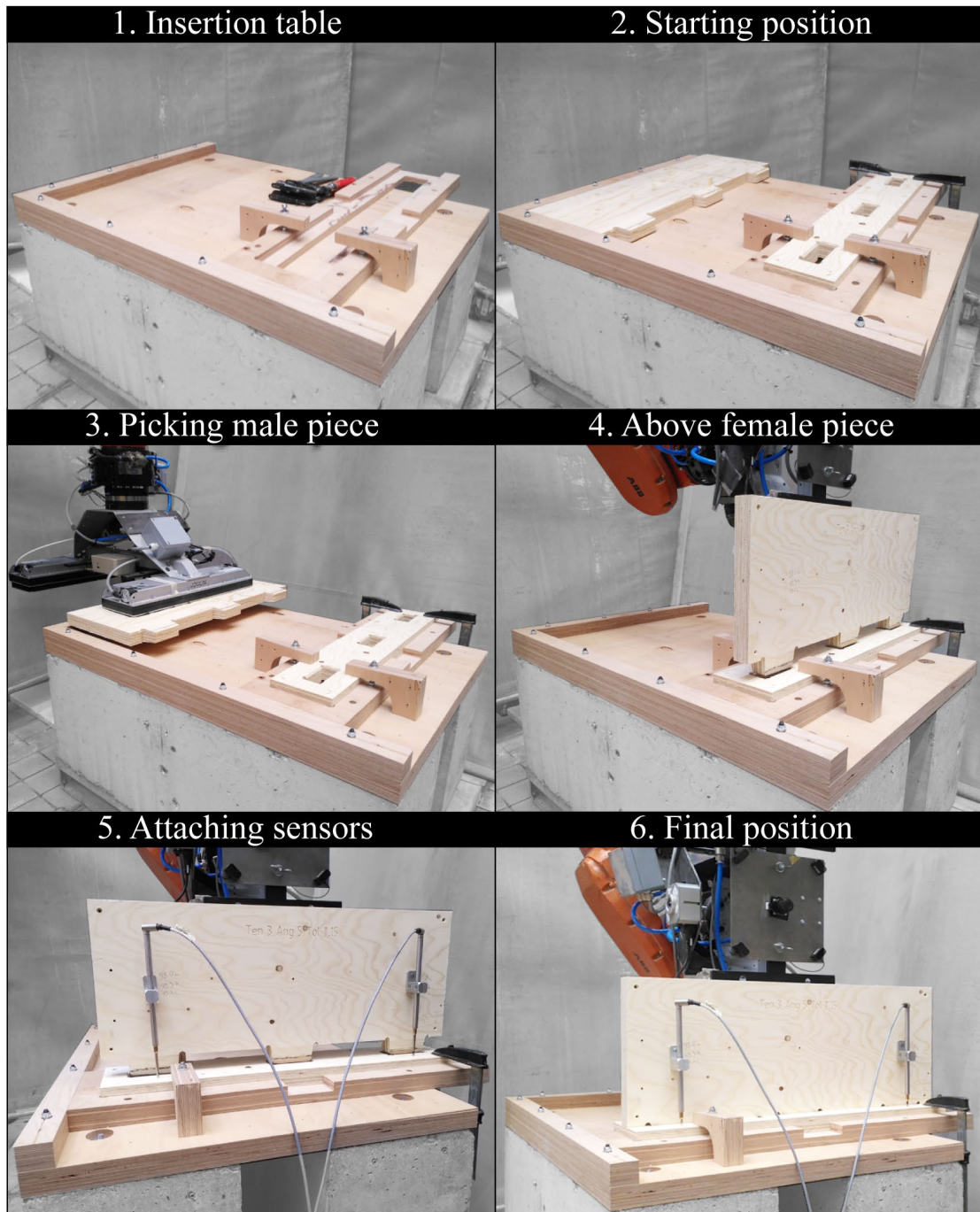


Figure 6.5: Procedure for testing each sample with the 6-axis robotic arm.

6.5.2 Chamfer and offset parameter

For the second batch of tests, the four edges of the mortises were chamfered over a distance of 5 mm (see Figure 6.3). This value was chosen based on previous research work showing that a chamfer of 5 mm at a 45 degrees angle was sufficient to compensate for robot positioning

Chapter 6. Design considerations for robotically assembled through-tenon joints

Table 6.3: Insertion completion as a function of the offset parameter and number of tenons. Orange cells represent samples with partial insertion while green cells represent fully inserted samples.

Insertion (%)		Nbr Tenons			
		2	3	4	5
Offset (mm)	0	1.06	-	-	-
	0.05	1.97	-	-	-
	0.10	3.59	74.45	51.73	46.30
	0.15	2.26	97.07	59.57	50.96
	0.20	97.74	97.96	97.51	96.19
	0.25	98.67	-	-	-

Table 6.4: Maximum load (F) as a function of the offset parameter and number of tenons.

F (N)		Nbr Tenons			
		2	3	4	5
Offset (mm)	0	1947	-	-	-
	0.05	1772	-	-	-
	0.10	2057	1997	2012	1721
	0.15	1888	1942	2035	2016
	0.20	1021	726	1005	1430
	0.25	824	-	-	-

errors [Rog+20]. In addition, a chamfer was applied on the tenon but only on the smaller sides, as shown in Figure 6.3. This removes the need to flip the tenon plate during fabrication in order to chamfer the side facing the CNC table. This new feature allowed the insertion of a 2-tenons plate with an offset parameter of 0.10 mm instead 0.20 mm (see Table 6.5). The chamfer reduces the risk of blocking situations and helps to guide the tenon into the mortise in case of initial misalignment. Figure 6.6 shows the linear progression of the frictional forces during the insertion with 0.05 mm and 0.10 mm of offset. For 0.05 mm, the robot stopped at about one-third of the mortise as it reached a force of 1800 N. For 0.10 mm, a first spike can be observed around 15%. This is where the tenon hit the chamfer before sliding into the mortise.

Table 6.5: Insertion completion and maximum load (F) as a function of the offset parameter with a chamfer of 5 by 5 mm.

Offset (mm)	Insertion (%)	F (N)
0.05	36.87	1754
0.10	95.53	933

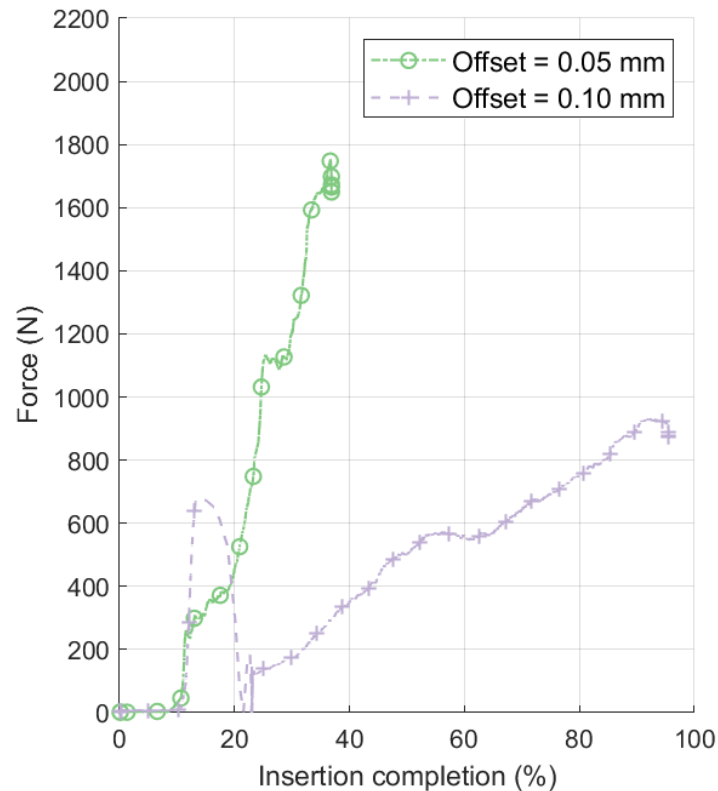


Figure 6.6: Influence of the offset parameter on the insertion of 2 tenons with a chamfer of 5 by 5 mm (angle parameter: 0 degree).

6.5.3 Angle parameter

While combining a 5 mm chamfer and 0.10 mm offset allows the insertion of a plate with two tenons, the required force increases with the number of tenons. To avoid introducing more clearance and loosening the connection, another solution based on the tapering of the joint was investigated (see angle parameters in Figure 6.3). Taper angles ranging from 1 to 15 degrees were applied on 4 faces of the tenons and the mortises. This required cutting the joints in 5-axis and flipping the tenon plate on the CNC table to mill the bottom face of the panel. This bevel angle has the advantage of minimizing friction during most of the insertion. Indeed, even with a small angle of 1 degree, forces rose only after 60% of insertion (see Figure 6.7). However, as the space between the mortise and the tenon shrinks until reaching 0 mm at 100% of insertion (see Figure 6.8), forces rise abruptly during the last millimeters. This prevented the robot from progressing further than 80 to 95% for all tested angles (see Table 6.6). Nevertheless, completely eliminating the clearance has the advantage of improving the rigidity of the connection compared to previous results obtained by varying the offset parameter. Finally, for an angle parameter larger than 5 degrees, no significant gain in the assembly insertion was achieved.

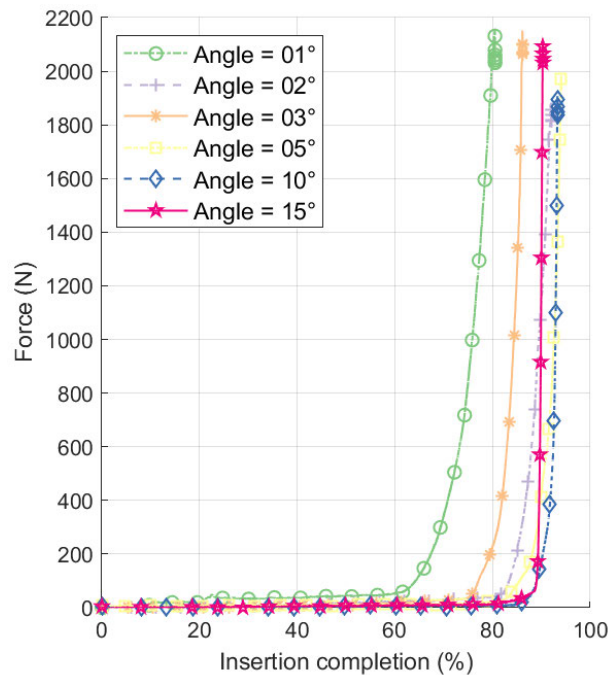


Figure 6.7: Influence of the angle parameter on the insertion of 2 tenons (offset parameter: 0 mm, chamfer: 5 by 5 mm).

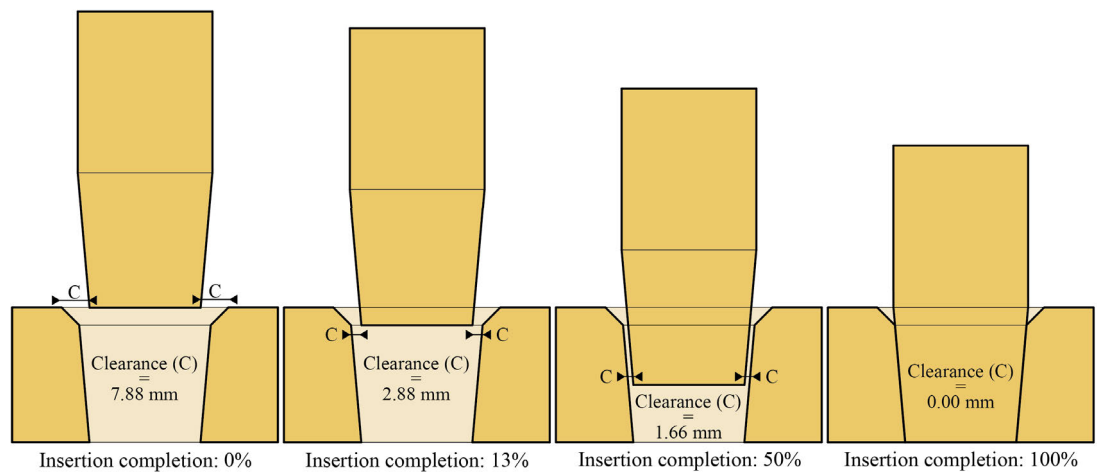


Figure 6.8: Progressive diminution of clearance for a bevel angle of 5 degrees without offset and with a chamfer of 5 by 5 mm. The clearance (C) is defined as the distance between the edges of the tenon and the internal faces of the mortise hole. The distance is measured perpendicularly to the vector of insertion.

Table 6.6: Insertion completion and maximum load (F) as a function of the angle parameter

Angle (°)	Insertion (%)	F (N)
1	80.52	2159
2	92.03	1883
3	86.18	2152
5	94.09	1984
10	93.33	1907
15	90.32	2111

6.5.4 Combined parameters

The bevel angle alone does not allow the full insertion of the joints. Therefore, we studied if combining the offset and angle parameters could solve this issue. The angle was set to 5 degrees for all tests as it scored best in the previous series. Results for the insertion of 2 to 5 tenons with an angle of 5 degrees and an offset of 0.05, 0.10, and 0.15 mm are shown in Table 6.7. Corresponding maximum forces are also reported in Table 6.8, and detailed graphs are available in Appendix A.6.2. We observed that only a minimal amount of offset is required as, with 0.05 mm, all tests were successfully inserted. Besides, the number of tenons no longer seems to affect the performance of the insertion. While for 5 tenons and 0.15 mm offset, the insertion was slightly under the threshold value, results for 0.05 mm and 0.10 mm showed that 5 tenons could be fully inserted with the same parameters as for 2, 3, and 4 tenons.

Table 6.7: Insertion completion as a function of the offset parameter and the number of tenons with an additional angle of 5 degrees.

		Nbr Tenons			
Insertion (%)		2	3	4	5
Offset (mm)	0	94.09	-	-	-
	0.05	96.12	96.16	95.76	95.69
	0.10	95.50	97.98	97.14	96.45
	0.15	97.66	97.48	95.58	93.31

Table 6.8: Maximum load (F) with an additional angle of 5 degrees.

		Nbr Tenons			
F (N)		2	3	4	5
Offset (mm)	0	1984	-	-	-
	0.05	1716	1850	1723	1850
	0.10	1716	1751	1666	1751
	0.15	1621	1613	1669	1873

6.5.5 Extrapolation to a box girder

Previous tests carried out on 80 cm long samples showed that an angle of 5 degrees and an offset of 0.05 mm enabled the robotic insertion of 2 to 5 tenons. To determine whether this would work for larger pieces, with a greater number of tenons, and for other robotic configurations, the assembly of a 250 cm long box girder was performed with the robot (see Figure 6.9). The girder was made out of two vertical webs and two horizontal flanges. Each panel was connected by 8 through-tenon joints with chamfers of 5 by 5 mm, an offset of 0.05 mm, and an angle of 5 degrees.

The position of the bottom flange was manually referenced in the robot space. Then, both webs were assembled following a similar protocol as for smaller samples. LVDTs were attached to the first and last tenons of the plate (Figure 6.9, left). For the top flange, the situation was different. First, mortises were inserted into the tenons instead of the opposite. Therefore, LVDTs were again attached to the webs and placed in the upward direction on opposite tenons (Figure 6.9, right). Second, the orientation of the reaction force compared to the vacuum gripper was changed from tangential to normal. Third, two plates needed to be inserted simultaneously.

Finally, while 8 and 16 joints needed to be simultaneously assembled for the webs and the top flange, respectively, the robotic insertion of the three plates was successful. We noted that, in this configuration, measured forces could reach 3000 N without triggering collision detection. This is because the robot is working at a closer range and can, therefore, take higher loads. However, as the last part of the insertion curves in Figure 6.10 is almost vertical, the effective insertion of each plate actually required about half of the maximum force.

6.6 Conclusion

This experimental study allowed the identification of optimal design parameters for through-tenon joints assembled by a robotic arm. The main issue at stake consisted in finding a balance between the rigidity of the connections and the ease of assembly for the robot. The augmentation of the required force when assembling multiple joints simultaneously was considered a major challenge in previous research work. Standard industrial robotic arms are indeed quite limited in the force they can apply before detecting a collision. The tests carried out allowed the development of a precise protocol to compare the insertion performance for different geometric parameters quantitatively. This included the influence of 3-axis offset and 5-axis bevel angles, as well as the presence of chamfers.

The results indicate that the offset parameter alone considerably reduces the rigidity of the connections. Nevertheless, it has the advantage of keeping the manufacturing process in 3-axis, which might be appreciated in smaller industries where 5-axis cutting is not always available. In such case, our experiments show that, between 2 and 5 tenons, an offset of at least 0.2 mm should be applied to ensure the robotic assembly. However, this number could

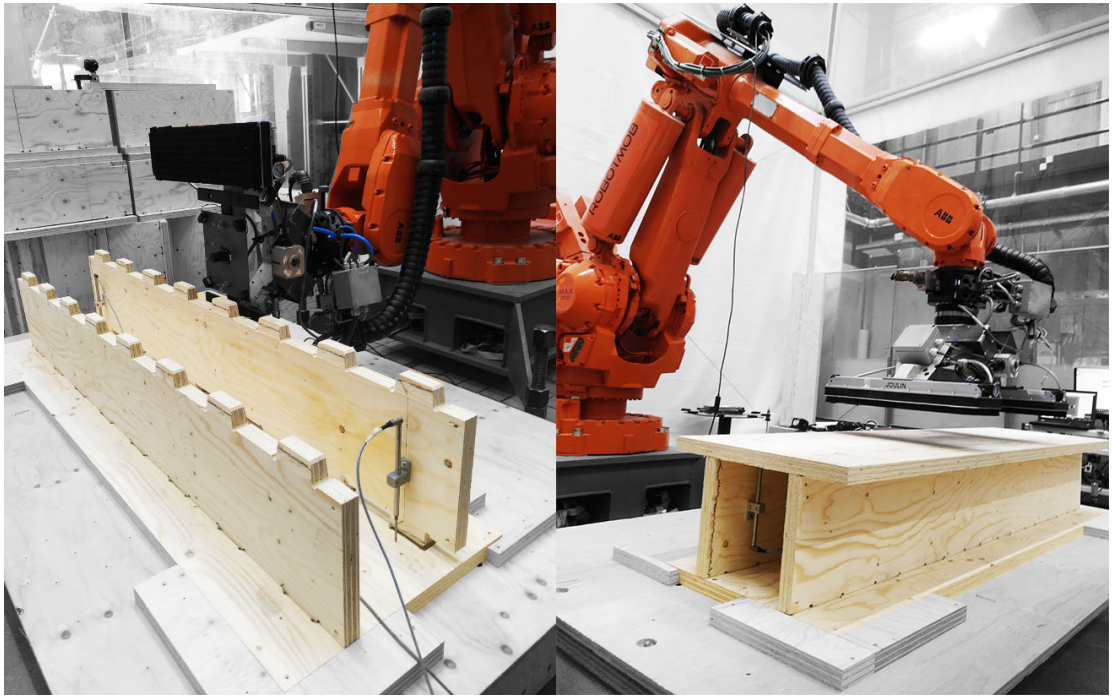


Figure 6.9: Robotic assembly of a box girder. The four plates are connected by eight through-tenon joints each.

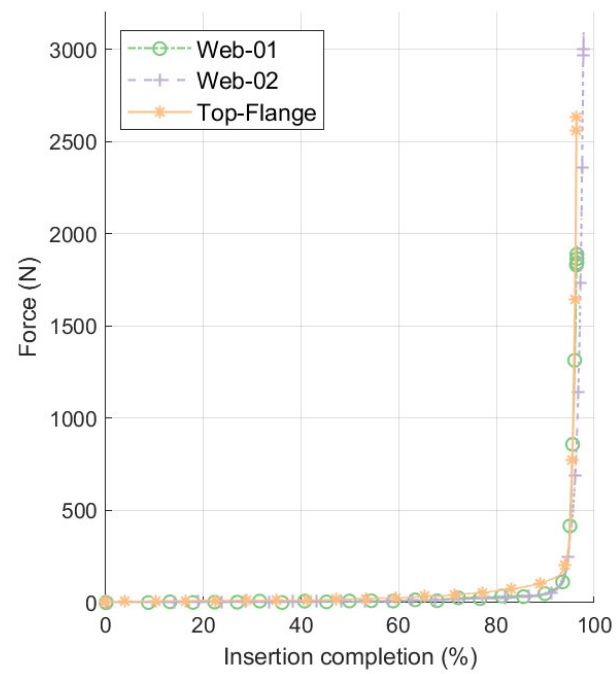


Figure 6.10: Successful insertion of the three elements of the box girder.

Chapter 6. Design considerations for robotically assembled through-tenon joints

be revised upward for an increasing number of tenons as the reaction forces could increase with the number of tenons.

Specific CNC milling bits with a 45 degrees angle can also be used to chamfer the edges of the joint while remaining in 3-axis. A 5 by 5 mm chamfer will reduce blocking situations and help to guide the tenon inside the mortise. It makes it possible to insert two tenons with an offset of only 0.10 mm.

To insert a wide configuration of tenons without loosening the connection too much, we investigated the tapering of the joints in 5-axis. We demonstrated that the offset parameters could be reduced to 0.05 mm by combining a bevel angle of 5 degrees and a chamfer of 5 mm. The conic shape eliminates friction forces during most of the insertion and ultimately reduces the clearance. The assembly of a 2.5 m long box girder, with up to 16 joints that needed to be assembled simultaneously, confirmed that this combination of parameters was optimal for the robotic assembly of large-scale timber plate structures.

Further investigations would be needed to extend the design guidelines depending on the types of panels, wood species, and the size of the elements. While the current study focused on the insertion of spruce LVL panels, it is expected that the resulting friction forces will differ for Cross-Laminated Timber (CLT) and Oriented Strand Board (OSB) panels which are also commonly used in construction. The choice of panel types and tree species will influence the texture and hardness of the wood. Using a softer wood will tend to increase the tolerance and facilitate the insertion. Similarly, smooth surfaces will more easily slide against each other. A quantitative analysis of these phenomena would, therefore, be an interesting complement to this research.

Furthermore, the influence of humidity and temperature on the joints has been excluded from the study so far. As the samples were assembled with the robotic arm right after being cut with the CNC, potential deformations due to those environmental factors could be neglected. However, future research could focus on assessing the validity of the findings if the samples were affected by dimensional variations. Hygroscopic swelling could also be exploited by performing the robotic insertion with a low humidity level and letting the joints expand subsequently to increase the rigidity of the connections naturally.

To conclude, this research paves the way for the automated assembly of structures connected by wooden joints. It provides an alternative to existing nailing and gluing methods for timber framing. While further research needs to be carried out to extend this technique to industrial processes and assess its performance, the establishment of design guidelines and the development of a testing methodology is a substantial achievement toward its application to real case studies.

6.7 Acknowledgments

This research was supported by the NCCR Digital Fabrication, funded by the Swiss National Science Foundation (NCCR Digital Fabrication Agreement #51NF40-141853). In addition, the authors would like to thank François Perrin, Frédérique Dubugnon, Gilles Guignet, and Jonathan Martin from the Structural Engineering Platform at EPFL for their involvement in the development of the testing setup.

Conclusion and outlook **Part IV**

7 Research output

7.1 Summary of research achievements

7.1.1 Computational design framework

The first part of the research (Chapters 3 and 4) focused on the development of a computational framework for the design of IATPS. A significant achievement concerns the establishment of a general approach to the design of IATPS, as opposed to existing project-specific workflows. This was attained by compiling the set of all possible contact situations between two panels and proposing a topological classification for IATPS. This harmonization effort was continued with the analytical parameterization of four types of timber joints. As a result, mathematical equations have been derived and can be easily implemented in any software to compute the 3D geometry of those joints.

Furthermore, the research also addressed the complexity of the insertion constraints associated with modular assembly sequences. An innovative method relying on graph theory and the geometric intersection of insertion domains has been introduced. It extends the capacity of existing algorithms by allowing the computation of compatible insertion vectors for cases where several plates need to be assembled simultaneously.

Another achievement lies in generating and simulating robot trajectories directly inside the design interface. A method for generating robot trajectories from the vectors of insertion associated with each panel has been presented. Besides, a real-time simulation of the robot moves in Grasshopper using the open-source plugin Robots has been introduced. A streamlined data exchange process has also been established between Grasshopper and Unity to enable connection with the workflow of an existing timber construction company. This work demonstrated the ability of the developed framework to adapt to the industrial context. Ultimately, all those achievements give the possibility to design IATPS while taking robotic constraints into account.

Results from previous IBOIS theses on the digital fabrication and structural analysis of IATPS

were also integrated into the workflow. Building upon the works of Dr. Hani Buri, Dr. Christopher Robeller, and Dr. Petras Vestartas, it is now possible to generate, simulate, and export CNC toolpaths from Grasshopper. In addition, a collaboration with Dr. Aryan Rezaei Rad led to the implementation of a feedback loop to automatically assess the structural performance of IATPS. The solver relies on the COMPAS framework to perform a Finite Element analysis and display the results directly in Grasshopper.

7.1.2 Automated Construction workflow

The second part of the research (Chapters 5 and 6) focused on tackling the challenges associated with the robotic assembly of IATPS. One achievement of the research lies in the successful collaboration with an industrial partner to develop a streamlined workflow from computational design to robotic construction. A custom programming language was implemented to facilitate communication with the robot controller and could be transposed to other cases of robotic prefabrication. Besides, several prototypes have been assembled with an industrial 6-axis robotic arm, highlighting two significant challenges of the robotic insertion of timber joints: precision and friction.

Consequently, another research achievement lies in the enhancement of the robot's precision through the development of a visual feedback loop. Computer vision algorithms were implemented to detect fiducial markers located on timber plates. This allows updating the position of inserted panels before inserting the following panels. Further research also demonstrated the benefit of combining laser range sensors with a camera to improve the accuracy of the results obtained through image processing.

Regarding the challenge posed by friction forces, the research achieved the introduction of design guidelines for through-tenon joints that minimize reaction forces during the robotic assembly while maximizing the structural performance. A series of experiments allowed the determination of optimal clearance parameters. The robotic assembly of a 2,5 m box girder demonstrated that following those guidelines enables the insertion of many joints simultaneously.

7.2 Impact of the research

7.2.1 Impact on the design team

One of the major outcomes of this thesis is the publication of a Grasshopper plugin for IATPS. This interactive design tool makes IATPS more accessible to designers, architects, and engineers. It allows them to integrate fabrication, assembly, and engineering considerations in the design process. Besides, the tool is not limited to one structural topology (e.g., vaults, walls, slabs,...). It can be used for a wide variety of applications as long as the initial design consists of an assembly of timber panels.

The developed tool proposes a paradigm change in the design of timber structures. Two approaches can be currently distinguished in practice. On the one hand, modular prefabrication strategies focus on a standardized catalog of modules that are assembled following a repetitive process. On the other hand, bespoke architectural projects require custom geometric algorithms and fabrication techniques. With this thesis, a hybrid "*system-based*" approach is proposed by taking advantage of the geometric properties of IATPS. The advantage is that custom architectural projects can be designed while relying on a fully automated workflow that simplifies construction logistics (Figure 7.1).

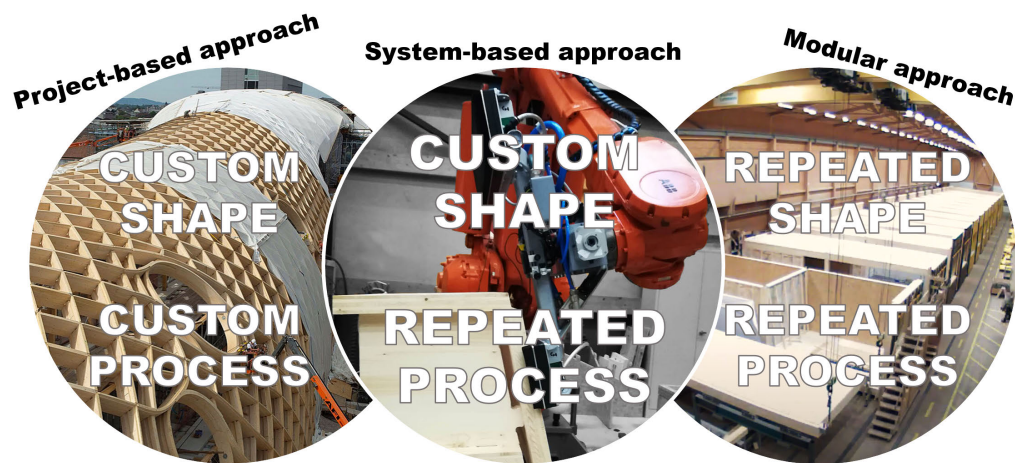


Figure 7.1: Using the developed tool, custom IATPS can be built with a fully automated process combining the advantages of modular prefabrication and bespoke architecture. (Credits for left and right pictures: Blumer Lehmann AG).

Furthermore, as discussed partially in chapter 4, the framework facilitates collaboration between architects and engineers by reuniting the different aspects associated with the project's constructability directly inside the design interface. While conventional design processes usually require frequent back and forth between engineers and architects, the developed tool gives the possibility to discuss and negotiate the different design parameters to satisfy fabrication, assembly, and structural constraints. From a broader perspective, the research demonstrates that system-based approaches have the potential to increase collaboration and efficiency through the development of integrated design interfaces.

Lastly, the developed tool could also be used by non-experts for the creation of smaller timber structures such as self-built houses or furniture pieces. The intuitive interface fosters the democratization of the design process by facilitating the 3D modeling of the connections and automating the generation of fabrication and assembly instructions. Taking examples from the models developed by Wikihouse [Ope] in England, EMARF [VUI] in Japan, or iWood.care [iwo] in Switzerland, the cutting of the pieces could be handled by a distributed network of manufacturers. In conclusion, this research impacts wood construction on all scales, from domestic furniture to the realization of large spatial structures, and can engage both the novice maker and the experienced practitioner.

7.2.2 Impact on timber construction companies

While the first part of the thesis focused on the computational design of IATPS, the second part focused on the challenge of automating their construction. Timber construction companies will likely benefit more from the outcomes of this second part. More specifically, this research paved the way for implementing production chains where panels are assembled solely through interlocking. This would simplify construction logistics by removing gluing and screwing steps.

The research demonstrated the feasibility of inserting timber panels into each other with a robotic arm. However, it also highlighted the need to adapt the connections' shape in consequence and equip the robot with feedback loops to reach enough precision. In addition, design guidelines that describe optimal clearance parameters have been established and could be easily implemented by timber construction companies interested in using timber joints.

Similarly, the results obtained through the development of the visual feedback loop have a high potential for industrial applications. The combination of cameras and lasers explored in this thesis is an efficient solution to increase the accuracy of a robotic arm at a low cost. The research on the detection of engraved markers also has promising applications that extend beyond the field of automated assembly. While further developments are required, the technique could be used to embed more data into a construction element than just its location in space.

7.2.3 Impact on society

As stated in the introduction of this dissertation, increasing the use of timber in buildings has the potential to reduce the environmental footprint of the construction sector. Furthermore, digitization is a key to making timber construction more efficient and competitive. The chair of Sustainable Construction at ETH Zurich identified four categories of interventions related to the potential of digital fabrication, computational design, and construction automation to build more sustainably [AH16]:

- Enriching structures with additional functions (thermal, acoustic...)
- Making construction processes more efficient
- Reducing materials quantity
- Fostering the use of more sustainable materials (reused, bio-based)

As far as sustainability is concerned, the impact of the thesis aligns with the last three categories of interventions. First, automating the assembly of IATPS with a robotic arm increases the efficiency of the construction process. Second, facilitating the use of timber joints reduces the quantity of steel needed for the connections. Third, making available an intuitive design-to-construction workflow for IATPS encourages the use of this construction system and, more broadly, the use of wood as a building material.

The energy consumption of the CNC and robot used in this research has yet to be quantified and should be considered for a proper life cycle assessment of IATPS. However, studies have shown that the environmental impact of digital fabrication technologies is almost negligible compared to the production of building materials [AH16]. Therefore, in this thesis, digitization is regarded as a means to spread the use of low embodied-energy materials, contributing significantly to improving construction sustainability.

7.2.4 Impact on architectural education

The developed tool also has an educational vocation. The plugin *Manis* was tested by architecture students at EPFL and in a workshop at the 2022 CAADRIA conference in Sydney. Some structures designed by the participants are shown in Appendix A.3. It was concluded from user feedback that the tool was intuitive enough to be adopted by beginners in parametric design. Moreover, the tool has been used for very different projects in terms of scale and topology, demonstrating the wide range of potential applications of this research.

At a broader level, this research contributes to reinstating fabrication and assembly issues at the heart of architectural education. Although construction principles were once central to the design process, technological advances in the 20th century have favored the emergence of strong architectural shapes often detached from building considerations. However, the challenges of the 21st century require us to rethink not only how we build but also how we design and teach architecture. To create a more sustainable environment, it is necessary to develop a more holistic approach integrating logistics aspects within the design process and considering the entire life cycle of architectural projects.

Besides, computational tools like the one introduced in this thesis provide students with means of dealing with the growing complexity of architectural projects. More generally, developing a computational mindset in the architecture cursus is essential to foster systems thinking and move away from traditional linear workflows. Furthermore, as for practitioners, this tool encourages students to adopt an interdisciplinary approach by bridging the gap between disciplines and bringing knowledge from different fields into the design interface.

8 Research outlook

8.1 Limitations and future research needs

8.1.1 Computational design framework

This research focused on expanding the scope of IATPS and assumed that the structures considered were exclusively composed of panels. However, concomitant research carried out at IBOIS by Petras Vestartas on the digital fabrication of round wood structures showed many similarities between panels, beams, and logs regarding the parametrization of the connections. Therefore, it is possible to consider a generalization of the methods developed in this thesis to other building elements and other connection types. First, the automated 3D modeling of timber joints could be extended to any geometry of wood pieces. Second, it would be interesting to study how the algorithms developed to solve assembly constraints for IATPS could be used to optimize construction logistics for more standard construction systems.

Another limitation of the computational framework is its dependency on the Rhinoceros-Grasshopper environment. This restricts the use of the plugin to a specific piece of CAD software. Furthermore, there is a considerable risk that future program updates will make the plugin obsolete in the long term. Although it is conceivable to transpose the algorithms to another software, future research could also focus on establishing an independent solution relying entirely on open-source libraries.

The current framework places the responsibility on users to adjust the various design parameters until the structure satisfies architectural, fabrication, assembly, and engineering requirements. Although this gives a lot of design freedom, going through this iterative process may take a long time, especially for large structures with many different pieces. Therefore, it would be interesting to investigate the implementation of a multi-criteria optimization tool to assist users in the design phase. As a first step, assembly sequences could be computed by automating the trial and error process instead of requiring input from the user. As a second step, optimal assembly sequences that ensure structural stability during all construction phases could be investigated. In this regard, it would be relevant to complete the developed frame-

work with an algorithm that can compute self-supporting assemblies, such as introduced in [Wan21].

Moreover, the generation of robotic trajectories could benefit from recent research in robotic path planning to reach a fully automated workflow. For example, the current algorithm could be enhanced with a collision solver to optimize robot trajectories and automatically compute a suitable path. This particular issue has notably been addressed in the thesis and publications of Yijiang Huang [Hua18; Hua+21]. However, further research is needed to facilitate the generation of robotic trajectories for non-expert users.

8.1.2 Automated Construction workflow

Although this thesis demonstrated the feasibility of assembling IATPS with a robotic arm, it also highlighted challenges that should be addressed in future research. First, robotic assembly experiments carried out in chapter 4 and 5 have shown the difficulty of inserting panels when the insertion force is not perpendicular to the ground. While temporary supports can help provide a sufficient reaction force, another option would be to use a second robotic arm to hold the pieces during the insertion. Cooperative robots were notably used in Stefana Parascho's thesis to assemble structures made from welded steel tubes [Par19]. A similar setup could be developed for IATPS. One challenge would lie in accurately synchronizing and calibrating the robots. Motion planning algorithms, such as Choreo [HGM18], should also be investigated to avoid collisions between the robots and the panels.

The experiments in chapter 6 have also emphasized that the force required to insert tight-fit timber joints quickly reaches the force threshold of standard industrial robotic arms. Therefore, although this thesis has introduced guidelines about the amount of clearance required for the robotic assembly of IATPS, another solution would consist in increasing the robot's force. For example, this could be achieved by adding a jackhammer on the robot end effector to provide additional pulses during the insertion of the joints. Christopher Robeller et al. [Rob+17] also explored the use of a vibrating device as a solution to overcome friction forces. As promising results were obtained with oversized tenons, this should be further investigated.

Future research could also focus on further developing feedback loops to assist the robotic insertion. In addition to the visual detection of fiducial markers through computer vision, haptic sensors could be coupled with deep learning algorithms, such as those introduced in [Apo+21b; Kra+22; Ode+19] to facilitate the insertion of the joints. Machine learning techniques could also be employed with a camera tracking system to locate timber panels around the robot and remove the need for any marker. Moreover, further work is necessary to combine the results obtained in Chapter 5 and 6. Future robotic insertion experiments should integrate both the visual feedback loop and the optimized joint shape.

8.2 Perspectives for robotic timber construction

To place this thesis in a broader context, it is first necessary to recall that it was funded by the National Center of Competence in Research Digital Fabrication (NCCR DFAB), supported by the Swiss National Science Foundation (SNSF). The NCCR DFAB is a cross-disciplinary research initiative aiming to accelerate the integration of digital technologies in the Architecture, Engineering, and Construction (AEC) sector. Since its launch in 2014, more than a hundred researchers from various disciplines have collaborated through different research clusters to move forward on this issue. This research is part of the cluster "*Spatial Timber Assemblies*", which tackles the development of computational design, digital fabrication, and robotic assembly strategies for timber structures composed of beams and panels.

In June 2022, the NCCR DFAB entered its third and final funding period, focusing on defining a straightforward approach to feasible research implementations and ensuring innovation transfer into practice. While the short-term prospects of the research have already been raised in the previous sections of this chapter, the longer-term prospects for further digitizing the timber construction sector are discussed here. Considering ongoing works at the NCCR DFAB and other leading research centers in the field (e.g., IntCDC in Stuttgart, IAAC in Barcelona...), two significant trends can be distinguished. The first prospect consists in moving toward automated on-site construction, while the second consists in moving toward human-robot collaboration.

8.2.1 Toward automated on-site construction

Automating on-site construction has several benefits, such as reducing the risk of accidents, increasing building precision and efficiency, and reducing the risk of errors and associated material waste. Mobile robotic platforms have been developed by several research institutes [Wag+20b; Gif+17]. Well-known applications consist in stacking bricks or stones for autonomous wall construction. However, as wood is particularly adapted to off-site prefabrication, there is currently limited research on automating timber structure assembly on-site. Working in a closed and controlled environment offers many advantages. However, performing the assembly on-site simplifies the logistics as flat-packed construction elements can be transported instead of larger modules. Besides, it avoids the need to segment the buildings into smaller parts that can fit the width of a standard truck and allow a single continuous assembly sequence.

Therefore, future research could expand upon the processes described in this thesis to tackle the robotic assembly of IATPS on-site. This will not necessarily involve standard industrial robots, like the one used in this thesis, but more likely automated cranes and gantries with a more extensive range. For more accessibility on the construction site, a robotic manipulator could also be coupled with an elevating work platform. A significant challenge is that working sites are unpredictable environments that may be difficult for robots to navigate. Consequently, efficient haptic and visual feedback loops must be developed to allow for more tolerance

during assembly.

8.2.2 Toward human-robot collaboration

The progressive automation of the timber construction sector questions the place and role of human workers. The development of automated construction chains has led to a reduction of 25% in employment in wood products manufacturing between 2000 and 2020 in Europe [Eur20]. Meanwhile, round and sawn wood production increased respectively by 21% and 11% [Eur20]. Overall, the number of small companies has also significantly decreased in favor of larger companies capable of investing in the digital transition.

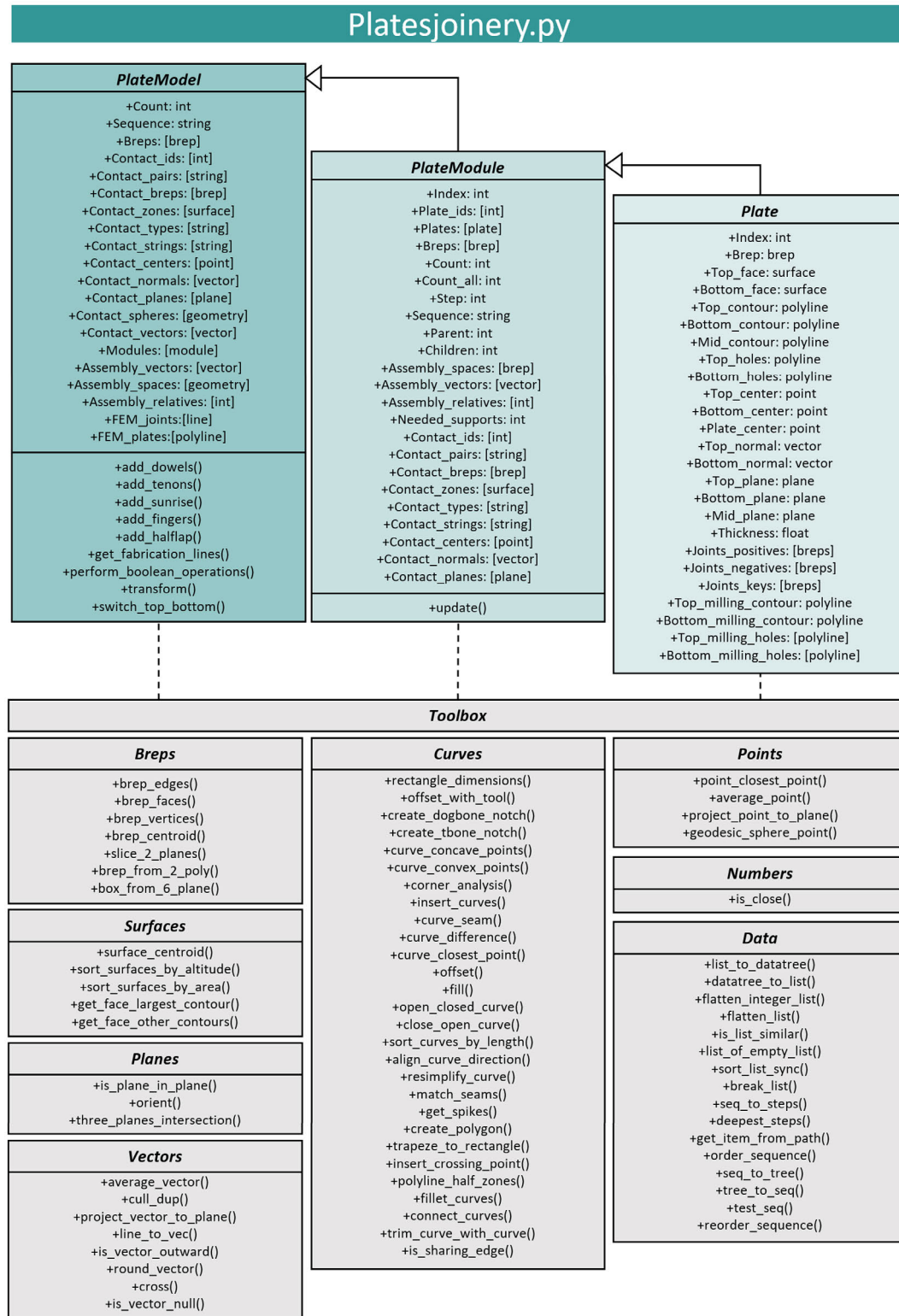
However, the lack of flexibility in fully automated solutions has led to the reintroduction of more manual work alongside robotic chains. In addition, the inherent variability of architectural projects demands a certain level of adaptability, which usually requires human intervention. Therefore, researchers and industries are increasingly investigating how robots and humans can collaborate in the same work environment.

Human-robot collaboration can take multiple forms and operate at different levels (from working asynchronously to working together on the same task) [Mat+19]. For example, a worker can teach a robot to perform a task using hand guidance functions. A robot can also be equipped with sensors to slow down when a person approaches, enabling the worker to work safely in the same space. Augmented-Reality (AR) devices are also becoming increasingly popular in assisting workers in assembling or stacking structural elements. In this situation, the worker is at the center of the action, and the machine helps him by providing visual guidance.

While this thesis focused on developing a fully automated robotic solution, the challenges raised in the previous sections suggest that human intervention could also be beneficial for assembling IATPS. For example, the vector of insertions of the pieces could be displayed through an AR headset to guide workers during the assembly. In addition, providing the exact direction for the insertion would reduce friction forces and make it easier to insert the panels.

A Appendix

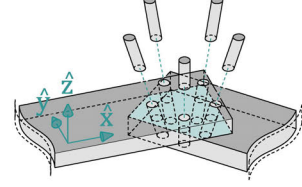
A.1 UML diagram of the joinery solver



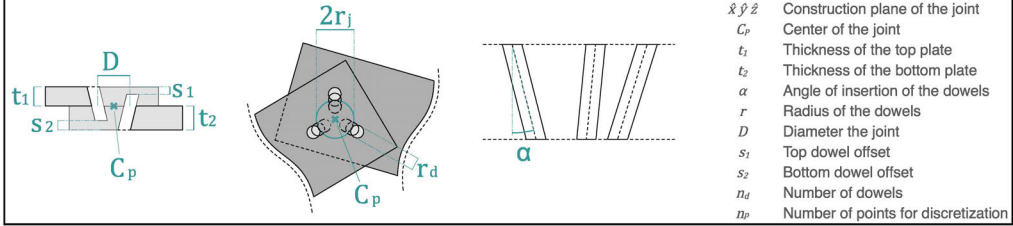
A.2 Mathematical parametrization of timber joints

Dowel joint

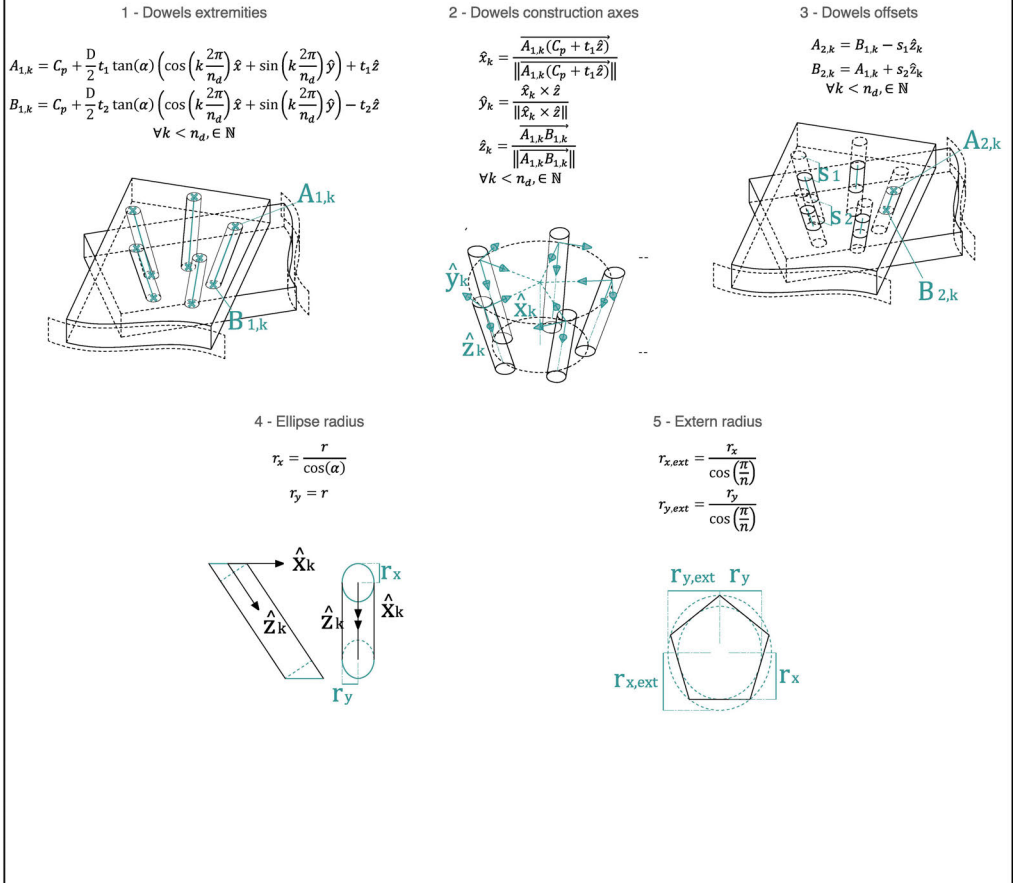
Dowel joints can be used to connect timber plates with coplanar faces. With one single dowel, the pieces can rotate freely and the connection is a pin. With more dowels distributed in a circle, a more rigid connection can be created. This mathematical definition gives the possibility to incline the dowels to better lock the parts. The depth of the holes can be controlled to hide the joint from one or both sides for aesthetic or practical purposes. The radius of the dowel and of circular pattern can also be specified by the user.



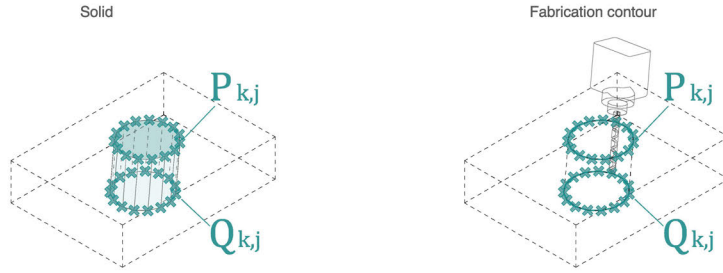
Initial parameters



Intermediary steps



Final equations

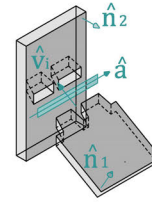


$$P_{k,j} = A_{2,k} + r_{x,ext} \cos\left(\frac{2\pi j}{n_p}\right) \hat{x}_k + r_{y,ext} \sin\left(\frac{2\pi j}{n_p}\right) \hat{y}_k \quad Q_{k,j} = B_{2,k} + r_{x,ext} \cos\left(\frac{2\pi j}{n_p}\right) \hat{x}_k + r_{y,ext} \sin\left(\frac{2\pi j}{n_p}\right) \hat{y}_k$$

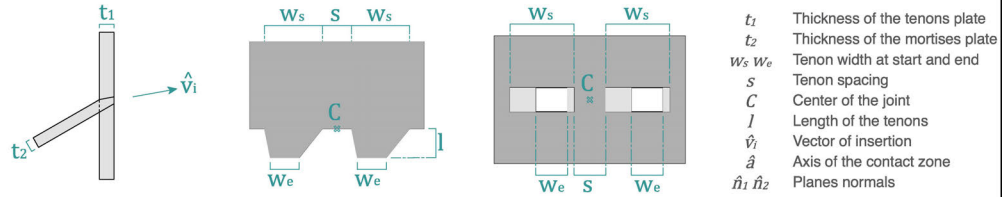
$$\forall j < n_p, j \in \mathbb{N}$$

Trough-tenon joint

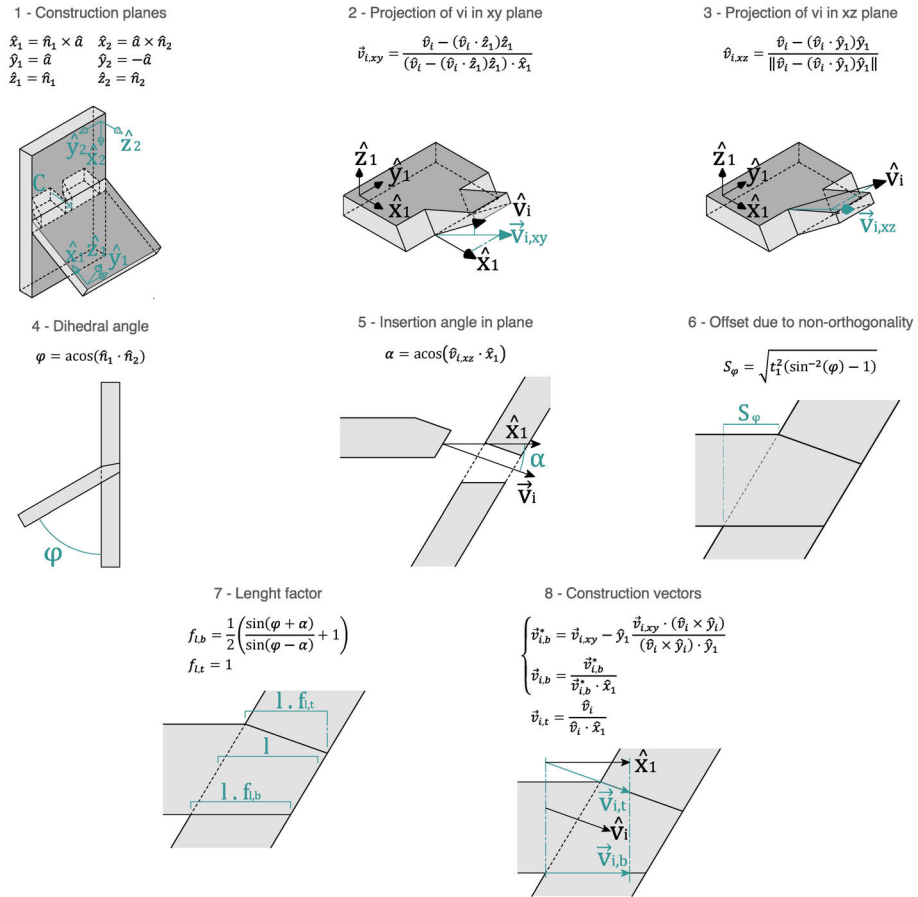
Through-tenon or mortise-and-tenon joints are commonly used in woodworking to join two pieces with a right angle. This joint usually consists of inserting a rectangular tongue formed on one plate into a rectangular hole on the corresponding plate. This mathematical definition extends the insertion space by accepting in-plane and out-of-plane vectors of insertion. Depending on the angle between this vector and the normals of each plate, the joint is then sheared and/or chamfered. Among the different parameters, the length of the tenon can be adjusted to create a stub mortise with the tenon embedded in the plate.



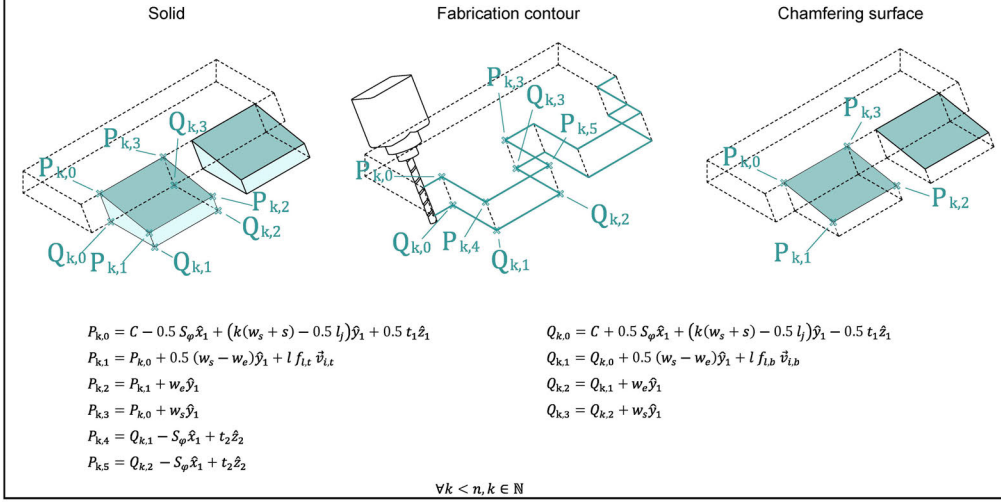
Initial parameters



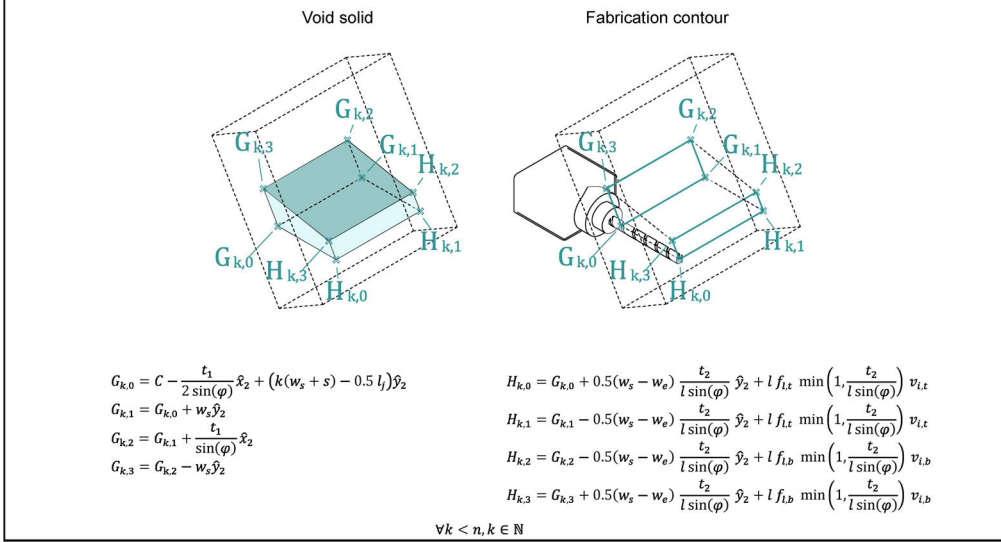
Intermediary steps



Points of the tenons

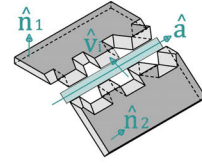


Points of the mortises

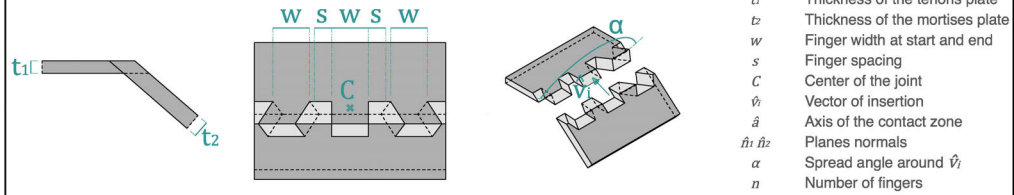


Sunrise dovetail joint

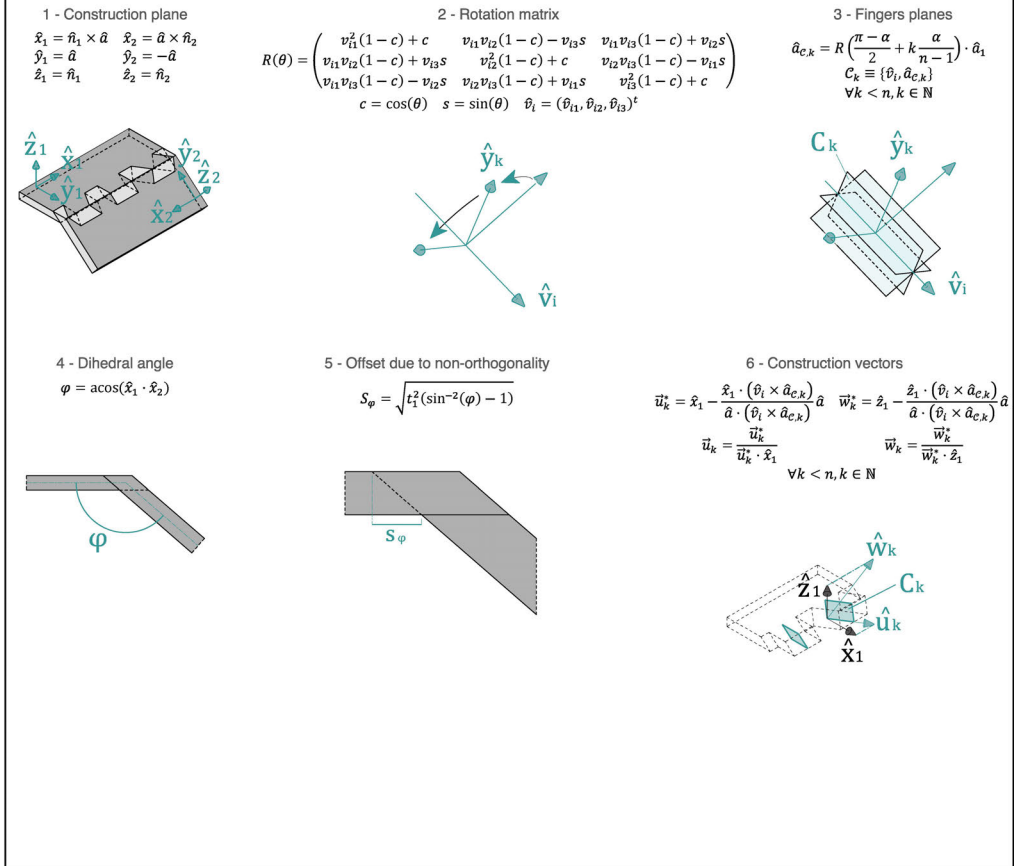
Sunrise dovetails, also called nejiri arigata in Japan, are a particular case of dovetail joints with multiple fingers oriented in different directions. This highly aesthetic joint has a unique vector of insertion which can be found by intersecting all the planes of the different fingers. This mathematical definition allows controlling the maximum angle between two planes as well as the number of fingers. The final shape of the joint is given by the orientation of the vector of insertion specified by the user.



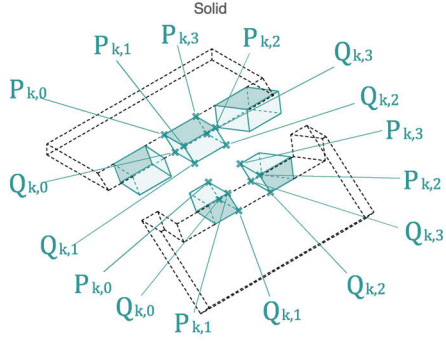
Initial parameters



Intermediary steps

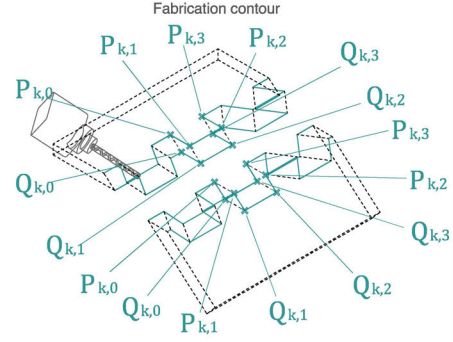


Final equations



$$\begin{aligned}
 P_{k,0} &= C - 0.5 S_{\varphi} \hat{x} + ((w+s)k - 0.5(n(w+s) - s))\hat{y} + 0.5 t \hat{z}_1 \\
 P_{k,1} &= P_{k,0} + \frac{t_2}{\sin(\varphi)} \vec{u}_k \\
 P_{k,2} &= P_{k,1} + w\hat{y} \\
 P_{k,3} &= P_{k,0} + w\hat{y}
 \end{aligned}$$

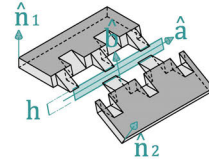
$$\forall k \leq n, k \in \mathbb{N}$$



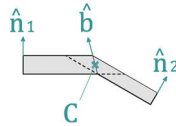
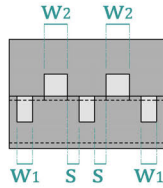
$$\begin{aligned}
 Q_{k,0} &= P_{k,0} + S_{\varphi} \vec{x}_{k,y} \\
 Q_{k,1} &= P_{k,1} + S_{\varphi} \vec{x}_{k,y} \\
 Q_{k,2} &= P_{k,2} + S_{\varphi} \vec{x}_{k,y} \\
 Q_{k,3} &= P_{k,3} + S_{\varphi} \vec{x}_{k,y}
 \end{aligned}$$

Finger joint

Finger joints or comb joints are traditionally used to interlock two pieces end to end. This can be done to cover a longer span or a larger area than what is permitted by the size of the pieces. The principle consists in creating a complementary pattern on both sides of the contact zone so that for each finger on one side, there is a corresponding hole on the other side. This mathematical definition generalizes the finger joint to non-orthogonal cases with potentially different thicknesses of plates. The number of fingers on each side, their width and their spacing can also be controlled.



Initial parameters



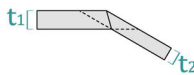
w_1, w_2	Widths of the fingers of the plates
s	Distance between fingers
h	Height of the contact zone
\hat{a}	Longitudinal axis of the contact zone
\hat{b}	Longitudinal axis of the contact zone
\hat{n}_1, \hat{n}_2	Planes normals
n_1, n_2	Number of fingers of the plates

Intermediary steps

1 - Plates thickness

$$t_1 = d \cdot |\hat{z}_1 \cdot \hat{b}|$$

$$t_2 = d \cdot |\hat{z}_2 \cdot \hat{b}|$$

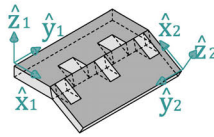


2 - Construction plane

$$\hat{x}_1 = \hat{n}_1 \times \hat{a} \quad \hat{x}_2 = \hat{a} \times \hat{n}_2$$

$$\hat{y}_1 = \hat{a} \quad \hat{y}_2 = -\hat{a}$$

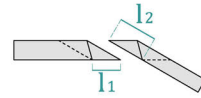
$$\hat{z}_1 = \hat{n}_1 \quad \hat{z}_2 = \hat{n}_2$$



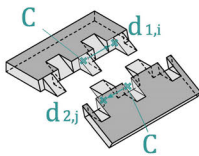
3 - Length of the fingers

$$l_1 = \frac{t_2}{|\hat{z}_1 \cdot \hat{x}_2|}$$

$$l_2 = \frac{t_1}{|\hat{z}_2 \cdot \hat{x}_1|}$$



4 - Finger start location for $n_1 \geq n_2$



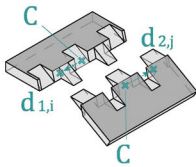
$$d_{1,i} = \begin{cases} i(w_1 + s) - \frac{l_j}{2} & k < \left\lfloor \frac{\Delta n}{2} \right\rfloor \\ \left\lfloor \frac{\Delta n}{2} \right\rfloor (w_1 + s) + \left(i - \left\lfloor \frac{\Delta n}{2} \right\rfloor \right) (w_1 + w_2 + 2s) - \frac{l_j}{2} & \left\lfloor \frac{\Delta n}{2} \right\rfloor \leq k < \left\lfloor \frac{\Delta n}{2} \right\rfloor + n_2 \\ \left\lfloor \frac{\Delta n}{2} \right\rfloor (w_1 + s) + n_2(w_1 + w_2 + 2s) + \left(i - \left\lfloor \frac{\Delta n}{2} \right\rfloor - n_2 \right) (w_1 + s) - \frac{l_j}{2} & \left\lfloor \frac{\Delta n}{2} \right\rfloor + n_2 \leq k < n_1 \end{cases}$$

$$d_{2,j} = (\Delta n + 1)(w_1 + s) + j(w_1 + w_2 + 2s)$$

$$l_j = n_1(w_1 + s) + n_2(w_2 + s) - s$$

$$\Delta n = |n_1 - n_2|$$

4 - Finger start location for $n_1 < n_2$



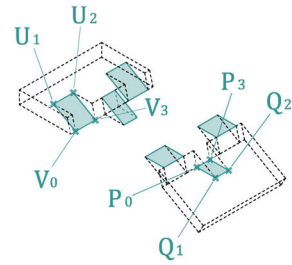
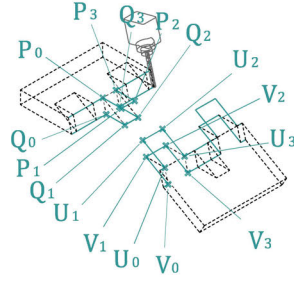
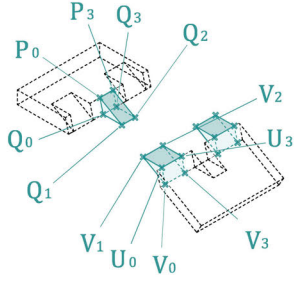
$$d_{1,i} = (\Delta n + 1)(w_2 + s) + i(w_1 + w_2 + 2s)$$

$$d_{2,j} = \begin{cases} j(w_2 + s) - \frac{l_j}{2} & k < \left\lfloor \frac{\Delta n}{2} \right\rfloor \\ \left\lfloor \frac{\Delta n}{2} \right\rfloor (w_2 + s) + \left(j - \left\lfloor \frac{\Delta n}{2} \right\rfloor \right) (w_1 + w_2 + 2s) - \frac{l_j}{2} & \left\lfloor \frac{\Delta n}{2} \right\rfloor \leq k < \left\lfloor \frac{\Delta n}{2} \right\rfloor + n_1 \\ \left\lfloor \frac{\Delta n}{2} \right\rfloor (w_2 + s) + n_2(w_1 + w_2 + 2s) + \left(j - \left\lfloor \frac{\Delta n}{2} \right\rfloor - n_1 \right) (w_2 + s) - \frac{l_j}{2} & \left\lfloor \frac{\Delta n}{2} \right\rfloor + n_1 \leq k < n_2 \end{cases}$$

$$l_j = n_1(w_1 + s) + n_2(w_2 + s) - s$$

$$\Delta n = |n_1 - n_2|$$

Final equations



$P_{k,0} = C + d_{1,i}\hat{a} + \frac{h}{2}\hat{b}$	$Q_{k,0} = C + d_{1,i}\hat{a} - \frac{h}{2}\hat{b}$	$U_{k,0} = C + d_{2,j}\hat{a} + \frac{h}{2}\hat{b}$	$V_{k,0} = C + d_{2,j}\hat{a} -$
$P_{k,1} = P_{k,0} + l_1\hat{x}_1$	$Q_{k,1} = Q_{k,0} + l_1\hat{x}_1$	$U_{k,1} = U_{k,0} + l_2\hat{x}_2$	$V_{k,1} = V_{k,0} + l_2\hat{x}_2$
$P_{k,2} = P_{k,1} + w_1\hat{a}$	$Q_{k,2} = Q_{k,1} + w_1\hat{a}$	$U_{k,2} = U_{k,1} + w_2\hat{a}$	$V_{k,2} = V_{k,1} + w_2\hat{a}$
$P_{k,3} = P_{k,0} + w_1\hat{a}$	$Q_{k,3} = Q_{k,0} + w_1\hat{a}$	$U_{k,3} = U_{k,0} + w_2\hat{a}$	$V_{k,3} = V_{k,0} + w_2\hat{a}$

A.3 Examples of structures designed with Manis

A.3.1 Projects of Master students from the architecture studio at EPFL)

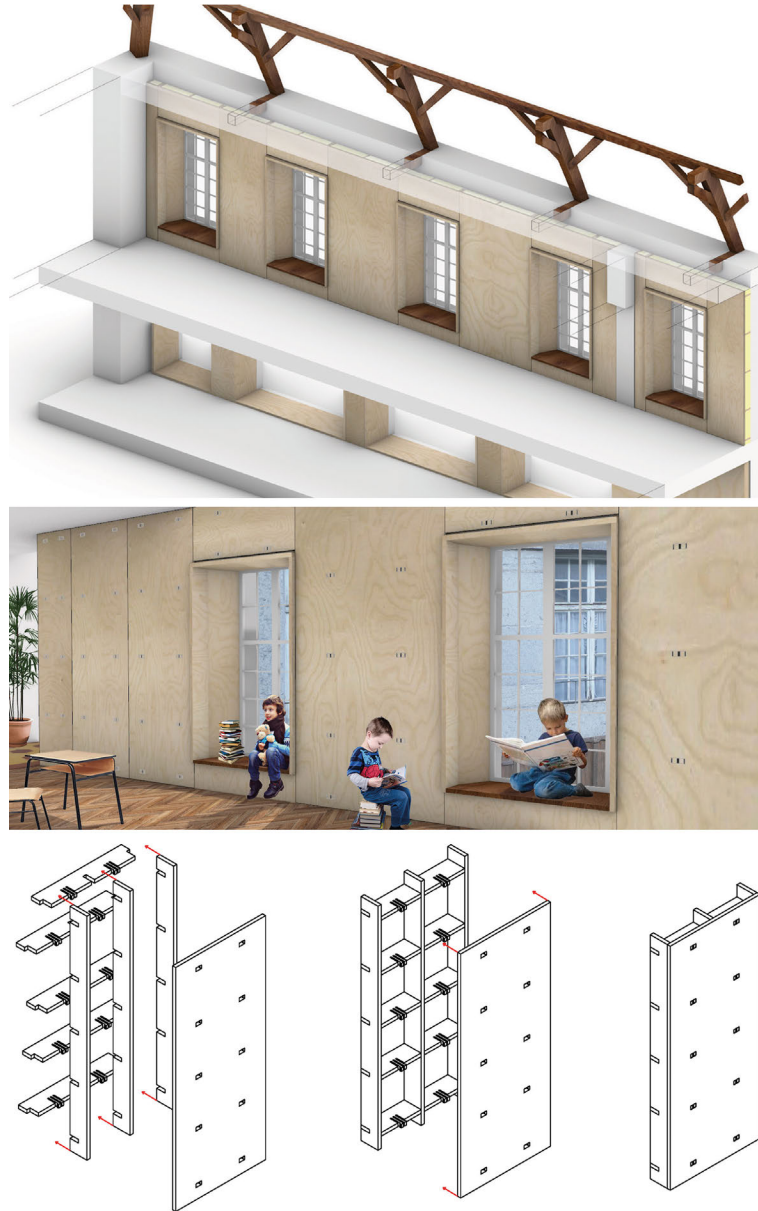


Figure A.1: Using Manis for a renovation project in a Swiss castle (student: Nicolas Otti, Spring 2020).

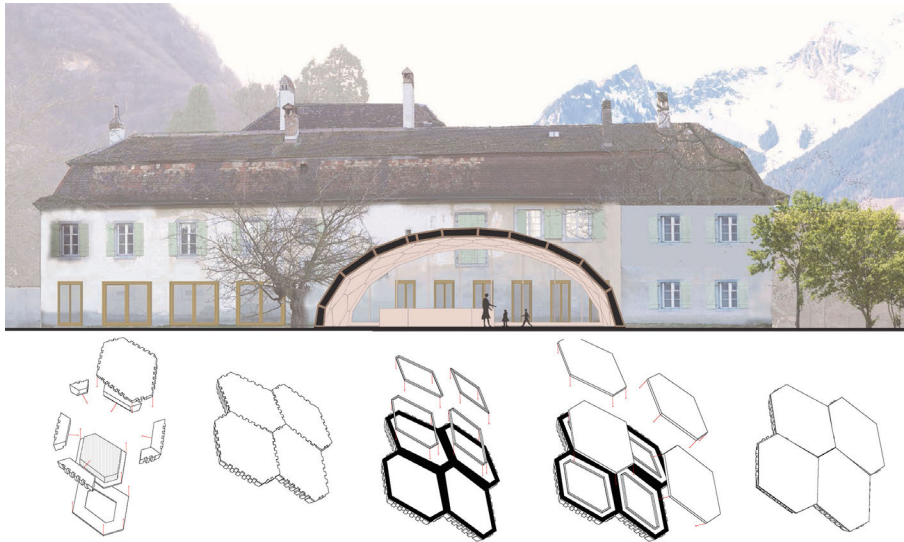


Figure A.2: Using Manis for a bespoke timber shell (student: Nicolas Otti, Spring 2020).

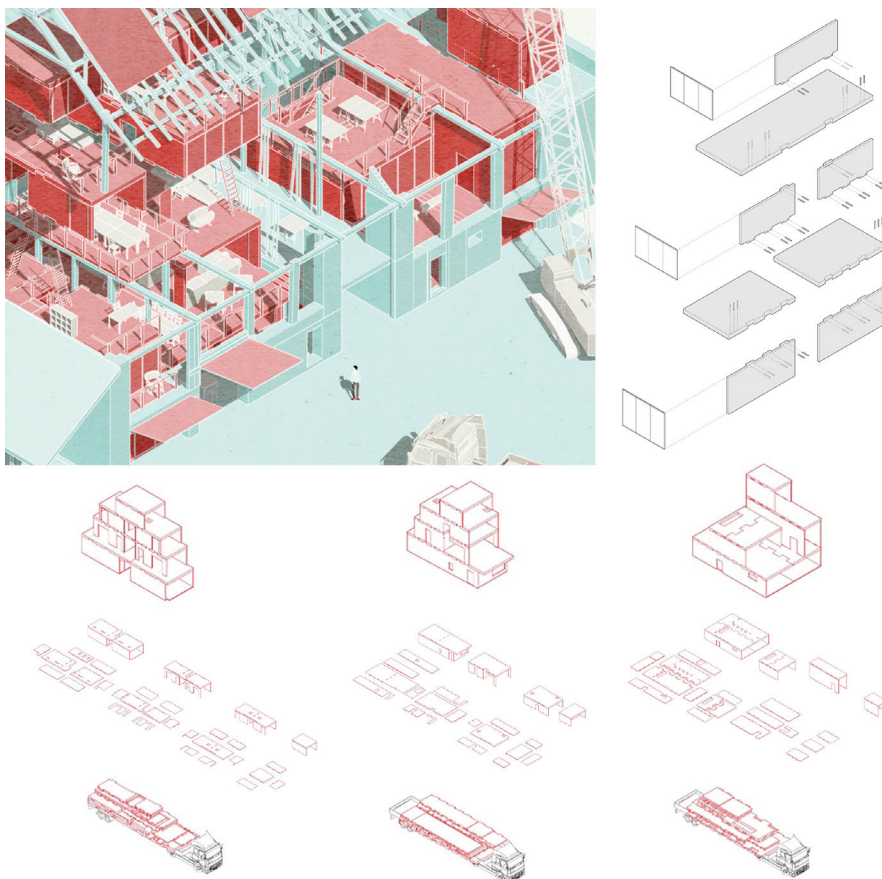


Figure A.3: Using Manis for prefabricated housing boxes (student: Tomohiko Nakamura, Spring 2020).

A.3.2 Workshop at the 2022 CAADRIA conference in Sydney

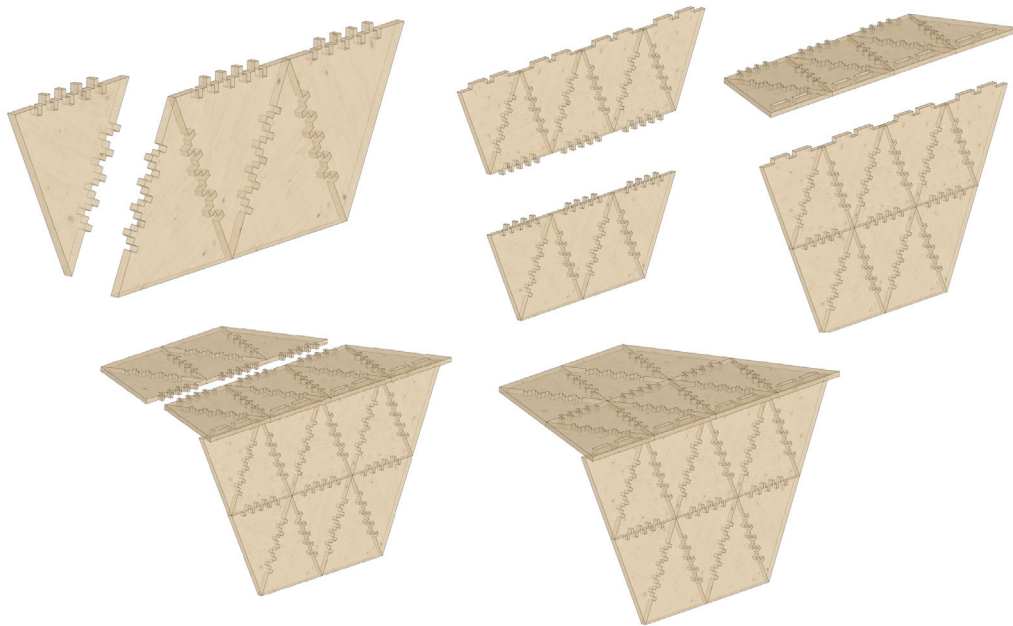


Figure A.4: Using Manis for a bike shelter (participant: Jacinta Alves, April 2022).

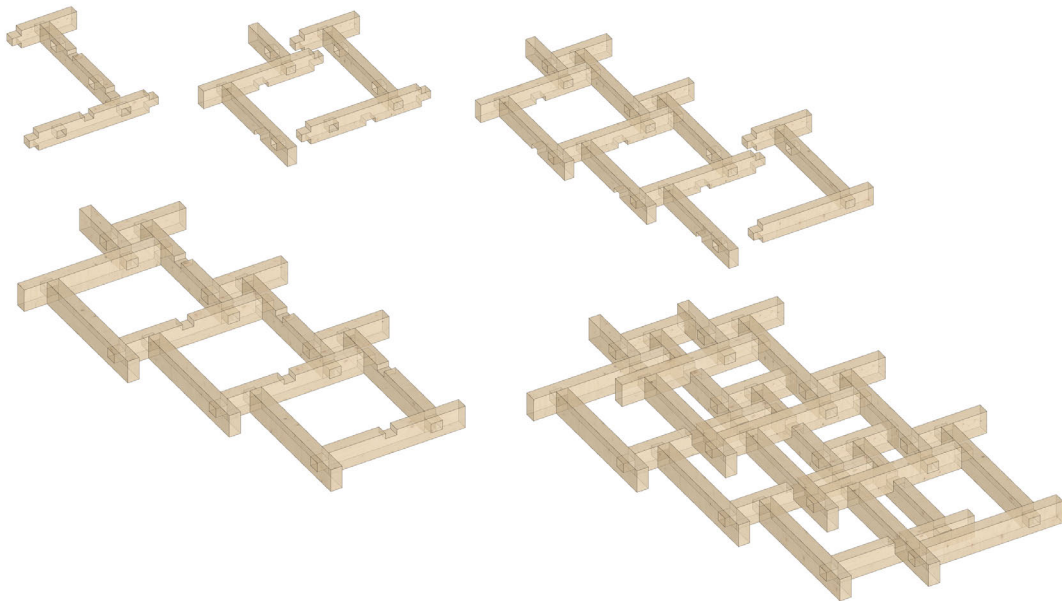


Figure A.5: Using Manis for a reciprocal structure (participant: Rin Masuda, April 2022).

A.3.3 Architectural investigations

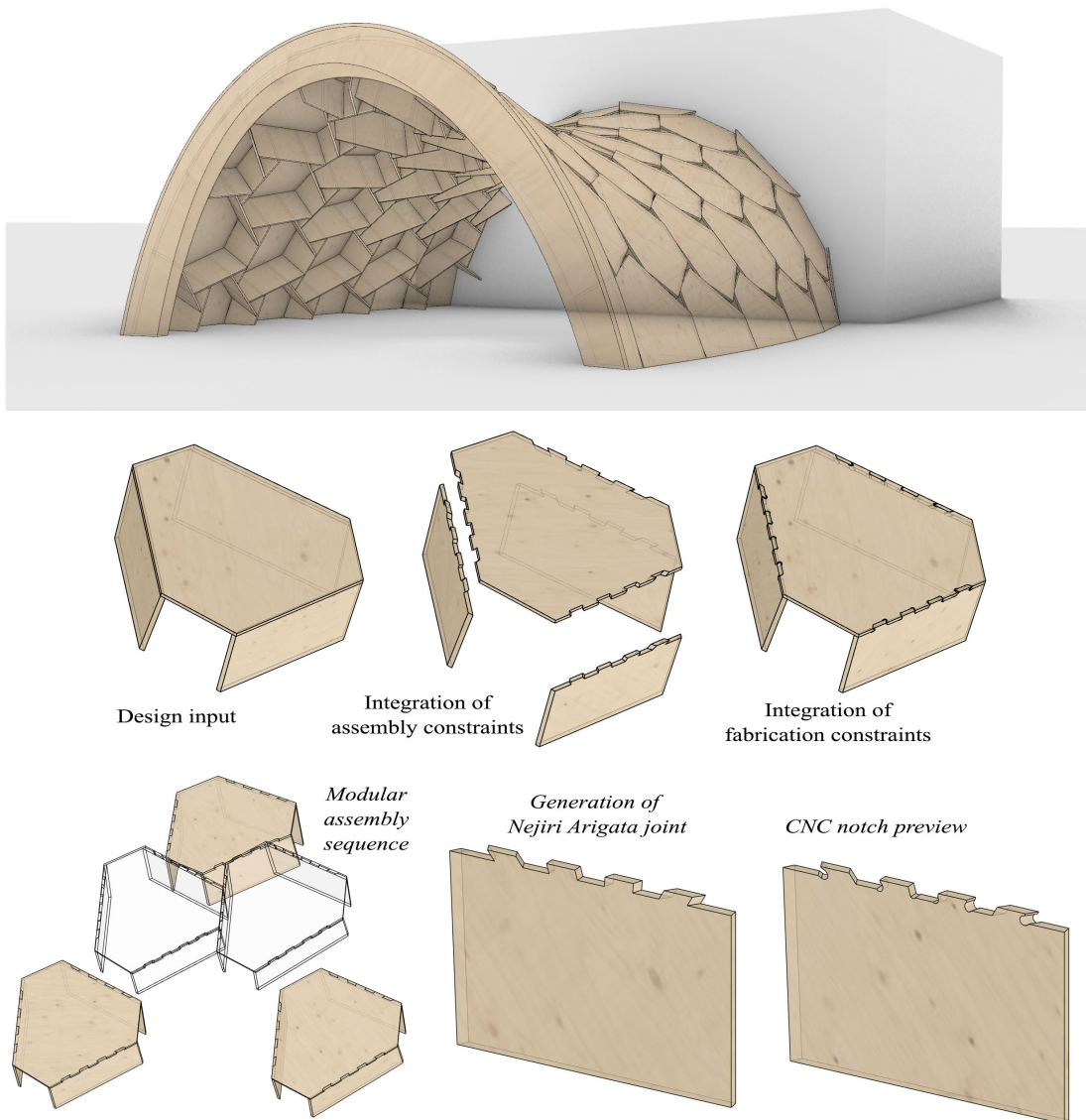


Figure A.6: Using Manis to design a boxed vault.

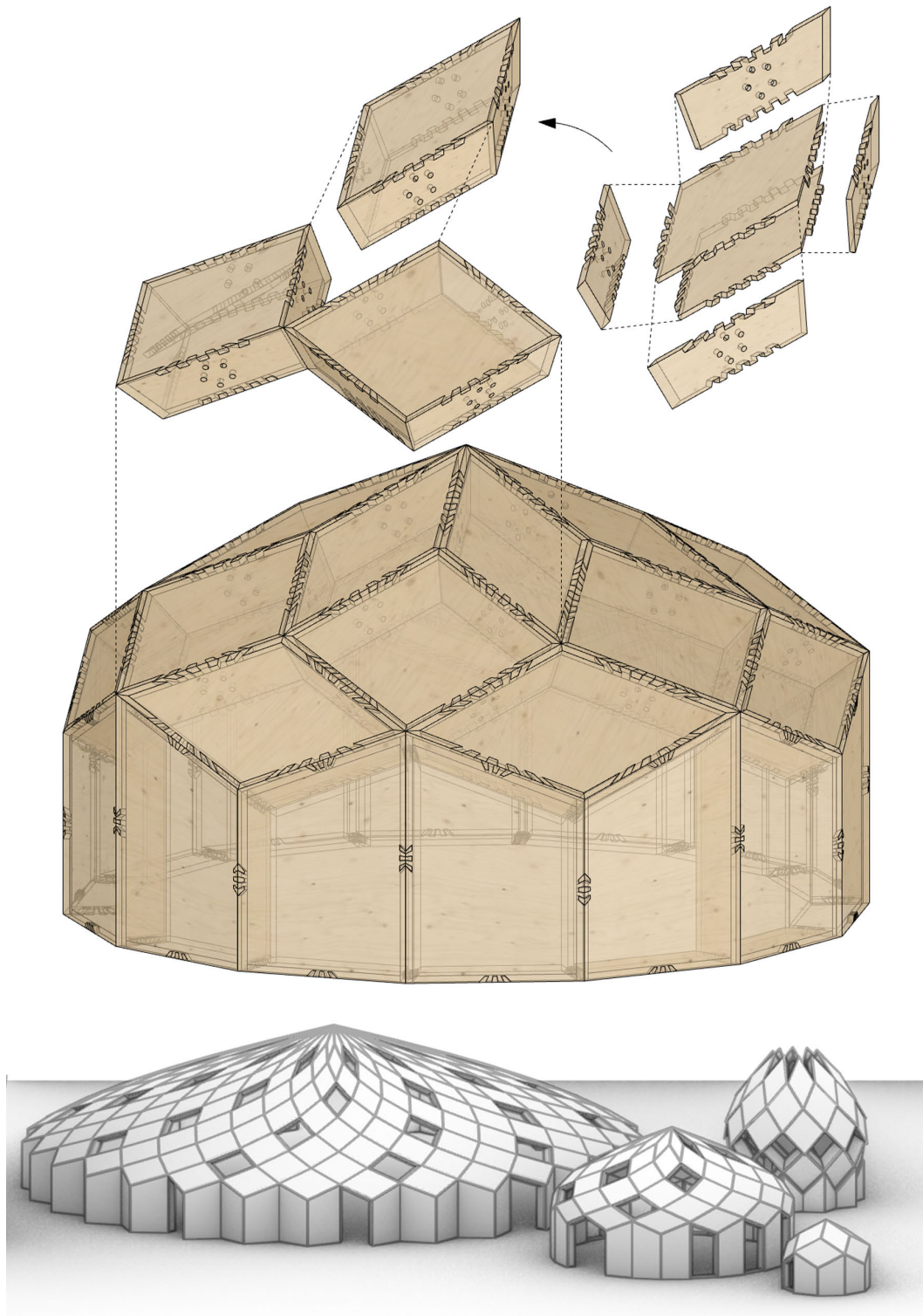


Figure A.7: Using Manis to design zome structures (spiral-shaped domes).

A.4 Pseudo-code of the indexing algorithm for the macro model of the structure of Annen

Using :	rhinoscriptsyntax library	<i>// basic geometry functions</i>
Input :	C (list of all Cells as polylines), S, B and P (associated Strip, Box and Plate identifiers as list of integers), J (list of all Joints as segments), Js and Je (associated list of tags associated to start and end plate of each joint)	
Output:	N, E, G (lists of strings for Nodes, Beam Elements, and Geometric Transformation commands)	<i>// following OpenSees standards</i>
Initializing:	nodesInfo = []	<i>// temporary storage for nodes data</i>
Tag		
1	for i = 0 to i = length of C -1	<i>// calling each plate</i>
1.1	tag = 1000*S[i] + 10*B[i] + P[i]	
Corners		
1.2	points = corners of C[i]	
1.3	for j = 0 to 3	
1.3.1	Add to N: 'node' + (100000*tag + j+1) + x,y,z coordinates of points[j]	<i>// id format: SBBP000j</i>
1.3.2	Add to nodesInfo: ((100000*tag + j+1), points[j], (100000*tag + j+1))	
Corner hinges		
1.4	hinge1 = copy of points[0] translated 10mm in direction of points[1]	
1.5	Add to N: 'node' + (100000*tag + 5001) + x,y,z coordinates of hinge1	<i>// id format: SBBP5001</i>
1.6	Add to nodesInfo: ((100000*tag + 5001), hinge1, (100000*tag + 5001))	
1.7	hinge2 = copy of points[0] translated 10mm in direction of points[0]	
1.8	Add to N: 'node' + (100000*tag + 5002) + x,y,z coordinates of hinge2	<i>// id format: SBBP5002</i>
1.9	Add to nodesInfo: ((100000*tag + 5002), hinge2, (100000*tag + 5002))	
1.10	hinge3 = copy of points[1] translated 10mm in direction of points[2]	
1.11	Add to N: 'node' + (100000*tag + 5003) + x,y,z coordinates of hinge3	<i>// id format: SBBP5003</i>
1.12	Add to nodesInfo: ((100000*tag + 5003), hinge3, (100000*tag + 5003))	
1.13	hinge4 = copy of points[2] translated 10mm in direction of points[1]	
1.14	Add to N: 'node' + (100000*tag + 5004) + x,y,z coordinates of hinge4	<i>// id format: SBBP5004</i>

A.4 Pseudo-code of the indexing algorithm for the macro model of the structure of Annen

```

1.15      Add to nodesInfo: ((100000*tag + 5004), hinge4, (100000*tag +
1.16      hinge5 = copy of points[2] translated 10mm in direction of
           points[3])
1.17      Add to N: 'node' + (100000*tag + 5005) + x,y,z coordinates of // id format: SBBP5005
           hinge5
1.18      Add to nodesInfo: ((100000*tag + 5005), hinge5, (100000*tag +
           5005))
1.19      hinge6 = copy of points[3] translated 10mm in direction of
           points[2]
1.20      Add to N: 'node' + (100000*tag + 5006) + x,y,z coordinates of // id format: SBBP5006
           hinge6
1.21      Add to nodesInfo: ((100000*tag + 5006), hinge6, (100000*tag +
           5006))
1.22      hinge7 = copy of points[3] translated 10mm in direction of
           points[0]
1.23      Add to N: 'node' + (100000*tag + 5007) + x,y,z coordinates of // id format: SBBP5007
           hinge7
1.24      Add to nodesInfo: ((100000*tag + 5007), hinge7, (100000*tag +
           5007))
1.25      hinge8 = copy of points[0] translated 10mm in direction of
           points[3]
1.26      Add to N: 'node' + (100000*tag + 5008) + x,y,z coordinates of // id format: SBBP5008
           hinge8
1.27      Add to nodesInfo: ((100000*tag + 5008), hinge8, (100000*tag +
           5008))

Geom.
Transf.
1.28      vector1 = vector from points[0] to points[1]
           vector2 = vector from points[0] to points[3]
           normal = cross product between vector 1 and 2
           Add to G: 'geomTransfLinear'+tag+x,y,z coordinates of normal

Fiber parallel
beams
1.29      if P[i] == 1 or P[i] == 2
1.29.1      mat = '$A_P12_base $E_P12_base $G_P12_base // assign material
           $J_P12_base $Iy_P12_base $Iz_P12_base' + tag // properties
1.30      if P[i] == 3
1.30.1      mat = '$A_P3_base $E_P3_base $G_P3_base $J_P3_base // assign material
           $Iy_P3_base $Iz_P3_base' + tag // properties
1.31      if P[i] == 4
1.31.1      mat = '$A_P4_base $E_P4_base $G_P4_base $J_P4_base // assign material
           $Iy_P4_base $Iz_P4_base' + tag // properties
1.32      Create an array of 4 hatches (bH) parallel to segment [points[0],
           points[1]] // see figure 5.10
1.33      for j = 0 to 3
1.33.1      bH_tag = 10000*tag + 1000 + j+1

```

Appendix A. Appendix

1.33.2	Add to N: 'node' + (bH_tag + '1') + x,y,z coordinates of bH[j] start point	// id format: SBBP100j1
1.33.3	Add to N: 'node' + (bH_tag + '2') + x,y,z coordinates of bH[j] end point	// id format: SBBP100j2
1.33.4	Add to E: 'element elasticBeamColumn' + bH_tag + (bH_tag + '1') + (bH_tag + '2') + mat	// id format: SBBP100j
1.33.5	Add to nodesInfo: (bH_tag + '1'), bH start point, (bH_tag + '1')	
1.33.6	Add to nodesInfo: (bH_tag + '2'), bH end point, (bH_tag + '2')	
Fiber perpendicular beams		
1.34	if P[i] == 1 or P[i] == 2	
1.340.1	mat = '\$A_P12_perp \$E_P12_perp \$G_P12_perp \$J_P12_perp \$Iy_P12_perp \$Iz_P12_perp' + tag	// assign material properties
1.35	if P[i] == 3	
1.35.1	mat = '\$A_P3_perp \$E_P3_perp \$G_P3_perp \$J_P3_perp \$Iy_P3_perp \$Iz_P3_perp' + tag	// assign material properties
1.36	if P[i] == 4	
1.36.1	mat = '\$A_P4_perp \$E_P4_perp \$G_P4_perp \$J_P4_perp \$Iy_P4_perp \$Iz_P4_perp' + tag	// assign material properties
1.37	Create an array of 6 hatches (pH) perpendicular to segment [points[0], points[1]]	// see figure 5.10
1.38	for j = 0 to 5	
1.38.1	pH_tag = 10000*tag + 2000 + j+1	
1.38.2	Add to N: 'node' + (pH_tag + '1') + x,y,z coordinates of pH[j] start point	// id format: SBBP200j1
1.38.3	Add to N: 'node' + (pH_tag + '2') + x,y,z coordinates of pH[j] end point	// id format: SBBP200j2
1.38.4	Add to E: 'element elasticBeamColumn' + pH_tag + (pH_tag + '1') + (pH_tag + '2') + mat	// id format: SBBP200j
1.38.5	Add to nodesInfo: (pH_tag + '1'), pH start point, (pH_tag + '1')	
1.38.6	Add to nodesInfo: (pH_tag + '2'), pH end point, (pH_tag + '2')	
Joints		
2	for i = 0 to i = length of J -1	
2.1	J_num = i+1	// short string for OpenSees
2.2	J_tag = Js[i] + Je[i] + J_num	// long string with adjacency information
2.3	Add to E: 'element twoNodeLink' + J_num + (J_num+'1') + (J_num+'2') + '-mat \$Stiffness_Tension \$Stiffness_IP \$Stiffness_OOP \$Stiffness_about_Tension \$Stiffness_about_OOP \$Stiffness_about_IP -dir 1 2 3 4 5 6 -orient -1 0 0.01'	// id format: S _A B _A B _A P _A S _B B _B B _B P _{Bi} // assign connection properties

A.4 Pseudo-code of the indexing algorithm for the macro model of the structure of Annen

```

2.4      Add to N: 'node' + (J_num+'1') + x,y,z coordinates of J[i] start point // id format:
                                                SABABAPASBBBBBPBi1
2.5      Add to N: 'node' + (J_num+'2') + x,y,z coordinates of J[i] end point // id format:
                                                SABABAPASBBBBBPBi2
2.6      Add to nodesInfo: (J_tag + '1'), J[i] start point, (J_num+ '1')
2.7      Add to nodesInfo: (J_tag + '2'), J[i] end point, (J_num+ '2')
Boundary
elements
3        for i = 0 to i = length of C -1
3.1      Initialize PointsOnPline = [] // list for sorting all
                                                points on the contour
3.2      tag = 1000*S[i] + 10*B[i] + P[i]
3.3      normal = cross product between vector from points[0] to points[1]
                                                and vector from points[0] to points[3]
3.4      mat = ' $A_cont $E_cont $G_cont $J_cont $Iy_cont $Iz_cont' + // assign material
                                                tag properties
3.5      for j = 0 to j = length of nodesInfo -1 // convert points to
                                                curve parameter
3.5.1      if length of nodesInfo[j][0] < 10 // tags of all corners and
                                                hatches
3.5.1.1      if the four first digits of nodesInfo[j][0] correspond to the // select only points
tag of the cell lying on the polyline
3.5.1.1.1      Add to PointsOnPline: nodesInfo[j][2], curve parameter
at nodesInfo[j][1]
3.5.2      else // tags of all joints
3.5.2.1      if the four first digits of nodesInfo[j][0] correspond to the // select only points
tag of the cell and the last one is 1 lying on the polyline
3.5.2.1.1      Add to PointsOnPline: nodesInfo[j][2], curve parameter
at nodesInfo[j][1]
3.5.2.2      if the four next digits of nodesInfo[j][0] correspond to the // select only points
tag of the cell and the last one is 2 lying on the polyline
3.5.2.2.1      Add to PointsOnPline: nodesInfo[j][2], curve parameter
at nodesInfo[j][1]
3.6      Sort PointsOnPline by curve parameters
3.7      for j = 0 to j = length of PointsOnPline -1
3.7.1      cont_tag = 10000*tag + 4000 + j + 1 // base identifier for
                                                contour elements
3.7.2      string = 'element elasticBeamColumn' + cont_tag + // id format: SBBP400j
PointsOnPline [j][0] + PointsOnPline [j+1][0] + mat
3.7.3      if (the element connects corner nodes to corner pins) // modify string of hinge
                                                elements
3.7.3.1      Replace 'elasticBeamColumn' by 'twoNodeLink' in string
3.7.4      Add string to E
Export
4        Export G, N and E as text in .tcl format

```

A.5 Global overview of the robotic insertion test campaign

Table A.1: List of tested samples (each sample was tested three times).

Test number	Number of tenons	Offset (mm)	Chamfer (mm)	Angle (°)	Insertion (%)
1	2	0.00	none	0	1.06
2	2	0.05	none	0	1.97
3	2	0.10	none	0	3.59
4	2	0.15	none	0	2.26
5	2	0.20	none	0	97.74
6	2	0.25	none	0	98.67
7	3	0.10	none	0	74.45
8	3	0.15	none	0	97.07
9	3	0.20	none	0	97.96
10	4	0.10	none	0	51.73
11	4	0.15	none	0	59.57
12	4	0.20	none	0	97.51
13	5	0.10	none	0	46.30
14	5	0.15	none	0	50.96
15	5	0.20	none	0	96.19
16	2	0.05	5x5	0	36.87
17	2	0.10	5x5	0	95.53
18	2	0.00	5x5	1	80.52
19	2	0.00	5x5	2	92.03
20	2	0.00	5x5	3	86.18
21	2	0.00	5x5	5	94.09
22	2	0.00	5x5	10	93.33
23	2	0.00	5x5	15	90.32
24	2	0.05	5x5	5	96.12
25	2	0.10	5x5	5	95.50
26	2	0.15	5x5	5	97.66
27	3	0.05	5x5	5	96.16
28	3	0.10	5x5	5	97.98
29	3	0.15	5x5	5	97.48
30	4	0.05	5x5	5	95.76
31	4	0.10	5x5	5	97.14
32	4	0.15	5x5	5	95.58
33	5	0.05	5x5	5	95.69
34	5	0.10	5x5	5	96.45
35	5	0.15	5x5	5	93.31
36	8	0.05	5x5	5	96.47
37	8	0.05	5x5	5	97.85
38	16	0.05	5x5	5	96.39

A.6 Insertion graphs for different joint parameters

A.6.1 Offset only

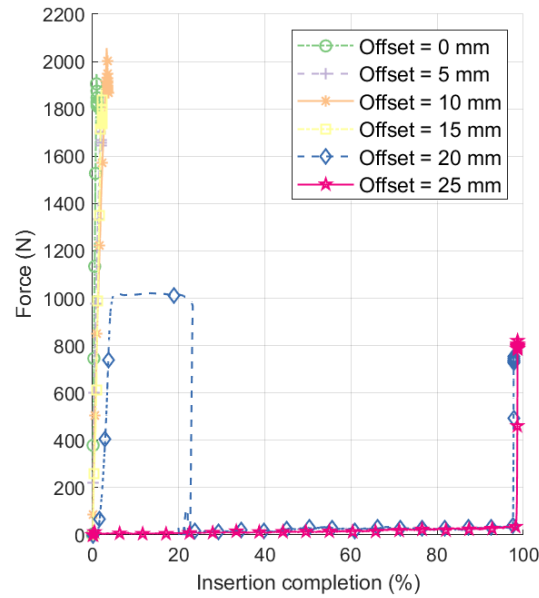


Figure A.8: Influence of the offset parameter (mm) on the insertion of 2 tenons (angle parameter: 0 degree, chamfer: none).

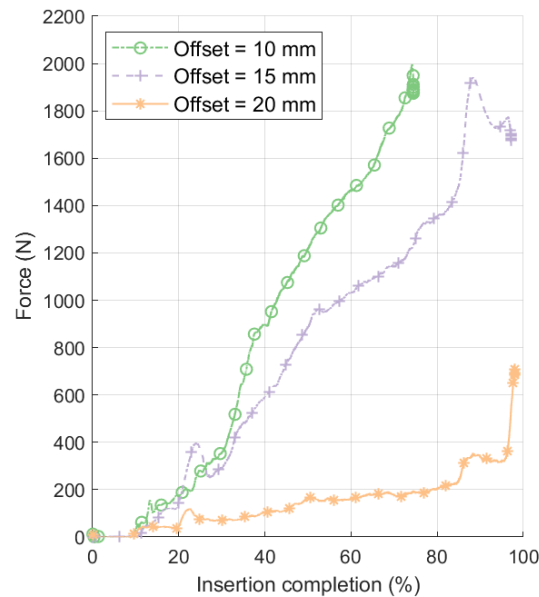


Figure A.9: Influence of the offset parameter (mm) on the insertion of 3 tenons (angle parameter: 0 degree, chamfer: none).

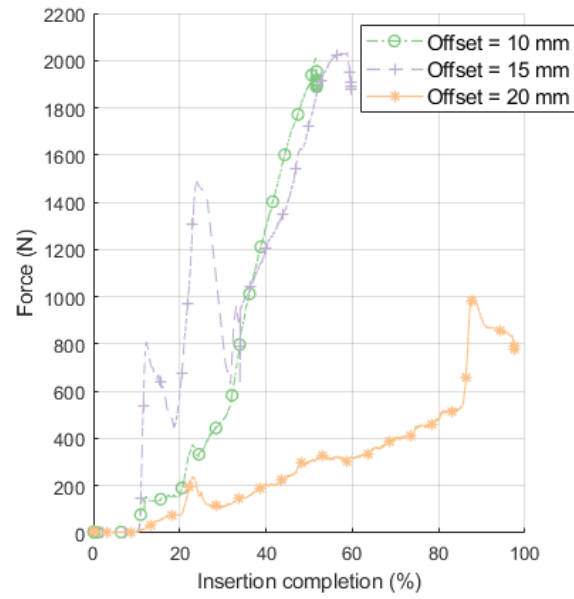


Figure A.10: Influence of the offset parameter (mm) on the insertion of 4 tenons (angle parameter: 0 degree, chamfer: none).

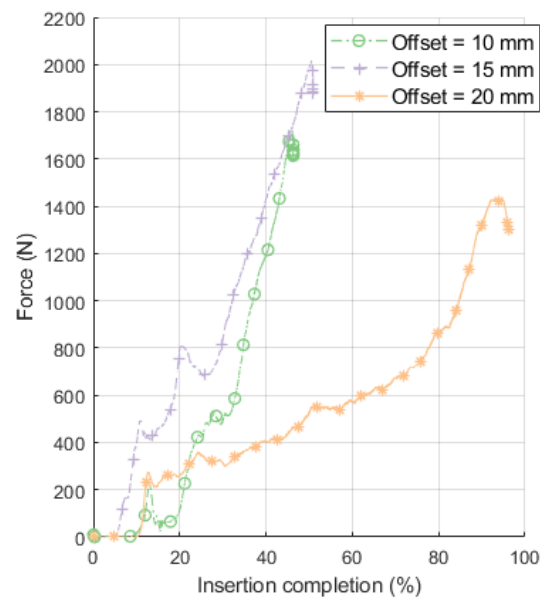


Figure A.11: Influence of the offset parameter (mm) on the insertion of 5 tenons (angle parameter: 0 degree, chamfer: none).

A.6.2 Offset and angle

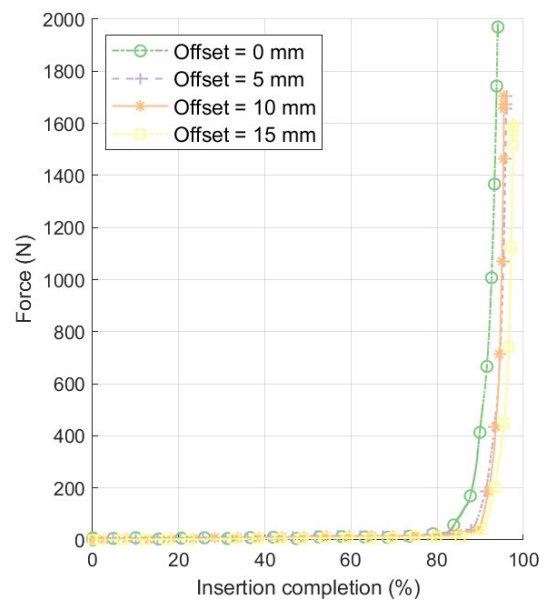


Figure A.12: Influence of the offset parameter (mm) on the insertion of 2 tenons (angle parameter: 5 degree, chamfer: 5 by 5 mm).

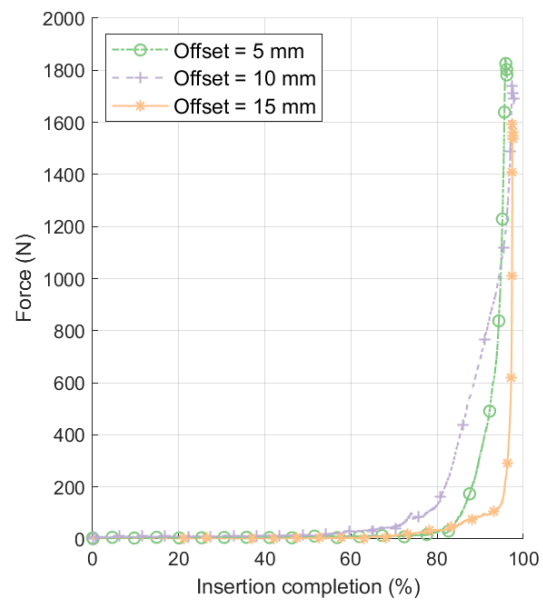


Figure A.13: Influence of the offset parameter (mm) on the insertion of 3 tenons (angle parameter: 5 degree, chamfer: 5 by 5 mm).

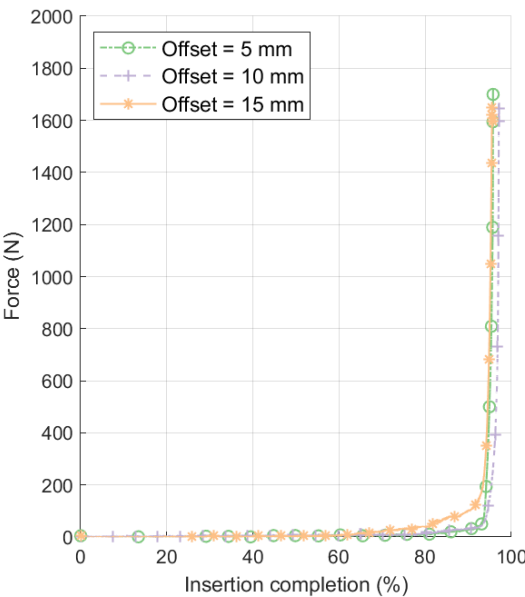


Figure A.14: Influence of the offset parameter (mm) on the insertion of 4 tenons (angle parameter: 5 degree, chamfer: 5 by 5 mm).

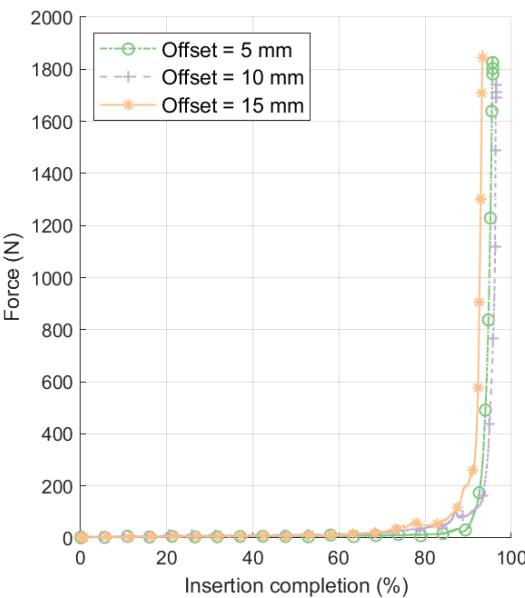


Figure A.15: Influence of the offset parameter (mm) on the insertion of 5 tenons (angle parameter: 5 degree, chamfer: 5 by 5 mm).

Bibliography

- [ABB01] ABB Automation Technology Products AB. *Product Specification IRB 6400R M2000*. Västerås, 2001.
- [ACS16] Agarwal, R., Chandrasekaran, S., and Sridhar, M. *Imagining construction's digital future*. <https://www.mckinsey.com/capabilities/operations/our-insights/imagining-constructions-digital-future>. Accessed: 2022-09-15. 2016.
- [AH16] Agustí-Juan, I. and Habert, G. "Environmental Implications and Opportunities of Digital Fabrication". In: *Expanding Boundaries: Systems Thinking in the Built Environment*. Ed. by G. Habert and A. Schlueter. Sustainable Built Environment (SBE) Regional Conference Zurich 2016. 2016. Zurich, Switzerland: vdf Hochschulverlag an der ETH Zürich, Jan. 2016, pp. 304–308. ISBN: 978-3-7281-3774-6. DOI: 10.3218/3774-6_49.
- [Ali16] Alison Brooks Architects. *The Smile*. <https://www.alisonbrooksarchitects.com/project/the-smile/>. Accessed: 2022-09-15. 2016.
- [Ami+20] Amiri, A., Ottelin, J., Sorvari, J., and Junnila, S. "Cities as carbon sinks—classification of wooden buildings". In: *Environmental Research Letters* 15.9 (Aug. 2020), p. 094076. ISSN: 1748-9326. DOI: 10.1088/1748-9326/aba134.
- [Apo+16] Apolinarska, A. A., Bärtschi, R., Furrer, R., Gramazio, F., and Kohler, M. "Mastering the "Sequential Roof" Computational Methods for Integrating Design, Structural Analysis, and Robotic Fabrication". In: *Advances in Architectural Geometry 2016*. Ed. by S. Adriaenssens, F. Gramazio, M. Kohler, A. Menges, and M. Pauly. 5th Edition of the Advances in Architectural Geometry (AAG) Symposium. Zurich, Switzerland: vdf Hochschulverlag an der ETH Zürich, Sept. 2016, pp. 240–258. ISBN: 978-3-7281-3777-7. DOI: 10.3218/3778-4-17.
- [Apo+21a] Apolinarska, A. A., Kuhn, M., Gramazio, F., and Kohler, M. "Performance-Driven Design of a Reciprocal Frame Canopy - Timber structure of the FutureTree". In: *Towards a new, configurable architecture – Proceedings of the 39th International Hybrid Conference on Education and Research in Computer Aided Architectural Design in Europe*. eCAADe, 2021, pp. 497–504. DOI: 10.3929/ethz-b-000506420.

Bibliography

- [Apo+21b] Apolinarska, A. A., Pacher, M., Li, H., Cote, N., Pastrana, R., Gramazio, F., and Kohler, M. "Robotic assembly of timber joints using reinforcement learning". In: *Automation in Construction* 125 (2021), p. 103569. ISSN: 0926-5805. DOI: 10.1016/j.autcon.2021.103569.
- [Ass] Association for Robots in Architecture. *Kuka PRC*. <https://www.food4rhino.com/en/app/kukaprc-parametric-robot-control-grasshopper>. Accessed on 2022-08-12.
- [Bal+02] Balaguer, C., Abderrahim, M., Navarro, J., Boudjabeur, S., Aromaa, P., Kahkonen, K., Slavenburg, S., Seward, D., Bock, T., Wing, R., and Atkin, B. "FutureHome: An integrated construction automation approach". In: *IEEE Robotics & Automation Magazine* 9.1 (2002), pp. 55–66. DOI: 10.1109/100.993155.
- [Bau+19] Baudisch, P., Silber, A., Kommana, Y., Gruner, M., Wall, L., Reuss, K., Heilman, L., Kovacs, R., Rechlit, D., and Roumen, T. "Kyub: A 3D Editor for Modeling Sturdy Laser-Cut Objects". In: *Proceedings of the 2019 CHI Conference on Human Factors in Computing Systems*. Glasgow, Scotland Uk: Association for Computing Machinery, 2019, pp. 1–12. ISBN: 9781450359702. DOI: 10.1145/3290605.3300796.
- [Ben81] Benson, T. *Building the timber frame house: The revival of a forgotten craft*. Simon and Schuster, 1981. ISBN: 9781439107072.
- [BFD19] Brugnaro, G., Figliola, A., and Dubor, A. "Negotiated Materialization: Design Approaches Integrating Wood Heterogeneity Through Advanced Robotic Fabrication". In: *Digital Wood Design: Innovative Techniques of Representation in Architectural Design*. Ed. by F. Bianconi and M. Filippucci. Springer International Publishing, 2019, pp. 135–158. ISBN: 978-3-030-03676-8. DOI: 10.1007/978-3-030-03676-8_4.
- [Bod+19] Bodea, S., Dambrosio, N., Zechmeister, C., Menges, A., Pérez, M. G., Koslowski, V., Rongen, B., Knippers, J., Dörstelmann, M., and Kyjánek, O. "BUGA FIBRE PAVILION". In: *Architecture Research Building* (2019).
- [Boi20] Boissieu, A. de. "Super-utilisateurs ou super-spécialistes ? Cartographie des catalyseurs de la transformation numérique en agence d'architecture". In: *Les Cahiers de la recherche architecturale urbaine et paysagère* 9|10 (2020). DOI: 10.4000/craup.5551.
- [Bur10] Buri, H. "Origami - Folded Plate Structures". PhD thesis. 2010. DOI: 10.5075/epfl-thesis-4714.
- [Cad] Cadwork. *Variant*. <https://en.cadwork.com/cwen/Modules/Variant-parametric>. Accessed on 2022-27-07.
- [Can86] Canny, J. "A Computational Approach to Edge Detection". In: *IEEE Transactions on Pattern Analysis and Machine Intelligence* PAMI-8.6 (1986), pp. 679–698. DOI: 10.1109/TPAMI.1986.4767851.

- [Car13] Carpo, M. "Introduction: Twenty Years of Digital Design". In: *The Digital Turn in Architecture 1992–2012*. Ed. by M. Carpo. John Wiley & Sons, Ltd, 2013. Chap. 0, pp. 8–14. ISBN: 9781118795811. DOI: 10.1002/9781118795811.ch0.
- [Car17] Carpo, M. *The Second Digital Turn: Design Beyond Intelligence*. The MIT Press, Oct. 2017. ISBN: 9780262341240. DOI: 10.7551/mitpress/9976.001.0001.
- [Chu+20] Churkina, G., Organschi, A., Reyser, C. P. O., Ruff, A., Vinke, K., Liu, Z., Reck, B. K., Graedel, T. E., and Schellnhuber, H. J. "Buildings as a global carbon sink". In: *Nature Sustainability* 3 (2020), pp. 269–276.
- [Cla+21] Claypool, M., Retsin, G., Garcia, M. J., Jaschke, C., and Saey, K. "Automation and the Discrete: Exploring New Potentials for Streamlining Production in Architectural Design Research". In: *Journal of Architectural Education* 75.1 (2021), pp. 108–114. DOI: 10.1080/10464883.2021.1859893.
- [Cur20] Curtis, C. "Architecture at Scale: Reimagining One-Off Projects as Building Platforms". In: *Architectural Design* 90.2 (2020), pp. 96–103.
- [Dal21] Dalla Valle, A. "Challenge of Managing the Design Team Multidisciplinarity in View of Environmental Goals". In: *Change Management Towards Life Cycle AE(C) Practice*. Cham: Springer International Publishing, 2021, pp. 65–71. ISBN: 978-3-030-69981-9. DOI: 10.1007/978-3-030-69981-9_8.
- [Dan16] Dangel, U. *Turning Point in Timber Construction: A New Economy*. Birkhäuser, 2016. ISBN: 9783035608632. DOI: doi:10.1515/9783035608632.
- [Das] Dassault Systèmes. *Abaqus*. <https://www.3ds.com/fr/produits-et-services/simulia/produits/abaqus/derniere-version/>. Accessed on 2022-08-08.
- [De +16] De Wolf, C., Yang, F., Cox, D., Charlson, A., Hattan, A. S., and Ochsendorf, J. "Material quantities and embodied carbon dioxide in structures". In: *Proceedings of the Institution of Civil Engineers - Engineering Sustainability* 169.4 (2016), pp. 150–161. DOI: 10.1680/jensu.15.00033.
- [Def81] Deforge, Y. *Le graphisme technique: son histoire et son enseignement*. Editions Champ Vallon, 1981.
- [Dil+19] Dilsiz, A. D., Felkner, J., Habert, G., and Nagy, Z. "Embodied versus operational energy in residential and commercial buildings: where should we focus?" en. In: vol. 1343. *Climate Resilient Cities – Energy Efficiency & Renewables in the Digital Era (CISBAT 2019)*; Conference Location: Lausanne, Switzerland; Conference Date: September 4-6, 2019. Bristol: Institute of Physics, Nov. 2019, p. 012178. DOI: 10.3929/ethz-b-000381312.
- [DSB19] Devadass, P., Stumm, S., and Brell-Cokcan, S. "Adaptive Haptically Informed Assembly with Mobile Robots in Unstructured Environments". In: *Proceedings of the 36th International Symposium on Automation and Robotics in Construction (ISARC)*. Ed. by M. Al-Hussein. Banff, Canada: International Association for Au-

- tomation and Robotics in Construction (IAARC), May 2019, pp. 469–476. ISBN: 978-952-69524-0-6. DOI: 10.22260/ISARC2019/0063.
- [EG14] Elashry, K. and Glynn, R. “An Approach to Automated Construction Using Adaptive Programing”. In: *Robotic Fabrication in Architecture, Art and Design 2014*. Ed. by W. McGee and M. Ponce de Leon. Cham: Springer International Publishing, 2014, pp. 51–66. ISBN: 978-3-319-04663-1. DOI: 10.1007/978-3-319-04663-1_4.
- [ERN22] ERNE AG Holzbau. *Histoire de ERNE AG Holzbau*. <https://www.erne.net/fr/entreprise/histoire/>. Accessed: 2022-09-15. 2022.
- [Eur11] European Commission (DG ENV). *SERVICE CONTRACT ON MANAGEMENT OF CONSTRUCTION AND DEMOLITION WASTE – SR1 - Final Report Task 2*. Tech. rep. Feb. 2011.
- [Eur20] Eurostat. *Generation of waste by waste category, hazardousness and NACE Rev. 2 activity*. https://ec.europa.eu/eurostat/databrowser/view/env_wasgen/default/table?lang=en. Accessed: 2022-09-15. 2020.
- [Eur21] Eurostat. *Wood products - production and trade*. https://ec.europa.eu/eurostat/statistics-explained/index.php?title=Wood_products_-_production_and_trade. Accessed on 2022-10-31. 2021.
- [FIB] FIBois. *PACTE BOIS BIOSOURCES: Île-de-France*. <http://fibois-idf.fr/sites/default/files/inline-files/FIBOIS%20IDF%20-%20PACTE%20v13%20avril%202021%200.4.pdf>. Accessed: 2022-09-15.
- [FM21] Fang, D. and Mueller, C. “Mortise-and-tenon joinery for modern timber construction: Quantifying the embodied carbon of an alternative structural connection”. In: *Architecture, Structures and Construction* (2021). DOI: 10.1007/s44150-021-00018-5.
- [For20] Forest Europe. *State of Europe’s Forests 2020*. Tech. rep. 2020. URL: https://foresteurope.org/wp-content/uploads/2016/08/SoEF_2020.pdf.
- [Gam20] Gamero, J. “Development of Novel Standardized Structural Timber Elements Using Wood-Wood Connections”. In: *EPFL Doctoral Thesis* (2020), p. 214. DOI: 10.5075/epfl-thesis-8302.
- [Gan+18] Gandia, A., Parascho, S., Rust, R., Casas, G., Gramazio, E., and Kohler, M. “Towards automatic path planning for robotically assembled spatial structures”. In: *Robotic fabrication in architecture, art and design*. Springer. 2018, pp. 59–73.
- [Gar+14] Garrido-Jurado, S., Muñoz-Salinas, R., Madrid-Cuevas, F., and Marín-Jiménez, M. “Automatic generation and detection of highly reliable fiducial markers under occlusion”. In: *Pattern Recognition* 47.6 (2014), pp. 2280–2292. ISSN: 0031-3203. DOI: 10.1016/j.patcog.2014.01.005.

- [Gaw+19] Gawel, A., Blum, H., Pankert, J., Krämer, K., Bartolomei, L., Ercan, S., Farshidian, F., Chli, M., Gramazio, F., Siegwart, R., Hutter, M., and Sandy, T. “A Fully-Integrated Sensing and Control System for High-Accuracy Mobile Robotic Building Construction”. In: *2019 IEEE/RSJ International Conference on Intelligent Robots and Systems (IROS)*. 2019, pp. 2300–2307. DOI: 10.1109/IROS40897.2019.8967733.
- [GBW20a] Gamero, J., Bocquet, J. F., and Weinand, Y. “Experimental investigations on the load-carrying capacity of digitally produced wood-wood connections”. In: *Engineering Structures* 213 (2020), p. 110576. ISSN: 0141-0296. DOI: 10.1016/j.engstruct.2020.110576.
- [GBW20b] Gamero, J., Bocquet, J. F., and Weinand, Y. “A Calculation Method for Interconnected Timber Elements Using Wood-Wood Connections”. In: *Buildings* 10.3 (2020). ISSN: 2075-5309. DOI: 10.3390/buildings10030061.
- [Gem] Gemeente Amsterdam. *Nelson Mandelabuurt: nieuwe woonwijk naast het park*. <https://www.amsterdam.nl/projecten/nelson-mandelabuurt/>. Accessed: 2022-09-15.
- [GFB94] Gullapalli, V., Franklin, J., and Benbrahim, H. “Acquiring robot skills via reinforcement learning”. In: *IEEE Control Systems Magazine* 14.1 (1994), pp. 13–24. DOI: 10.1109/37.257890.
- [Gif+17] Giftthaler, M., Sandy, T., Dörfler, K., Brooks, I., Buckingham, M., Rey, G., Kohler, M., Gramazio, F., and Buchli, J. “Mobile robotic fabrication at 1:1 scale: the In situ Fabricator”. In: *Construction Robotics* 1.1-4 (June 2017), pp. 3–14. DOI: 10.1007/s41693-017-0003-5.
- [GLW18] Gamero, J., Lemaître, I., and Weinand, Y. “Mechanical characterization of timber structural elements using integral mechanical attachments”. In: *WCTE 2018 - World Conference on Timber Engineering*. Seoul, 2018. DOI: 10.5075/epfl-ibois-256646.
- [Goe+18] Goessens, S., Rogeau, N., De Beusscher, G., Mueller, C., and Latteur, P. “Parametric Design of Drone-Compatible Architectural Timber Structures”. In: *Proceedings of IASS Annual Symposia* 2018.9 (2018), pp. 1–8. ISSN: 2518-6582. URL: <https://www.ingentaconnect.com/content/iass/piass/2018/00002018/00000009/art00016>.
- [Gra92] Graubner, W. *Encyclopedia of wood joints - A Fine woodworking book*. Taunton Press, 1992. ISBN: 9780713470918.
- [Gru22] Gruppe, L. *Robot Wood Construction*. <https://www.leidorf.com/en/robotik-holzbau/>. Accessed: 2022-10-27. 2022.
- [Gui09] Guinard, D. “La filière bois en Europe et dans le monde”. In: *Annales des Mines - Responsabilité et environnement* 53.1 (2009), pp. 49–55. DOI: 10.3917/re.053.0049.
- [Guo+19] Guo, P., Zhang, Z., Liu, Y., Sun, W., and Li, Z. “Precision assembly method based on coaxial alignment and force control”. In: *Journal of Physics: Conference Series* 1303.1 (Aug. 2019), p. 012152. DOI: 10.1088/1742-6596/1303/1/012152.

Bibliography

- [HaB05] Haneca, K., acker, J. V., and Beeckman, H. "Growth trends reveal the forest structure during Roman and Medieval times in Western Europe: a comparison between archaeological and actual oak ring series (*Quercus robur* and *Quercus petraea*)". In: *Annals of Forest Science* 62.8 (Oct. 2005), pp. 797–805. DOI: 10.1051/forest:2005085.
- [Han08] Hani Buri, Y. W. "Die provisorische Kapelle von St. Loup". In: *Bulletin Schweizerische Arbeitsgemeinschaft für Holzforschung SAH* (2008).
- [Hel+18] Heller, F., Thar, J., Lewandowski, D., Hartmann, M., Schoonbrood, P., Stönner, S., Voelker, S., and Borchers, J. "CutCAD - An Open-Source Tool to Design 3D Objects in 2D". In: *Proceedings of the 2018 Designing Interactive Systems Conference*. DIS '18. Hong Kong, China: Association for Computing Machinery, 2018, pp. 1135–1139. ISBN: 9781450351980. DOI: 10.1145/3196709.3196800.
- [HGM18] Huang, Y., Garrett, C. R., and Mueller, C. T. "Automated sequence and motion planning for robotic spatial extrusion of 3D trusses". In: *Construction Robotics* 2.1 (Dec. 2018), pp. 15–39. ISSN: 2509-8780. DOI: 10.1007/s41693-018-0012-z.
- [HHT17] Hildebrandt, J., Hagemann, N., and Thrän, D. "The contribution of wood-based construction materials for leveraging a low carbon building sector in europe". In: *Sustainable Cities and Society* 34 (2017), pp. 405–418. ISSN: 2210-6707. DOI: 10.1016/j.scs.2017.06.013.
- [HKN21] Hansen, S. G., Kunic, A., and Naboni, R. "A reversible connection for robotic assembly of timber structures". In: *Engineering Structures* 245 (2021), p. 112795. ISSN: 0141-0296. DOI: 10.1016/j.engstruct.2021.112795.
- [HO18] Hemingway, E. G. and O'Reilly, O. M. "Perspectives on Euler angle singularities, gimbal lock, and the orthogonality of applied forces and applied moments". In: *Multibody System Dynamics* 44.1 (Sept. 2018), pp. 31–56. ISSN: 1573-272X. DOI: 10.1007/s11044-018-9620-0.
- [Hol] Hollander, J. *MakerCase*. <https://www.makercase.com/>. Accessed on 2022-27-07.
- [HP20] Hart, J. and Pomponi, F. "More Timber in Construction: Unanswered Questions and Future Challenges". In: *Sustainability* 12.8 (2020). ISSN: 2071-1050. DOI: 10.3390/su12083473.
- [Hua+21] Huang, Y., Victor, L. P. Y., Garrett, C., Gramazio, F., Kohler, M., and Mueller, C. "The new analog: A protocol for linking design and construction intent with algorithmic planning for robotic assembly of complex structures". In: *Symposium on Computational Fabrication*. SCF '21. Association for Computing Machinery, 2021. DOI: 10.1145/3485114.3485122.
- [Hua18] Huang, Y. "Automated Motion Planning for Robotic Assembly of Discrete Architectural Structures". MA thesis. Massachusetts Institute of Technology, 2018.

- [IKB19] Iturralde, K., Kinoshita, T., and Bock, T. “Grasped Element Position Recognition and Robot Pose Adjustment during Assembly”. In: *Proceedings of the 36th International Symposium on Automation and Robotics in Construction (ISARC)*. Ed. by M. Al-Hussein. Banff, Canada: International Association for Automation and Robotics in Construction (IAARC), May 2019, pp. 461–468. ISBN: 978-952-69524-0-6. DOI: 10.22260/ISARC2019/0062.
- [Ing11] Ingerson, A. “Carbon storage potential of harvested wood: summary and policy implications”. In: *Mitigation and Adaptation Strategies for Global Change* 16.3 (Mar. 2011), pp. 307–323. ISSN: 1573-1596. DOI: 10.1007/s11027-010-9267-5.
- [Int] International Organization for Standardization. *ISO 6983-1:2009, Automation Systems and Integration, Numerical Control of machines, Program Format and Definitions of Address Words, Part 1: Data Format for Positioning, Line Motion and Contouring Control System*. <https://www.iso.org/standard/34608.html>. Accessed on 2022-27-07.
- [iwo] iwood.care. *iwood.care*. <https://iwood.care/>. Accessed on 2022-06-10.
- [Jap22] Japanese Ministry of Agriculture, Forestry and Fisheries. *Sustainable Wood Use Promotion in Wood Producing Economies*. Tech. rep. Accessed: 2022-09-15. 2022.
- [KCC] Kim, P., Chen, J., and Cho, Y. K. “Autonomous Mobile Robot Localization and Mapping for Unknown Construction Environments”. In: *Construction Research Congress 2018*, pp. 147–156. DOI: 10.1061/9780784481264.015.
- [KK14] Kotradyová, V. and Kaliňáková, B. “Wood as Material Suitable for Health Care and Therapeutic Facilities”. In: *Advanced Materials Research* 1064 (2014), pp. 362–366. DOI: 10.4028/www.scientific.net/amr.1041.362.
- [KM13] Knippers, J. and Menges, A. “ICD/ITKE Research Pavilion 2011”. In: *Architectural Material & Texture*. Ed. by C. Hu. Vol. I. 2013, pp. 266–273. ISBN: 978-7-214-08683-9.
- [Kni+21] Knippers, J., Kropp, C., Menges, A., Sawodny, O., and Weiskopf, D. “Integrative computational design and construction: Rethinking architecture digitally”. In: *Civil Engineering Design* 3.4 (2021), pp. 123–135. DOI: 10.1002/cend.202100027.
- [Koh+13] Kohoutek, T. K., Droschel, D., Mautz, R., and Behnke, S. “Indoor Positioning and Navigation Using Time-Of-Flight Cameras”. In: *TOF Range-Imaging Cameras*. Ed. by F. Remondino and D. Stoppa. Berlin, Heidelberg: Springer Berlin Heidelberg, 2013, pp. 165–176. ISBN: 978-3-642-27523-4. DOI: 10.1007/978-3-642-27523-4_8.
- [Kra+22] Kramberger, A., Kunic, A., Iturrate, I., Sloth, C., Naboni, R., and Schlette, C. “Robotic Assembly of Timber Structures in a Human-Robot Collaboration Setup”. In: *Frontiers in Robotics and AI* 8 (2022). ISSN: 2296-9144. DOI: 10.3389/frobt.2021.768038.

Bibliography

- [Kri+15] Krieg, O. D., Schwinn, T., Menges, A., Li, J.-M., Knippers, J., Schmitt, A., and Schwieger, V. “Biomimetic Lightweight Timber Plate Shells: Computational Integration of Robotic Fabrication, Architectural Geometry and Structural Design”. In: *Advances in Architectural Geometry 2014*. Ed. by P. Block, J. Knippers, N. J. Mitra, and W. Wang. Cham: Springer International Publishing, 2015, pp. 109–125. ISBN: 978-3-319-11418-7.
- [Lar+20] Larsson, M., Yoshida, H., Umetani, N., and Igarashi, T. “Tsugite: Interactive Design and Fabrication of Wood Joints”. In: *Proceedings of the 33rd Annual ACM Symposium on User Interface Software and Technology*. New York, NY, USA: Association for Computing Machinery, 2020, pp. 317–327. ISBN: 9781450375146.
- [Leh22] Lehmann, B. *Free Form Holzbau*. <https://www.lehmann-gruppe.ch/holzbau/free-form.html>. Accessed: 2022-09-15. 2022.
- [Leu+21] Leung, P. Y., Apolinarska, A. A., Tanadini, D., Gramazio, F., and Kohler, M. “Automatic Assembly of Jointed Timber Structure using Distributed Robotic Clamps”. en. In: *‘PROJECTIONS’ – Proceedings of the 26th International Conference of the Association for Computer-Aided Architectural Design Research in Asia (CAADRIA 2021)*. Ed. by A. Globa, J. van Ameijde, A. Fingrut, N. Kim, and T. T. Sky Lo. Vol. 1. Hongkong: Association for Computer Aided Architectural Design Research in Asia (CAADRIA), 2021, pp. 583–592. ISBN: 978-988-78917-5-8. DOI: 10.3929/ethz-b-000481928.
- [Lig] Lignocam. *THE BTL FORMAT*. <https://lignocam.com/btlx/?lang=en>. Accessed on 2022-27-07.
- [Maa] McNeel and associates. *Grasshopper*. <https://www.grasshopper3d.com/>. Accessed on 2022-27-07.
- [Mab] McNeel and associates. *Rhino*. <https://www.rhino3d.com/>. Accessed on 2022-27-07.
- [Mac] McNeel and associates. *RhinoCommon*. https://developer.rhino3d.com/api/RhinoCommon/html/R_Project_RhinoCommon.htm. Accessed on 2022-27-07.
- [Mac+19] Machado, C. G., Winroth, M., Carlsson, D., Almström, P., Centerholt, V., and Hallin, M. “Industry 4.0 readiness in manufacturing companies: challenges and enablers towards increased digitalization.” In: *Procedia CIRP* 81 (2019). 52nd CIRP Conference on Manufacturing Systems (CMS), Ljubljana, Slovenia, June 12-14, 2019, pp. 1113–1118. ISSN: 2212-8271. DOI: 10.1016/j.procir.2019.03.262.
- [Mar22] Marks Barfield Architects. *Cambridge Mosque*. <https://marksbarfield.com/projects/cambridge-mosque/>. Accessed: 2022-09-15. 2022.
- [Mat+19] Matheson, E., Minto, R., Zampieri, E. G. G., Faccio, M., and Rosati, G. “Human–Robot Collaboration in Manufacturing Applications: A Review”. In: *Robotics* 8.4 (2019). ISSN: 2218-6581. DOI: 10.3390/robotics8040100.

- [Maz+] Mazzoni, S., McKenna, F., Scott, M., and Fenves, G. *OpenSees: The open system for earthquake engineering simulation*. <http://opensees.berkeley.edu/>. Accessed on 2022-05-08.
- [Mes18] Mesnil, R. “A Re-Parameterization Approach for the Construction of Domes with Planar Facets”. In: *Journal of the International Association for Shell and Spatial Structures* 59.4 (2018), pp. 286–295. ISSN: 1028-365X. DOI: doi:10.20898/j.iass.2018.198.016.
- [Mob22] Mobic SA. *Notre entreprise*. <https://www.mobicsa.be/notre-entreprise/>. Accessed: 2022-10-27. 2022.
- [Mol] Molloy, D. *Chapter 1 - Introduction to Object-oriented Programming*. <http://www.eeng.dcu.ie/~ee553/>. Accessed on 2022-27-07.
- [Mor+17] Mork, J. H., Luczkowski, M., Dyvik, S. H., Manum, B., and Rønnquist, A. “A parametric toolkit for advanced timber structures”. In: *6th Forum Wood Building Nordic Trondheim*. Trondheim, Norway, 2017.
- [Mor87] Morrison, H. *Early American Architecture: From the First Colonial Settlements to the National Period*. Courier Corporation, 1987.
- [Nat] Nations, U. *Sustainable Development Goals*. <https://sustainabledevelopment.un.org/>. Accessed on 2022-28-07.
- [Ngu20] Nguyen, A. C. “A Structural Design Methodology for Freeform Timber Plate Structures Using Wood-Wood Connections”. PhD thesis. Ecole Polytechnique Fédérale de Lausanne, 2020. DOI: 10.5075/epfl-thesis-7847.
- [Nob06] Noble, G. *Neolithic Scotland: timber, stone, earth and fire*. Edinburgh University Press, 2006.
- [NVW19] Nguyen, A. C., Vestartas, P., and Weinand, Y. “Design framework for the structural analysis of free-form timber plate structures using wood-wood connections”. In: *Automation in Construction* 107 (2019), p. 102948. ISSN: 0926-5805. DOI: 10.1016/j.autcon.2019.102948.
- [Ode+19] Odehnl, B., Hornung, P., Santorso, K., Ambrosz, B., Sampl, G., Golob, E., Brell-Cokçan, S., Braumann, J., and Cokçan, B. *Robotic Woodcraft - towards the craftsmanship of the future*. University of Applied Arts Vienna, 2019.
- [Ope] Open Systems Lab. *WikiHouse*. <https://www.wikihouse.cc/mission>. Accessed on 2012-16-08.
- [OT10] Oti, A. H. and Tizani, W. “Developing incentives for collaboration in the AEC Industry”. In: *Proceedings of the International Conference on Computing in Civil and Building Engineering*. Ed. by W. Tizani. Cham: Nottingham University Press, 2010, pp. 65–71. ISBN: 978-3-030-69981-9. DOI: 10.1007/978-3-030-69981-9_8.
- [Pad] Padfield, N. *More elegant CNC dogbones*. <https://fablab.ruc.dk/more-elegant-cnc-dogbones/>. Accessed on 2022-27-07.

Bibliography

- [Par19] Parascho, S. “Cooperative Robotic Assembly. Computational Design and Robotic Fabrication of Spatial Metal Structures”. en. Doctoral Thesis. Zurich: ETH Zurich, 2019. DOI: 10.3929/ethz-b-000364322.
- [PB15] Pásztor, E. and Barna, J. P. “Neolithic Longhouses and Bronze Age Houses in Central Europe”. In: *Handbook of Archaeoastronomy and Ethnoastronomy*. Ed. by C. L. Ruggles. New York, NY: Springer New York, 2015, pp. 1307–1316. ISBN: 978-1-4614-6141-8. DOI: 10.1007/978-1-4614-6141-8_126.
- [Pel21] Peltonen, P. *The Finnish Bioeconomy Strategy*. <https://www.bioeconomy.fi/facts-and-contacts/the-finnish-bioeconomy-strategy/>. Accessed: 2022-09-15. 2021.
- [Pic10] Picon, A. *Digital Culture in Architecture: An Introduction for the Design Professions*. Birkhäuser Basel, 2010. ISBN: 9783034602594.
- [Pot+08] Pottman, H., Asperl, A., Hoffer, M., Killian, A., and Brown, A. “Book Review: Architectural Geometry”. In: *International Journal of Architectural Computing* 6.2 (2008), pp. 215–216. DOI: 10.1260/147807708785850131.
- [Pyt] Python Software Foundation. *Python*. <https://www.python.org/>. Accessed on 2022-27-07.
- [Qin+16] Qin, Z., Wang, P., Sun, J., Lu, J., and Qiao, H. “Precise Robotic Assembly for Large-Scale Objects Based on Automatic Guidance and Alignment”. In: *IEEE Transactions on Instrumentation and Measurement* 65 (2016), pp. 1398–1411.
- [Rad12] Radkau, J. *Wood: a history*. Polity, 2012.
- [Rat22] Ratnasingam, J. “Furniture Manufacturing Systems”. In: *Furniture Manufacturing: A Production Engineering Approach*. Singapore: Springer Singapore, 2022, pp. 21–28. ISBN: 978-981-16-9412-7. DOI: 10.1007/978-981-16-9412-7_3.
- [RBW20] Rezaei Rad, A., Burton, H. V., and Weinand, Y. “Macroscopic Model for Spatial Timber Plate Structures with Integral Mechanical Attachments”. In: *Journal of Structural Engineering* 146.10 (2020), p. 04020200. DOI: 10.1061/(ASCE)ST.1943-541X.0002726.
- [Rey+21] Reyes, N., Rodríguez, B., Wiegand, E., Zilic, F., Ramage, M., Bukauskas, A., Debnath, R., Shah, D. U., Colman, T., De Wolf, C., Koronaki, A., Gatoó, A., Gin, Y., Ossio, F., and Ahumada, M. “Achieving zero carbon emissions in the construction sector: The role of timber in decarbonising building structures”. In: *Engineering* (Nov. 2021). DOI: 10.33774/coe-2021-hgd6q-v2.
- [Rez+21] Rezaei Rad, A., Burton, H., Rogeau, N., Vestartas, P., and Weinand, Y. “A framework to automate the design of digitally-fabricated timber plate structures”. In: *Computers & Structures* 244 (2021), p. 106456. ISSN: 0045-7949. DOI: 10.1016/j.compstruc.2020.106456.
- [Rez20] Rezaei Rad, A. “Mechanical Characterization of Integrally-Attached Timber Plate Structures: Experimental studies and macro modeling technique”. PhD thesis. Ecole Polytechnique Fédérale de Lausanne, 2020. DOI: 10.5075/epfl-thesis-8111.

- [RGW17] Robeller, C., Gamarro, J., and Weinand, Y. “Théâtre Vidy Lausanne A Double-Layered Timber Folded Plate Structure”. In: *Journal of the International Association for Shell and Spatial Structures* 58.4 (2017), pp. 295–314. ISSN: 1028-365X. DOI: doi:10.20898/j.iass.2017.194.864.
- [RLW21] Rogeau, N., Latteur, P., and Weinand, Y. “An integrated design tool for timber plate structures to generate joints geometry, fabrication toolpath, and robot trajectories”. In: *Automation in Construction* 130 (2021), p. 103875. ISSN: 0926-5805. DOI: 10.1016/j.autcon.2021.103875.
- [RNW14] Robeller, C., Nabaei, S. S., and Weinand, Y. “Design and Fabrication of Robot-Manufactured Joints for a Curved-Folded Thin-Shell Structure Made from CLT”. In: *Robotic Fabrication in Architecture, Art and Design 2014*. Ed. by W. McGee and M. Ponce de Leon. Cham: Springer International Publishing, 2014, pp. 67–81. ISBN: 978-3-319-04663-1. DOI: 10.1007/978-3-319-04663-1_5.
- [Rob+16] Robeller, C., Konakovic, M., Dedijer, M., Pauly, M., and Weinand, Y. “A Double-Layered Timber Plate Shell - Computational Methods for Assembly, Prefabrication, and Structural Design”. In: *Advances in Architectural Geometry 2016*. Ed. by S. Adriaenssens, F. Gramazio, M. Kohler, A. Menges, and M. Pauly. Zurich: Hochschulverlag AG an der ETH Zürich, 2016, pp. 104–122. ISBN: 978-3-7281-3778-4. DOI: doi:10.3218/3778-4_9.
- [Rob+17] Robeller, C., Weinand, Y., Helm, V., Thoma, A., Gramazio, F., Kohler, M., Menges, A., Sheil, B., Glynn, R., and Skavara, M. “ROBOTIC INTEGRAL ATTACHMENT”. In: *Fabricate 2017*. UCL Press, 2017, pp. 92–97. ISBN: 9781787350007. URL: <http://www.jstor.org/stable/j.ctt1n7qkg7.16> (visited on 06/14/2022).
- [Rob15] Robeller, C. “Integral Mechanical Attachment for Timber Folded Plate Structures”. PhD thesis. 2015. DOI: 10.5075/epfl-thesis-6564.
- [Roc17] Roche, S. “Semi-Rigid Moment-Resisting Behavior of Multiple Tab-and-Slot Joint for Freeform Timber Plate Structures”. PhD thesis. 2017. DOI: 10.5075/epfl-thesis-8236.
- [Rog+20] Rogeau, N., Tiberghien, V., Latteur, P., and Weinand, Y. “Robotic Insertion of Timber Joints using Visual Detection of Fiducial Markers”. In: *Proceedings of the 37th International Symposium on Automation and Robotics in Construction (ISARC)*. Ed. by H. Osumi, H. Furuya, and K. Tateyama. Kitakyushu, Japan: International Association for Automation and Robotics in Construction (IAARC), Oct. 2020, pp. 491–498. ISBN: 978-952-94-3634-7. DOI: 10.22260/ISARC2020/0068.
- [Rog+22] Rogeau, N., Rezaei Rad, A., Vestartas, P., Latteur, P., and Weinand, Y. “A Collaborative Workflow to Automate the Design, Analysis, and Construction of Integrally-Attached Timber Plate Structures”. In: vol. 2. Paper presented at Post-Carbon, the 27th International Conference of the Association for Computer-Aided Architectural Design Research in Asia (CAADRIA). Sydney, 2022, pp. 151–160. DOI: 10.52842/conf.caadria.2022.2.151.

Bibliography

- [Rog21] Rogeau, N. *Manis - Annen case study (Part 1: General workflow)*. Vimeo. 2021. URL: <https://vimeo.com/635127909>.
- [RR21] Rogeau, N. and Rezaei Rad, A. *Manis - Annen case study (Part 2: Focus on integrated structural design)*. Vimeo. 2021. URL: <https://vimeo.com/635128815>.
- [RT17] Rossi, A. and Tessmann, O. “Collaborative Assembly of Digital Materials”. In: *Proceedings of the 37th Annual Conference of the Association for Computer Aided Design in Architecture*. ACADIA. Cambridge, Nov. 2017, pp. 512–521. ISBN: 978-0-692-96506-1. DOI: 10.52842/conf.acadia.2017.512.
- [RV18] Robeller, C. and Viezens, V. “Timberdome: construction system for CLT-segmental plate shells without screws”. In: *24th International Timber Construction Forum*. Garmisch Partenkirchen, 2018.
- [RV20] Robeller, C. and Von Haaren, N. “Recycleshell: Wood-only Shell Structures Made From Cross-Laminated Timber (CLT) Production Waste”. In: *Journal of the International Association for Shell and Spatial Structures* 61.2 (2020), pp. 125–139. ISSN: 1028-365X. DOI: doi:10.20898/j.iass.2020.204.045.
- [RW15] Robeller, C. and Weinand, Y. “Interlocking Folded Plate – Integral Mechanical Attachment for Structural Wood Panels”. In: *International Journal of Space Structures* 30.2 (2015), pp. 111–122. DOI: 10.1260/0266-3511.30.2.111.
- [SB13] G. Schickhofer and R. Brandner, eds. *Starrer und nachgiebiger Verbund bei geschichteten, flächenhaften Holzstrukturen*. deutsch. 1st ed. Vol. 1. Monographic Series TU Graz. Verlag der Technischen Universität Graz, 2013. ISBN: 978-3-85125-262-0.
- [Sch] Schwartz, T. *HAL Robotics Framework*. <https://www.food4rhino.com/en/app/hal-robotics-framework>. Accessed on 2022-08-12.
- [Sch+19] Schwinn, T., Sonntag, D., Grun, T., Nebelsick, J. H., Knippers, J., and Menges, A. “Potential applications of segmented shells in architecture”. In: *Biomimetics for Architecture: Learning from Nature*. Ed. by J. Knippers, U. Schmid, and T. Speck. Birkhäuser, 2019, pp. 116–125. DOI: doi:10.1515/9783035617917-015.
- [SE] Sanderson, G. and Eater, B. *Visualizing quaternions: An explorable video series*. <https://eater.net/quaternions>. Accessed on 2022-08-18.
- [See21] Seewang, L. “From Forest to Frame: Representation and Exception in the Regional Modernism of the Pacific Northwest”. In: *Architectural Theory Review* 25.1-2 (2021), pp. 7–27. DOI: 10.1080/13264826.2021.1986083.
- [SEM] SEMA. *Prefabrication*. <https://www.sema-soft.de/en/software/timber-construction/prefabrication/>. Accessed on 2022-27-07.
- [Shi19] Shigeru Ban Architects. *SWATCH OMEGA*. http://www.shigerubanarchitects.com/works/2019_SO51/index.html. Accessed: 2022-09-15. 2019.
- [Sol] Soler, V. *Robots*. <https://github.com/visose/Robots/wiki>. Accessed on 2022-27-07.

- [SP13] Schwartzburg, Y. and Pauly, M. “Fabrication-aware Design with Intersecting Planar Pieces”. In: *Computer Graphics Forum* 32.2pt3 (2013), pp. 317–326. DOI: 10.1111/cgf.12051.
- [Str88] Strip, D. R. “Technology for robotic mechanical assembly: Force-directed insertions”. In: *AT&T Technical Journal* 67 (1988), pp. 23–34.
- [Svi20] Svilans, T. “Integrated material practice in free-form timber structures”. English. PhD thesis. 2020.
- [SZP18] Suárez-Ruiz, F., Zhou, X., and Pham, Q.-C. “Can robots assemble an IKEA chair?”. In: *Science Robotics* 3.17 (Apr. 2018). ISSN: 2470-9476. DOI: 10.1126/scirobotics.aat6385.
- [Tag20] Tagliaboshi, E. V. “HexBox Canopy: a Rapid Assembly Segmented Timber Shell with Wedge Joints”. MA thesis. Università di Pisa, 2020.
- [Tak81] Takase, Y. “An assessment of the potential of the United States stick-built house for self-help construction”. PhD thesis. Massachusetts Institute of Technology. Dept. of Architecture., 1981.
- [Tan+16] Tang, T., Lin, H.-C., Zhao, Y., Chen, W., and Tomizuka, M. “Autonomous alignment of peg and hole by force/torque measurement for robotic assembly”. In: *2016 IEEE International Conference on Automation Science and Engineering (CASE)*. 2016, pp. 162–167. DOI: 10.1109/COASE.2016.7743375.
- [Teg+12] Tegel, W., Elburg, R., Hakelberg, D., Stäuble, H., and Büntgen, U. “Early Neolithic Water Wells Reveal the World’s Oldest Wood Architecture”. In: *PLOS ONE* 7.12 (Dec. 2012), pp. 1–8. DOI: 10.1371/journal.pone.0051374.
- [Tho+20] Thoma, A., Jenny, D., Helmreich, M., Gandia, A., Gramazio, F., and Kohler, M. “Cooperative Robotic Fabrication of Timber Dowel Assemblies”. en. In: *Research Culture in Architecture: Cross-Disciplinary Collaboration*. Ed. by C. Leopold, C. Robeller, and U. Weber. Basel: Birkhäuser, Dec. 2020, pp. 77–88. ISBN: 978-3-0356-2014-6. DOI: 10.1515/9783035620238-008.
- [TW+59] Timoshenko, S., Woinowsky-Krieger, S., et al. *Theory of plates and shells*. Vol. 2. McGraw-hill New York, 1959. ISBN: 9780070647794.
- [Uni] Unity Technologies. *Unity*. <https://unity.com/>. Accessed on 2022-28-07.
- [Uni18] United Nations (Department of Economic and Social Affairs). *The World’s Cities in 2018*. Tech. rep. 2018.
- [Uni20] United Nations Environment Programme, Global Alliance for Buildings and Construction. *2020 Global Status Report for Buildings and Construction: Towards a Zero-emissions, Efficient and Resilient Buildings and Construction Sector - Executive Summary*. 2020. URL: <https://wedocs.unep.org/20.500.11822/34572>.
- [Van+17] Van Mele, T., Liew, A., Méndez Echenagucia, T., Rippmann, M., et al. *COMPAS: A framework for computational research in architecture and structures*. 2017.

Bibliography

- [VBV19] Vincke, S., Bassier, M., and Vergauwen, M. “IMAGE RECORDING CHALLENGES FOR PHOTOGRAMMETRIC CONSTRUCTION SITE MONITORING”. In: *The International Archives of the Photogrammetry, Remote Sensing and Spatial Information Sciences* (2019).
- [Ves+20] Vestartas, P., Rogeau, N., Gamarro, J., and Weinand, Y. “Modelling Workflow for Segmented Timber Shells Using Wood-Wood Connections”. In: *Impact: Design With All Senses*. Ed. by C. Gengnagel, O. Baverel, J. Burry, M. Ramsgaard Thomsen, and S. Weinzierl. Cham: Springer International Publishing, 2020, pp. 596–607. ISBN: 978-3-030-29829-6.
- [VTT16] VTT Expert Services Ltd. *Kerto-S and Kerto-Q Structural laminated veneer lumber by Metsä Wood*. Finland, 2016.
- [VUI] VUILD Architects. *EMARF*. <https://emarf.co/>. Accessed on 2022-27-07.
- [Wag+20a] Wagner, H. J., Alvarez, M., Groenewolt, A., and Menges, A. “Towards digital automation flexibility in large-scale timber construction: integrative robotic pre-fabrication and co-design of the BUGA Wood Pavilion”. In: *Construction Robotics* 4.3 (Dec. 2020), pp. 187–204. ISSN: 2509-8780. DOI: 10.1007/s41693-020-00038-5.
- [Wag+20b] Wagner, H. J., Alvarez, M., Kyjanek, O., Bhiri, Z., Buck, M., and Menges, A. “Flexible and transportable robotic timber construction platform – TIM”. In: *Automation in Construction* 120 (2020), p. 103400. ISSN: 0926-5805. DOI: 10.1016/j.autcon.2020.103400.
- [Wan+08] Wang, W., Liu, Y., Yan, D., Chan, B., Ling, R., and Sun, F. *Hexagonal Meshes with Planar Faces*. Tech. rep. The University of Hong Kong, 2008.
- [Wan21] Wang, Z. “Computational Analysis and Design of Structurally Stable Assemblies with Rigid Parts”. In: (2021), p. 153. DOI: 10.5075/epfl-thesis-8964.
- [WMR21] Weber, R., Mueller, C., and Reinhart, C. “Building for Zero, The Grand Challenge of Architecture without Carbon”. In: *SSRN* (2021). DOI: 10.2139/ssrn.3939009.
- [WSF] Wang, S.-Y., Sheng, Y.-T., and Frank, F. *Taco ABB*. <https://www.food4rhino.com/en/app/taco-abb>. Accessed on 2022-08-12.
- [WSP18] Wang, Z., Song, P., and Pauly, M. “DESIA: A General Framework for Designing Interlocking Assemblies”. In: *ACM Trans. Graph.* 37.6 (Dec. 2018). ISSN: 0730-0301. DOI: 10.1145/3272127.3275034.
- [ZDB17] Zheng, C., Do, E. Y.-L., and Budd, J. “Joinery: Parametric Joint Generation for Laser Cut Assemblies”. In: *Proceedings of the 2017 ACM SIGCHI Conference on Creativity and Cognition*. C&C ’17. Singapore, Singapore: Association for Computing Machinery, 2017, pp. 63–74. ISBN: 9781450344036. DOI: 10.1145/3059454.3059459.

- [Zim+21] Zimmermann, R. K., Andersen, C. E., Kanafani, K., and Birgisdóttir, H. *Whole life carbon assessment of 60 buildings - Possibilities to develop benchmarks values for LCA of buildings*. Tech. rep. Department of the Built Environment, Aalborg University Copenhagen, 2021.
- [ZS21] Zhang, X. and Stottlemyer, A. “Lumber and timber price trends analysis during the COVID-19 pandemic”. In: *Retrieved on October 1* (2021), p. 2021.

Glossary

- *Adjacency list*: List of lists containing all neighbors of each cell of a graph.
- *Assembly sequence*: List of integers describing in which order building components must be assembled. Integers can also be grouped in subsidiary lists to express intermediary steps in a modular assembly process (see Subsequence). If the panels are inserted one after another without intermediary steps, the assembly sequence is linear (as opposed to modular).
- *B-rep (Boundary representation)*: Solid represented by its envelope.
- *Clearance*: Tolerance in a timber joint. For tenon and mortise joints, the clearance is defined as the distance between the faces of the mortise and the faces of the tenon.
- *CNC (Computer Numerical Control) machine*: Milling machine that can be controlled by a computer to automate the cutting of flat panels allowing the realization of bespoke structures from standardized elements.
- *Contact type*: Topological relation between two plates describing if two plates intersect each other or are juxtaposed and, for the second case, which of their faces is in contact with the other plate (e.g., if the top face of plate A is connected to a side face of plate B, the contact type is labeled “Face-to-side”). The contact type directly impacts the type of joints that can be created between both plates.
- *Contact vector*: a local vector of insertion associated with a contact zone between two plates. Contact vectors are determined according to the contact type.
- *Contact zone*: Planar surface resulting from the intersection of two juxtaposed plates.
- *Fabrication toolpath*: Pair of curves representing the trajectory of a cutting tool. The lower curve gives the position, while the upper curve gives the orientation.
- *G-code*: Standard programming language which can be interpreted by most CNC machines to execute a fabrication toolpath.
- *IATPS (Integrally Attached Timber Plate Structures)*: Structure composed of standard timber panels connected by timber joints. The joints are integrated into the shape of the elements and prefabricated using a CNC machine.

- *Insertion domain*: Set of vectors representing all possible directions to assemble two pieces. Timber joints geometry constraints the insertion domain to specific directions of assembly. Insertion domains can be described in the 3D space as pieces of spheres.
- *Insertion vector*: Vector representing the direction of the assembly of one element or one group of elements (module).
- *Instantiation*: In object-oriented programming, construction of a distinct object based on a class containing specific methods and attributes. All class instances share the same data structure but store different values.
- *IRA (Industrial Robotic Arm)*: Articulated robot composed of a chain of connected links which can be programmed to perform actions similar to a human arm.
- *Plate (class)*: A python class that stores the plate geometry and other attributes such as the plate contour, the plate thickness, and the geometry of the associated joints.
- *Plate (geometry)*: Closed polyhedron with its two largest faces parallel to each other. In addition, all vertices must be trivalent, and each vertex of the top face should also be directly connected to exactly one vertex of the bottom face and conversely.
- *Plate faces*: Top and bottom faces of a plate, parallel to each other and larger than all other faces.
- *Plate model*: A Python class representing a collection of plates. The adjacency graph and the assembly sequence are its main attributes.
- *Plate module*: A Python class representing a portion of a plate model. In addition to the model attributes, the module is characterized by a subsequence and a vector of insertion.
- *Plate neighbor*: Adjacent plate sharing a contact zone (surface or volume) with another plate.
- *Plate sides*: Faces forming the edges of the plates between the top and bottom plate faces.
- *Robotic trajectory*: Series of robot positions expressed as a list of frames.
- *Subsequence*: Part of an assembly sequence defining the order of insertion for the plates of a specific module in the plate model.
- *Timber joinery*: Technique to connect two pieces of wood solely through their geometry (form-closure) and without the use of mechanical (nails, screws) or chemical (glue) fasteners.



CURRICULUM VITAE

Dr. NICOLAS ROGEAU

Engineer-architect and researcher looking for more sustainable construction methods.

MAILING ADDRESS:

Chemin Aimé-Steinlen, 5
1004, Lausanne, Vd, Switzerland

PHONE: +41 78 200 40 42

E-MAIL: nicolas.rogeau@gmail.com

EDUCATION

- Ph.D. 03/2019-02/2023 Laboratory for Timber Constructions (IBOIS), École Polytechnique Fédérale de Lausanne (EPFL), Switzerland. Thesis: Robotic assembly of Integrally-Attached Timber Plate Structures, under the supervision of Prof. Dr. Yves Weinand and Prof. Dr. Pierre Lateur.
- M.Sc. 09/2016-06/2018 Civil Engineer-Architect, Faculty of Architecture, Architectural Engineering and Urbanism (LOCI), Université Catholique de Louvain (UC Louvain), Belgium. Thesis: Parametric Design of Drone-Compatible Architectural Timber Structures, under the supervision of Prof. Pierre Lateur, in collaboration with the Massachusetts Institute of Technology (MIT).
- Exch. 09/2016-06/2017 Mercator international exchange program at the faculties of Architecture, Civil engineering, and Visual arts at Université Laval (UL), Québec, Canada.
- B.Sc. 09/2013-06/2016 Civil Engineer-Architect, Faculty of Architecture, Architectural Engineering and Urbanism (LOCI), Université Catholique de Louvain (UC Louvain), Belgium.

OTHER CERTIFICATIONS

- 05/2021 MOOC Circular economy applied to building, design, and furniture, Les Canaux, Paris, France.
- 05/2019 Public Space Public Life, Gehl Architects, Lausanne, Switzerland.
- 04/2016 European First Aid Certificate, Belgian Red Cross.
- 09/2015 Driving License (A1, B).

EMPLOYEMENT

- 03/2023-current Postdoctoral researcher and lecturer at the Laboratory for Timber Constructions (IBOIS), École Polytechnique Fédérale de Lausanne (EPFL). Topics: interdisciplinary collaboration and architectural pedagogy.
- 03/2019-02/2023 Doctoral candidate and teaching assistant at the Laboratory for Timber Constructions (IBOIS), École Polytechnique Fédérale de Lausanne (EPFL). Topics: computational design and robotic timber construction.
- 03/2019-08/2022 Researcher at the National Centre of Competence in Research Digital Fabrication (NCCR DFAB), Eidgenössische Technische Hochschule Zürich (ETHZ). Cluster: Spatial Timber Assemblies.
- 09/2018-02/2019 Internship at the Laboratory for Timber Constructions (IBOIS), École Polytechnique Fédérale de Lausanne (EPFL). Topic: Digital fabrication of round wood structures.
- 04/2017-06/2017 Design and construction of a public square for the city of Québec, Canada. Project: Sympathique Place Ouverte à Tous (SPOT) in collaboration with Hatem+D and Tergos Architecture.



AWARDS

01/2023	Nomination for the EPFL Doctorate Award, Lausanne, Switzerland.
04/2022	Young CAADRIA Award, The Association for Computer-Aided Architectural Design Research in Asia.
06/2018	Alumni Award for best Thesis Presentation, Louvain School of Engineering, UC Louvain, Belgium.
06/2018	Alumni Award for best Thesis Innovation, Louvain School of Engineering, UC Louvain, Belgium.
02/2017	Laureate of the interdisciplinary student competition "Cecobois Challenge", Centre d'Expertise sur la Construction Commerciale en Bois, Québec, Canada.
06/2016	Best design award at the timber structure challenge "Project P4/construction", UC Louvain, Belgium.

GRANTS

02/2023	Continuing Education Call for the creation of a postgrad course on digital timber construction.
12/2022	Postdoc.mobility grant from the SNSF for a 24 months research stay at the University of Tokyo, Japan.
06/2019	ENAC Special Call for Equipment (45'000 CHF) to perform research experiments with a 6-axis robotic arm.
02/2019	Swiss National Science Foundation (SNSF) grant to conduct research within the National Centre of Competence in Research Digital Fabrication (NCCR DFAB), grant number: 51NF40-141853.
05/2016	Mercator Scholarship to finance a year of study at Université Laval (UL), Québec, Canada.

TEACHING ACTIVITIES

02/2023-current	Ludic streets: Observe, Design, Build, Adjust , course for 3 rd year students in architecture, civil engineering, and environmental engineering at EPFL. Topics: urban design, inclusive public furniture, timber construction.
02/2022-current	Introduction to Computational Architecture , course for 3 rd year Bachelor students of the Architecture School at EPFL. Topics: computational thinking, parametric design, 3D modeling, interactive pedagogy.
02/2021-current	ENAC Week Land of thousand dances , interdisciplinary one-week design-to-construction workshop for 2 nd year Bachelor students at EPFL. Topics: reuse of timber, care and maintenance, on-site experimentations.
09/2018-current	Architectural design studio for 3 rd year Bachelor and 1 st year Master students of the Architecture School at EPFL. Topics: sustainable design, timber structures, digital tools, and construction performance.
02/2022-07/2022	Supervision of the Master project (2 nd year Master) of Liliana Da Cunha and Lisa Baseggio: <i>Requalification d'une parcelle industrielle à Delémont en un lieu de vie multi-usages et polyvalent</i> .
09/2021-01/2022	Supervision of the Theoretical essay (2 nd year Master) of Liliana Da Cunha and Lisa Baseggio: <i>Les structures hospitalières temporaires</i> .
09/2020-02/2021	Supervision of the Semester project (1 st year Master) of Florian Genilloud: <i>Implementation of Computer Vision with Time of Flight sensors for Robot Positioning</i> .
09/2018-12/2018	Teaching assistant for Designing structures , a course for 3 rd year Bachelor students of the Architecture School at EPFL. Topics: structural design, 3D modeling, timber construction.



Site visit in Rossinière with students of the Design Studio, Autumn 2021



3D scan of a timber barn in Switzerland with students of the Design Studio, Spring 2020



Transformation of a timber structure in Evian with students of the ENAC week, Spring 2022

PEER-REVIEWED PUBLICATIONS

- 09/2022 **Rogeanu, N.**, Gamero, J., Latteur, P., & Weinand, Y. (2022). Design considerations for robotically assembled through-tenon timber joints. *Construction Robotics*.
DOI: [10.1007/s41693-022-00080-5](https://doi.org/10.1007/s41693-022-00080-5)
- 04/2022 **Rogeanu, N.**, Rezaei Rad, A., Vestartas, P., Latteur, P., & Weinand, Y. (2022). A collaborative workflow to automate the design, analysis, and construction of Integrally-Attached Timber Plate Structures. In *Proceedings of the 27th CAADRIA Conference*, University Of New South Wales, Sydney.
DOI: [10.52842/conf.caadria.2022.2.151](https://doi.org/10.52842/conf.caadria.2022.2.151)
- 10/2021 **Rogeanu, N.**, Latteur, P., & Weinand, Y. (2021) An integrated design tool for timber plate structures to generate joints geometry, fabrication toolpath, and robot trajectories. *Automation in Construction*, 130.
DOI: [10.1016/j.autcon.2021.103875](https://doi.org/10.1016/j.autcon.2021.103875)
- 02/2021 Rezaei Rad, A., Burton, H., **Rogeanu, N.**, Vestartas, P., & Weinand, Y. (2021) A framework to automate the design of digitally-fabricated timber plate structures. *Computers & Structures*, Volume 244.
DOI: [10.1016/j.compstruc.2020.106456](https://doi.org/10.1016/j.compstruc.2020.106456)
- 10/2020 **Rogeanu, N.**, Tiberghien, V., Latteur, P., & Weinand, Y. (2020). Robotic Insertion of Timber Joints using Visual Detection of Fiducial Markers. In *Proceedings of the 37th International Symposium on Automation and Robotics in Construction*, Kitakyushu, Japan.
DOI: [10.22260/isarc2020/0068](https://doi.org/10.22260/isarc2020/0068)
- 08/2019 Vestartas, P., **Rogeanu, N.**, Gamero, J., & Weinand, Y. (2019). Modelling workflow for segmented timber shells using wood-wood Connections. In *Proceedings of the Design Modelling Symposium*, Berlin.
DOI: [10.1007/978-3-030-29829-6_46](https://doi.org/10.1007/978-3-030-29829-6_46)
- 07/2018 Goessens, S., **Rogeanu, N.**, De Beusscher, G., Mueller, C., & Latteur, P. (2018), Parametric design of drone-compatible architectural timber structures. In *Proceedings of IASS Annual Symposia*, Boston.
ISSN: [2518-6582](https://doi.org/10.22260/isarc2020/0068)

OUTREACH ACTIVITIES

- 02/2023 *Teaching Circular Architecture On-site*. Matters of Abstraction, KU Leuven, Ghent.
- 11/2022 *Robotic timber construction*. Swiss Robotics Day, Lausanne.
- 10/2022 *Timber industry 4.0*. Implenia at EPFL, Lausanne.
- 06/2022 *IATPS: from computational design to robotic construction*. Construction Robotics Symposium, Zurich.
- 04/2022 *A collaborative workflow for the design and construction of IATPS* (online workshop). CAADRIA, Sydney.
- 04/2022 *Building timber structures... with robots*. EPFL Reiseziel innovation, Thun.
- 12/2021 *No screws loose, an app for timber construction* (interview). Horizons, the Swiss Research Magazine.
- 03/2021 *Designing inside a point cloud*. Matters of Abstraction, KU Leuven (online).
- 10/2020 *Robotic insertion of timber joints with fiducial markers*. ISARC, Kitakyushu (online).
- 11/2019 *Building in timber with robots*. EPFL Alumni 50th homecoming, Lausanne.
- 07/2018 *Drone-compatible timber structures*. BESIX, Brussels.
- 07/2018 *Parametric design of drone-compatible architectural timber structures*. IASS, Boston.
- 02/2017 *Introduction to parametric design* (workshop). Student association, LOCI, UC Louvain.

ACADEMIC SERVICE AND MEMBERSHIP

- 03/2023 Reviewer of the New European Bauhaus Prizes 2023, European Commission.
- 04/2022-current Member of the *Research Network for Advancing Architecture, Engineering and Construction (AdvanceAEC)*.
- 09/2022-current Reviewer of the 27th and 28th CAADRIA Conferences, Sydney.
- 08/2021 Reviewer of 38th International Symposium on Automation and Robotics in Construction, Dubai.
- 09/2013-06/2016 Student representative, UC Louvain, Belgium.

LANGUAGES

French	Native
English	Highly proficient
Dutch	Intermediate
Japanese	Elementary

COMPUTER SKILLS

Rhinoceros3D and Grasshopper	Highly proficient
Microsoft Word, Excel, and PowerPoint	Highly proficient
Adobe Photoshop, Illustrator, and Premiere	Proficient
Python and C#	Proficient
Unity and 3ds Max	Intermediate

HOBBIES

Hiking, cycling, sailing, doing improvisation, and playing the piano.